Development of New Parameter Extraction Schemes and Maximum Power Point Controllers for Photovoltaic Power Systems

Raseswari Pradhan

Department of Electrical Engineering
National Institute of Technology Rourkela
2014

Development of New Parameter Extraction Schemes and Maximum Power Point Controllers for Photovoltaic Power Systems

A thesis submitted in partial fulfillment of the
requirements for the degree of

Doctor of Philosophy

in

Electrical Engineering

by

Raseswari Pradhan
Roll-509EE111

Under the Guidance of

Prof. Bidyadhar Subudhi

Department of Electrical Engineering
National Institute of Technology Rourkela
Rourkela-769008
2010-2013

Department of Electrical Engineering

National Institute of Technology Rourkela

C E R T I F I C A T E

This is to certify that the thesis entitled ***"Development of New Parameter Extraction Schemes and Maximum Power Point Controllers for Photovoltaic Power Systems"*** *by* ***Ms. Raseswari Pradhan****, submitted to the National Institute of Technology, Rourkela for the award of Doctor of Philosophy in Electrical Engineering, is a record of bonafide research work carried out by her in the Department of Electrical Engineering , under my supervision. I believe that this thesis fulfills part of the requirements for the award of degree of Doctor of Philosophy.The results embodied in the thesis have not been submitted for the award of any other degree elsewhere.*

Prof. Bidyadhar Subudhi

Place:Rourkela
Date:

To My Loving Family and Friends

Acknowledgements

First and foremost, I am truly indebted to my supervisors Prof. Bidyadhar Subudhi for his inspiration, excellent guidance and unwavering confidence through my study, without which this thesis would not be in its present form. I also thank him for his gracious encouragement throughout the work.

I express my gratitude to the members of Doctorate Scrutiny Committee, Prof. A.K. Panda, Prof. K.K. Mohapatra, Prof. S. Das and Prof. K.B. Mohanty, for their advise and care. I am also very much obliged to Prof. A.K. Panda, Head of the Department of Electrical Engineering, NIT Rourkela for providing all the possible facilities towards this work. My special thanks to Prof. P.K. Ray, Prof. S. Gosh, Prof. S. Maity, Prof. S. Samanta and Prof. C. Babu for their useful suggestions and comments. Thanks also to other faculty members in the department.

My special thanks to Lab staffs Sahadev Swain and Budhhu Oram for their unforgettable help. I would like to thank Raja, Chhavi, Pradosh, Soumya, Rakesh, Dushmanta, Basant, Satyam, Santanu, Debabrata, Subhasis, Satyajeet and all the research scholars at Center for Industrial Electronics and Robotics, NIT Rourkela, for their coperation.

I also want to thank Runa, Meena, Honny, Devasmita, Smita, Archala, Aparajita, Sushmita and all other C.V. Raman hostel mates in making my stay enjoyable during this Ph.D. duration. I thanks my friends Archana, Aliva, Suchismita and Sandhya for their encouragement and support.

My wholehearted gratitude to my parents, Gitanjali Pradhan and Sitaram Pradhan, my sisters, Anupama and Pinky for keeping faith on me and always shower me with their unconditional love.

Raseswari Pradhan

Abstract

In the recent years, in every parts of the world, focus is on supplementing the conventional fossil fuel based power generation with power generated from renewable sources such as photovoltaic (PV) and wind systems. PV technology is one of the fastest growing energy technologies in the world owing to its abundant availability. But unfortunately, the cost of PV energy is higher than that of other electrical energy from other conventional sources. Therefore, a great deal of research opportunities lie in applying power electronics and control technologies for harvesting PV power at higher efficiencies and efficient utilization. Simulation and control studies of a PV system require an accurate PV panel model. Further, for efficient utilization of the available PV energy, a PV system should operate at its maximum power point (MPP). A maximum power point tracker (MPPT) is needed in the PV system to enable it to operate at the MPP.

The output characteristic of a PV system is non-linear and its output power fluctuates to a large extent in accordance with the variation of solar irradiance and temperature. A lot of research is being pursued on this area and several MPPT techniques have been proposed and implemented. But, still there is a lot of scope on designing new parameter extraction algorithms to achieve fast and accurate extraction of PV panel parameters. Further, there is need of development of efficient MPPT algorithms that can be adapted to different weather conditions with minimal fluctuations in input PV current and voltage.

The work described in the thesis involves development of some new parameter extraction and robust adaptive MPPT algorithms. Two parameter extraction algorithms have been proposed namely a hybrid Newton-Raphson method (hybrid NRM) and an evolutionary computational technique called Bacterial Foraging Optimization (BFO). These two parameter extraction techniques are found to be extracting parameters of a PV panel accurately in all weather conditions with less computational overhead. Further, these two parameter extraction techniques do not suffer from singularity problem during convergence. BFO technique being a global optimization technique provides accurate PV panel parameters.

Although hybrid NRM exhibits a good convergence for obtaining PV panel parameters but it is unsuitable for shading conditions. From the simulation and experimental results, it is observed that BFO algorithm yeilds good parameter extraction performance both in shading and non-shading conditions. Thus, BFO technique is considered to be more effective in achieving accurate parameter extraction compared to the hybrid NRM algorithm.

After having developed efficient parameter extraction algorithms for a PV panel, the thesis subsequently proposes five new MPPT algorithms such as an Auto-tuned Adaptive MPPT (ATAMPPT), Adaptive predictive error filter controller based MPPT (APEFC-MPPT), Double integral sliding mode controller based MPPT (DISMC-MPPT), Adaptive DISMC-MPPT and Self-tuned adaptive MPPT. All these developed MPPT algorithms have been implemented on a 0.2kW PV stand-alone system, in MATLAB/SIMULINK, OPAL-RT and on a prototype hardware PV control set-up. From obtained results, it is found that these MPPTs adjust effectively the power of a PV system to its maximum power value smoothly with fast response and accuracy whilst reducing the fluctuations in its power. Tracking performance of all these proposed MPPT algorithms are found to be superior to some of the existing MPPTs such as perturb and observe (P&O), incremental conductance (INC) and P&O adaptive perturbation size (APO. Further more, a PV system is observed to be stable with all these proposed MPPTs. It is found that the proposed self-tuned adaptive MPPT exhibits better MPP tracking performance in terms of quick settling time and least steady state error. Further, less voltage fluctuation and less maximum overshoot are observed in the case of the proposed self-tuned adaptive MPPT amongst all the proposed MPPT algorithm.

Contents

List of Abbreviations

Abbreviation	Description
PV	Photovoltaic
STC	Standard Testing Condition
MPP	Maximum Power Point
OC	Open Circuit
SC	Short Circuit
MPPT	Maximum Power Point Tracker
PWM	Pulse Width Modulation
DPWM	Discrete PWM
NRM	Newton-Raphson Method
PI	Proportional-Integral
PID	Proportional-Integral-Derivative
IPID	Incremental Proportional-Integral-Derivative
DPID	Discrete PID
Z-N	Ziegler-Nichols
PSO	Particle Swarm Optimization
GA	Genetic Algorithm
BFO	Bacterial Foraging Optimization
FPGA	Field Programmable Gate Array
VHSIC	Very-High-Speed Integrated Circuits
VHDL	VHSIC Hardware Description Language
RT	Real-Time
RTW	Real-Time Workshop
HIL	Hardware-in-Loop
FSCI	Fractional Short-Circuit Current
FOCV	Fractional Open-Circuit Voltage
OCC	One-Cycle Control
LUT	Look-up Table Technique
Diffrn	Differentiation Technique

Abbreviation	Description
FV	Feedback Voltage
FPVV	Feedback of Power Variation with Voltage
FPVC	Feedback of Power Variation with Current
P&O	Perturbation and Observation
INC	Incremental Conductance
FO	Forced Oscillation
RCC	Ripple Correlation Control
CS	Current Sweep
EPP	Estimated-Perturb-Perturb
Par Cap	Parasitic Capacitance
LVM	Load Voltage Maximization
DLCDC	DC Link Capacitor Droop Control
Linr	Linearization
FLC	Fuzzy Logic Control
ANN	Artificial Neural Network
SMC	Sliding-Mode Control
ISMC	Integral Sliding-Mode Control
DISMC	Double Integral Sliding-Mode Control
G-N	Gauss-Newton
SD	Steepest-Descent
Analyt	Analytic
CF	Curve Fitting
DMPPT	Distributed Maximum Power Point Tracking
MVMPPT	Multi-variable MPPT
TEODI	Technique on Equalization of Output for forced Displacement of Input
ATAMPPT	Auto-Tuned Adaptive MPPT
APO	Adaptive Perturb and Observe
APEFC	Adaptive Predictive Error Filter Controller
RLS	Recursive Least square
LMS	Least Mean Square
NLMS	Normalized Least Mean Square
VSLMS	Variable Step-size LMS
CVSLMS	Correlation based Variable Step-size LMS
RCVSLMS	Robust Correlation based Variable Step-size LMS
GASLMS	Gradient Adaptive Step-size LMS
GALSLMS	Gradient Adaptive Limited Step-size LMS
MSE	Mean Steady-state Error

Abbreviation	Description
SSE	Steady-State Error
SISO	Single-Input-Single-Output
GMV	Generalized Minimum Variance
IGMV	Incremental Generalized Minimum Variance
PC	Personal computer
DSO	Digital Storage Oscilloscope
ADC	Analogue to Digital Converter
DAC	Digital to Analogue Converter
PWM	Pulse width Modulation
GUI	Graphical User Interface
NI	National Instruments
DAQ/DAS	Data Acquisition System

List of Figures

List of Tables

Chapter 1

Introduction

1.1 Background

1.1.1 Photovoltaic Power Generation

Due to limited stock and rising prices of conventional energy sources such as coal and petroleum etc. and their adverse impacts on the environment, there is a strong motivation to supplement the energy requirement from nonconventional energy or renewable energy sources such as solar energy, wind, hydro, geothermal, etc. for electrical power generation [2]. Among the different renewable sources, solar or photovoltaic (PV) power system becomes popular [3, 4] due to the fact that

- Solar irradiance is abundantly available with no cost on fuel
- No pollution and waste products involved in PV power generation
- Less maintenance needed than that of other alternatives
- Unattended operation and minimum periodic maintenance so less labor cost
- High initial cost, but in long term cost effectiveness
- Locally generate energy, without the need of long transmission lines

The word photovoltaic (PV) is combination of the two words 'photo', which means light, and 'voltaic', which implies the production of electricity. PV technology is concerned with generation of electricity from light. A solar cell is a device that converts the energy of sunlight directly into electricity using photovoltaic effect [5].

Although PV generated power benefit both the economy and the environment at a long run compared to that of conventional energy resources such as coal and oil but unfortunately, at present PV power generation is not economically beneficial [6, 7, 8]. Therefore, a lot research oppotunities exist on PV power generation aspects.

1.1.2 Challenges in PV Power Generation

In a PV system, the conversion of solar energy to electricity is facilitated by means of a PV array and a power-electronic converter system with a control mechanism. The dynamic behavior and its impact on the distribution network of a PV system are greatly influenced due to the nonlinear characteristics of the PV array and converter system together with its control. Accurate mathematical models of the PV systems are necessary to study and characterize the transient responses. These mathematical models must have the capability of being augmented with those of the distribution networks to allow comprehensive analytical and simulation studies. However, design of such mathematical models is not a straightforward task because the design parameters of the PV panels are usually not provided by manufacturer. Therefore, the only viable option is the development of mathematical models of PV panel that are based on understanding of dynamics of the PV system such that the models can capture the I-V and P-V characteristics of the real PV systems [9].

Solar arrays are among the best renewable energy resources and PV is the fastest growing energy technology in the world. But energy conversion technologies of PV system suffer from some serious drawbacks such as intermittence and seasonality of sunlight and per unit generation cost. The output of PV power station fluctuates greatly due to the intrinsic fluctuation and randomness of PV power generation. The output characteristic of a PV cell is non-linear and its output power fluctuates to a large extent by solar irradiance and temperature. Specially, the maximum power point of the PV cells changes a lot with change of solar irradiance and temperature [10].

PV system can generate electricity only when sunlight is available. The lack of inexpensive and efficient energy converters and also poor match between the solar and electrical demand peaks in many locations and applications are the main hurdles for the PV system. Another drawback is its low power density because solar power received at Earth's surface varies over day to night and winter to summer in a particular location. Therefore, energy conversion technologies are required to equip with good converters, controllers, filters and storage devices. It brings another drawback with it that is increase in cost per unit of energy generation. Thus, the PV systems are expensive and are still not competent with typical retail prices for grid electricity [11, 8]. Therefore, even if customers are aware of the benefits of the PV system applications, they still prefer buying the conventional electricity due to high unit price in case of PV power. Average power generation efficiency of a commercial PV panel is only around 20% [12, 13]. But that generated PV power can be made available for practical use only by the help of an efficient device called maximum power point tracker (MPPT) which extracts the peak of the available PV power. This device must be constructed with a good MPPT algorithm and a controller with efficient control system [14]. Therefore, research on MPPT is of great significance for improving the utilization of PV panels.

1.1.3 Photovoltaic Energy Conversion

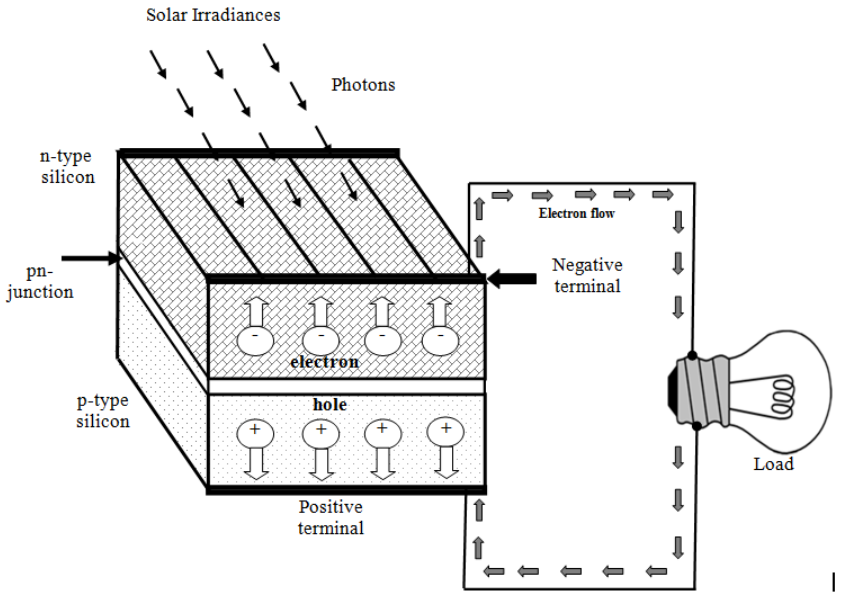

Figure 1.1: Conversion mechanism of Solar light into electricity in a PV cell

When a photon (a light particle) hits a PV cell of the PV panel, it has enough energy to knock an electron loose, allowing it to flow freely as shown in Fig.1.1. All PV cells have two layers of silicon; one is positively charged and another one is negatively charged. When light strikes the PV cell, the electric field across the junction between these two layers causes electricity to flow. The PV cell behaves as a current source [15]. The greater the intensity of the solar irradiance, the greater is the generation of current in this PV cell. The PV panel contains several PV cells in series and parallel according to the output power requirement. When this PV panel is connected to a load then the electrons started moving in a certain direction, creating a useful current through the load.

The PV cell can be of three types such as Mono-crystalline, Poly-crystalline and thin-film. Characteristics of these solar cells are shown in Fig.1.2 and compared in Table 1.1.

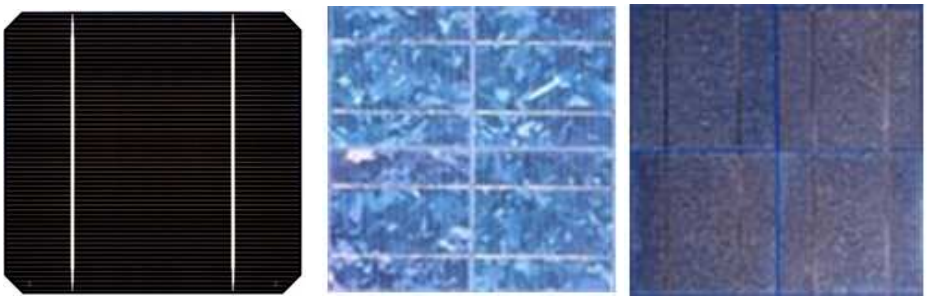

Figure 1.2: (a) Mono-crystalline, (b) Poly-crystalline and (c) Thin-film PV cell

Although PV cell becomes a current source in presence of solar light, but its generated

Table 1.1: Types of PV cells [1]

SL. No.	Types of PV Cell	Properties
1	Mono-crystalline	∗ Made up of a single material called silicon. ∗ Most efficient in power generation in good weather conditions. ∗ Energy conversion efficiency is 12-15%.
2	Poly-crystalline	∗ Made up of a material called Poly-crystalline silicon which is composed of a number of small silicon crystals. ∗ It is also efficient in good light conditions. ∗ But, it has less embodied energy than mono-crystalline. ∗ Energy conversion efficiency is 11-14%.
3	Thin-film	∗ Made up of materials like CdTe, CIGS, CIS, Amorphous Silicon (a-Si). ∗ It is efficient even in poor light conditions. ∗ Very low embodied energy. Most environmental friendly. ∗ Energy conversion efficiency is 6-12%.

current is insignificant for any useful work. Therefore, many PV cells need to be connected in series and parallel according to supply a required voltage and current ratings of load. A PV module with power rating in watts consists of these series and parallel combination of PV cells. For the requirement of a higher rating of supply such as kW and MW, PV arrays are used [16]. These PV arrays are made by connecting many PV modules in series and parallel as shown in Fig.1.3. The PV array power output depends on the power output of individual PV modules. By choosing appropriate sized and series-parallel combinations of PV modules, PV array of given power rating can be obtained.

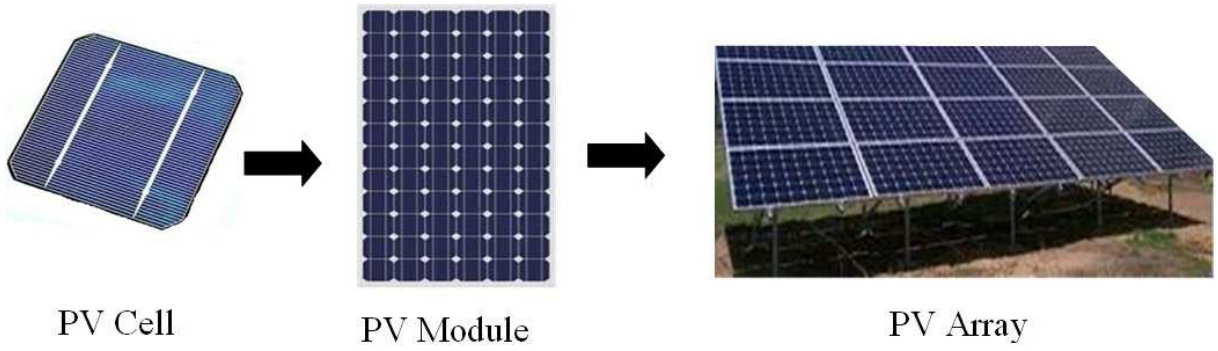

Figure 1.3: Relationship between PV cell, module and array

1.1.4 Types of PV system

Grid Connected

It is the most popular type of PV system for homes and business centers. The PV system is connected to the local electricity network allowing the surplus amount of the generated solar electricity to be sold to the utility. Electricity can be taken back from the network in absence of sun light like night, cloudy sky etc. An inverter is used in this PV system to convert the DC power produced by its PV array to AC power as AC power is needed to run electrical equipments.

Stand-alone

This type of PV system is completely independent of the utility grid. In this type of PV system, the PV array is directly connected to a battery which stores the generated electricity and acts as the main power supply. An inverter can be used to convert AC power from DC power generated by the PV array of the PV system, enabling the use of normal appliances without mains power.

Hybrid System

A PV system can be combined with one or more other sources of power such as biomass generator, wind turbine or diesel generator etc. to ensure a consistent supply of electricity. A hybrid system can be grid connected, stand alone or grid supported type [17].

1.1.5 Modeling of PV Panel

Accurate modeling of a photovoltaic cell is an important requirement for designing an efficient PV system since photovoltaic cell is the basic element of a PV system. In the past, a number of research works have been directed on both modeling of PV module and on topological descriptions which are used in either isolation or integrated to a grid. Choice of topology system is also important for successful modeling of a PV array.

A number of mathematical models of PV cell such as ideal model, two-diode model and single-diode model are available in literature. According to law of Physics, an ideal model of the PV module [18] can be represented by a photo-generated current source I_{ph} and a diode both in parallel to each other (Fig.1.4 (a)). The diode D represents the p-n junction of the PV module and current through this diode I_d represents the escaping current through the p-n junction due to the diffusion mechanism. This model assumed to be lossless and is the simplest model. But this model does not represent an accurate structure of a PV module. To improve the accuracy, a series resistance R_s of the PV module has been considered in [19] as shown in Fig.1.4 (b) which represents the conductance loss. To further increase the accuracy, another resistance R_{sh} that represents the leakage current in the p-n junction has been added to Fig.1.4 (c) which is represented in Fig.1.4 (c) [20].

A second diode has been added to the structure of the Fig.1.4 (c) in order to increase the

modeling accuracy further and the modified model is called a two-diode model as shown in Fig.1.4 (d) [26]. In this model, current I_{d1} through diode D_1 represents the diffusion current due to major charges while current I_{d2} through diode D_2 represents the recombination current due to minor charges. Although behavior of a two-diode model closely matches with that of the physical PV module but the model is non-linear and complex. Its mathematical analysis is very difficult.

The single diode model of PV module is although non-linear but simple in structure than that of the two-diode model. Hence, analysis of this model is easier than that of the two-diode model [21]. It also responds quickly to any changes in the system conditions. On comparing the reported different models of PV module, the single-diode-five-parameter model represented using five parameters namely series resistance (R_s), shunt resistance (R_{sh}), diode-ideality factor (a), dark saturation current (I_0) and photo-generated current (I_{ph}) is suitable in maintaining optimized balance between imitations of the physical PV module and the ease of implementation in mathematical analysis hence widely used. Therefore, a single diode five-parameter model is considered in this work [22].

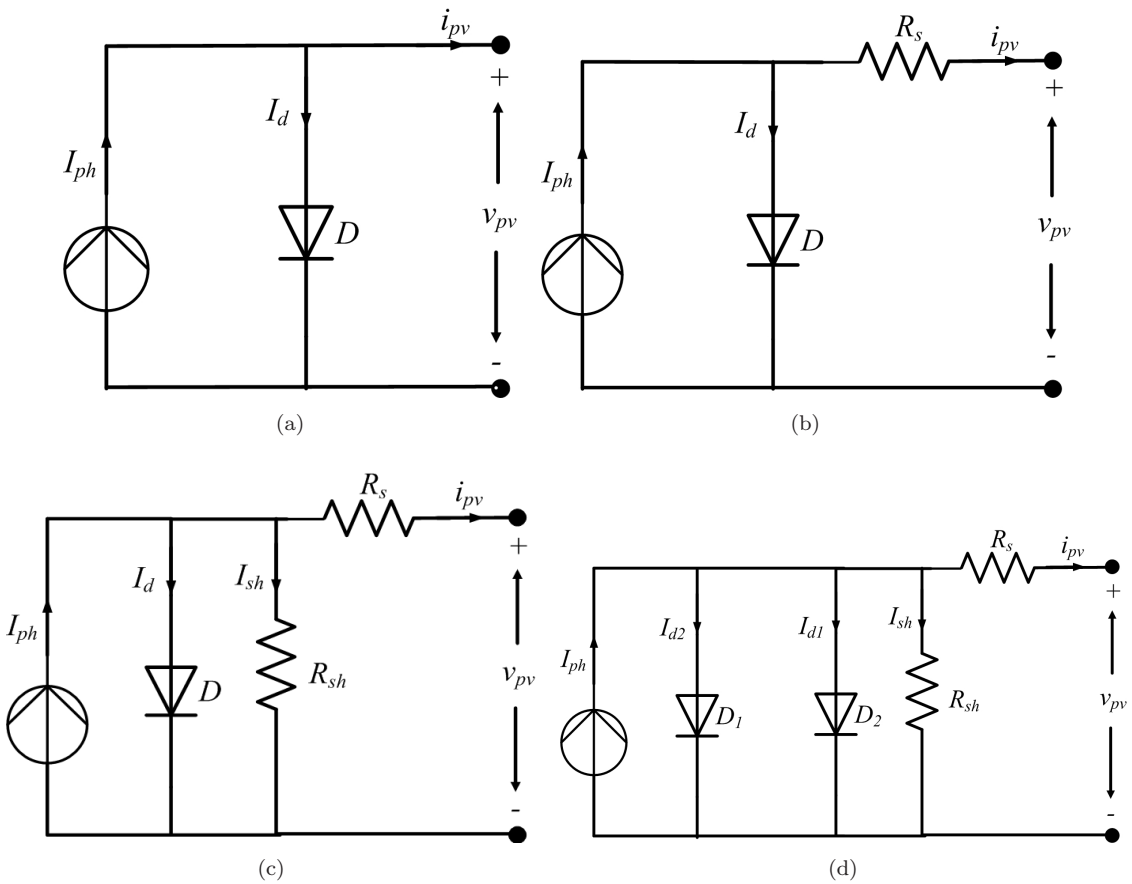

Figure 1.4: (a) Ideal Model, (b) Single-diode-four-parameter Model, (c) Single-diode-five-parameter Model and (d) Two-diode Model of a PV module

Usually, information regarding values of short-circuit current (I_{sc}), open-circuit voltage (V_{oc}), voltage at MPP (V_{mpp}) and current at MPP (I_{mpp}) are provided in the Manufacturer's data-sheet. But, values of parameters i.e. I_{ph}, I_0, R_s, R_{sh} and a are unknown to the user since they are not mentioned in manufacturers' data-sheet. Hence, the first step towards this PV panel modeling involves finding values of parameters i.e. I_{ph}, I_0, R_s, R_{sh} and a. For efficient design of the PV panel, it is essential to use the accurate values of the panel parameters and hence the parameters need to be extracted by a suitable extraction method before designing a PV panel.

1.1.6 Maximum Power Control using MPPT

Although PV energy conversion into electrical energy is one of the rapidly growing technology in various countries but, PV system has limitations such as high installation cost, low energy conversion efficiency and irregularity in power generation due to dependency on environment [23]. As the output characteristic of the PV panel of a PV system is non-linear, fluctuation in its output PV power value to a large extent is affected by solar irradiance and temperature. Hence, the output of PV power system fluctuates greatly due to the fluctuation and randomness of PV power generation. Specially, the maximum power point of the PV cells changes a lot with varying solar irradiance and temperature [24].

Commercial PV panels have very less average power generation efficiency. But that generated PV power can be made available for practical use only by the help of a MPPT with a good tracking algorithm to find the MPP in a short time and an efficient controller. Therefore, research in MPPT is of great significance for improving the utilization of PV cells [25].

A lot of research has been directed in the past to improve the efficiency and power quality of PV system [26]. PV systems have low energy conversion efficiency due to their nonlinear and time-varying I-V and P-V characteristics with respect to variation in solar irradiance and PV cell temperature. Hence, the PV systems need to be operated at their MPPs because at MPP, a PV panel operates most efficiently as it delivers the maximum power. To track the MPP, a maximum power point tracker (MPPT) is usually used in the PV system. MPPT controller controls the PV system with view to improve the power generation efficiency of the PV system. Hence, MPPT is considered as an integral component in a PV system [27].

There exists a single point called MPP (V_{mpp}, I_{mpp}) at which output power of PV panel is the maximum. When a load is directly coupled to the PV panel as shown in Fig.1.5 (a), then the operating point of load is defined by the intersection of its I-V characteristics with the load line as in Fig.1.5 (b). There are two operating points ***A*** and ***B*** for two different values of R_L. Powers at these points A and B are definitely less than MPP as they are not aligned with MPP. This means that the operating point of PV panel with direct coupled load is defined by the load and there is under use of maximum possible power. When load varies, then the operating points of PV system also changes which is undesirable.

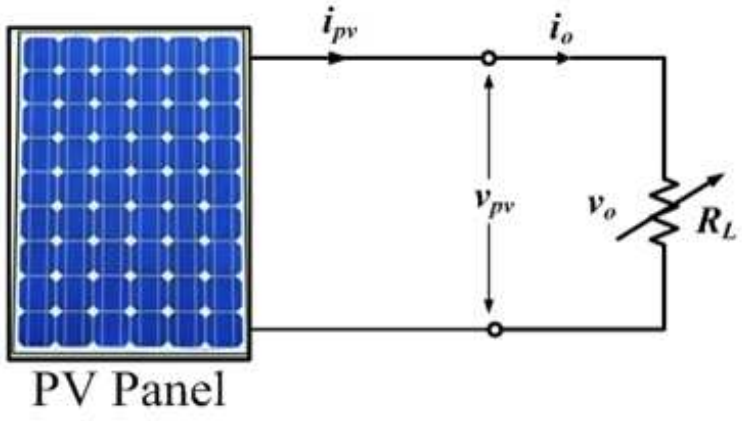

(a)

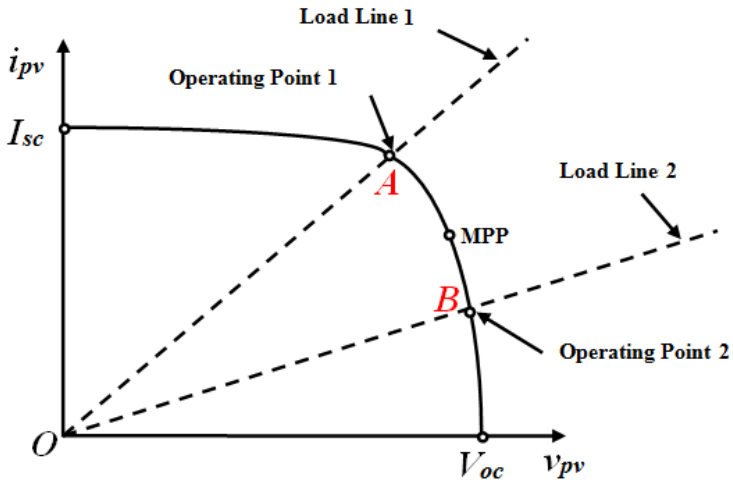

(b)

Figure 1.5: (a) PV panel with directly connected load and (b) Operating point of a PV system with direct coupled load

Therefore, a mechanism is to be devised to pull the operating point of the load to the MPP which is accomplished by a MPPT algorithm along with a DC/DC converter installed in between the PV panel and the load as shown in Fig.1.6. The MPPT algorithm calculates the reference operating point (V_{ref}) at which power is maximum and then the DC/DC converter forces the PV system to operate at that reference point.

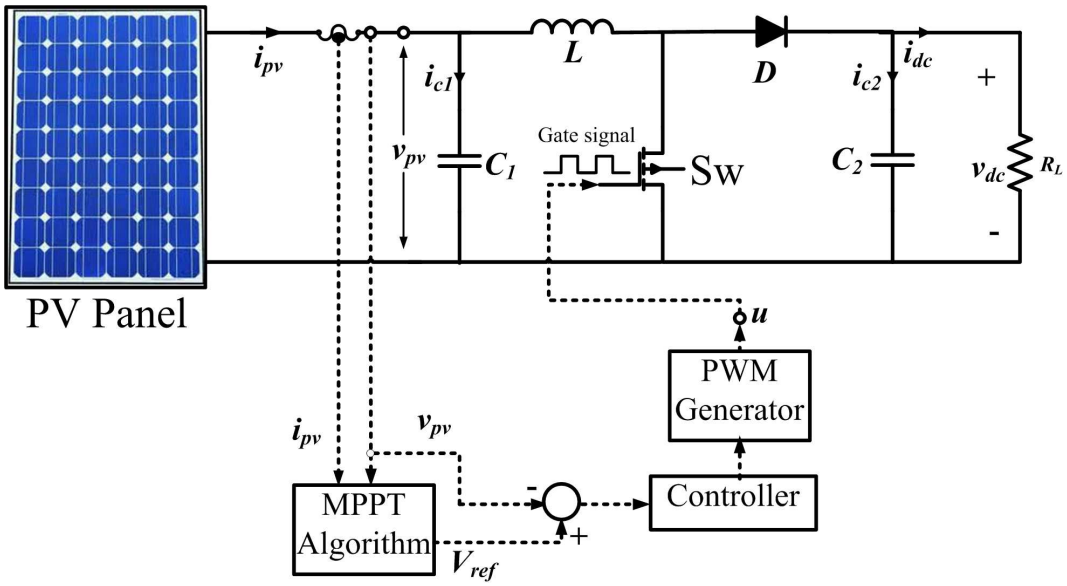

Figure 1.6: A Stand-alone PV system with MPPT

The MPPT system would be considered as an efficient system if it changes its operating point along with the MPP of the PV panel, ensuring the maximum power at all environmental conditions. MPPT tracks the maximum power of the PV panel at different environmental conditions [28, 29]. The solution of this MPP problem is actually very challenging as the MPP is not known a priori and MPP has non-linear dependencies with environmental conditions (Fig.1.7 and Fig.1.8). This point must be determined either by mathematical calculations using an accurate mathematical model of PV system or by using some search algorithms [30].

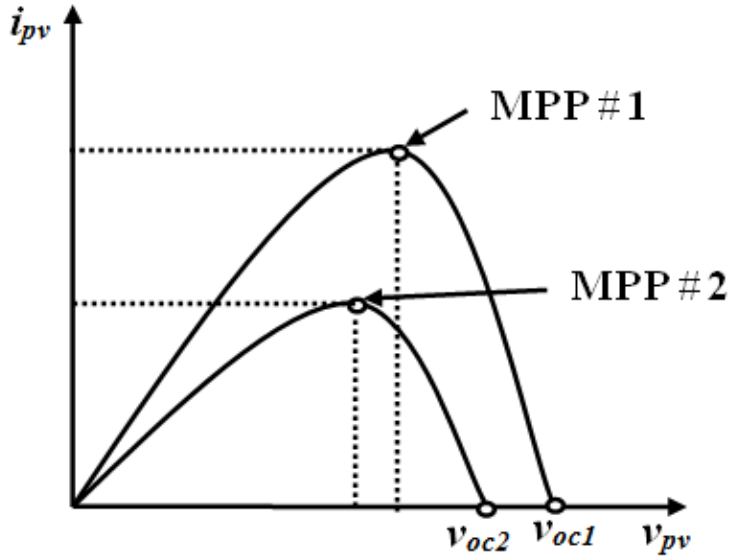

Figure 1.7: MPPTs of PV system at different irradiance under no shading condition

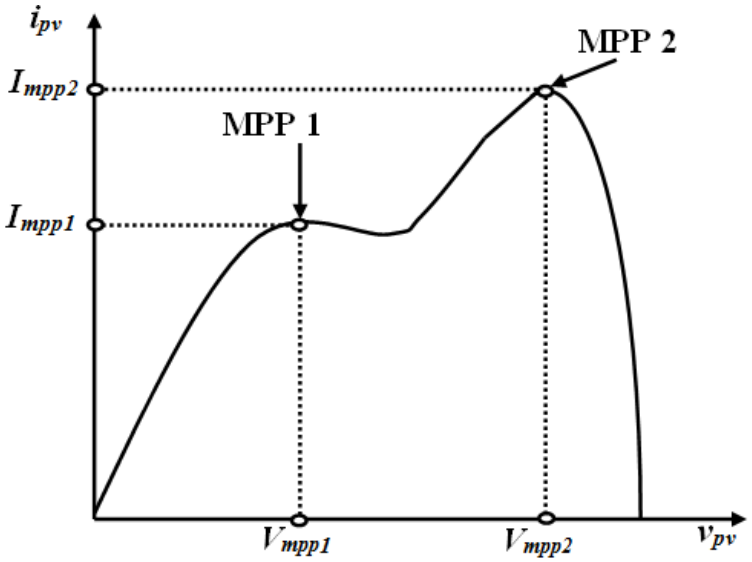

Figure 1.8: MPPTs of PV system at different solar irradiance under partial shading

1.1.7 MPPT Applications and Efficiency

Solar technologies are usually tested and validated by National Renewable Energy Laboratory. Though some other countries are venturing into the MPPT productions, but MPPTs are primarily manufactured in Germany, Japan, mainland China, Taiwan and USA. Some of the practical applications of MPPT techniques are in solar water pumping system, solar vehicles (car, flights), satellite power supply, off-grid and grid-tied power supply system, small electronics applications (mobile charging), etc. To get maximum profit from a grid-connected PV system, it requires knowledge about efficiencies of the PV modules and inverters. Three different efficiencies such as conversion efficiency, European efficiency, static and dynamic MPPT efficiencies are defined combined with their procedure of evaluation in [31]. Out of these efficiencies, the most important efficiency that need attention is the MPPT efficiency as it focuses on the amount of power drawn from the PV panel. The MPPT efficiency is calculated as follows in (1.1).

$$\eta_{mppt} = \frac{v_{pv} \times i_{pv}}{P_{mpp}} \tag{1.1}$$

This MPPT efficiency calculation can be applied to the stand-alone system as well. Static-MPPT efficiency means MPPT efficiency at constant weather conditions and dynamic-MPPT efficiency means MPPT efficiency at variable weather conditions. Researchers, users and commercial manufacturers of MPPT should test the developed MPPT system for the static and dynamic MPPT efficiencies. Using buck, boost and cuk converters, detailed efficiency comparison of INC and *P&O* MPPT techniques has been done in [32].

1.2 Literature Review on Parameter Extraction and MPPT Techniques of PV Panel

1.2.1 Literature Review on Parameter Extraction Methods

In the past, several extraction methods have been proposed as reported in literature. The extraction methods proposed during 1969 to 2012 have been reviewed and presented here. From an intensive literature survey of so far available parameter extraction methods so far, it is found that in general these methods can be classified into three categories such as analytic, iterative and evolutionary computational methods (Fig.1.9).

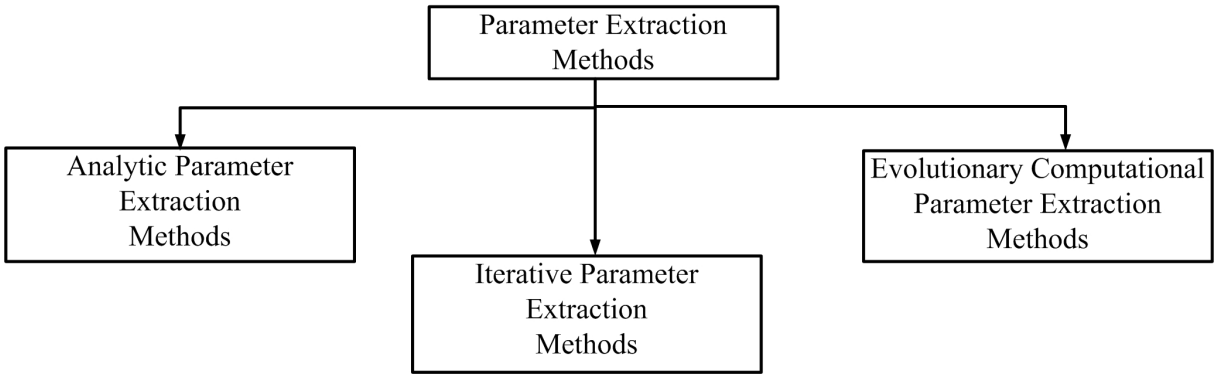

Figure 1.9: Classifications of Parameter Extraction Methods of the PV panel

An analytic parameter extraction method solve only explicit mathematical equations like $f(x) = k_1 x + k_2$ where x is the parameter to be extracted and k_1 and k_2 are constants [19]. Hence, these methods are usually preferred for dealing with ideal models (Fig.1.4 (a)) with the mathematical equation $v_{pv} = \left(\frac{n_s V_t}{n_p}\right) \times \left(\frac{I_{ph}+I_0-i_{pv}}{I_0}\right) - i_{pv}R_s$ and single-diode-four-parameter model (Fig.1.4 (b)) with the mathematical equation as $v_{pv} = \left(\frac{n_s V_t}{n_p}\right) \times \left(\frac{I_{ph}+I_0-i_{pv}}{I_0}\right)$ [38]. These mathematical models of the PV panel are represented by empirical relationships between voltage v_{pv} and current i_{pv}. The empirical relation between v_{pv} and i_{pv} can be determined by measuring v_{pv} and i_{pv} at different loads which is determined at standard testing condition (STC). Analytical methods of parameter extraction are very simple and need very less computational time as only a single iteration is required for this. [33] has proposed a simple analytical method. This method is constructed without considering the magnitude of R_{sh} hence applicable to four-parameter model only. Although this paper has suggested that the theoretical I-V characteristics derived by it exactly fit with that of the experimental characteristics with error less than 1% but, in this method, the magnitude of a is usually very large (> 50). If solar panel with such a p-n junction in which a considered is very large than, a large amount of energy would be lost due to recombination effects of the carriers and hence efficiency of the panel would be very small. Hence, this type of model is very uneconomical and hence not preferred. The commercial panels generally use crystalline materials in which diode-ideality factor varies from 1 to 2. Although these

analytical methods perform efficiently at STC for some models but these methods are found to be unsuitable for single-diode-five-parameter model Fig.1.4 (c) for wide range of changing the weather conditions [34]. Because, the mathematical model of PV panel represented is implicit in nature, hence it cannot be solved analytically.

Iterative methods are probably the best options for parameter extraction. A number of iterative methods are available in the literature. Some of them have been described next. From the above literature review on different iterative parameter extraction methods, it is observed that Newton-Raphson method (NRM) is one of the best root-finding methods. But improper choice of the initial conditions affects its accuracy and convergence. Hence, most of the previous parameter extraction works such as [35], [21], [36], [37], [38], [39], [40] and [41] are based on NRM.

But, in all these methods, five independent equations are necessary for extraction of the five unknown parameters such as I_{ph}, I_0, R_s, R_{sh} and a for a single-diode-five-parameter model. Computation of a Jacobian matrix is required in the NRM algorithm. This Jacobian matrix consists of twenty-five numbers of double-derivative terms $\frac{\partial^2 f(X)}{\partial X^2}$ in addition to same number of single derivative terms $\frac{\partial f(X)}{\partial X}$ where $X = [I_{pv}, I_0, a, R_s, R_{sh}]$ and *f(X)* is any five unique functions dependent on X. Due to this reason, NRM is usually very complex, lengthy and error prone. The jacobian matrix has been further simplified by Sera et al [42] for finding R_s, R_{sh} and a. Here, I_{ph} and I_0 are calculated solving two pre-defined equations that are dependent on R_s, R_{sh} and a.

Still, there is an inherent problem in all NRM methods [35]-[42] i.e. singularity problem which is division by zero (due to existence of zero value of second derivative term at some voltages and currents) may arise if initial conditions of the parameters (I_{ph}, I_0, R_s, R_{sh} and a) are chosen improperly. Also, these NRM methods have not considered the boundary limits of the parameters R_s, R_{sh} and a. A lot of assumptions are required in these methods in order simplify the five-parameter extraction problem which results in low value of R_s and high value of R_{sh} denoting the ideal conditions of PV module. Hence, the parameters so obtained by these NRMs are found to be incorrect.

The singularity problem is resolved in a parameter extraction method named as comprehensive parameter extraction method [43] of PV module where parameters (I_{ph}, I_0, R_s, R_{sh} and a) are calculated by varying each of these parameters in five dependent loops until the maximum power of PV module matches with the power at MPP. This method has guaranteed convergence. This parameter extraction method is simple and very accurate as very less numbers of assumptions are needed. But, this method consumes a lot of time as it involves computation in five loops consisting of many equations. It is also not reliable for weather conditions other than STC because power at MPP at STC is only known from manufacturer's data-sheet.

[44] proposed another comprehensive parameter extraction method where the five loop problem of [52] has been simplified to a single loop problem by assuming a as a constant and I_{ph} and I_0 are represented with equations that are dependent on R_s, R_{sh} and a. In this method, R_{sh} is calculated by increasing R_s until the maximum PV power becomes equal to MPP power. But, the accuracy of [44] approach depends on how smaller is the step size chosen and hence needs more numbers of iterations. It states that any initial value of a can be taken and adjusted later according to necessity. This introduces further delay in the process. Also, changing values of a might change the curvature of the I-V and P-V characteristics. This method is suitable to solve parameter extraction problem accurately at STC but may fail in other weather conditions, because it assumed values of R_s, R_{sh} and a independent of weather conditions and partial shedding conditions.

To resolve above issues, evolutionary computational algorithms can be used because these evolutionary algorithms are global optimization techniques [45]. In [46], performances of five such evolutionary computational approaches i.e. genetic algorithms (GA) method, mimetic algorithm method, particle swarm optimization (PSO) method, ant-colony optimization method and shuffled frog leaping method have been compared. It has remarked that PSO performs better than that of other four algorithms in terms of success rate and solution quality. This PSO based parameter extraction method is suitable in all types of conditions such as changing weather conditions and complete or partial shedding conditions.

PSO based parameter extraction method has been presented in [47] which considers inverse barrier constraints for R_s, R_{sh} and a. It obtains optimized values of parameters R_s, R_{sh} and a at any temperature condition. This method depends only on its objective function and it is not sensitive to initial condition and gradient information. These features of PSO make the algorithm computationally inexpensive, simple to implement and has low CPU and memory requirements. However, some experimental results show that although the global search ability of PSO is quite good but the local search ability around the optima is very poor [**?**]. This results in premature convergence in the calculation in case of existence of multiple optima in P-V curve of the PV panel because of shedding effect. This results in performance degradation hence PSO is inconsistence. Again PSO needs large number of iterations for finding solutions.

1.2.2 Remarks from Literature Review on Parameter Extraction Methods

From the discussions presented in section 1.3.1, the following observations can be made. These are

- All the existing parameter extraction methods can be broadly categorized into three groups such as analytic, iterative and evolutionary computational methods.

- Analytical methods of parameter extraction are very simple and need very less computational time as only a single iteration is required for this. But, they are applicable for only ideal PV model and single-diode-four-parameter PV model.
- Iterative methods like NRM is probably the best option for parameter extraction of single-diode-five-parameter PV model because of its accuracy and fast convergence nature provided the initial conditions are proper. But, NRM suffers from singularity problem.
- Comprehensive type iterative parameter extraction methods do not suffer from singularity problem. They are simple and have guaranteed convergence for solution. But, their accuracy and convergence time are dependent upon the step-size of the iterations.
- Analytic and iterative methods are suitable for local optimum points. Hence, they may fail in conditions like fast weather change and partial shedding where multiple local optimum points are available.
- Evolutionary computational parameter extraction methods such as PSO, GA are good in providing solution in fast varying weather conditions and partial shedding conditions. But, these methods suffer from the problem of premature convergence in presence of multiple local optimum points.

1.3 Review on Maximum Power Point Techniques

Referring [22], [48] and [49] the following acceptable MPPT techniques that applied on various PV applications such as space satellite, solar vehicles and solar water pumping etc.

1. Curve-Fitting (CF)Technique
2. Fractional Short-Circuit Current (FSCI) Technique
3. Fractional Open-Circuit Voltage (FOCV) Technique
4. Look-up Table (LUT) Technique
5. One-Cycle Control (OCC) Technique
6. Differentiation (Diffrn) Technique
7. Feedback Voltage (FV) or Current Technique
8. Feedback of Power Variation with Voltage (FPVV) Technique
9. Feedback of Power Variation with Current (FPVC) Technique
10. Perturbation and Observation (P&O) and Hill-Climbing Technique

11. Incremental Conductance (INC) Technique
12. Forced Oscillation (FO) Technique
13. Ripple Correlation Control (RCC) Technique
14. Current Sweep (CS) Technique
15. Estimated-Perturb-Perturb (EPP) Technique
16. Parasitic Capacitance (PC) Technique
17. Load Current/Load Voltage Maximization (LVM) Technique
18. DC Link Capacitor Droop Control (DLCDC) Technique
19. Linearization (Linr) Based MPPT Technique
20. Intelligence MPPT Techniques
    i. Fuzzy Logic (FLC) Based MPPT Technique
    ii. Artificial Neural Network (ANN) Based MPPT Technique
    iii. Particle Swarm Optimization Based MPPT (PSO-MPPT) Technique
21. Sliding-Mode Control (SMC) Based MPPT Technique
22. Gauss-Newton (G-N) Technique
23. Steepest-Descent (SD) Technique
24. Analytic (Analyt) Based MPPT Technique

It is very difficult to analyze all of these MPPT techniques by studying their individual structures, because each technique has its pros and cons. The MPPTs can only be analyzed by comparing of them considering classification, advantages, disadvantages, control strategy, control variables, circuitry, and applications. Classifications of the MPPT techniques have been attempted based on features, like, number of control variables involved, types of control strategies, circuitry, and applications.

1.3.1 Classification of Existing MPPTs

Classification according to Control Strategies

Control strategies can be of three types, such as indirect control (Indcntr), direct control and Evolutionary (Evolun) computational methods. Indirect control techniques are based on use of a database that includes parameters and data such as characteristics curves of the PV panel for different irradiance and temperature or on using some mathematical empirical formula to

estimate MPP Fig.1.10. Direct control strategies can seek MPP directly by taking account the variations of the PV panel operating points without any a priori knowledge of the PV panel parameters like R_s, R_{sh}, a, I_0 and I_{ph}. Direct Control strategies can be further classified into two types such as, sampling (Sampl) methods and modulation (Moduln) methods. In sampling methods, first a sample is made from PV panel voltage v_{pv} and current i_{pv} like power p_{pv}, $\frac{dp_{pv}}{dv_{pv}}$, $\frac{di_{pv}}{dv_{pv}}$ etc. and then gathering the past and present information of the sample, the location of the MPP is tracked. In modulation methods, MPP can be tracked by generating oscillations automatically by the feedback control. Evolutionary computational methods like, FLC and ANN etc methods do not need exact mathematical models, they can work with vague inputs and can handle nonlinearities and are adaptive in nature. These are rule based techniques which are very difficult to generate.

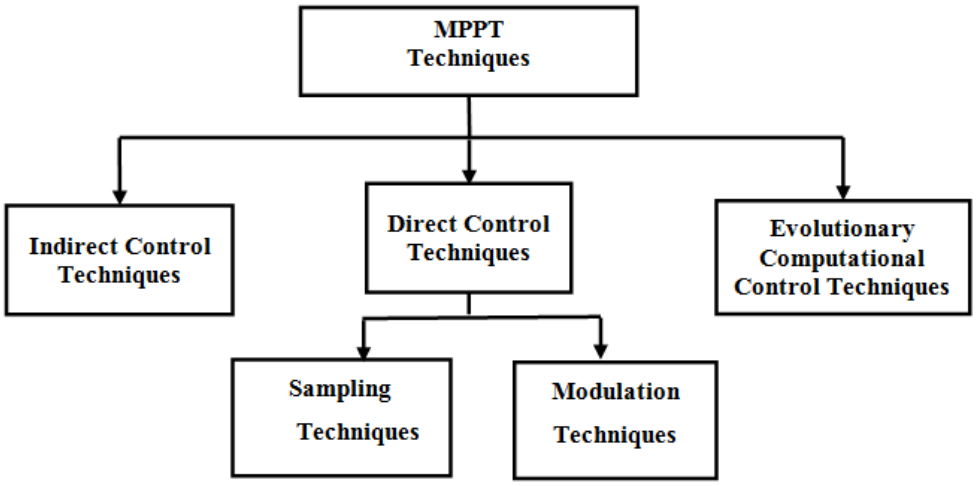

Figure 1.10: Classification according to control strategies

Two types of sampling (Sampl) techniques are adopted namely (a) Voltage-Feedback Control and (b) Power-Feedback Control. In voltage-feedback control, output voltage of the PV panel is used as the control variable. The MPPT control system keeps the operating point of the PV panel close to its maximum power point (MPP) by regulating the panel's output voltage until it matches to voltage at MPP. This technique has the following drawbacks.

- The effects of the irradiance and temperature of the solar array are neglected
- It cannot be widely applied to battery energy storage system

Therefore, this type of control method is only suitable for use at constant irradiance, such as in satellite system, because it cannot automatically track the maximum power point of the array when variations in irradiance and temperature occur. In power-feedback control, maximum power control is achieved by forcing the derivative $(\frac{dp_{pv}}{dv_{pv}})$ to be equal to zero under power feedback control. A common approach in power feedback control is measurement and

maximization of the power at the load terminal. This has an advantage that unnecessary knowledge of the solar array characteristics is not mandatory. But, the main drawback of this method is that it maximizes power to the load not power from the solar array.

Classification according to Number of Control Variables

Two different control variables are often chosen to achieve the maximum power control. According to the variables need to be sensed, MPPT techniques can be classified into two types, such as one-variable techniques and two-variable techniques (Fig.1.11). It is easier and inexpensive to implement voltage sensor whereas current sensor is bulky and expensive and hence implementation of current sensor is inconvenient in PV power systems.

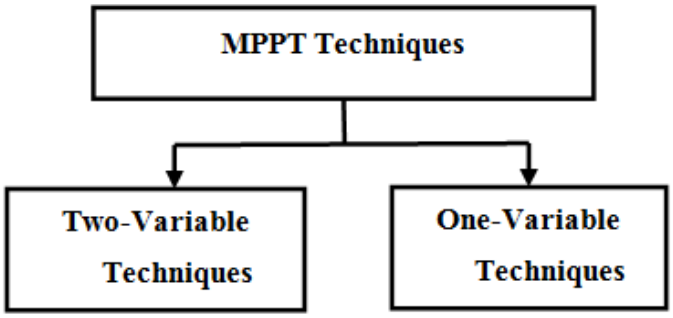

Figure 1.11: Classification according to number of control variables of PV panel

Classification according to Types of Circuitry

The circuitry involved in MPPT techniques are of two types such as analog circuit and digital circuit. Preference of MPPT techniques is also dependent upon the fact that some users are comfortable with analog techniques while others like the digital techniques. The MPPT techniques can be classified based on the type of circuitry used (Fig.1.12).

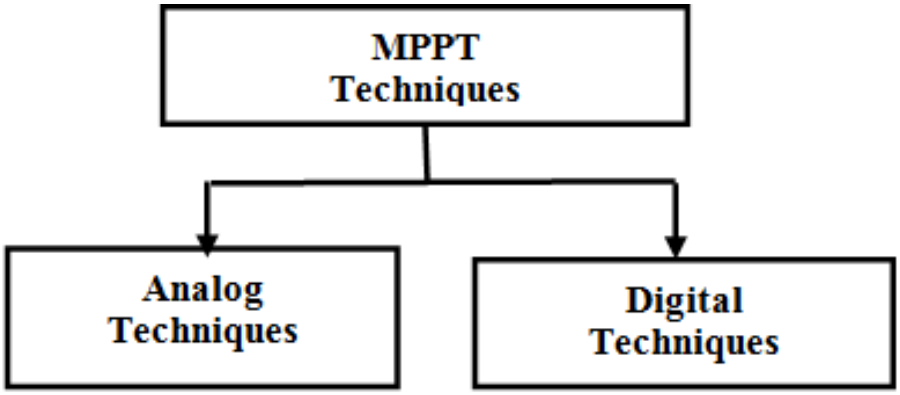

Figure 1.12: Classification according to number of control variables of PV panel

Classification according to Types of Application

MPPT techniques can be also classified based on the type of application of the PV power systems as shown in Fig.1.13. Some applications need accurate MPPT and cost not an issue, such as, satellite power system, solar vehicles, Industry and large scale residential premises. But, some systems like residential applications need simple and cheap MPPT technique. Expensive applications generally use advanced and complex circuitry because accuracy and fast response are main priorities there.

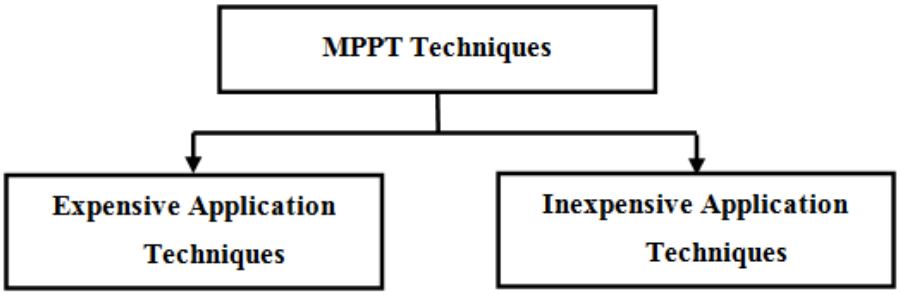

Figure 1.13: Classification according to types of applications

Analyzing the structure and behavior of all the discussed MPPT techniques, they can be categorized according to control strategy adopted, control variables chosen, circuitry used and applications intended for. Table 1.2 presents a comparison of different MPPT techniques according to the different category of classifications.

1.3.2 Advantage and Disadvantage of Different MPPT Techniques

Curve-Fitting Technique [43]

Advantages:

- Cost effective and simple because it does not require sensors for measurements of voltage and current during MPP tracking

Disadvantages:

- Not universal
- Needs a large memory capacity for its mathematical calculations
- Also requires accurate information regarding the PV system

Table 1.2: Comparison of Different MPPT Techniques

MPPT Technique	Control Strategy	Control Variable	Circuitry (A / D)	Necessity of parameter Tuning	Complexity of calculation and hardware implementation
CF	Ind-Contr	v_{pv}	D	Y	simple
FOCV	Ind-Contr	v_{pv}	both	Y	simple
FOCV	Ind-Contr	i_{pv}	both	Y	simple
LUT	Ind-Contr	v_{pv} and i_{pv}	D	Y	simple
OCC	Sampl	v_{pv} and i_{pv}	both	Y	simple
Diffrn	Sampl	v_{pv} and i_{pv}	both	Y	complex
FV	Sampl	v_{pv} and i_{pv}	D	N	simple
FPVV	Sampl	v_{pv} and i_{pv}	D	N	complex
FPVC	Sampl	v_{pv} and i_{pv}	D	N	medium
P&O	Sampl	v_{pv} and i_{pv}	both	N	complex
INC	Sampl	v_{pv} and i_{pv}	D	N	complex
FO	Moduln	v_{pv} or i_{pv}	A	Y	complex
RCC	Moduln	v_{pv} or i_{pv}	A	Y	complex
CS	Moduln	v_{pv} and i_{pv}	D	Y	complex
EPP	Moduln	v_{pv} and i_{pv}	both	N	complex
PC	Moduln	v_{pv} and i_{pv}	D	Y	Simple
LVM	Moduln	v_{pv}	A	N	Medium
DLCDC	Moduln	v_{pv}	both	Y	Simple
Linr	Moduln	Irradiance	D	Y	Medium
FLC	Evolun	v_{pv} or i_{pv}	D	Y	Medium
ANN	Evolun	v_{pv} or i_{pv}	D	Y	Medium
SMC	Evolun	v_{pv} or i_{pv}	D	N	Complex
G-N	Sampl	v_{pv} or i_{pv}	D	N	Medium
SD	Sampl	v_{pv} or i_{pv}	D	N	Medium
Analyt	Ind-Contr	v_{pv} or i_{pv}	both	Y	Medium
			A - Analog D - Digital	Y- yes N- no	

FOCV and FSCI Techniques [50]

Advantages:

- Simple and fast
- Elimination of dummy cells for reference calculation makes it more efficient, less expensive and no oscillations in steady state

Disadvantages:

- Calculated MPP is the approximate one and not the actual MPP
- frequently short-circuiting or open-circuiting at the load end add complexities in implementation and also power loss

- dependency on irradiations, temperature levels and degradation (aging, dirt) effects of panel

Look-up Table Technique [48]

Advantages:

- Simple and fast to implement

Disadvantages:

- Needs a large memory capacity for storing data
- the nonlinear and time-varying nature of solar cells and their dependency on irradiations, temperature levels and degradation i.e. dirt, aging, etc. effects, make it difficult to record MPPs and store them in all possible system conditions

OCC Technique [51]

Advantages:

- Constant switching frequency operating mode and its hardware implementation does not require any digital signal processors or multipliers
- With the adoption of a single-stage inverter, make the whole system inexpensive and reliable

Disadvantages:

- Even after the parametric optimization, it is not able to provide good MPPT performance under variable weather conditions

Differentiation Technique [52]

Advantages:

- Fast MPP tracking

Disadvantages:

- Fast MPP tracking
- Large numbers of terms are involved in MPP equation. Hence, very complex calculation

Feedback Voltage/Current Technique [53]

Advantages:

- Simple and inexpensive control system

Disadvantages:

- Cannot be used only in systems with battery as load
- it is unable to adapt to frequent environmental changing conditions

Feedback of Power Variation with Voltage and Current Technique [28]

Advantages:

- Very accurate as calculate MPP at zero value of derivative of PV power with respect to PV voltage

Disadvantages:

- The calculation and implementation of the derivative term that is derivative of PV power with respect to PV voltage is very difficult
- Hence the circuits involved in this technique are very complex

P&O and/or Hill Climbing Technique [54], [55] and [56]

Advantages:

- Accurate result
- Reliable and efficient technique
- Independent of the panel properties and characteristics

Disadvantages:

- Accuracy and required time are dependent on size of perturbation
- Not suitable for fast changing environmental conditions
- Output voltage and current signals of PV panel oscillate even at steady state

Incremental Conductance Technique [57]

Advantages:

- Efficiency same as P&O
- Good yield under rapidly changing atmospheric conditions

Disadvantages:

- Requires complex and costly control circuits
- Needs four sensors to accomplish its MPPT action
- Here also output voltage and current signals of PV panel oscillate even at steady state

Forced Oscillation Technique [58], [59]

Advantages:

- Adaptive in nature
- Accurate result for a wide range
- Easy to implement with cheap and easily available components

Disadvantages:

- Variable operating frequency and related complex filters
- Difficult to control

RCC Technique [60]

Advantages:

- No need of artificial perturbation as it is inherited by DC/DC converter
- Accurate result for a wide range

Disadvantages:

- Complex
- Time consuming technique

Current Sweep Technique [61], [62]

Advantages:

- Reference point is frequently updated in a fixed interval of time
- Accurate result if proportionality coefficients are properly chosen

Disadvantages:

- Not a generalized technique as proportionality coefficients depends on panel material and characteristics

EPP Technique [63]
Advantages:

- Tracking speed is faster and more accurate than that of P&O method
- Considers the nonlinear PV characteristic
- Accurate result also in wide irradiance-changing conditions

Disadvantages:

- Need three modes, such as two perturbs and in between one estimate mode, time consuming and complex

Parasitic Capacitance Technique [64]
Advantages:

- Considers effect of the solar cells parasitic junction capacitance and charge storage in the p-n junctions of the solar cells
- More compatible and close with the real PV panel

Disadvantages:

- More complex than Incremental Conductance technique

Load Current/Load Voltage Maximization Technique [65]
Advantages:

- No need of complex algorithm or calculation steps
- Easy to implement with a simple circuitry
- Pre-knowledge of panel characteristics not required

Disadvantages:

- Time taking tuning
- Power loss during tuning
- Limited range
- Not suitable to fast changing conditions

DC Link Capacitor Droop Control Technique [49]

Advantages:

- MPP calculation needs values of panel voltage
- DC-link voltage and power across inverter
- Pre-knowledge of panel characteristics not needed

Disadvantages:

- Needs a DC-link
- Limited applications
- restricted to only PV system that is connected in parallel with an AC system line

Linearization Technique [66]

Advantages:

- MPP estimated through a set of simple linear equations
- Easy calculation

Disadvantages:

- Calculated MPP is approximate one and hence usually differs greatly from the actual MPP
- Limited range of operating conditions

FLC Based MPPT Technique [67]

Advantages:

- Very good performance in terms of fast response, no overshoot and less steady state error
- Suitable for rapid temperature and irradiance variations
- Do not require pre-knowledge of the exact model of the PV panel

Disadvantages:

- Rules based technique
- Construction of rules are difficult

ANN Based MPPT Technique [68]

Advantages:

- Intelligent learning based technique
- No detail information about the PV system required
- On-line tracking is possible
- Accurate and fast once it is tuned
- Independent of environmental conditions

Disadvantages:

- Relation of MPP is calculated from a long observation on PV system
- Needs a great deal of time for tuning
- Obtained rules during MPP tracking process of a PV panel is not universal and he rules are limited to the same PV panel only

Sliding-Mode Based MPPT Technique [69]

Advantages:

- Simple MPP tracking and control laws
- Guaranteed stability
- Considers nonlinear behavior of PV panel and MPPT converter
- easy hardware implementation because it is compatible with a wide range of devices such as DSP, microcontroller, FPGA, etc.

Disadvantages:

- Required exact assessment of switching coefficients
- Chattering even at steady state
- Need good filters for variable frequency operation or necessity of extra circuitry to change variable operating frequency to fixed one

Gauss-Newton Technique [70]

Advantages:

- One of the fastest technique if initial conditions are properly chosen
- Accurate result
- Pre-knowledge of exact model of PV panel is not required

Disadvantages:

- Accuracy, speed and stability are dependent on initial conditions
- Complex calculation because need to calculate derivative and double derivative terms

Steepest Descent Technique [70]

Advantages:

- Fast MPPT performance
- Less complex than that of Gauss-Newton because double derivative terms not present in algorithm

Disadvantages:

- Accuracy, speed and stability are dependent on initial conditions and perturbation step-size
- For fixed step size range of operation is less and for variable step size algorithm is lengthy hence lead to complexity and inaccuracy while execution of the algorithm
- Slow convergence of error if Euler method is used for calculation of derivative terms

Analytic Based MPPT Technique [71]

Advantages:

- Simple heuristic strategy based on observations and experimental results
- Need information of panel voltage and current only, pre-knowledge of exact model
- Pre-knowledge of exact model not necessary

Disadvantages:

- Calculated MPP oscillates around the actual MPP
- The algorithm changes panel to panel hence one the developed algorithm is not valid for all panels

1.3.3 Hybrid MPPT (HMPPT) Techniques

P&O and Incremental Conductance techniques are the most extensively used MPPTs in commercially because of their straight forwardness, accuracy in MPP calculation and ease in implementation. Therefore, these two techniques are most often revised or extended [84]. But, the accuracy and tracking time of these techniques depend on perturbation size of the

control variable PV voltage or PV current or duty-ratio of converter. If this perturbation size is very small, then the accuracy is more but it needs more tracking time. On the other hand if the perturbation size is large it results in quick convergence but the accuracy in the MPP tracking is less. Again, these two algorithms are not intelligent enough to handle fluctuations in solar irradiance. For an example, these algorithms react to every change in solar irradiance like for momentarily change in irradiance like shadowing by cloud conditions also the algorithm reacts as if real changes in irradiation and varies the operating point. This quick variation in operating point gives more pressure on the DC/DC converter and eventually shortens its life. Hence, many kinds of modification have been introduced to the P&O technique. As both the panel characteristic and DC/DC converter are highly nonlinear and time-varying in nature, for their proper control some hybrid control techniques are essential [72].

In a recent proposed hybrid MPPT technique with both P&O and ANN, the perturbation step is continuously approximated by using ANN. It is an intelligent learning based technique and no detail information about the PV system required. Using this P&O-ANN hybrid MPPT [73], on-line MPP tracking is possible. It is accurate, fast and once tuned; it is independent of environmental conditions.
For strengthening searching capability of ANN based MPPT technique, its agents should be properly tuned. Considering this, genetic algorithm (GA) concept is used for tuning parameters of ANN algorithm. Similarly, a GA optimized fuzzy based MPPT is proposed by [74]. In this technique, membership functions and control rules are simultaneously found by GA.

Further, poor stability and power fluctuation due to the highly non-linear nature of the PV characteristics using simple P&O can be eliminated using Adaptive Neuro-Fuzzy inference system (ANFIS) is used in [75]. Once properly trained, this system can interpolate and extrapolate the MPP with high accuracy.

These techniques are developed considering a wide range of operating conditions. They are suitable for multi-array PV system also. Most of these techniques are a combination of two or more techniques hence more advanced and accurate and a priori knowledge of exact PV model is not necessary. But, it results in complex calculation for fast changing operating conditions and is difficult for implementation as control law changes with operating conditions.

1.3.4 MPPT Techniques for Mismatched Conditions

A PV plant comprises of number of arrays. Therefore, it may so happen that there may be different orientations of PV modules belonging to the same PV field. Further, there could be shadowing effects by clouds and bodies surrounding the plant. There could be manufac-

turing tolerances, non-uniformity of ambient temperature in proximity of each panel due to uneven solar irradiation and air circulation, dust and spot dirtiness (leaves, bird droppings). Mismatched conditions have strong impact on the shape of the P-V characteristics of the PV arrays and the energy productivity of mismatched strings can drop down to 20% of that of the not mismatched strings. In addition, in case of mismatch, the P-V characteristic of the PV field may have more than one peak. Hence, MPPT algorithms may fail causing a drastic drop in the overall system efficiency [30]. Therefore, some advanced MPPTs have been developed especially for these mismatched conditions such as

1. Distributed Maximum Power Point Tracking (DMPPT)
2. Multi-variable MPPT (MVMPPT)
3. Technique is based on the Equalization of the Output operating points in correspondence of the forced Displacement of the Input operating points (TEODI)

DMPPT

DMPPT [76] alleviates the above mismatched problems, because in DMPPT technique, each module uses a single MPPT. Five different distinct approaches in DMPPT are described in [76] as follows.

- MPPT with DC/DC converter outputs connected in strings to a central inverter
- MPPT with DC/DC converter outputs connected in parallel directly to the central
- String MPPT with DC/DC converter outputs connected in parallel to a central inverter
- MPPT with DC/AC module inverters
- String MPPT with DC/AC string inverters or a multi-input central inverter

An example of DMPPT is shown in Fig.1.14. In this figure, there are n-number of PV panels $PV_1, PV_2, ..., PV_n$ are connected in series. Instead of using a single MPPT for all PV panels, individual PV panel have their own MPPT. One centralized inverter has been connected to them as shown in the figure to converter total dc voltage $v_{dc} = v_1 + v_2 + ... + v_n$ to ac voltage v_{ac} . Since, individual PV panel have their MPPTs to harvest maximum possible power from that panel for the available solar irradiance to the panel, hence mismatched in solar irradiance to the PV panels can be handled. In other words, DMPPT ensures higher energy efficiency in presence of mismatching conditions than other MPPTs as shown in Table 1.1 and Table 1.2. Some of the commercial products that have used DMPPT are: Parallux (eIQ energy, San Jose, California), Powerbox (solar-edge technologies, UK), Solar Magic (National Semiconductor, America), Maximizer-ES and Maximizer-EP (Tigo Energy, California) and

Sun Mizer (Xandex, California).

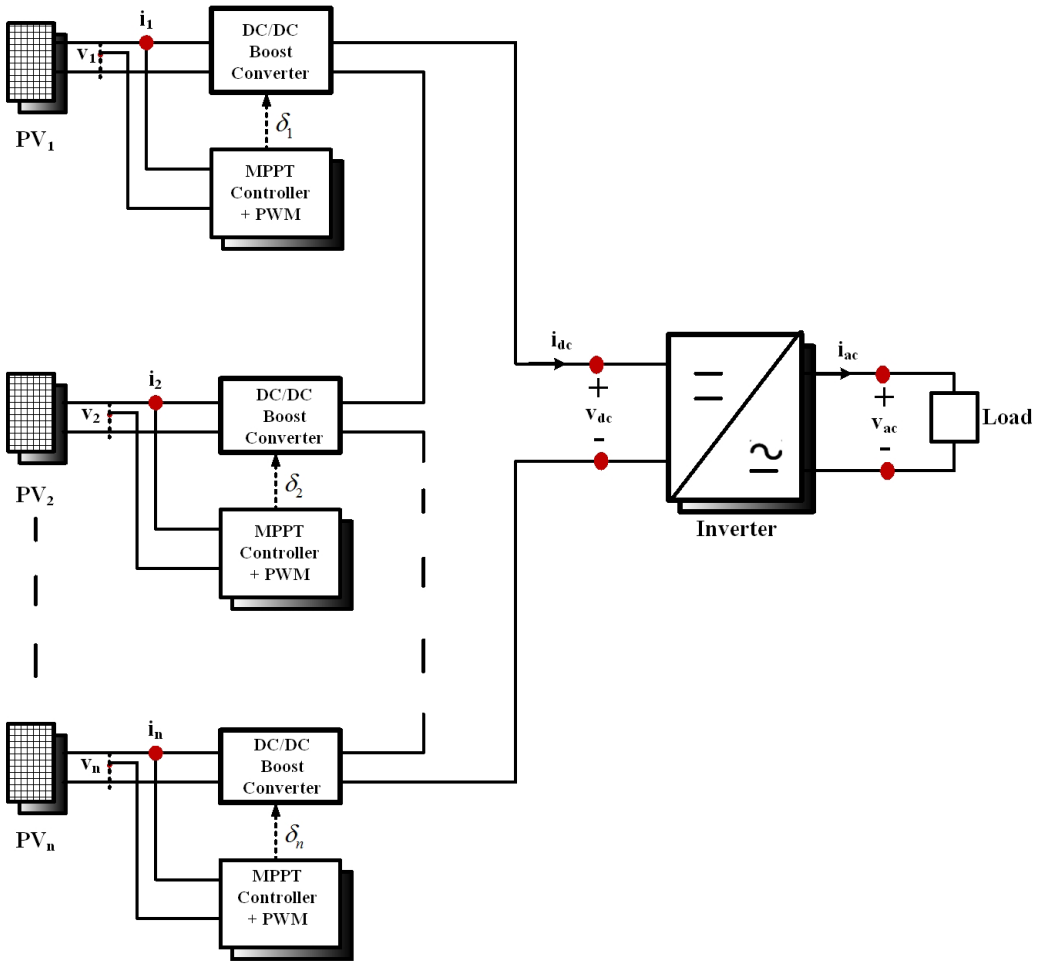

Figure 1.14: DMPPT in a PV array with n-number of PV panels connected in series

TEODEI

This MPPT technique is an advanced fully analog form of DMPPT. It does not require any data to be kept in memory. It is based on the equalization of the output operating points of two or more identical PV systems. An example of TEODI-MPPT [77] applied to two parallel connected PV panels is shown in Fig.1.15. Due to the parallel connection of the output ports of the two DC/DC boost converters, it is $v_{o1} = v_{o2} = v_{dc}$. Therefore, output currents of the converters are also same as shown in eq(1.2) and eq(1.3)

$$i_{o1} = i_{o2} \tag{1.2}$$

and

$$i_{dc} = i_{o1} + i_{o2} = 2i_{o1} = 2i_{o2} \tag{1.3}$$

The powers delivered from the two DC/DC boost converters should have the same value.

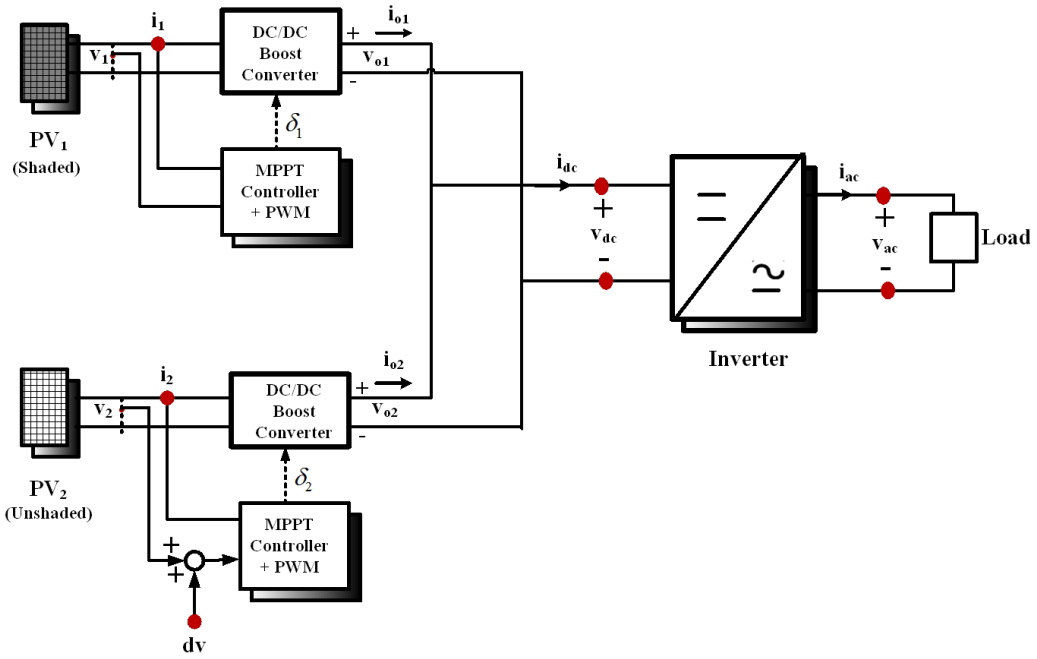

Figure 1.15: TEODI in a PV array with two PV panels connected in parallel

Assuming same efficiencies of the power stages of these two DC/DC converters, the power extracted by the two PV panels must have the same value. If first PV panel becomes shaded, then output voltage $v_{o1} < v_{o2}$. To maintain condition given by eq(1.4), the reference output voltage of second converter has been increased by dv.

$$v_{dc} = 2v_{o2} \tag{1.4}$$

where $dv = v_{o2} - v_{o1}$. Hence, the output currents of the two converters i_{o1} and i_{o2} remain equal to each other. Hence, total output power of the DC/DC boost converters remains equal to that of the expected MPP power. In TEODI-MPPT [77], each PV panels of a PV array has their own DC/DC converter but of the all the DC/DC converters are centralized controlled by a single control block.

MV-MPPT

An example of traditional P&O applied to two PV panels is shown in Fig.1.16(a) [78]. Here, two MPPT blocks with &O algorithm are required one for each PV panel. But, in case of MV-MPPT type MPPT control, only a single MV-MPPT block is sufficient for controlling both the PV panels as shown in Fig.1.16 (b). The control unit of this MV-MPPT takes current and gives the signal for the controlled switches of the DC/DC boost converters.

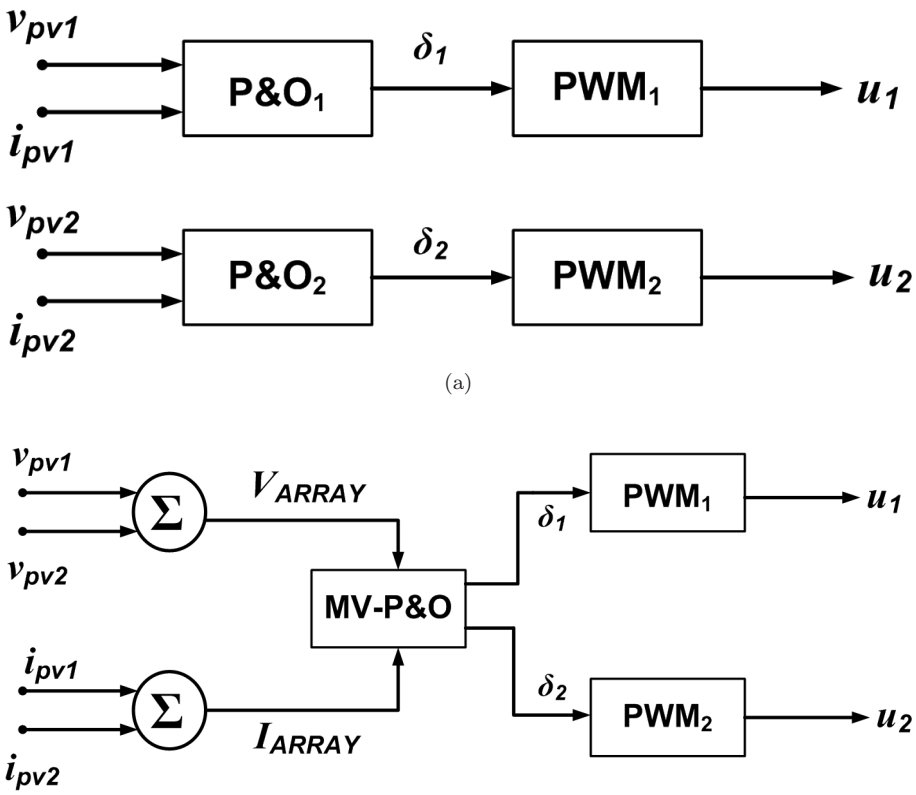

Figure 1.16: Comparison between (a) traditional P&O and (b) multi-variable P&O structures

As shown in Fig.1.16 (a), in P&O based MPPT technique, the number of required P&O blocks is equal to number of switching control variables (δ_1, δ_2) whereas as shown in Fig.1.16 (b), one block of MV-P&O is sufficient to generate multiple control variables. In MV-P&O number control stages are reduced compared to that of P&O. Hence, power loss in the whole MPPT system is reduced considerably maximizing the PV power at the output of the converter.

1.3.5 Remarks from Literature Review on MPPT

From the discussions presented in section 1.3, the following observations are highlighted here. mismatched

- MPPT is one of the integral components of a PV system.
- MPPT consists of one MPPT algorithm that estimates the MPP and another control mechanism that forces the operating point of PV system to a line on the calculated MPP.
- Many MPPTs are available which may be having direct or indirect MPPT algorithms.

- MPPTs are applied to PV system either with a DC/DC converter or an inverter according to the types of applications.
- It is very difficult to suggest any MPPT as best for a user by the researcher because each MPPT has its individual merits and demerits. Hence, it is better to let the user select MPPT according to the requirements.
- MPPT algorithms are available that can tackle conditions like fast weather changes and partial shedding where multiple local MPPs are available.
- A well designed controller i.e. an adaptive controller is necessary for increasing efficiency of the MPPT.

1.4 Motivation the Thesis

The motivations of the thesis are as follows.

- No matter whatever may be the topology of a PV system for example, grid-connected, stand-alone or hybrid, a well-developed model of a PV panel is necessary for its simulation studies.
- For successful design and analysis of a PV system necessitates an accurate mathematical model of its PV panel. A number of models of the PV panel are available such as ideal model, single-diode-four-parameter model, single-diode-five-parameter model and double-diode model. These models are represented through appropriate parameters of the PV panel. Accurate mathematical model must be developed to study and characterize the transient responses of a PV system. However, the development of such mathematical model is not a straightforward task because this involves accurate extraction of parameters of a PV panel. Therefore, it is necessary to extract the aforesaid parameters of the PV panel.
- From literature review, it is found that analytical parameter extraction algorithms are based on empirical relationship between v_{pv} and i_{pv} and iterative algorithms require a lot of time to converge. These two techniques work efficiently in STC but may not be efficient and accurate in weather conditions other than STC. NRM algorithms suffer from singularity problem. All these discussed algorithms assume R_s, R_{sh} and a to be constant with changing weather conditions. But, in actual case like I_{ph} and I_0, parameters R_s, R_{sh} and a too changes with weather conditions [94]. There are no boundary limits of the parameters demarcated in any of the above algorithms. Also, they are not applicable to shedding conditions where multiple maxima occur in the P-V characteristics of PV panels. Although PSO algorithm resolve above problems, but it

suffers from premature convergence fast changing weather conditions. Therefore, new parameter extraction algorithms need to be developed to extract parameters accurately in full solar irradiance, shedding condition and in fast changing weather conditions. The new parameter extraction algorithms should consider upper and lower boundary limits of the parameters of PV panel. They should not suffer from singularity and premature convergence problems.

- PV panels have low energy conversion efficiency. Further, efficiency can be increased only if a PV panel can be operated at its MPP. In other words, a PV panel is utilized fully only when it operates at its MPP.
- A MPPT is operated using a buck or boost DC/DC converter. A DC/DC converter performs adjustment of the operating point of PV system such that transferring maximum power from the PV panel to the load. The simplest way of implementing an MPPT is to operate a PV panel under constant voltage and power reference to modify the duty cycle of the DC/DC converter.
- For operating a PV panel at MPP, it is necessary to calculate the MPP using a suitable tracking algorithm. This algorithm must be efficient enough to calculate MPP of the PV panel by reading samples of PV voltage and current. This MPPT algorithm needs to be designed to handle changing environmental conditions such as temperature and solar radiation. Reported MPPT algorithms in literature have a number of shortcoming like high tracking error, fluctuation around the actual MPP depending on the perturbation size, in efficiency to cope to the changing weather conditions, singularity problem and slow response problems etc. Therefore, there is need of developing new MPPT algorithms considering the above discussed problems.
- To further improve efficiency of a PV system, a controller needs to be included in the MPPT of a PV system for maximum utilization of the available solar power in fast and wide range of changing environmental conditions. So far, main emphasis has given on design on MPPT algorithms and in most papers only PI or PID-controllers with fixed gains are employed. But, it is found that even if the MPPT algorithm is efficient but a well-tuned controller is necessary to accomplish the MPP adjustment in fast and wide range of changing environmental conditions. Therefore, MPPTs with properly tuned controllers are required.

1.5 Objective of the Thesis

- To review the reported parameter extraction algorithm for modeling of a PV panel.
- To propose efficient algorithms in terms of fast convergence and accuracy for extraction of parameters of a PV panel.
- To develop a mathematical model of a PV panel having obtained parameters by the proposed parameter extraction algorithms.
- To evaluate efficiency of the proposed parameter extraction algorithms through both simulated and experimental results.
- To review on the reported approaches to MPPT design.
- To propose new MPPT algorithms such that the accuracy in tracking reference voltage can be achieved in less time.
- To propose new adaptive controllers for MPPT considering the uncertainties of the PV system dynamics due to changing solar irradiance at different weather conditions.
- To simulate the proposed MPPT algorithms in MATLB/SIMULINK and real-time simulation model in OPAL-RT simulator.
- To develop a prototype of a PV control set-up and implement the proposed MPPT algorithms in hard-ware set-up.
- To evaluate the efficacy of the proposed MPPT algorithms.

1.6 Thesis Organization

The thesis consists of eight chapters that are organized as follows.

CHAPTER 1 presents a comprehensive review on different approaches to mathematical modeling of a PV panel reported together with different parameter extraction techniques. Subsequently, the chapter also reviews available maximum power control techniques. This chapter has presented broad categorization of some of the selected the existing parameter extraction methods into three groups such as analytic, iterative and evolutionary computational techniques. Further, merits and demerits of these categories and scope of developing new parameter extraction techniques are also discussed. Similarly, literatures on some of the distinct available MPPTs have been collected and analyzed with respect to their merits, demerits, applications etc. Then necessity of designing new direct MPPTs in increasing efficiency of the MPPT is suggested.

CHAPTER 2 proposed a new iterative technique called hybrid Newton-Raphson Method (NRM) and another new heuristic technique called Bacterial Foraging Optimization (BFO)

based parameter extraction technique for the PV panel. This hybrid NRM does not suffer from singularity problem during convergence process like Newton-Raphson techniques of parameter extraction but is found to have faster convergence and more accurate than that of Newton-Raphson techniques and existing comprehensive parameter extraction technique. But, this hybrid NRM shares one common feature with that of existing Newton-Raphson and comprehensive parameter extraction technique such as dependency of its speed of convergence on initial conditions of the unknown PV panel parameters. Therefore, it is found to be not ideal for fast changing weather conditions and partial shedding conditions. In the other proposed BFO based parameter extraction technique, unknown PV panel parameters are heuristically chosen. Like hybrid NRM, it does not suffer from singularity problem during convergence process but unlike hybrid NRM, it can efficiently works in both fast changing weather conditions and partial shedding conditions.

CHAPTER 3 proposed a new auto-tuned adaptive MPPT technique called Auto-tuned-adaptive-MPPT (ATAMPPT) for maximum power control of PV systems. The ATAMPPT technique can estimate the MPPs of a PV system on-line using a recursive-least-square (RLS) based system identifier and a NRM algorithm. Its effectiveness is verified compared with three existing MPPTs such as perturb and observe (P&O), Incremental-conductance (INC) and adaptive perturb and observe (APO) presenting simulation results in MATLAB/SIMULINK, real-time simulation results in OPAL-RT and experimental results using a 0.2kW prototype set-up.

CHAPTER 4 proposed a new adaptive predictive error filter controller based MPPT (APEFC-MPPT). This MPPT uses an adaptive predictive FIR filter in which filter weight is updated using a RLS method with variable forgetting factor. The APEFC-MPPT consists of a new MPPT algorithm and an adaptive proportional-integral-derivative-controller (PID-controller). This MPPT is capable of both tracking and filtering operations. Testing with simulation, real-time simulation and experimental results, it is found that MPP tracking with this APEFC-MPPT possesses both faster response and lesser steady-state error than that of ATAMPPT.

CHAPTER 5 presented two Double integral sliding mode controller MPPTs (DISMC-MPPTs). These two DISMC-MPPTs have been constructed with new sliding surfaces. The PWM mechanism adds advantages such as simple control structure and fixed frequency operation to these two DISMC-MPPTs. In the first DISMC-MPPT, controller coefficients are considered fixed whilst in the adaptive DISMC-MPPT, controller coefficients are updating with changing weather conditions. The DISMC-MPPT is constructed following procedure suggested by Slotine-Lee [79]. With simulation and real-time simulation results, the MPP tracking capability of this DISMC-MPPT is verified to be better than that of Integral sliding mode controller MPPT (ISMC-MPPT) and Sliding mode controller MPPT (SMC-MPPT).

In case of the proposed adaptive DISMC-MPPT, the sliding mode control coefficients are selected taking account the reaching and stability conditions and hence it facilitates with fast response and guaranteed stability. This proposed adaptive DISMC-MPPT is verified to possess better tracking behavior such as tracking time, steady-state error and chattering as compared to DISMC-MPPT, Tan's DISMC-MPPT and Jiao's DISMC-MPPT.

CHAPTER 6 presents a new self-tuned-MPPT with an Incremental-PID-controller (IPID-controller), RLS identifier and Incremental Generalized minimum variance (IGMV) control law for maximum power control problem. This MPPT is found to be better than that of self-tuned-MPPT with Generalized-Minimum-Variance (GMV) control law and self-tuned-MPPT with pole-placement control law. The effectiveness of the proposed controller is validated with simulation, real-time simulation and experimental results. Comparing with tracking performances of MPPTs such as ATAMPPT, APEFC-MPPT and adaptive DISMC-MPPT, it is seen that overall efficiency of this self-tuned MPPT is more.

CHAPTER 7 describes the concluding remarks and suggestions for some future research problems as extensions of the work described in the thesis.

Chapter 2

Hybrid NRM & BFO Parameter Extraction Algorithms for Photovoltaic Panels

2.1 Introduction

From the literature survey pursued on parameter extraction methods provided in chapter 1, it is found that Newton-Raphson based methods (NRMs) are fast and accurate provided the initial conditions are chosen appropriately. Hence, most of the previous parameter extraction methods have exploited NRMs. But, in these methods, five independent equations are required for extraction of the five unknown parameters such as I_{ph}, I_0, a, R_s and R_{sh} for example, NRM applied by [21]. This method is very complex, lengthy and error prone due to the involvement of single and double derivative terms. Subsequently, the algorithm length and complexity of NRM algorithm has been simplified in [42]. Here, instead of extracting the five parameters the problem was simplified by modifying it to a three parameter extraction problem using standard assumptions. As a result, fast convergence is achieved and the method becomes less complex, but it suffers from singularity problem.

As discussed earlier in Chapter 1, in NRM algorithm unknown parameter $X = [I_{ph}, I_0, a, R_s, R_{sh}]$ are extracted by solving the five unique equations $\frac{\partial F(X)}{\partial X} = 0$. If the initial points of X are not properly chosen, then it is found that some the elements of its Jacobian matrix $\frac{\partial F^2(X)}{\partial X^2}$ become zero before reaching $\frac{\partial F(X)}{\partial X} = 0$. Hence, there is a possibility of premature convergence or no convergence condition. This problem is called singularity problem as encountered in NRM. In order to resolve this singularity problem, a comprehensive method which is a direct iterative three parameter extraction method for solving $X = [a, R_s, R_{sh}]$ [44]. Therefore, it does not require Jacobian matrix so that singularity problem can be avoided. This method has a guarantee of solutions and very less numbers of assumptions have been taken. But, the accuracy of this approach depends on how small is the step size chosen and hence needs more numbers of iterations. It states that any initial value of a can

be chosen and can be adjusted if needed later. This introduces further delay in the process. Also, changing value of a might change the curvature of the I-V and P-V characteristics.

Considering all the above problems, a new parameter extraction method is proposed in this chapter that is based on both NRM and comprehensive method. This method is developed for single-diode-five-parameter model of PV panel (Fig.3.3). This method uses comprehensive iterative method to calculate parameter a whereas a simplified two parameter NRM is used to estimate parameters R_s and R_{sh}. Rest two parameters I_{ph} and I_0 are calculated by some pre-defined equations that are dependent on the values of a, R_s and R_{sh}.

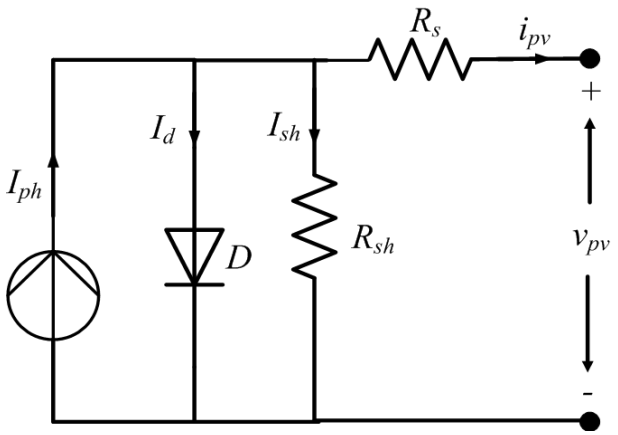

Figure 2.1: Single-diode-five- parameter Model of a PV module

2.2 Parameter Extraction Problem Formulation

The output current i_{pv} of a single-diode five-parameter model (Fig.3.3) is given by

$$\begin{aligned} i_{pv} &= I_{ph} - I_d - I_{sh} \\ \Rightarrow i_{pv} &= I_{ph} - I_0 \left[\exp\left(\frac{n_p v_{pv} + i_{pv} R_s}{n_s V_t}\right) - 1\right] - \frac{n_p v_{pv} + i_{pv} R_s}{R_{sh}} \end{aligned} \tag{2.1}$$

where n_s and n_p denote the number of series cells and parallel cells in the pv panel respectively. V_t is the thermal generated voltage, k_b denotes the Boltzman's constant, T is the PV panel temperature and q is the charge of an electron. In case, there presents only series cells in the pv panel, then n_p=1.
In this condition, eq (2.1) can be written as eq (2.2).

$$\begin{aligned} i_{pv} &= I_{ph} - I_d - I_{sh} \\ \Rightarrow i_{pv} &= I_{ph} - I_0 \left[\exp\left(\frac{n_p v_{pv} + i_{pv} R_s}{n_s V_t}\right) - 1\right] - \frac{n_p v_{pv} + i_{pv} R_s}{R_{sh}} \end{aligned} \tag{2.2}$$

An accurate knowledge of PV panel parameters is important for the design, control of solar cells and for estimation of their performance. the accuracy of these parameters is accepted

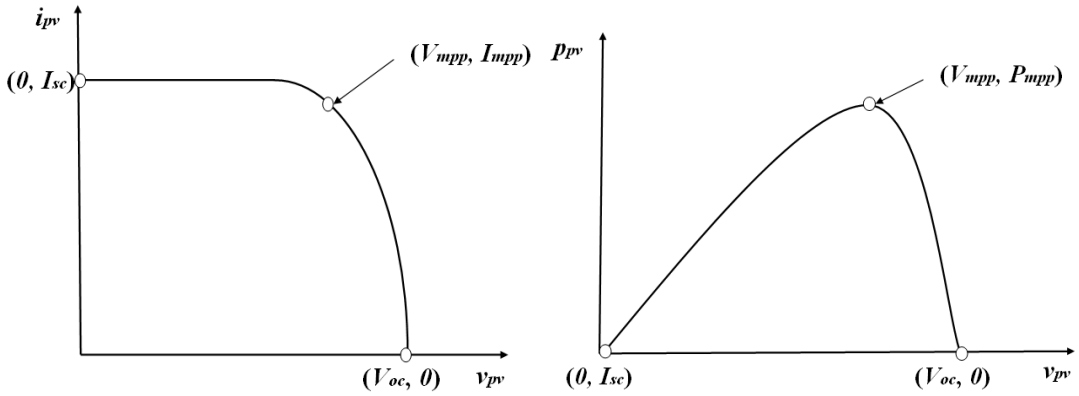

Figure 2.2: I-V characteristics, (b) I-V characteristics of a PV panel

if I-V and P-V curve constructed using these parameters match with that of curves shown in Fig.2.2.

It may be noted that only one implicit equation eq (2.1) is available to solve the five parameter extraction problem of the single-diode-five-parameter model of PV panel. In addition to that, information regarding values of I_{mpp}, V_{mpp}, V_{oc} and I_{sc} at standard testing condition is available in the Manufacturer's data-sheet. But, five independent equations are required to calculate the unknown parameters I_{ph}, I_0, a, R_s and R_{sh} using NRM. It is required to initialize the unknown parameters properly for avoiding singularity problem. In order to reduce time and error in calculation, the parameter extraction problem needs to be simplified. But in view of simplification of the problem, more number of assumptions will jeopardise the accuracy. Keeping these facts into consideration, a new parameter extraction method is proposed in this chapter which is described in the subsequent sections.

2.3 Proposed Hybrid Newton-Raphson based Parameter Extraction Method

The proposed parameter extraction method is a Newton-Raphson based method with some modifications. In this method, the complex five-degree NRM parameter extraction problem for solving $X = [I_{ph}, I_0, a, R_s, R_{sh}]$ has been simplified to a two-degree NRM parameter extraction problem for solving $X = [R_s, R_{sh}]$. The value of parameter a varies between 1 and 2. Hence, a can be solved easily and quickly by normal iterative method instead of increasing complexity of the NRM by adding an extra degree. Also, I_{ph} and I_0 can be converted to functions that are dependent on a, R_s and R_{sh}, so that only two of the parameters R_s and R_{sh} are needed to be solved by NRM. Hence, the five parameter extraction problem is simplified to a two parameter extraction problem to be solved by NRM. It is defined as hybrid Newton-Raphson method (hybrid NRM).

2.3.1 Description of the Proposed Hybrid Newton-Raphson Method

Accuracy and time requirement of NRM is strongly dependent on the initial points of tracking, hence it is very essential to consider proper initial conditions of the unknown variables R_s and R_{sh} whilst solving them using NRM.

$$\begin{aligned} R_s &= R_{s,min} \\ R_{sh} &= R_{sh,min} \end{aligned} \tag{2.3}$$

At first the unknown parameters are initialized using eq (2.3). For accurate and fast evaluation of parameters R_s and R_{sh}, the value $R_{s,min}$ and $R_{sh,min}$ need to be properly selected. In literature, many sets of initial conditions for R_s and R_{sh} have been defined. The most accepted set of initial conditions is shown in eq (2.4) where $\frac{dv_{pv}}{di_{pv}}\Big|_{o.c.}$ and $\frac{dv_{pv}}{di_{pv}}\Big|_{s.c.}$ can be calculated from the I-V characteristic curve of the PV panel.

$$\begin{aligned} R_{s,min} &= -\frac{dv_{pv}}{di_{pv}}\bigg|_{o.c.} \\ R_{sh,min} &= -\frac{dv_{pv}}{di_{pv}}\bigg|_{s.c.} \end{aligned} \tag{2.4}$$

This method of initial condition evaluation is very difficult if the I-V characteristic is not known beforehand. Another set of initial conditions of $X = [R_s,\, R_{sh}]$ as shown in eq (2.5) has been suggested by [3].

$$\begin{aligned} R_{s,min} &= 0 \\ R_{sh,min} &= \frac{V_{mpp}}{I_{sc} - I_{mpp}} - \frac{V_{oc} - V_{mpp}}{I_{mpp}} \end{aligned} \tag{2.5}$$

But unfortunately, no convincing logic behind the construction of eq (2.5) has been defined in [3]. Considering these problems, a set of initial conditions for R_s and R_{sh} has been suggested in this section. As the magnitude of R_s is very less, hence its initial value $R_{s,min}$ can be taken as zero.

$$\left(\frac{\partial v_{pv}}{\partial i_{pv}}\right)\bigg|_{\substack{i_{pv} = I_{sc} \\ v_{pv} = 0}} = \frac{1 + A_1 - A_2}{-B_1 - B_2} \tag{2.6}$$

where

$$\begin{aligned} A_1 &= \frac{\left(I_{sc}R_{sh,min} - V_{oc} + I_{sc}R_{s,min}\right) e^{\frac{I_{sc}R_{s,min} - V_{oc}}{N_s V_t}}}{N_s V_t R_{sh,min}} \\ A_2 &= \frac{R_{s,min}}{R_{sh,min}} \\ B_1 &= \frac{\left(I_{sc}R_{sh,min} - V_{oc} + I_{sc}R_{s,min}\right) e^{\frac{I_{sc}R_{s,min} - V_{oc}}{N_s V_t}}}{N_s V_t R_{sh,min}} \\ B_2 &= \frac{1}{R_{sh,min}} \end{aligned} \tag{2.7}$$

Applying the initial value of $R_{s,min}$ calculated from eq (2.5) in eq (2.6), $R_{sh,min}$ is rewritten as follows.

$$\begin{aligned} R_{se,min} &= 0 \\ R_{sh,min} &= \frac{N_s V_t - I_{sc}}{N_s V_t + I_{sc} exp\left(\frac{I_{sc}R_{s,min} - V_{oc}}{N_s V_t}\right)} \end{aligned} \tag{2.8}$$

Then I_{ph} and I_0 can be represented in terms of R_s and R_{sh} and a as follows.
At open circuit condition $((i_{pv} = 0, v_{pv} = V_{oc}))$,

$$0 = I_{ph,stc} - I_{0,stc} e^{\frac{V_{oc}}{N_s V_t}} - \frac{V_{oc}}{R_{sh}} \tag{2.9}$$

At MPP $((i_{pv} = I_{mpp}, v_{pv} = V_{mpp}))$,

$$i_{pv}|_{mpp} = I_{ph,stc} - I_{0,stc} e^{\frac{V_{mpp} + I_{mpp}R_s}{N_s V_t}} - \frac{V_{mpp} + I_{mpp}R_s}{R_{sh}} \tag{2.10}$$

At short circuit condition $((i_{pv} = I_{sc}, v_{pv} = 0))$,

$$I_{sc} = I_{ph,stc} - I_{0,stc} e^{\frac{I_{sc}R_s}{N_s V_t}} - \frac{I_{sc}R_s}{R_{sh}} \tag{2.11}$$

Analyzing eq (2.9) and eq (2.10); $I_{ph,stc}$ and $I_{0,stc}$ can be obtained using eq (2.12) and eq (2.13).

$$I_{ph,stc} = I_{0,stc} e^{\frac{V_{oc}}{N_s V_t}} - \frac{V_{oc}}{R_{sh}} \tag{2.12}$$

$$I_{0,stc} = \frac{I_{sc} - \frac{V_{oc} - I_{sc} R_s}{R_{sh}}}{e^{\frac{V_{oc}}{N_s V_t}} - e^{\frac{I_{sc} R_s}{N_s V_t}}} \tag{2.13}$$

The second exponential term in eq (2.13) is very small thus negligible in comparison to that of the first term and hence one obtains

$$I_{0,stc} = \left[I_{sc} - \frac{V_{oc} - I_{sc}R_s}{R_{sh}}\right] e^{-\frac{V_{oc}}{N_s V_t}} \tag{2.14}$$

It is necessary to select two independent equations to be used in Newton-Raphson method for the evaluation of parameters R_s and R_{sh}. Eq (2.17) and eq (**??**) are those two independent equations. These are derived as follows.

The PV output power is given by

$$p_{pv} = v_{pv} i_{pv} \tag{2.15}$$

At MPP, the PV output power becomes

$$P_{mpp} = V_{mpp}\, i_{pv}|_{mpp} \tag{2.16}$$

Applying value of $i_{pv}|_{mpp}$ from eq (2.10) in eq (2.16), P_{mpp} is derived as

$$P_{mpp} = V_{mpp}\left[I_{ph,stc} - I_{0,stc} e^{\frac{V_{mpp} + I_{mpp}R_s}{N_s V_t}} - \frac{V_{mpp} + I_{mpp}R_s}{R_{sh}}\right] \tag{2.17}$$

Again at MPP, the derivative of PV output power with its output voltage can be written as

$$\frac{\partial p_{pv}}{\partial v_{pv}} = i_{pv}|_{mpp} + V_{mpp}\left(\frac{\partial i_{pv}}{\partial v_{pv}}\right)\Bigg|_{\substack{i_{pv}=I_{mpp}\\ V=V_{mpp}}} = 0 \tag{2.18}$$

where

$$\left(\frac{\partial i_{pv}}{\partial v_{pv}}\right)\Bigg|_{\substack{i_{pv}=I_{mpp}\\ V=V_{mpp}}} = \frac{-\frac{(I_{sc}R_{sh}-V_{oc}+I_{sc}R_s)e^{\frac{V_{mpp}+I_{mpp}R_s-V_{oc}}{N_sV_t}}}{N_sV_tR_{sh}} - \frac{1}{R_{sh}}}{1+\frac{(I_{sc}R_{sh}-V_{oc}+I_{sc}R_s)e^{\frac{V_{mpp}+I_{mpp}R_s-V_{oc}}{N_sV_t}}}{N_sV_tR_{sh}} - \frac{R_s}{R_{sh}}} \tag{2.19}$$

I-V and P-V characteristics of a PV panel are very sensitive to the accurate combinations of its parameters $[I_{ph}, I_0, a, R_s, R_{sh}]$. This fact has been given special priority while designing the proposed parameter extraction method. Again for different PV-models, the range of effective values of a are different. In this method, a is incremented gradually from 1 to 2 and for each value of a, eq (2.17) and eq (**??**) are solved using NRM. During this procedure it is observed that for all values of a, feasible solutions is not possible. Only a small range between 1 and 2 gives feasible solution. That particular range of value of a is selected and the mean of these value of a is selected as the final value for a. Again, using this value of a, the magnitude of parameters R_s and R_{sh} are extracted solving eq (2.17) and eq (**??**). Then, $I_{ph,stc}$ and $I_{0,stc}$ are calculated using eq (2.12) and eq (2.14). This method gives flexibility or choice to designer for parameter selection because of the availability of the more than one set of solutions. In this method, it is assumed that the values of R_s, R_s and a remain fixed for a panel and does not change with environmental conditions. Only I_{ph} and I_0 vary with environmental conditions and these can be calculated using eq (2.20) and eq (2.21).

$$I_{ph} = G_c\frac{[I_{pv,stc} + K_I\,(T_c - 298)]}{1000} \tag{2.20}$$

$$I_0 = \frac{I_{sc} + K_I\,(T_c - 298)}{exp\left(\frac{V_{oc}+K_v(T_c-298)}{aV_t}\right) - 1} \tag{2.21}$$

The proposed hybrid NRM based parameter extraction method is presented in Table 2.1. The efficacy of the proposed hybrid NRM based parameter extraction method is verified by comparing with that of two other methods, such as conventional Method 1 [42] and Method 2 [44].

2.3.2 Results and Discussions

For comparison of the proposed hybrid NRM parameter extraction algorithm with that existing algorithms such as NRM and comprehensive algorithms, each one of set of the two initial conditions are taken one at a time for all these three parameter extraction algorithms using the SSI-M6-205 PV panel model. The Manufacturer's data-sheet of SSI-M6-205 PV panel is in Table 2.2.

Table 2.1: Proposed Hybrid NRM Algorithm

Steps to calculate parameter *a*
i. Parameter a is incremented gradullay from 1 to 2. ii. For each value of a, eq (2.17) and (2.18) are solved using NRM iii. The mean value of a is determined finally
Steps to calculate parameter R_s and R_{sh}
i. R_s and R_{sh} are extracted by solving equation eq (2.17) and (2.18) using NRM
Steps to calculate parameter I_{ph} and I_0
i. $I_{ph,stc}$ and $I_{0,stc}$ are calculated solving eq (2.12) and eq (2.13) respectively ii. I_{ph} and I_0 are calculated solving eq (2.20) and eq (2.21) respectively

Table 2.2: Manufacturer's data-sheet Parameters of PV Panels

	Mono-Crystalline	**Mono-Crystalline**	**Poly-Crystalline**	**Thin-Film**
Parameters	**Shell SQ85**	**PM648**	**SSI-M6-205**	**Shell ST40**
I_{sc} (A)	5.45	2.8	7.91	2.68
V_{oc} (V)	22.2	21.6	35.55	23.3
I_{mpp} (A)	4.95	2.2	7.31	2.41
V_{mpp} (V)	17.2	18.2	28.04	16.6
K_I(V/^{0}C)	-0.0725	-0.076	-0.036	-0.1
K_V(A/^{0}C)	0.0008	0.002	0.0006	0.00035
K_P(%/^{0}C)	-0.0043	-0.0045	-0.004	-0.006
n_s	36	36	60	36

The feasible values of the five unknown parameters $[I_{ph}, I_0, a, R_s, R_{sh}]$ of SSI-M6-205 PV panel are shown in Table 2.3 and Table 2.4 considering two different sets of initial conditions shown in eq (2.4) and eq (2.5) respectively. In Table 2.3, the bold terms such as 1.203, 0.3944, 471.4416, 3.77×10^{-8} and 7.9034 are the calculated values of parameters I_{ph}, I_0, a, R_s and R_{sh} respectively for initial conditions given in eq (2.4). Similarly, in Table 2.4, the bold terms such as 1.16, 0.4083, 831.8043, 1.852×10^8 and 7.9061 are the calculated values of parameters I_{ph}, I_0, a, R_s and R_{sh} respectively for initial conditions given in eq (2.5). As per the algorithm described in Table 2.1, the value of a such as 1.203 is the mean of other values of a for initial condition given by eq (2.4) and 1.16 is the mean of other values of a for initial condition given by eq (2.5) respectively. The values 0.3944, 471.4416, 3.77×10^{-8} and 7.9034 for parameters I_{ph}, I_0, a, R_s and R_{sh} respectively are calculated using $a = 1.203$. Similarly, the values 0.3944, 471.4416, 3.77×10^{-8} and 7.9034 for parameters I_{ph}, I_0, a, R_s and R_{sh} respectively have been calculated using $a = 1.16$.

To decide which initial condition is the appropriate one among initial conditions given by eq (2.4) and eq (2.5), a comparison of the performance of the proposed hybrid NRM method with that of Method 1 [42] and Method 2 [44] has been made. For this, first initial condition

given by eq (2.4) has been taken in all cases and the parameters are extracted. Then, the parameters are extracted considering the initial condition given by eq (2.5) for all the above three methods. The results of the extracted parameters are shown in Table 2.5 for initial conditions of eq (2.4) and eq (2.5) respectively.

Referring Table 2.5 and Table 2.6, it can be observed that

- Absolute error for parameter extraction is less in case of proposed hybrid NRM for both the initial conditions than that of Method 1 and Method 2.
- Method 1 takes less time than that of Method 2 and hybrid NRM. But, if parameters are observed then it can be seen that Method 1 is close to ideal condition with high value of R_{sh} (negligible I_{sh}) which is strongly undesirable. Between Method 2 and hybrid NRM, time taken by the hybrid NRM is less than Method 2. Hence, performance of the proposed method is better than that of Method 1 and Method 2.
- Comparing initial conditions given by eq (2.4) with the proposed initial condition given by eq (2.5), the results obtained using the proposed one are more accurate as both the absolute error of maximum power (%) and time consumption is lesser than that of the other initial condition.
- The proposed set of initial conditions of unknown parameters I_{ph}, I_0, a, R_s and R_{sh} suits the hybrid NRM.

Fig.2.3 and Fig.2.4 show the comparison of I-V and P-V characteristics of SSI-M6-205 PV panel with parameters obtained from proposed hybrid NRM with that of Method 1 and Method 2 at STC respectively. Therefore, to extract parameters of PV panel of prototype PV system, the proposed initial condition has been considered. The prototype PV system consists of five PM648 PV panels connected in series. This PM648 PV panel is mono-crystalline one. The simulated performances like estimated I-V and P-V characteristics of the studied PV panel have been compared with that of its experimentally evaluated one [80]. The experiment has been conducted using the PM648 PV panel on 27th May 2011 at 12 noon. The temperature and solar irradiance at that time has been recorded as 42.6 W/m^2

Table 2.3: Comparison of Extracted Parameters of SSI-M6-205 Solar Panel at STC by proposed hybrid NRM With initial conditions given in eq (2.4)(Tolerance of Peak Power = 10^{-8})

a	P_{max} (W)	R_s Ω	R_{sh} Ω	I_0 (A)	I_{pv} (A)	iterations
1.202	204.9724	0.394762	476.2545	3.71×10^{-8}	7.903444	17
1.203	204.9724	0.394444	471.4416	3.77×10^{-8}	7.903382	15
1.204	204.9724	0.394125	466.7238	3.38×10^{-8}	7.90332	18
1.203	**204.9724**	**0.3944**	**471.4416**	3.77×10^{-08}	**7.9034**	**15**

Table 2.4: Comparison of Extracted Parameters of SSI-M6-205 Solar Panel at STC by proposed hybrid NRM With initial conditions given in eq (2.5))(Tolerance of Peak Power = 10^{-8})

a	P_{max}	R_s	R_{sh}	I_0	I_{pv}	iterations
1.11	204.972399	0.424834	7095.645406	7.57×10^{-6}	7.909526	19
1.12	204.972398	0.421492	2836.321975	9.11×10^{-8}	7.908825	18
1.13	204.972399	0.418168	1771.433796	1.093×10^{-8}	7.908133	18
1.14	204.972395	0.414863	1287.387281	1.307×10^{-8}	7.907451	17
1.15	204.972396	0.411575	1010.784203	1.558×10^{-8}	7.906779	17
1.16	204.972398	0.408305	831.804299	1.852×10^{-8}	7.906117	17
1.17	204.972399	0.405053	706.51716	2.195×10^{-8}	7.905465	17
1.18	204.972389	0.401818	613.913056	2.594×10^{-8}	7.904823	16
1.19	204.97239	0.398601	542.6776	3.056×10^{-8}	7.90419	16
1.2	204.972392	0.3954	486.179906	3.592×10^{-8}	7.903567	16
1.21	204.9724	0.392217	440.275206	4.21×10^{-8}	7.902953	19
1.22	204.972399	0.424834	7095.645406	4.921×10^{-8}	7.909526	19
1.16	**204.9724**	**0.4083**	**831.8043**	1.852×10^{-8}	**7.9061**	**17**

Table 2.5: Comparison of Extracted Parameters of SSI-M6-205 Solar Panel at STC by different methods With initial conditions given in eq (2.4)

Parameters	Method 1 [42]	Method 2 [44]	Proposed Hybrid NRM
a	1.1034	1.3	1.203
I_0 (A)	6.68×10^{-9}	1.57×10^{-7}	3.77×10^{-8}
I_{ph} (A)	7.91	7.9146	7.9034
R_s (Ω)	0.427	0.2944	0.3944
R_{sh} (Ω)	4.58E+09	504.7124	471.4416
Time Taken (s)	2.94669	14.12139	3.89045
Absolute error maximum power (%)	4.863×10^{-4}	1.88×10^{-4}	8.7734×10^{-8}

and 47^0C respectively. The magnitudes of V_{oc}, I_{sc}, V_{mpp} and I_{mpp} along with the extracted values of the five unknown parameters I_{ph}, I_0, a, R_s and R_{sh} of the studied PV panel have been shown in Table 2.7.

2.3.3 Remarks on the Proposed Hybrid NRM Parameter Extraction Method

Advantages

- This method is simple and fast as the complex five-parameter-extraction-problem of NRM is simplified to two-parameter-extraction-problem of NRM.
- In this method, value of a is calculated from a range of values between 1 and 2 that give feasible solution. Hence, the singularity problem is not present in this method.

Table 2.6: Comparison of Extracted Parameters of SSI-M6-205 Solar Panel at STC by different methods With initial conditions given in eq (2.5)

Parameters	Method 1 [42]	Method 2 [44]	Proposed Hybrid NRM
a	1.1056	1.3	1.16
I_0 (A)	6.9629×10^{-9}	1.5742×10^{-7}	1.8519×10^{-8}
I_{ph} (A)	7.91	7.9146	7.9061
R_s (Ω)	0.4263	0.2944	0.4083
R_{sh} (Ω)	2.8544×10^{9}	504.7124	831.8043
Time Taken (s)	2.119657	8.34453	3.184309
Absolute error maximum power (%)	4.863×10^{-4}	3.8672×10^{-4}	6.063×10^{-8}

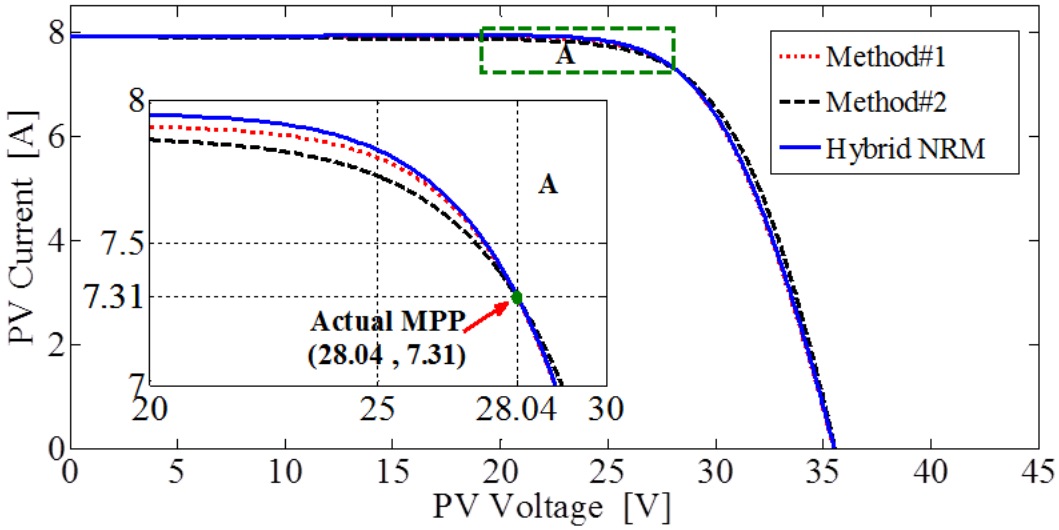

Figure 2.3: Comparison of derived I-V Characteristics of SSI-M6-205 PV panel using extracted parameters of proposed hybrid NRM with that of Method 1 and Method 2

Disadvantages

- It is dependent upon the initial conditions of the parameters to be extracted.
- Except the values of parameters I_{ph} and I_0, other parameters a, R_s and R_{sh} are assumed to be independent of weather conditions. But physically, values of R_s, R_{sh} and a also vary with weather conditions [29].
- This method is not applicable to PV panels with partial shading conditions.

From the above discussions, it is clear that the parameter extraction problem of a nonlinear PV model is implicit in nature and it is very difficult to solve accurately using traditional algorithms i.e. NRM. But, it is found that evolutionary algorithms are capable of accurate optimization in solution even where traditional algorithms fail [81]. Hence, evolutionary computational approaches can be used to solve the nonlinear implicit parameter extraction

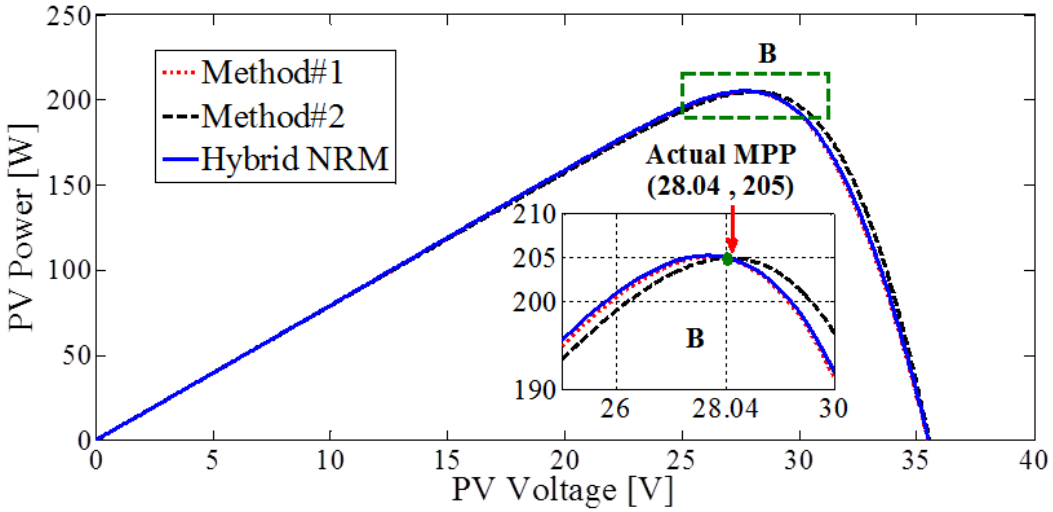

Figure 2.4: Comparison of derived P-V Characteristics of SSI-M6-205 solar panel using extracted parameters of proposed hybrid NRM with that of Method 1 and Method 2

Table 2.7: Measured and Extracted Parameters of PM648 PV Panel using Proposed Hybrid NRM on 27TH MAY 2011 AT 12 NOON

Measured Data	**Value**
V_{mpp} (V)	11.7
V_{oc} (V)	17.4
I_{mpp} (A)	0.675
P_{mpp} (W)	7.897492
Extracted Parameters	**Value**
R_s (Ω)	4.26193
R_{sh} (Ω)	96.709946
a	1.26
I_0(A)	2.76×10^{-7}
I_{ph}(A)	0.887459

problem. PSO is one of the best evolutionary global optimization technique. A PSO based parameter extraction method which considers inverse barrier constraints for R_s, R_{sh} and a. It obtains optimized values of parameters R_s, R_{sh} and a at any temperature condition. This method depends only on its objective function and sensitive to neither the initial condition nor the gradient information. This quality makes the algorithm computationally inexpensive, simple to implement and has low CPU and memory requirements. However, some experimental results show that PSO based parameter extraction method has following short-comings.

- Although the global search ability of PSO is quite good but the local search ability around the optima is very poor.
- Premature convergence in the fast weather changing conditions.

- Premature convergence in the in case of existence of multiple optima in P-V curve of the PV panel because of shedding effect.
- This results in performance degradation hence PSO is inconsistence.
- It needs large number of iterations for finding solutions.

Recently, another heuristic optimization technique called BFO has been widely used due to its optimization performance better than that of PSO in many problems. Hence, in this work an attempt has been made to exploit BFO for parameter extraction problem of PV panels. Hence, a BFO based parameter extraction method is developed which is discussed in the following section.

2.4 Proposed BFO based Parameter Extraction Method

Survival of species in any natural evolutionary process depends upon their fitness criteria, which relies upon their food searching (foraging) and motile behavior. BFO rests on a simple principle of the foraging (food searching) behavior of E.Coli bacterium in human intestine. There are mainly four stages in a BFO optimized process such as chemotactic, swarming, reproduction and elimination and dispersal. In chemotactic stage, bacterium can move in a predefined direction or change their directions of motion. In swarming, each bacterium provides a signal to other bacterium to move together. In reproduction, healthiest bacterium split into two and less healthy bacterium die. In elimination and dispersal phase, a sudden unforeseen event occurs. That may drastically alter the smooth process of evolution and cause the elimination of the set of bacteria and disperse them to a new environment. This unknown event may place a newer set of bacteria nearer to the food location.

2.4.1 Description of the BFO based Parameter Extraction Method

At solar irradiance G and temperature T, the output current of a PV module is given by

$$i_{pv} = I_{ph}(G,T) - I_0(G,T)\left[\exp\left(\frac{v_{pv} + i_{pv}R_s(G,T)}{n_s V_t(G,T)}\right) - 1\right] - \frac{v_{pv} + i_{pv}R_s(G,T)}{R_{sh}(G,T)} \quad (2.22)$$

Eq (2.9) and eq (2.11) can be rewritten as eq (2.22) for the value of open-circuit voltage V_{oc}, short-circuit current I_{sc} at any solar irradiance G and temperature T.

$$\begin{aligned} V_{oc}(G,T) &= R_{sh}(G,T)\left[I_{ph}(G,T) - I_0(G,T)\left\{\exp\left(\frac{v_{pv} + i_{pv}R_s(G,T)}{n_s V_t(G,T)}\right) - 1\right\}\right] \\ I_{sc}(G,T) &= \left(I_{ph}(G,T) - I_0(G,T)\left(\exp\left(\frac{v_{pv} + i_{pv}R_s(G,T)}{n_s V_t(G,T)}\right) - 1\right)\right) \\ &\quad \times \left(\frac{R_{sh}(G,T)}{R_s(G,T) + R_{sh}(G,T)}\right) \end{aligned} \quad (2.23)$$

Similarly, from eq (2.10) and eq (2.16), PV current and power at MPP under any solar irradiance G and temperature T can be re-derived as,

$$\begin{aligned} I_{mpp}(G,T) &= I_{ph}(G,T) - I_0(G,T)\exp\left(\frac{V_{mpp}(G,T)+I_{mpp}(G,T)R_s(G,T)}{n_s V_t(G,T)}\right) \\ &\quad - \frac{V_{mpp}(G,T)+I_{mpp}(G,T)R_s(G,T)}{R_{sh}(G,T)} \\ P_{mpp}(G,T) &= V_{mpp}(G,T)\times I_{mpp}(G,T) \end{aligned} \tag{2.24}$$

At a given solar irradiance G and temperature T, reference value of the short-circuit current $I_{sc}(G,T)$, open-circuit voltage $V_{oc}(G,T)$ and power at MPP, $P_{mpp}(G,T)$ can be calculated as follows [2-3, 7].

$$\begin{aligned} {I_{sc}}^*(G,T) &= \frac{G}{G_{STC}}\left[I_{sc}(STC)+K_I(T-T_{STC})\right] \\ {V_{oc}}^*(G,T) &= \left[V_{oc}(STC)+K_V(T-T_{STC})\right] \\ {P_{mpp}}^*(G,T) &= \frac{G}{G_{STC}}\left[P_{mpp}(STC)+K_P(T-T_{STC})\right] \end{aligned} \tag{2.25}$$

where ${I_{sc}}^*$(STC), ${V_{oc}}^*$(STC) and ${P_{mpp}}^*$(STC) are the reference values of the short-circuit current, open-circuit voltage and MPP power at STC respectively. G_{STC} and T_{STC} are the solar irradiance of 1000 W/m^2 and temperature of 298 ^{0}K at STC respectively. K_I, K_V and K_P are the temperature coefficients at short-circuit current, open-circuit voltage and MPP respectively. All of the above six parameters (${I_{sc}}^*$(STC), ${V_{oc}}^*$(STC), ${P_{mpp}}^*$(STC), K_I, K_V and K_P) are provided by manufacturer.

2.4.2 Formulation of the Parameter Extraction Problem

The parameters I_{ph}, I_0, R_s, R_{sh} and a of a PV module are dependent on G and T. At any G and T, the I_{ph} and I_0 can be calculated as follows.

$$\begin{aligned} I_0(G,T) &= \frac{I_{sc}(G,T)+K_I(T-T_{STC})}{\exp\left(\frac{V_{oc}(G,T)+K_V(T-T_{STC})}{n_s V_t(G,T)}\right)-1} \\ I_{ph}(G,T) &= \frac{G}{G_{STC}}\left\{I_{sc}\left[\frac{R_s(G,T)+R_{sh}(G,T)}{R_{sh}(G,T)}\right]+K_I(T-T_{STC})\right\} \end{aligned} \tag{2.26}$$

For any G and T, the values of I_{sc}, V_{oc} and P_{mpp} can be calculated from PV module model given by eq 2.23 and eq 2.24. I_{sc}, V_{oc} and P_{mpp} can be represented in terms of R_s, R_{sh} and a. The reference values of short-circuit current ((I_{sc}*), open-circuit voltage (V_{oc}*) and MPP power (P_{mpp}*) can be calculated analytically using eq 2.25 respectively. Difference between $\begin{bmatrix} I_{sc} & V_{oc} & P_{mpp} \end{bmatrix}^T$ and $\begin{bmatrix} I_{sc}^* & V_{oc}^* & P_{mpp}^* \end{bmatrix}^T$ are the short-circuit current, open-circuit voltage and MPP power errors respectively. The short-circuit current error (e_{sc}), open-circuit voltage error (e_{oc}) and MPP power error (e_{mpp}) need to be minimized by employing BFO algorithm

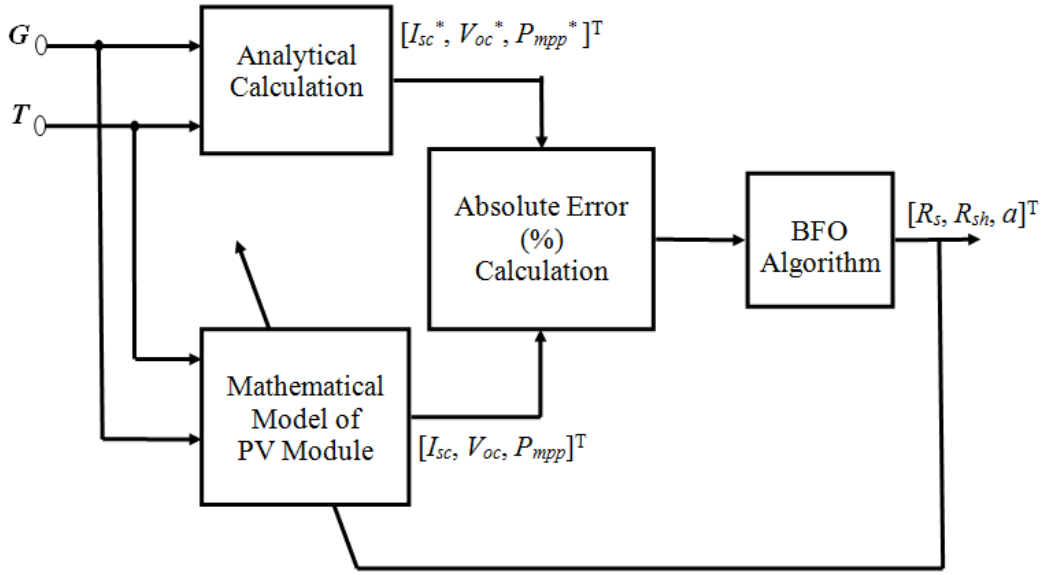

Figure 2.5: Comparison of Extracted Parameters of SSI-M6-205 PV Model using different Methods at -25^{0}C to 75^{0}C

formulating a suitable fitness function. The fitness function for this parameter extraction problem can be defined as

$$\min_{R_s,R_{sh},a,G,T} e_{fit} = e_{sc} + e_{oc} + e_{mpp} \tag{2.27}$$

where e_{sc}, e_{oc} and e_{mpp} are the absolute percentage of short-circuit current error, open-circuit voltage error and MPP power error respectively.

$$\begin{aligned} e_{sc} &= \left| \frac{I_{sc}(G,T) - {I_{sc}}^*(G,T)}{{I_{sc}}^*(G,T)} \right| \times 100 \\ e_{oc} &= \left| \frac{V_{oc}(G,T) - {V_{oc}}^*(G,T)}{{V_{oc}}^*(G,T)} \right| \times 100 \\ e_{mpp} &= \left| \frac{P_{mpp}(G,T) - {P_{mpp}}^*(G,T)}{{P_{mpp}}^*(G,T)} \right| \times 100 \end{aligned} \tag{2.28}$$

The structure of the proposed BFO based parameter extraction method is shown in Fig.2.5. The proposed parameter extraction method consists of a BFO-Parameter Extraction algorithm (Table 2.8). The following terms are used in this algorithm.

i = sample count

l = elimination-dispersal loop count

m = reproduction-dispersal loop count

n = chemo tactic loop count

$Samp$ = total number of samples

p_{opt}= number of parameters to be optimized

N_{sl} = swimming length

N_{ci} = number of chemotactic iterations

N_{re} = maximum number of reproduction steps
N_{ed} = maximum number of elimination and dispersal events
P_{ed} = probability of elimination and dispersal events
J(i,n,m,l) = fitness function
J_{health} = factor representing health/ fitness/ suitability of each sample of PV parameters i.e. R_s, R_{sh} and a
C(i) = step-size specified by each run or tumble in the random direction
$d_{attract}$, $\omega_{attract}$, $\omega_{repellant}$, $h_{repellant}$ = arbitrarily chosen weighing factors
For effective and accurate evaluation of the parameters of a PV module, upper and lower limit constraints are also been considered for each parameter. The fitness function shown in eq (2.27) can be solved to extract of the parameters (R_s, R_{sh} and a). For this, the inequality constraints for the parameters (R_s, R_{sh} and a) are considered as follows.

$$\begin{aligned} R_{s,\min} &\leq R_s \leq R_{s,\max} \\ R_{sh,\min} &\leq R_{sh} \leq R_{sh,\max} \\ a_{\min} &\leq a \leq a_{\max} \end{aligned} \tag{2.29}$$

2.4.3 Results and Discussions

The proposed BFO based parameter extraction method is verified using five PV modules (Shell SQ85, PM648, SSI-M6-205 and Shell ST40) whose data are given in Table 2.2. These five PV models are examined for some defined test conditions i.e., solar irradiances G (1000 W/m^2, 800 W/m^2, 600 W/m^2, 400 W/m^2 and 200 W/m^2) and temperatures T (-25^{0}C, 0^{0}C, 25^{0}C, 50^{0}C and 75^{0}C).

For each test condition, the BFO algorithm was implemented using MATLAB and individual set of parameters (R_s, R_{sh} and a) were evaluated. For this BFO approach to evaluate R_s, R_{sh} and a, a set of 200 numbers of populations were considered for each test condition. The parameters set giving lowest value of fitness function are selected as the best fit among all the population. Using that set of best fit parameters the MPP power is calculated. For testing the accuracy of the calculated MPP power using BFO, the lowest absolute percentage error of the MPP power was selected. The absolute error of MPP power (%), e_{mpp} is calculated by using eq (2.28). In the simulation of the proposed BFO-Parameter Extraction algorithm, the following BFO parameters are considered in this work.

$$\begin{cases} S = 200, p = 3, N_c = 5, N_{re} = 10, \\ N_{ed} = 10, P_{ed} = 0.1, C\,(i) = 0.001, d_{attract} = 0.05, \\ \omega_{attract} = 0.3, h_{repellant} = 0.05, \omega_{repellant} = 0.05 \end{cases}$$

For ease in simulation and parameters evaluation all the three parameters (R_s, R_{sh} and a) were considered to be bounded with the inequality constraints as defined in eq (2.29)

Table 2.8: Proposed BFO based Parameter Extraction Algorithm

Step-1: Initialization of BFO Parameters (R_s, R_{sh} and a)
Step-2: Elimination-dispersal loop: $l = l + 1$
Step-3: Reproduction loop: $m = m + 1$
Step-4: Chemo taxis loop: $n = n + 1$
a. For $i = 1, 2....Samp$ (total sample no) $J(i, n, m, l) = \min_{R_s, R_{sh}, a, G, T} e_{fit} = e_{sc} + e_{oc} + e_{mpp}$ i.e. add on the cell-cell attraction effect for swimming behavior End for loop b. For $i = 1, 2....Samp$, take tumble/swim decision Generate a random vector $\Delta(i)$ in the interval $[1, 1]$ i. Update unknown parameter $x^i(n+1, m, l) = x^i(n, m, l) + u \times C(i) \frac{\Delta(i)}{\sqrt{\Delta^T(i)\Delta(i)}}$ ii. Compute new $J(i, n+1, m, l)$ using new position Else exit swim loop c. Generate a random d. Go to next sample i+1 if $i \neq Samp$ [go to b] e. If $min(J) < tolerance$, exit from all the loops
Step-5: If $J < tolerancelimit$ (Chemotactic iterations), go to Step-6 $J < N_c$ End of 'for loop' (b) End of Chemo taxis loop
Step-6: Reproduction For $i = 1, 2....Samp$ and given m and l Compute $J_{health} = \sum_{j=1}^{N_C+1} J_{sw}(i, n, m, l)$ Sort parameters in ascending order of J_{health} End of for loop Set $S_r = \frac{S}{2}$ with highest J_{health} and other S_r will be removed with the best value split
Step-7: If $m < N_{re}$ (maximum no. of reproduction steps) go to Step-3 End of reproduction loop
Step-8: Elimination-dispersal For i=1, 2, , Samp, with probability P_{ed} (probability of elimination and disposal), eliminate and disperse each set of parameters End of 'Eliminate-dispersal' loop Obtain optimized values of unknown parameters (a, R_s, R_{sh})
Step-9: Selection of Best P-V characteristics Using the obtained parameters in Step-8, Simulate for P-V characteristics changing PV voltage v_{pv} from 0 to V_{oc}. Calculate e_{mpp} and check whether $e_{mpp} < tolerance$ If yes, select P-V curves and find parameters for different G and T

Table 2.9: Inequality Constraints for Unknown Parameters of PV Panels

	Mono-Crystalline	Mono-Crystalline	Poly-Crystalline	Thin-Film
Parameters	Shell SQ85	PM648	SSI-M6-205	Shell ST40
a_{min}	0.8	0.8	0.8	0.8
a_{max}	2	2	2	2
$R_{s,min}$	0.01	0.01	0.01	0.01
$R_{s,max}$	2	2	2	2
$R_{sh,min}$	140	140	140	140
$R_{sh,max}$	300	300	600	300

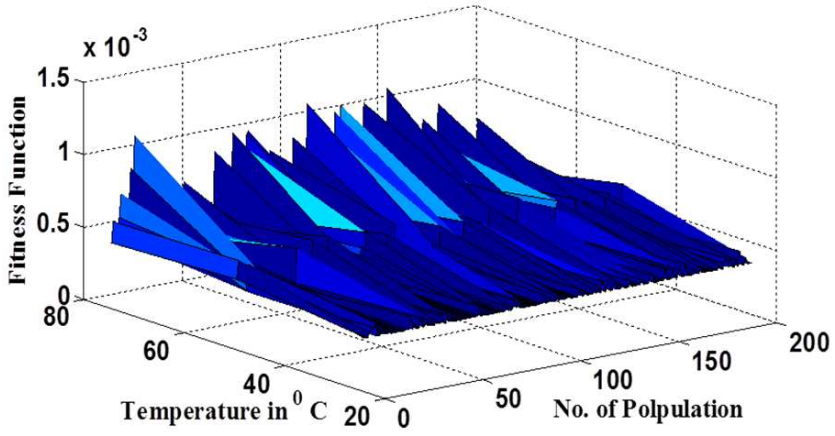

Figure 2.6: Comparison of Fitness Function of SSI-M6-205 PV Model for different populations at temperature variations

and Table 2.9. Fig.2.6 shows the 3D-plot of fitness function and number of population at different temperatures. This 3D-plot looks like a hilly curve and the global minimum of fitness function for each temperature is the deepest point in this curve. From this figure, it is clear that, for each temperature, the population that gives this deepest point is the fittest one. This fittest set of parameters (R_s, R_{sh} and a) were recorded. Using this procedure, the parameters (R_s, R_{sh} and a) were determined for all the test conditions (G (1000 W/m^2, 800 W/m^2, 600 W/m^2, 400 W/m^2 and 200 W/m^2) and temperatures T (-25^{0}C, 0^{0}C, 25^{0}C, 50^{0}C and 75^{0}C)).The Fig.2.7 demonstrates the global minimum of SSI-M6-205 PV Model at 0^{0}C. The efficacy of the proposed BFO parameter extraction method is verified by comparing its performance with that of three other existing parameter extraction methods such as hybrid NRM, comprehensive approach [44] and PSO [47]. The absolute percentage MPP power errors calculated by eq (2.28) at STC of all the above four parameter extraction methods are compared in Table 2.10 and Table 2.11. It can be seen from these tables that using BFO approach to parameter extraction yields e_{mpp} at STC only 0.000134%, 0.0016%, 0.0016%, 0.012% and 0.000507% for Shell SQ85, Shell SP70, SSI-M6-205 and ST40 PV modules re-

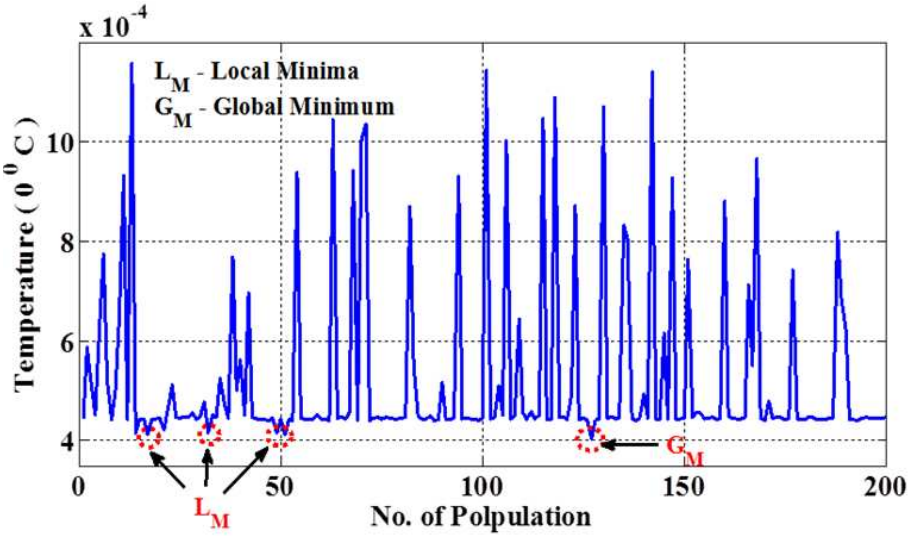

Figure 2.7: Fitness Function of SSI-M6-205 PV Model for different populations at 0^0C

Table 2.10: Comparison of Absolute MPP Power Error (%) at STC

PV Module	Hybrid NRM	PSO [47]	Comprehensive [44]	Proposed BFO
Shell SQ85	0.0044	0.0354	0.0473	0.00133
PM648	0.00485	0.0083	0.0334	0.00257
SSI-M6-205	0.003	0.004	0.013	0.00012
Shell ST40	0.00134	0.0016	0.0018	0.000507

Table 2.11: Comparison of Computational Time Burden (s) at STC

PV Module	Hybrid NRM	PSO [47]	Comprehensive [44]	Proposed BFO
PM648	3.58	5.65	14.36	2.36
SSI-M6-205	3.184309	6.13	14.28	1.86

spectively. It can be further seen that these values of e_{mpp} are lesser than that of hybrid NRM, comprehensive and PSO parameter extraction methods for all the above PV modules. From this comparison, it is confirmed that BFO approach to parameter extraction performs better at STC compared to hybrid NRM, comprehensive and PSO parameter extraction methods.

From Table 2.10 and Table 2.11, it is observed that the computational time taken by the proposed BFO method is also the least i.e. 2.36s as compared to that of 3.58s in the case of hybrid NRM, 5.65s of PSO [47] and 14.36s of comprehensive method [44] for the prototype PV panel. For SSI-M6-205 PV panel also computational time in case of BFO is the minimum than that of hybrid NRM, comprehensive and PSO methods. The calculated values of R_s,

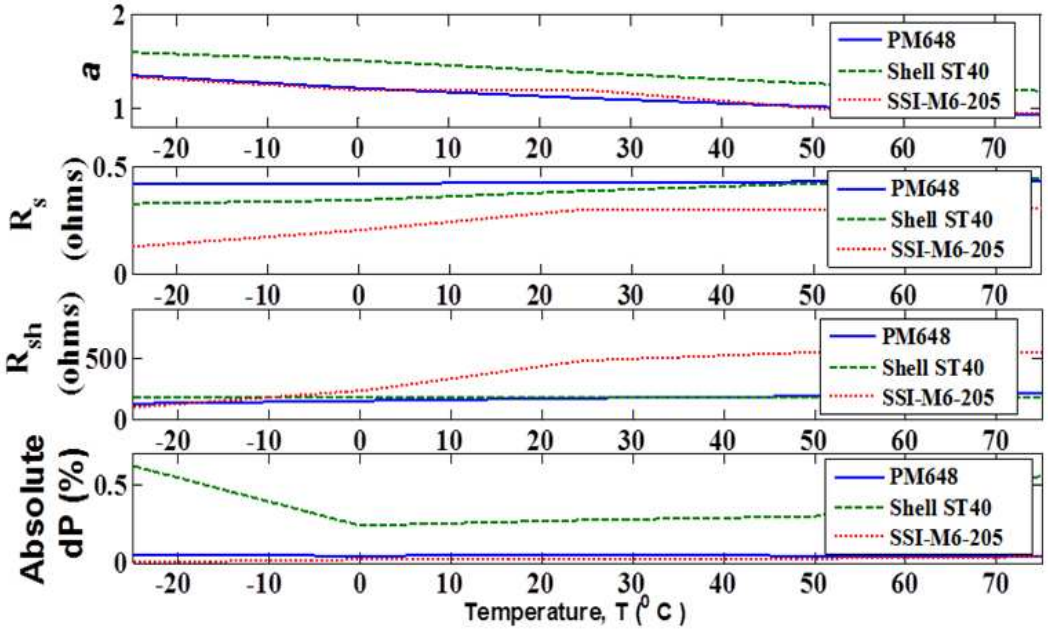

Figure 2.8: Comparison of Extracted Parameters of SSI-M6-205 PV Model using different Methods at -25^{0}C to 75^{0}C

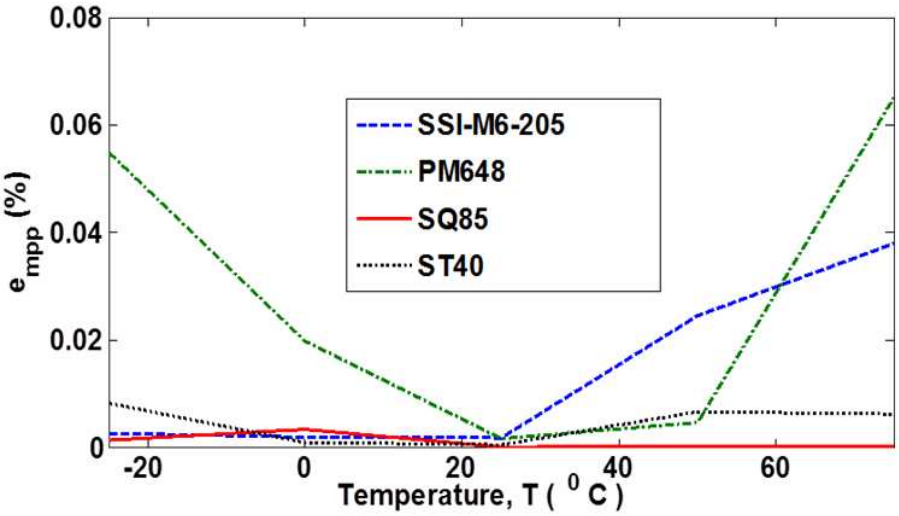

Figure 2.9: Estimation error in case of BFO Parameter Extraction Algorithm

R_{sh} and a for all the tested PV panels using the proposed BFO method are shown in Fig.2.8. From this Fig.2.8, it can be observed that BFO algorithm is converging to extract parameters at 0^{0}C. Hence, it is clear that application of BFO algorithm is not constraint only to STC and can be applicable to any other test conditions beyond STC. Although PSO method exhibits similar results [7] but average errors of power at MPP (e_{mpp}) at all test conditions for BFO is much less which is around 0.029% as compared to 0.18% for NRM and 0.073% for PSO (Fig.2.9). For experimental validation of the proposed BFO method, an experiment was conducted on a PM648 PV module whose data-sheet parameters are shown in Table

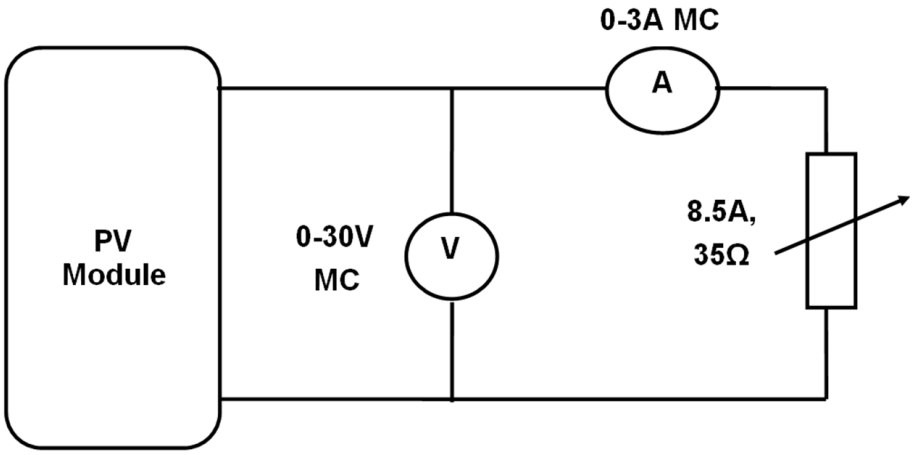

Figure 2.10: Experimental set-up to verify Proposed Parameter Extraction Algorithms

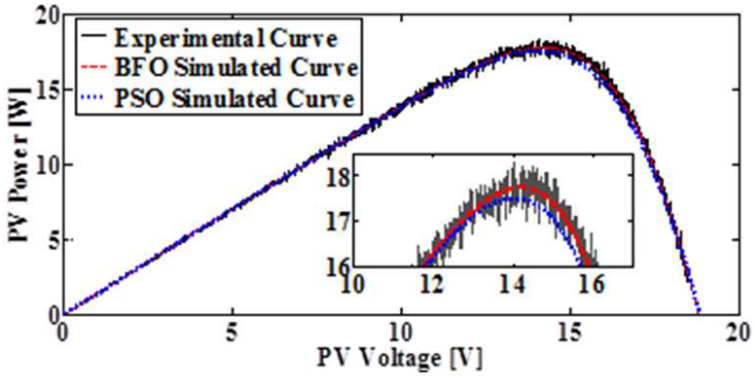

Figure 2.11: Comparison of P-V characteristics using Extracted Parameters of PM648 PV Model using proposed BFO Method with that of experimentally obtained curve at 658 W/m^2 and 23^0C at Unshaded condition

2.2. The experimental set-up for the above experiment is shown in Fig.2.10. Fig.2.11 further verifies the efficacy of the BFO parameter extraction method i.e. the BFO simulated P-V characteristics matching more with that of the experimentally obtained P-V characteristics than that of PSO. Fig.2.12 shows the comparison of P-V curve of PM648 PV Model with the BFO extracted parameters and the experimental P-V curve in shading condition. In this figure, Case-I is for the normal solar irradiance condition (V_{oc} = 18.46 V and I_{sc} = 1.42V) whereas Case-II is suggesting the partial shedding condition (V_{oc} = 17.65V and I_{sc} = 0.26V). It can be seen that the simulated P-V characteristic using BFO extracted parameters almost match with that of the experimentally obtained P-V curve. Hence, it is verified that the BFO method is efficiently working in partial shading condition.

2.4.4 Remarks from BFO based Proposed Extraction Method

- This method is independent of initial conditions.
- The singularity problem is not present in this method.

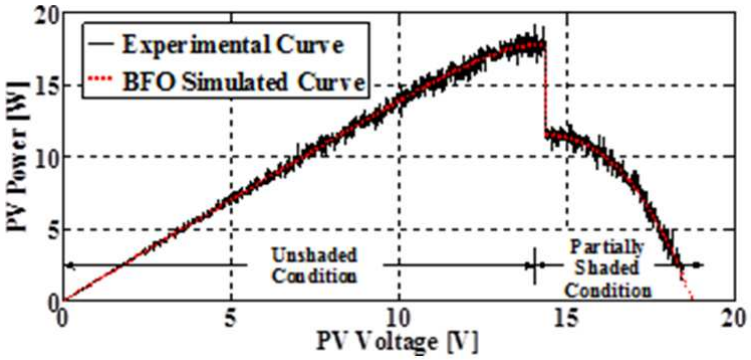

Figure 2.12: Comparison of P-V characteristics using Extracted Parameters of PM648 PV Model using proposed BFO Method with that of experimentally obtained curve at 658 W/m^2 and 23^0C at shaded condition

- In this method, values of all the PV model parameters I_{ph}, I_0, R_s, R_{sh} and a are varying with weather conditions satisfying the concept provided by [6] that PV model parameters are variable with respect to weather conditions.
- Works in partial shading condition also.

2.5 Chapter Summary

A new iterative method called hybrid NRM and another new evolutionary computational algorithm called BFO based parameter extraction algorithm are proposed for of PV panel. With the support of sufficient simulation and experimental results, hybrid NRM is found to have faster convergence and more accurate than that of other two existing methods i.e. NRM [42] and comprehensive method [44]. Unlike NRM, it does not suffer from singularity problem during convergence process. But, the accuracy and speed of convergence of this method are dependent on initial conditions of the unknown parameters. Also, it is not ideal for fast changing weather conditions and partial shading conditions. The other proposed BFO based parameter extraction method can efficiently works in both fast changing weather conditions and partial shedding conditions. It also does not suffer from singularity problem during convergence process. Therefore, BFO based parameter extraction algorithm is found to be better than that of NRM, comprehensive method and hybrid NRM.

Chapter 3

An Auto-Tuning based Adaptive Maximum Power Point Tracker for a Photovoltaic Power System

3.1 Introduction

This Chapter proposes a new Auto-tuning based MPPT for a PV system. A PV system can harvest maximum possible power if it is operated at MPP. In view of achieving this maximum PV power, a MPPT is employed between the PV panel and load. As discussed in Chapter 1, MPPT is a very important component of a PV system. It usually consists of a MPPT algorithm, a controller, PWM generator, comparator and a DC/DC boost converter as shown in Fig.3.1. The MPPT algorithm calculates the reference operating point of the PV system that aligns with the MPP. A DC/DC boost converter forces the PV system to operate at MPP calculated by the MPPT algorithm. The PWM generator generates gate-pulses according to the signal received from the controller. Designing a suitable MPPT algorithm and a controller are very important in achieving maximum power harvest in a PV system [82].

A good number of MPPT algorithms and their implementations are reported in [82], [48], [49] for constant and fast changing weather conditions and also for partial shedding mismatched conditions. Incremental Conductance (INC) and Perturb and Observe (P&O) methods are more popular MPPTs because of their simplicity and ease in implementations [83]. Also, INC and P&O MPPTs have been modified [84]-[85] to improve the PV power harvesting efficiency and MPP tracking accuracy. An adaptive P&O (APO) proposed in [86] is a low cost MPPT that involves a simple adaptive MPP tracking algorithm, a PI-controller and a voltage sensor.

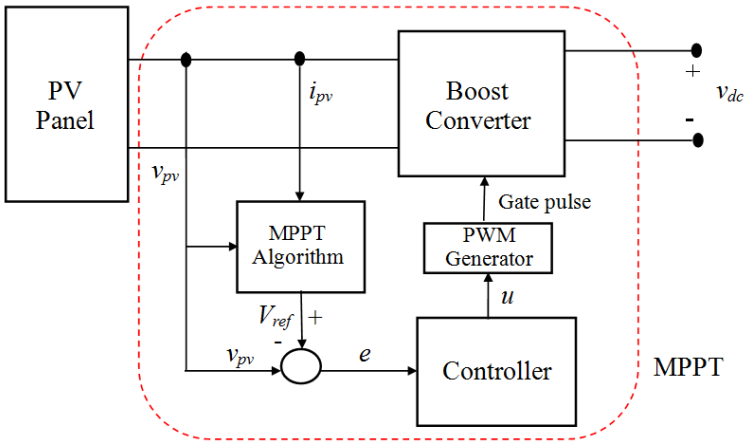

Figure 3.1: Stand-alone PV system with MPPT controller

Although these conventional MPPT control algorithms like P&O, INC and fractional open-circuit voltage MPPTs can make the PV system work at the maximum power point, but the adaptation factors such as MPP tracking speed and anti-disturbance ability of the PV system with any of these MPPTs are poor [84]. MPP tracking responses such as tracking accuracy and tracking time of P&O, INC and APO etc. are dependent on the perturbation size of tracking variable like PV voltage, current, duty-ratio of MPPT converter etc. Also, the tracking signal oscillates around its reference point even at the steady-state [50], [87]. On the other hand, Newton-Raphson method (NRM) based MPPT [70] is found to be an appropriate MPPT technique because it does not depend on empirical formula and also does not involve trial and error [11]. Although NRM algorithm deals with double integral term of the tracking signal, but the estimated MPPs using NRM are not oscillatory like P&O and INC MPPTs. Also, the NRM technique is a very convenient technique to calculate MPPs on-line by linearizing the model of the PV panel and DC/DC boost converter [58].

The main concern in maximum PV power harvesting applications is to design and implement a controller in the situation of fast changing weather conditions because the MPP of a PV panel is dependent on the weather conditions (Fig.3.2) [88]. PI and PID-controllers are commercially accepted controllers because of their easy practical implementation. But opportunities exist in modifying these controllers to achieve adaptive control actions [89]. A fixed gain PID-controller cannot handle fast variations in weather conditions for a wide operating range [90]. Although adaptive controllers such as the model reference adaptive controller (MRAC) and self-tuning regulator (STR) have been successfully applied to PID-controlled DC/DC converters but the parameter tuning algorithms of these adaptive controllers are very complex and dependent on plant parameters [91].

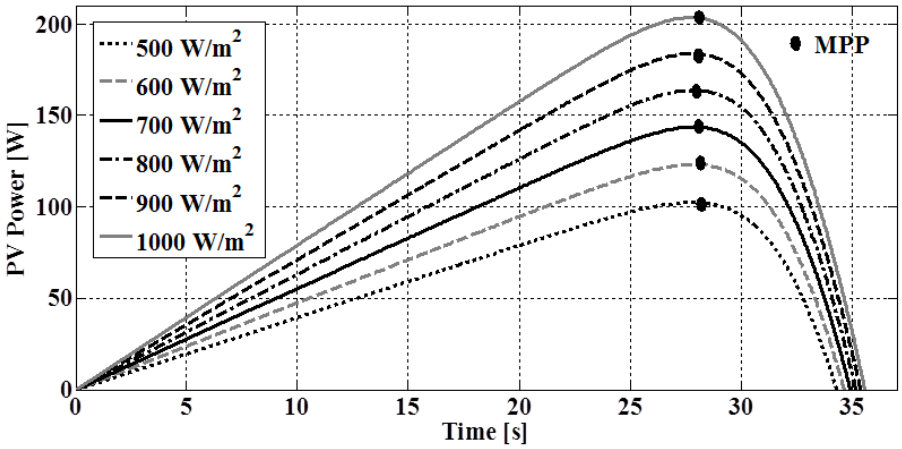

Figure 3.2: Variation of PV power p with PV voltage v for different solar radiations

For control action involving high frequency switching, the tuning algorithm should be simple [92]. The main challenge involved in designing an adaptive controller is the development of a parameter tuning algorithm that ensures stability and convergence of controller parameters [18]. For DC/DC power converter control, auto-tuning control has been successful in providing adaptive control action on-line [90]. It is also found that an auto-tuner is based on a simple and robust algorithm. It does not affect converter operation under normal condition [91]. The auto-tuners presented in [90] and [91] work efficiently for normal load regulation problem but may not efficient enough as MPPT controller has to work in a situation of fast changing weather conditions.

Adaptive algorithms should involve tuning of controller parameters efficiently and quickly for a PV system which has uncertain nonlinear dynamics. It becomes easier to design and implement an adaptive algorithm in MPPT by considering linear models of the PV panel and DC/DC boost converter. Hence, the auto-tuner proposed in this work is equipped with a tuning algorithm that is based on linearized models of PV panel and DC/DC boost converter. Although on-line MPPT operation is possible using an ideal PV panel model, but its accuracy is affected by the neglect of shunt and series-resistances [33]. Hence, a polynomial curve-fitting model [70] where recursive parameterizations is possible has been used. This polynomial model is constructed from real-time data of PV panel voltage, current and power, hence is independent of manufacturer's data-sheet. For construction of a polynomial model, a mathematical function is generated that approximately fits the data.

The performance of the proposed MPPT is compared with that of three existing MPPTs such as P&O [55], INC [57] and an APO [24] using appropriate simulation, real-time simulation and experimental studies. Real-time simulation results presented in this thesis are the outputs obtained from a real-time simulator such as OPAL-RT [93]. OPAL-RT operates efficiently with hardware-in-the-loop (HIL) simulation using the field-programmable gate array

(FPGA) over a wide time range such as from few seconds to hours [93]. For experimental studies in this thesis, a 0.2kW prototype PV system has been developed and used.

3.2 Problem Formulation

The equivalent circuit of a PV module is shown in Fig.3.3. When solar radiation G falls on the PV module, current I_{ph} is generated. At the output terminal of the PV system voltage v_{pv} and current i_{pv} are available.

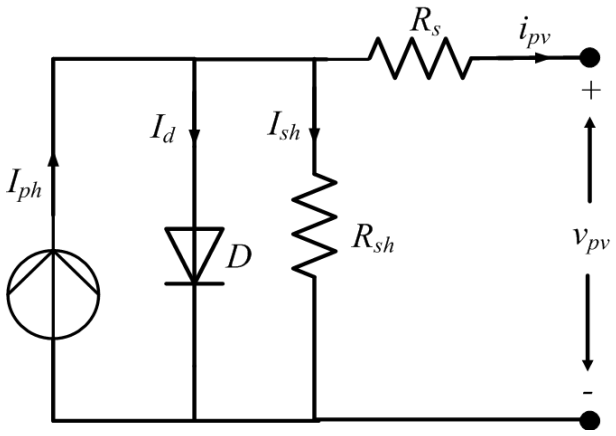

Figure 3.3: Equivalent Mathematical Model of a PV Panel

Applying Kirchhoff's current law to this PV module circuit, the output PV current can be expressed as

$$i_{pv} = I_{ph} - I_0 \left[\exp\left(\frac{v_{pv} + i_{pv} R_s}{n_s V_t} \right) - 1 \right] - \frac{v_{pv} + i_{pv} R_s}{R_{sh}} \tag{3.1}$$

where I_0 is the dark-saturation current, n_s, R_s and R_{sh} are number of series cells in the PV panel, series resistance and shunt resistance respectively. V_t is the thermal voltage of the PV system given by

$$V_t = \frac{a k_b T}{q} \tag{3.2}$$

where a is diode-ideality factor, k_b is Boltzmann's constant, T is junction temperature and q is the charge of an electron. The output power of the PV system is given by

$$p_{pv} = v_{pv} \times i_{pv} \tag{3.3}$$

There exists a single point called Maximum Power Point (MPP) at any solar irradiance at which output power of the PV system is the maximum as shown in Fig.3.2. Hence,

$$\frac{dp_{pv}}{dv_{pv}} = 0 \tag{3.4}$$

Voltage at MPP (V_{ref}) can be calculated by solving eq (3.4) using a MPPT algorithm. Then using a DC/DC boost converter as shown in Fig.3.4, the operating point of the PV system

can be adjusted to this calculated V_{ref}. The MPPT problem is concerned with estimation of the MPP using MPPT algorithm. Then the PV system is forced to operate at that estimated MPP by providing an appropriate duty-signal to the DC/DC converter. The MPPT algorithm and the controller both need to be efficient because their performances are directly related to the power conversion efficiency of the entire PV system.

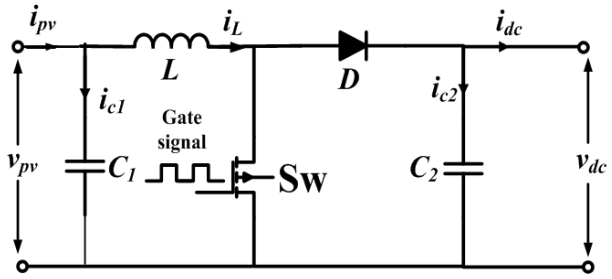

Figure 3.4: Equivalent Mathematical Model of a DC/DC Boost Converter

3.3 Proposed Auto-tuning based Adaptive MPPT

A PV system with the proposed MPPT controller is shown in Fig.3.5. PV panel voltage v_{pv} and current i_{pv} are sensed and sampled by an ADC to v(k) and i(k). These sampled signals v(k) and i(k) are supplied to the MPPT algorithm to generate v_{ref}(k). This v_{ref}(k) is the voltage at which operating point of PV system coincides with MPP of PV panel. v_{ref}(k) is compared with v(k) to generate an error signal e_1(k). Here, a simple PV system has been designed maintaining the output voltage v_{dc}(k) equal to $v_{dc,ref}$. Hence, the objective of the controller is to minimize the error e_2(k) between $v_{dc,ref}$(k) and v_{dc}(k). Therefore, the controller is designed such that the following error is minimized.

$$e\left(k\right) = e_1\left(k\right) + e_2\left(k\right) = \left[v_{ref}\left(k\right) - v\left(k\right)\right] + \left[v_{dc,ref}\left(k\right) - v_{dc}\left(k\right)\right] \tag{3.5}$$

The auto-tuner tunes the parameters of discrete PID in response to receiving a signal y(k) and parameter w from a linearized model of boost converter where y(k) is the boost converter output and w is the un-damped natural frequency component of the linearized model of boost converter. The signal u(k) is sent to a PWM generator so that it generates the required gate-pulse for the boost converter. Thus, the control operation consists of the following five distinct steps.

- Selection of the order the polynomial PV panel model
- Estimation of PV panel parameter (θ)
- Calculation of MPP voltage v_{ref}(k) using the MPPT algorithm
- Linearization of the DC/DC boost converter

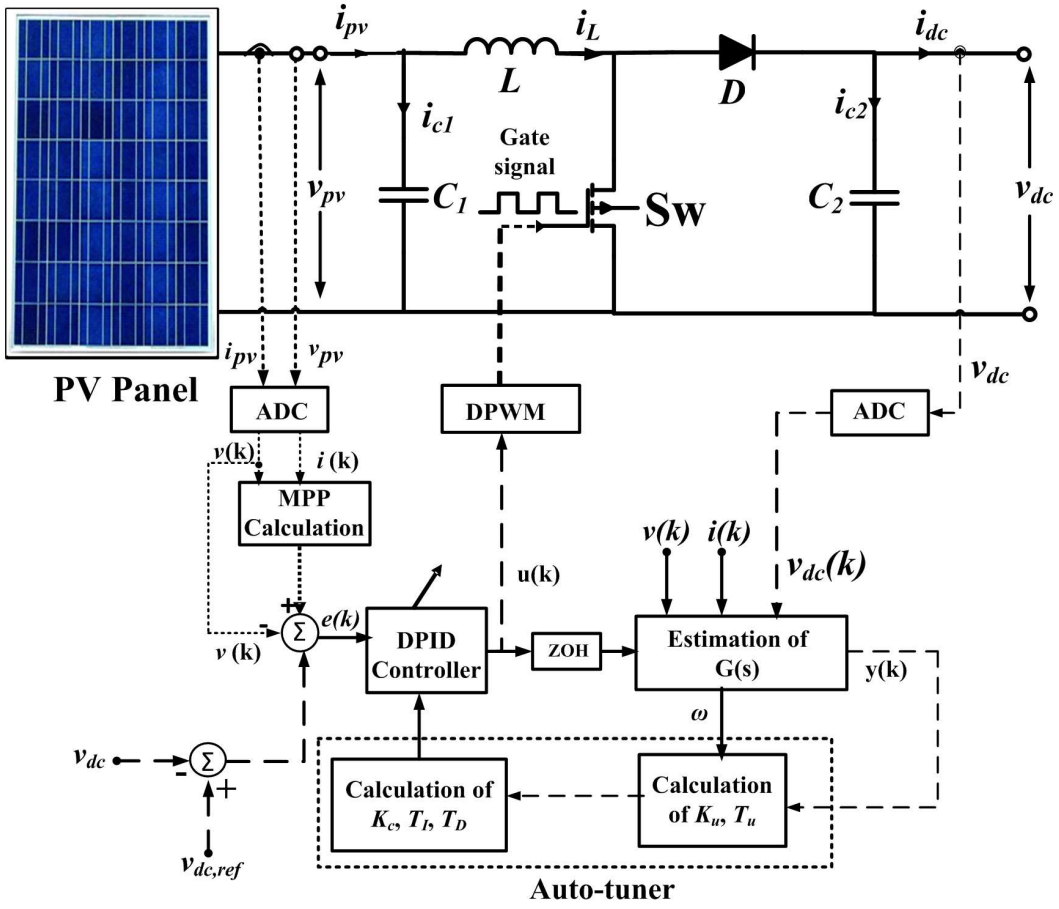

Figure 3.5: Proposed Auto-tuning based Auto-tuned Adaptive MPPT Controller for MPPT operation of PV Panel

- Tuning the discrete PID controller parameters using an auto-tuner

3.3.1 Selection of PV panel Model

In this work, a polynomial curve-fitting model for the PV system is considered. Typically system identification involves two distinct steps namely polynomial order determination and parameter estimation (estimating coefficients of polynomial describing PV system dynamics). The order of the polynomial curve-fitting model is selected as follows. Usually, the PV panel dynamics is identified by its I-V or P-V characteristics. The MPPs are more distinct in P-V curves than that of I-V curves. Hence, the P-V curve is chosen for curve-fitting [11]. Then, taking PV panel voltage sample v(k) and power sample p(k) as input and output respectively, the order of the polynomial model is determined. Here, p(k) is calculated by multiplying v(k) and i(k). At first, an n^{th}-order polynomial model is considered. The n^{th}-order polynomial describing the P-V characteristics of the PV-panel is given as

$$p(k) = b_0(k) + b_1(k)\, v(k) + b_2(k)\, v^2(k) + ... + b_n(k)\, v^n(k) \tag{3.6}$$

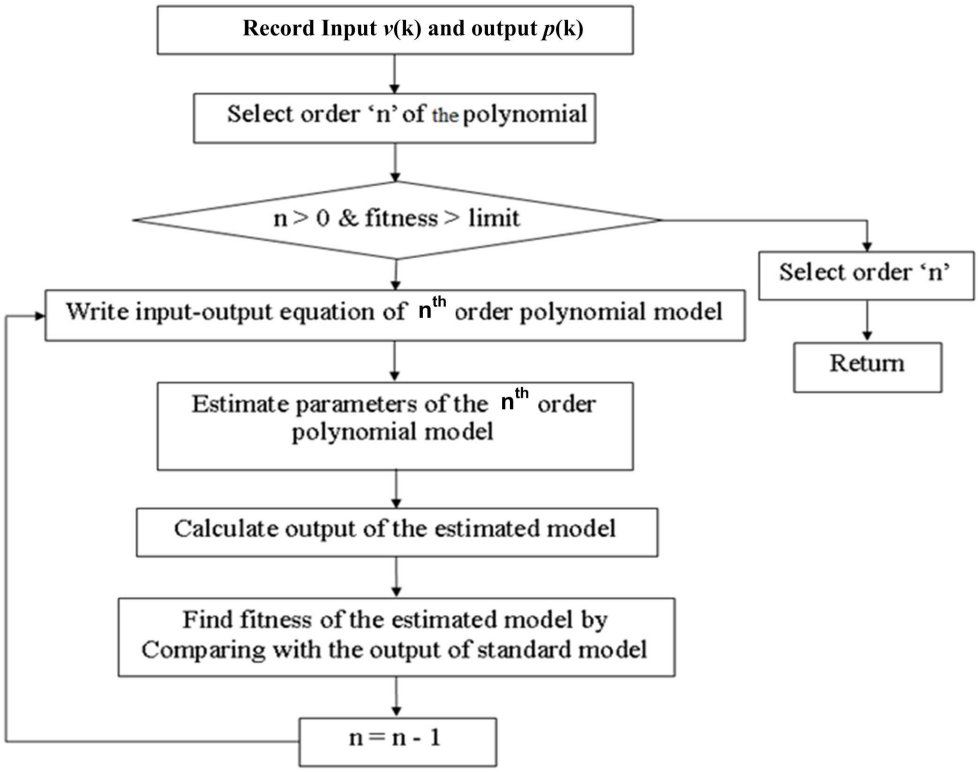

Figure 3.6: Selection of lowest possible polynomial order of curve-fitting-polynomial PV panel model

where k is the sample number. The order of the linearized polynomial model of PV panel represented by eq (3.7) can be selected following the steps shown in Fig.3.6. In this selection process, at first, order n is selected for the linearized polynomial model. Then the fitness of the polynomial can be evaluated using the following formula.

$$Fitness(\%age) = \left[1 - \left|\frac{p\,(k) - \hat{p}\,(k)}{p\,(k)}\right|\right] \times 100 \tag{3.7}$$

where $\hat{p}\,(k)$ is the estimated power sample by an n^{th} order polynomial model and is the power sample of the standard PV model. Then, the $(n-1)^{th}$ order is considered and its fitness is tested. The process is continued up the fitness becomes $\geq$ set lower limit 95%. It should be noted that the lowest possible ordered polynomial model of the PV panel should be considered to avoid complexity and unnecessary extra mathematical calculations during on-line system identification process. This above process is carried out at standard testing condition (STC) that is at 1000 W/m^2 and 25^{0}C. Then, the polynomial model is cross-validated at other weather conditions.

3.3.2 Estimation of PV Panel Parameters

Eq(3.7) can be rewritten in regressor form as

$$p\,(k) = \phi^T\,(k)\,\theta\,(k) \tag{3.8}$$

where the regressor vector ϕ and parameter vector θ are given by

$$\phi(k) = \begin{bmatrix} 1 & v(k) & . & . & . & v^n(k) \end{bmatrix};$$
$$\theta(k) = \begin{bmatrix} b_0(k) & b_1(k) & . & . & . & b_n(k) \end{bmatrix}^T; \tag{3.9}$$

A RLS algorithm can be employed for the PV parameters extraction. The k^{th} sampled panel voltage v(k) and power p(k) are selected as input and output of the RLS block. Signal p(k) is the product of v(k) and current i(k).The PV panel model in eq (3.8) is already in regressive form. Hence RLS algorithm can be applied directly to estimate θ as follows.

$$\hat{\theta}(k) = \hat{\theta}(k-1) + K(k)\left[p(k) - \varphi^T(k)\hat{\theta}(k-1)\right] \tag{3.10}$$

$$K(k) = \frac{C(k-1)\varphi^T(k)}{\lambda + \varphi^T(k)C(k-1)\varphi(k)} \tag{3.11}$$

$$C(k) = \frac{\left[I - K(k)\varphi^T(k)\right]C(k-1)}{\lambda} \tag{3.12}$$

where p(k), K(k), *lambda* and C(k) are the measured power, the Kalman-gain matrix, the forgetting factor such that $0 < \lambda < 1$ and the covariance-matrix respectively at k^{th} sample.

3.3.3 Determination of Reference voltage for MPPT operation

The procedure for calculation of v_{ref}(k) is shown in Fig.3.7. The P-V characteristics of a PV panel at different solar radiations indicate that with variations in solar radiation, the peak power point and corresponding voltage point change. That voltage point can be estimated as follows. Let, the derivative of actual PV power with respect to actual PV voltage is represented as f (v) such as

$$f(v) = \frac{dp}{dv} \tag{3.13}$$

Referring eq (3.4), at MPP f(v) becomes zero. Hence,

$$f(v) = 0 \tag{3.14}$$

Then, voltage at MPP can be determined by solving eq (3.14). This can be solved by using the Newton-Raphson method (NRM). Flowchart for NRM for finding MPP is shown in Fig.3.8.

Using NRM, the first-derivative $\frac{dp}{dv}$ and second-derivative $\frac{d^2p}{dv^2}$ of the n^{th}-order polynomial of PV panel can be written as

$$f(v) = \frac{dp}{dv} = \hat{b}_1(k) + 2\hat{b}_2(k)v(k) + 3\hat{b}_3(k)v^2(k) + ... + n\hat{b}_n(k)v^{n-1}(k)$$
$$\dot{f}(v) = \frac{d^2p}{dv^2} = 2\hat{b}_2(k) + 6\hat{b}_3(k)v(k) + 12\hat{b}_4(k)v^2(k) + ... + n(n-1)\hat{b}_n(k)v^{n-2}(k) \tag{3.15}$$

where $\hat{b}_i$ are the estimated parameters of the PV system. Although NRM is one of the fastest methods of root finding, but it does not have the guarantee of convergence unless $v(0)$ is properly chosen. This problem is clear from the relationship between $f(v)$ and v as shown in Fig.3.9. In this Fig.3.9, point '1' and '4' are the open-circuit and short-circuit points respectively. In between '1' and '4', true MPP lies at '3'. But, there exists a local minimum at point '2' where $\dot{f}(v)$ is zero and division of zero occurs during the calculation of MPP. If v is initialized from '1', then it will suffer from the unwanted division of zero problems in between the estimation procedure. Hence, it is advisable to choose initial point of v between '5' and '4' to avoid the divergence problem.

3.3.4 Linearization of DC/DC Boost Converter Model

A DC/DC converter is required to force the operating voltage of PV panel to the MPP voltage. In this work, a non-isolated boost type converter is used because this converter is widely used as PV system interface due to its simplicity and efficiency [24]. A DC/DC boost converter has been used in this paper for MPPT operation. The circuit of a boost converter is shown in Fig.3.4 and their equivalent circuits for different switching operations are shown in Fig.3.10 (a) and 3.10 (b). Here, v_{pv} and i_{pv} are voltage and current of the PV panel respectively, i_L is the current through inductor L, the voltage and current of load R_L are v_{dc} and i_{dc}, the current through capacitor C_2 is i_{c2}. The linearized system model of the DC/DC Boost converter can be determined by using the small-signal state-space modeling technique for a switch-mode power converter assuming that $v_{dc} = v_{dc,ref}$. Hence, the control signal of this reference linearized model would automatically materialized both the MPPT operation as well as the regulation of output voltage v_{dc}. The model is described as follows. When the switch is OFF, then switching control signal (Fig.3.10 (a))

$$\begin{aligned} i_{pv} &= i_{c1} + i_L \\ \Rightarrow \frac{v_{pv}}{r_{pv}} &= C_1 \frac{dv_{pv}}{dt} + i_L \\ \Rightarrow \frac{dv_{pv}}{dt} &= \frac{1}{r_{pv} C_1} v_{pv} - \frac{1}{C_1} i_L \end{aligned} \tag{3.16}$$

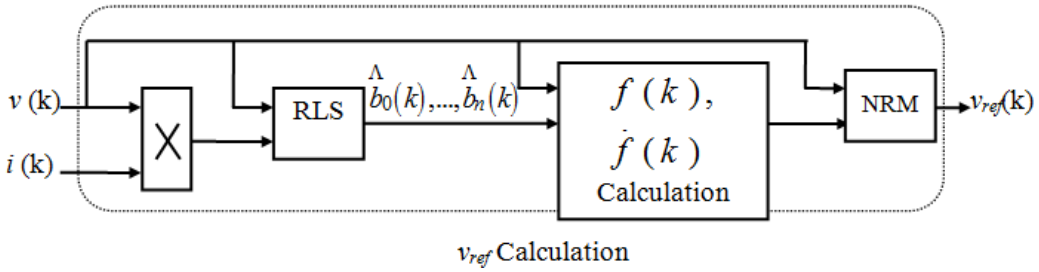

Figure 3.7: Calculation of reference PV voltage v_{ref} (k) for MPPT Operation

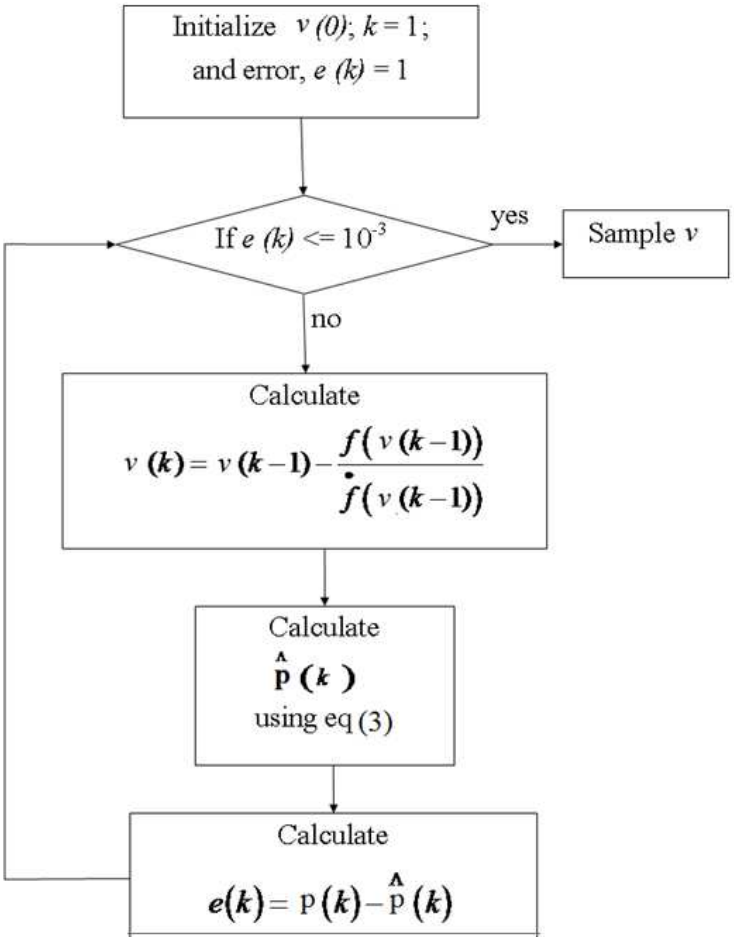

Figure 3.8: Flow-chart showing NRM method for MPP estimation

and

$$v_{pv} = L\frac{di_L}{dt} + v_{dc}$$
$$\Rightarrow \frac{di_L}{dt} = \frac{v_{pv}}{L} - \frac{v_{dc}}{L} \tag{3.17}$$

When the switch is ON (Fig.3.10 (b)), then

$$i_{pv} = i_{c1} + i_L$$
$$\Rightarrow \frac{dv_{pv}}{dt} = \frac{1}{r_{pv}C_1}v_{pv} - \frac{1}{C_1}i_L \tag{3.18}$$

and

$$v_{pv} = L\frac{di_L}{dt} \tag{3.19}$$

where r_{pv} is the dynamic resistance of the PV panel and is calculated as follows.

$$r_{pv} = -\frac{dv_{pv}}{di_{pv}} \tag{3.20}$$

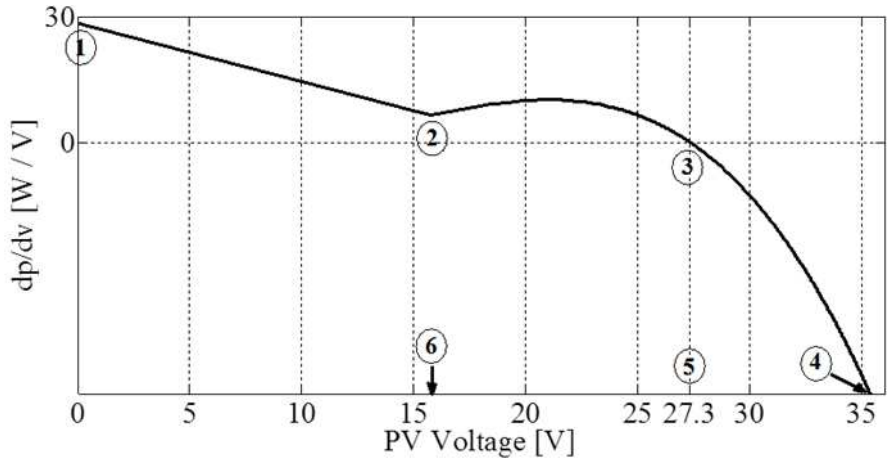

Figure 3.9: Relationship between $\frac{dp}{dv}$ and PV voltage v of SSI-M6-205 PV panel

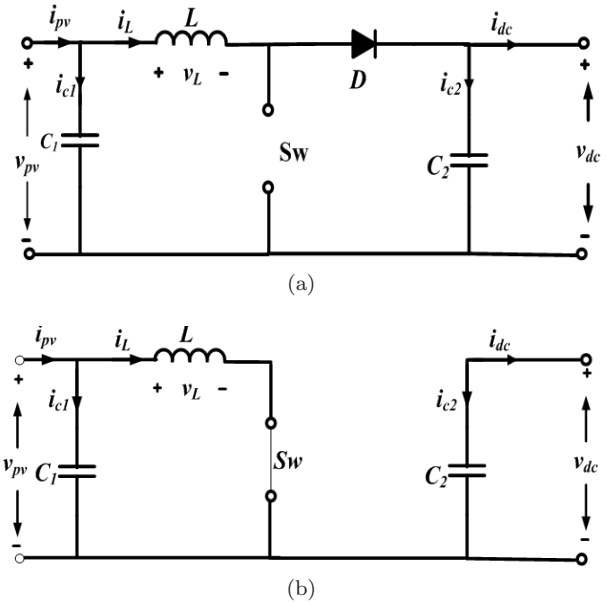

(a)

(b)

Figure 3.10: (a) Equivalent circuit of boost converter when Sw is open and (b) when Sw is closed

Let δ is the duty-ratio of the switching signal u, then eq (3.15)-eq (3.18) are combined as

$$i_{pv} = i_{c1} + i_L \tag{3.21}$$

$$\Rightarrow \frac{dv_{pv}}{dt} = \frac{1}{r_{pv}C_1}v_{pv} - \frac{1}{C_1}i_L \tag{3.22}$$

$$\frac{di_L}{dt} = \frac{1}{L}v_{pv} - \frac{v_{dc}}{L}\bar{\delta}$$

$$y = v_{pv}$$

Here, L and C_1 are kept fixed for a given DC/DC boost converter and only r_{pv} varies. The value of r_{pv} is usually negative near MPP [24]. Laplace transforming eq (3.21), we get

$$\begin{aligned} sV_{pv}(s) &= \frac{1}{r_{pv}C_1}V_{pv}(s) - \frac{1}{C_1}I_L(s) \\ sI_L(s) &= \frac{1}{L}V_{pv}(s) - \frac{V_{dc}}{L}\bar{D}(s) \\ Y(s) &= V_{pv}(s) \end{aligned} \tag{3.23}$$

Eq (3.23) can be rewritten in transfer function form as

$$G(s) = \frac{V_{pv}(s)}{\bar{D}(s)} = \frac{\frac{V_{dc}(s)}{LC_1}}{s^2 + \left(\frac{1}{r_{pv}C_1}\right)s + \left(\frac{1}{LC_1}\right)} \tag{3.24}$$

The general transfer function form of a 2^{nd}-order DC/DC boost converter dynamics is given by

$$G(s) = \frac{V_{pv}(s)}{\bar{D}(s)} = \frac{K_0}{s^2 + 2\zeta\omega s + \omega^2} \tag{3.25}$$

where K_0 and ζ are the system-gain and damping-ratio of the step-response of the DC/DC boost converter. Comparing eq (3.24) and eq (3.25),

$$\begin{aligned} K_0 &= \frac{V_{dc}(s)}{LC_1} \\ \omega &= \sqrt{\frac{1}{LC_1}} \\ \zeta &= \frac{1}{2r_{pv}LC_1\omega} \end{aligned} \tag{3.26}$$

Here, the magnitudes of L_1, C_1 and ω are fixed. The value of dynamic resistance of PV panel varies with changing weather conditions.

3.3.5 Auto-Tuning of PID-Controller Parameters

A discrete time PID-controller (DPID) has been chosen for the proposed ATAMPPT because it is easy to implement in digital computing platform. The k^{th}-sample switching signal to the boost converter with discrete DPID controller during MPPT operation is given as

$$u(k) = K_c\left[e(k) + \frac{T_c}{T_i}\sum_{n=0}^{k} e(n) + T_d\frac{e(k) - e(k-1)}{T_c}\right] \tag{3.27}$$

where K_c, T_i, T_d and T_c are the proportional-gain, integral-time, derivative-time and sampling period respectively of the controller. However, conventional DPID based MPPT controllers generally do not work well for actual systems, higher order systems, time-delayed linear systems, on-line operation and complex systems without precise mathematical models. To overcome these difficulties, the DPID controller has to provide necessary duty-ratio

of switching signal $u(\mathrm{k})$ so as to obtain actual v close to v_{ref} both in fixed and variable weather conditions in accordance with changing in environmental conditions. For varying weather conditions, parameters of DPID controller such as K_c, T_i and T_d are to be adjusted. The tuning procedure of these parameters is described as follows. The tuning of the DPID controller is based on experiment performed in closed loop. This tuning method is simple as values of ω and $G(s)|_{s=j\omega}$ is only required for the tuning of DPID-controller parameters. Taking ω as input, the new auto-tuner evaluates the tuning-parameters such as tuning-gain (K_u) and tuning-time-constant (T_u) using following equations.

$$\begin{aligned} K_u &= \frac{1}{|G(j\omega)|} \\ T_u &= \frac{2\pi}{\omega} \end{aligned} \tag{3.28}$$

where

$$\arg\left(G(j\omega)\right) = -\pi \tag{3.29}$$

In this ATAMPPT, the PID parameters K_c, T_i and T_d are tuned using values of (K_u) and (T_u) with the following empirical relationships.

$$\begin{aligned} K_c &= 0.6K_u \\ T_c &= 0.5T_u \\ T_d &= 0.125T_u \end{aligned} \tag{3.30}$$

The effectiveness and accuracy of the proposed ATAMPPT can be estimated by observing its (i) percentage of absolute error in MPP tacking and (ii) MPPT efficiency. The percentage of absolute error in MPP tacking and MPPT efficiency at STC can be estimated as

$$\begin{aligned} \varepsilon_{v_{mpp}} &= \left| \frac{v_{mpp\_actual} - v_{mpp\_estimated}}{v_{mpp\_actual}} \right| \times 100 \\ \varepsilon_{p_{\max}} &= \left| \frac{p_{\max\_actual} - p_{\max\_estimated}}{p_{\max\_actual}} \right| \times 100 \\ \eta_{MPPT} &= 1 - \varepsilon_{p_{\max}} \end{aligned} \tag{3.31}$$

3.4 Results and Discussion

In order to validate the efficacy of the proposed ATAMPPT controller, we first obtain the P-V characteristics at different weather conditions (Fig.2.2) of SSI-M6-205 PV system [13] whose manufacturer's data-sheet is shown in Table 3.1.

Table 3.1: Component of SSI-M6-205 PV Panel

Component	Value
Inductance,L (mH)	0.5
Capacitance,C_1 (μF)	180
Capacitance,C_2 (μF)	330
Sampling time,T_s (μs)	1
Time interval of MPPT (s)	5
Reference output voltage of DC/DC boost converter $v_{dc,ref}$ (V)	48

3.4.1 Simulation Results

The procedure of fixing up the order of the polynomial in selection of the PV panel prior to on-line evaluation of MPPs is presented next. For this order selection, fitness of the PV model polynomial with some selected order like 8^{th}, 6^{th} and 4^{th} is checked using eq (3.7). P-V characteristics of PV model with 8^{th}, 6^{th} and 4^{th} ordered polynomials are shown in Fig.3.11 with their absolute percentage of fitness.

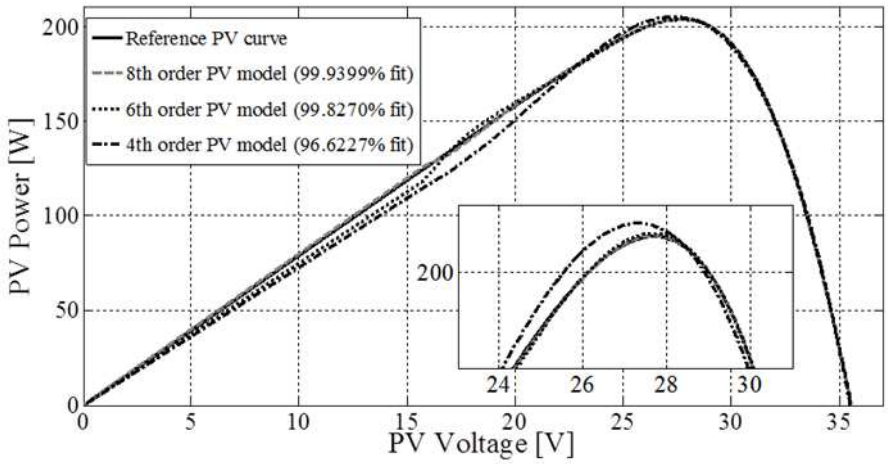

Figure 3.11: Comparison of different order of polynomial of SSI-M6-205 PV panel models with that of the Actual model at STC

Referring to Fig.3.11, it is observed that P-V characteristic in case of 8th order polynomial model of PV panel has as high as 99.9399 % of percentage fitness at STC with respect to the reference P-V characteristic. Meanwhile, P-V characteristics in case of the 6th and the 4th order polynomial models have 99.827 and 96.6227% of fitness respectively. To reduce the calculation complexities, the order of the polynomial model should be as low as possible. The fitness of the 4^{th} order polynomial model is having the simplest structure among 8^{th}, 6^{th} and 4^{th} order polynomials of PV panel and also having more than 95% of fitness. Hence, 4th order polynomial model for PV panel is considered in this paper. After selection of the

model, the next step is extraction of model parameters of the PV system.

After selection of the model, the next step is extraction of model parameters of the studied PV system. A 4^{th} order polynomial of a PV system is given as

$$p(k) = b_0(k) + b_1(k)\, v(k) + b_2(k)\, v^2(k) + b_3(k)\, v^3(k) + b_4(k)\, v^4(k) \tag{3.32}$$

where the regressor ϕ vector and the parameter vector θ are given by

$$\phi = \begin{bmatrix} 1 & v(k) & v^2(k) & v^3(k) & v^4(k) \end{bmatrix};$$
$$\theta = \begin{bmatrix} b_0(k) & b_1(k) & b_2(k) & b_3(k) & b_4(k) \end{bmatrix}^T \tag{3.33}$$

The proposed Auto-tuner based MPPT algorithm was implemented as follows. Auxiliary load is varied with a fixed number of steps and data of v and p are acquired and temporarily stored in the data base. Using those data of v and p in eq (3.32) and eq (3.33), θ is estimated as shown in Fig.3.12 and Table 3.2.

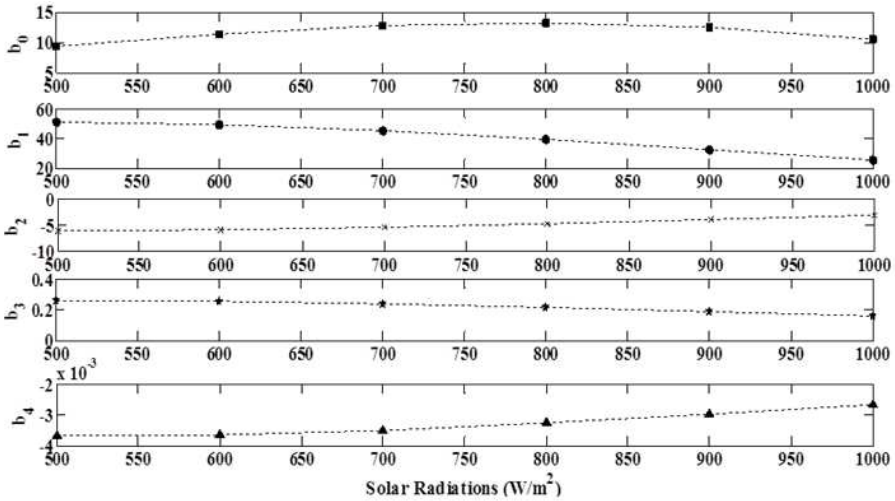

Figure 3.12: Variations in PV Panel parameters with solar radiations

Fig.3.12 and Table 3.2 show the estimated PV panel parameter vector such as b_0 - b_4 with variation in solar radiation. From Fig.3.12, it can be observed that with each change in

Table 3.2: Estimated PV panel parameters with variation in solar radiations

G (W/m^2)	T(^{0}C)	b_0	b_1	b_2	b_3	b_4
500	25	9.3598	51.1171	-6.1516	0.2617	-0.0037
600	25	11.4216	49.1796	-5.9143	0.2557	-0.0036
700	25	12.7764	44.9902	-5.4154	0.24	-0.0035
800	25	13.1865	39.294	-4.7357	0.2174	-0.0033
900	25	12.4703	32.7069	-3.9409	0.1903	-0.003
1000	25	10.5023	25.7226	-3.0837	0.1606	-0.0027

solar radiation, θ is also varying distinctly that leads to the variation in the operating point of DC/DC boost converter such as the voltage and current at MPP. Varying v with very small step-size of 0.5ms, p was evaluated using eq (3.32). The evaluated data of v and p were used in NRM block. Using NRM, voltage at MPP was evaluated as shown in Table 3.3 and used as the reference voltage point v_{ref} for DC/DC boost converter. Referring to Table 3.3, the percentage absolute error in estimated power at STC is only 0.4035%. Lowering the radiation this $\varepsilon_{p_{\max}}$ increases but still it is less than 4% at 500 W/m^2.

Table 3.3: Comparison of Estimated voltage and power at MPP (v_{ref} and P_{max} respectively) using NRM with that of simulated voltage and power with variation in solar radiations

G (W/m^2)	Actual P_{ref} (V)	Estimated v_{ref} (V)	$\varepsilon_{v_{\max}}$ (%)	Actual P_{max} (W)	Estimated (W)	$\varepsilon_{v_{\max}}$ (%)	η_{MPPT} (%)
500	27.61	26.24	4.962	100.5941	104.3101	3.694	96.306
600	27.78	26.44	4.8236	121.6577	124.7192	2.5165	97.4835
700	27.89	26.59	4.6612	142.6554	145.1007	1.7142	98.2858
800	27.96	26.71	4.4707	163.5504	165.4192	1.1426	98.8574
900	28	26.81	4.25	184.3157	185.6459	0.7217	99.2783
1000	28.04	26.88	4.0685	204.9302	205.7572	0.4035	99.5965

For a given DC/DC boost converter, the tuning of PID-controller parameter was accomplished by using the new auto-tuning method during MPP tracking process. In this procedure, the DPID-controller parameters vary with dynamic resistance of PV panel (r_{pv}) which again varies with solar radiation. Then, r_{pv} was calculated at $v = 20$ V. Using value of r_{pv} in eq (6.7), parameters of linear DC/DC boost converter model are estimated as shown in Table 3.4. The frequency of the PV system with the proposed ATAMPPT is shown in Fig.3.13. In this figure, $\omega_{pm} > \omega_{gm}$ and both GM and PM are positive. Therefore, the studied PV system with this new MPPT is stable.

A comparative analysis of MPP tracking performances of PV system with the proposed ATAMPPT and some of the existing renowned MPPTs such as P&O, INC and an adaptive

Table 3.4: Estimated PID controller parameters using proposed auto-tuning method with variation in solar radiations

G (W/m^2)	T(^{0}C)	K_u	ω	T_u	K_c	T_i	T_d
500	25	0.0393	55.1021	0.1140	0.0236	0.0536	0.0134
600	25	0.0391	68.0324	0.0924	0.0235	0.0509	0.0121
700	25	0.0389	80.0153	0.0785	0.0233	0.0376	0.0094
800	25	0.0386	90.3110	0.0696	0.0231	0.0308	0.0086
900	25	0.0384	98.4446	0.0638	0.0229	0.0296	0.0079
1000	25	0.0382	106.7915	0.0588	0.0228	0.0283	0.0071

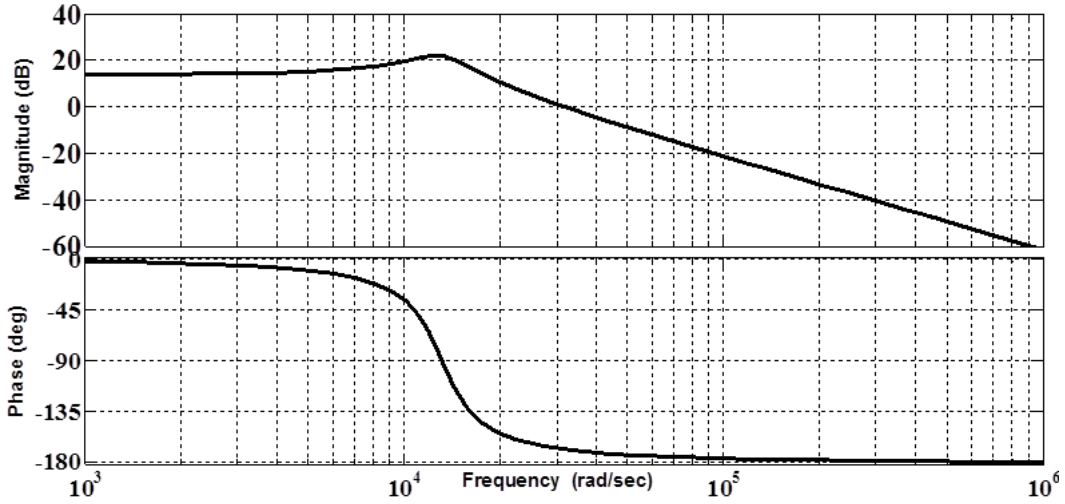

Figure 3.13: Frequency response of PV system with the Proposed ATAMPPT technique at STC

P&O (APO) can be seen in Fig.3.14 (a) and Fig.3.14 (b). Referring Fig.3.14 (a), it can be observed that the settling time of PV system with the proposed ATAMPPT is less than 0.04s whereas the settling times in case of APO, P&O and INC based MPPTs are 0.17s, 0.3s and 0.27s respectively (Fig.3.14 (b)). It can also be observed that there are voltage oscillations present in case of APO, P&O and INC based MPPTs as 1.5V, 2V and 2.4V respectively. But in case of the ATAMPPT, there is negligible voltage oscillation. For every change in solar radiation, reference voltage changes, hence PID-controller parameters have to be changed so that v_{ref} is tracked very accurately and effectively taking little tracking time as shown in Fig.3.15. This figure explains how effectively and quickly voltage of DC/DC converter is adjusted to vref with continuous variations in solar radiation between 500 W/m^2 and 1000 W/m^2 in every 40ms.

3.4.2 Real-time Simulation Results

The objective of conducting real-time simulation in this work is to verify the accuracy of the PV system output when using the real-time compensation of switching events. For proper verification of a controller that controls a converter, the real-time response of the converter is needed to be observed. The studied PV system consists of a solar panel, MPPT converter system with a controller and a load in which the effectiveness of the controller that we verified observing the load voltage. Hardware installation of all the components of the studied PV system is mimicked in real-time; the real-time responses are obtained by HIL simulation. In this paper, HIL simulation has been performed using an OPAL-RT simulator. The real-time results are obtained from the OPAL-RT output.

The controlled converter output voltage response from OPAL-RT is the real-time response of the proposed system due to its facilities for real-time computations. The layout of the

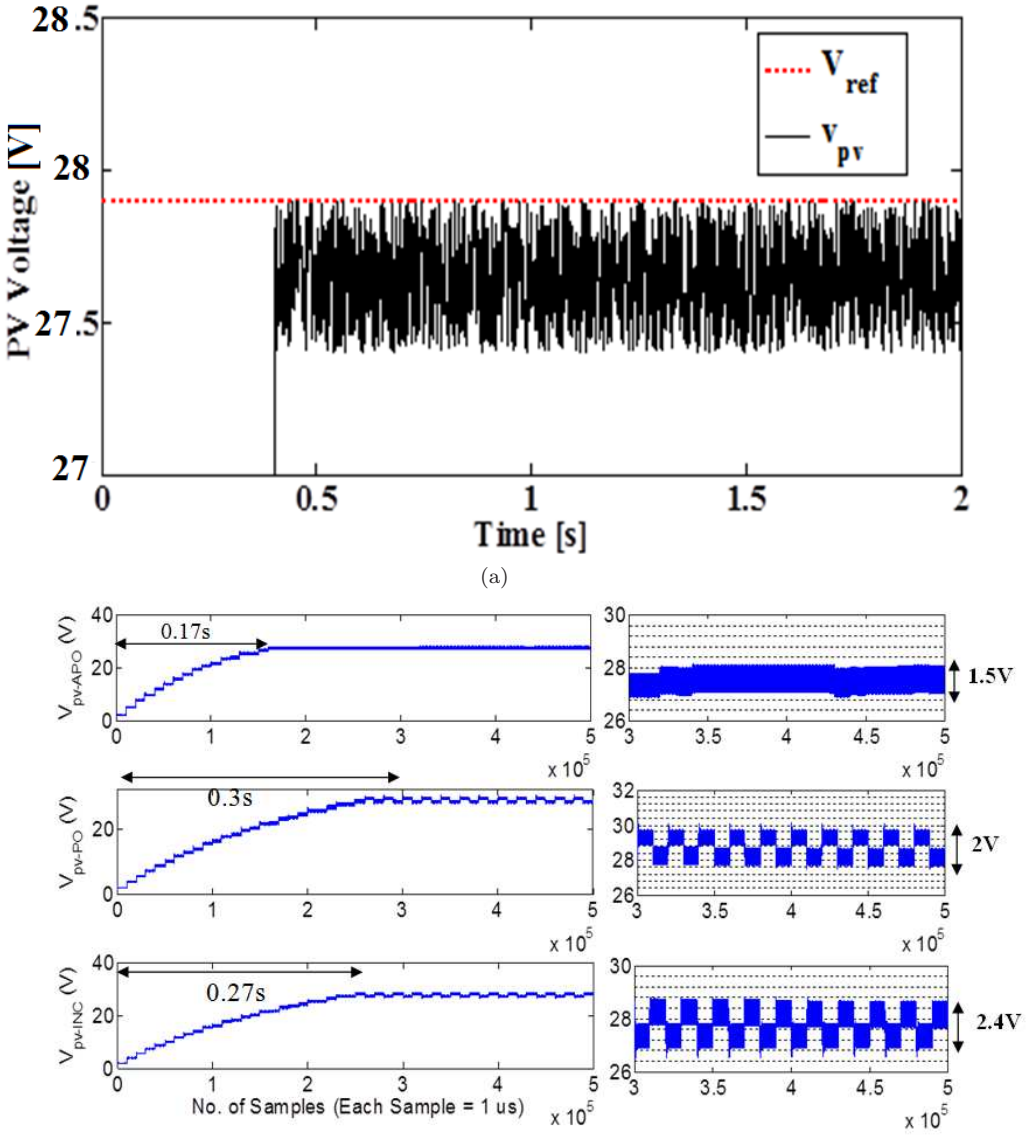

Figure 3.14: MPP Voltage tracking results of PV system with (a) proposed ATAMPPT and (b) APO, P&O and INC based MPPTs at STC

real-time HIL simulation set-up is shown in Fig.3.16.

The work-flow structure of the OPAL-RT simulator is shown in Fig.3.15. In this figure, XSG block enables users to generate custom, application specific models that can be implemented onto an FPGA device. The model of the PV system whose real-time response is needed first constructed in MATLAB/SIMULINK. The model created in SIMULINK has two subsystems such as master subsystem and console subsystem. In the master subsystem, the model to be simulated is kept whilst the console subsystem consists of scopes with outputs terminals for all the signals that are required to be observed. For obtaining its real-time output responses the output signals are linked to the Opal-RT simulator using

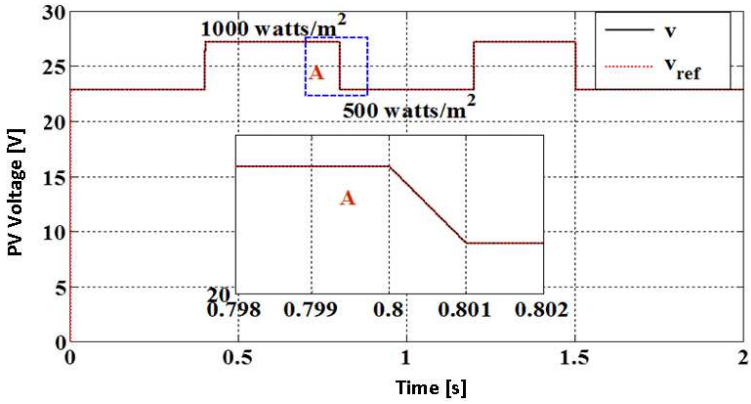

(a)

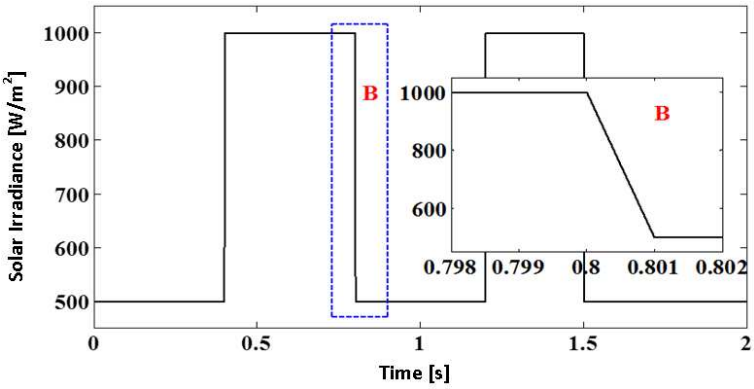

(b)

Figure 3.15: MPP Voltage tracking performances of PV system with (a) proposed ATAMPPT and (b) APO, P&O and INC based MPPTs at STC

an Op5142Ex1 Analog out block in master subsystem. In ordinary MATLAB/SIMULINK model, output terminals are directly connected to scopes to observe simulated results. But, in this real-time simulation between output terminals and scopes, a XILINK System Generator block is connected. The signal number in the XILINK System Generator block is set as same as number of output terminals. For C-code generation and compilation of the SIMULINK model, RT-LAB uses an established tool such as Real Time Workshop (RTW). The procedure of this real-time simulation consists of the following distinct steps.

- Construction of the tested model in discrete mode in MATLAB/SIMULINK
- Building the model
- Setting Hardware-in-Loop (HIL) option
- Selection of Red-Hat for code generation
- Loading the model
- Execution to obtain real-time outputs

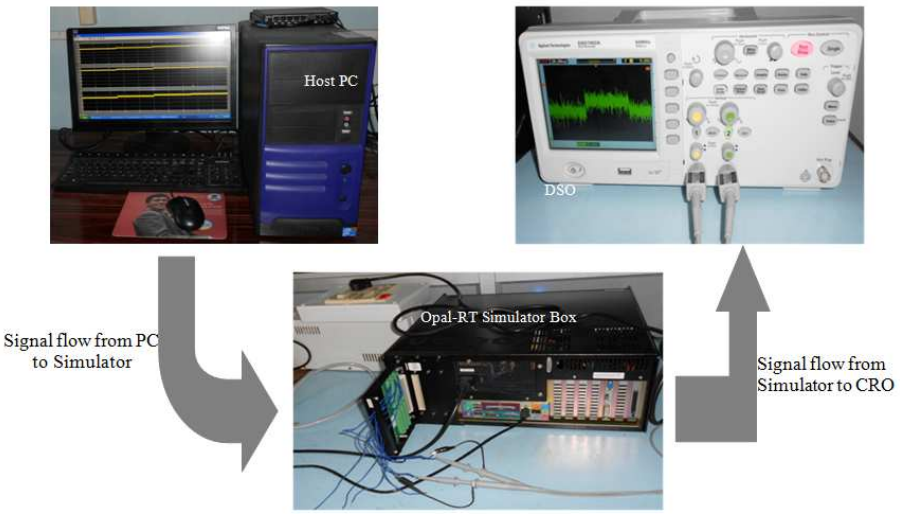

Figure 3.16: OPAL-RT Real-time Simulator Set-up

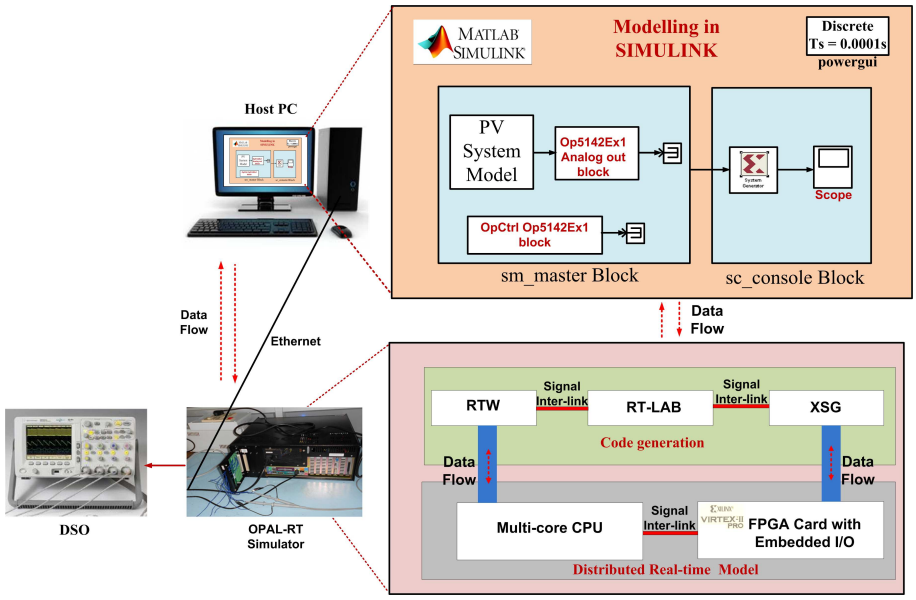

Figure 3.17: Work-Flow structure of OPAL-RT real-time Simulator

OPAL-RT simulator works in FPGA platform. A model is effectively run in OPAL-RT if it works in discrete domain. Hence, the proposed MPPT of the PV system has to be redesigned for discrete-domain domain. It should be noted that for facilitate FPGA implementation, the voltages and currents input to OPAL-RT simulator has been limited to one-tenth of their actual values. Fig.3.18 shows the real-time simulated tracking results such as PV current, voltage and dc-link voltage of the studied SSI-M6-205 PV system with the proposed ATAMPPT respectively. From this figure, the oscillations in of these real-time responses can be noted as 50mA in PV current, 30mV in PV voltage and 20mV in dc-link voltage respectively.

Fig.3.19 (a), (b) and (c) show the real-time simulated tracking results the same the studied

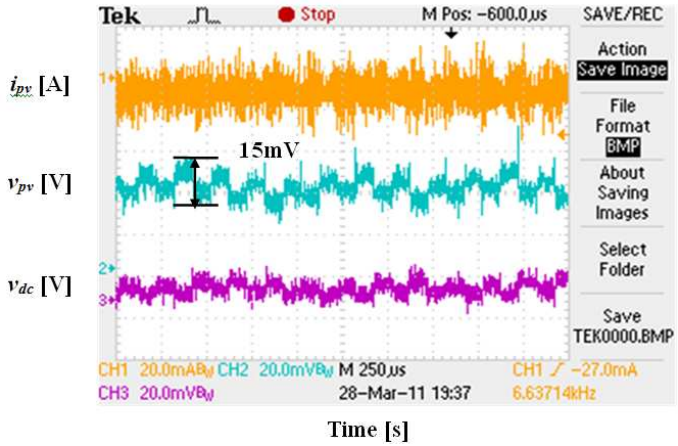

Figure 3.18: Real-time simulated MPP tracking results of the studied SSI-M6-205 PV system with the proposed ATAMPPT at STC

SSI-M6-205 PV system with APO-MPPT, P&O-MPPT and INC-MPPT respectively. From these figures, the oscillations in the PV voltages can be observed as 0.1V, 2V and 2.5V respectively.

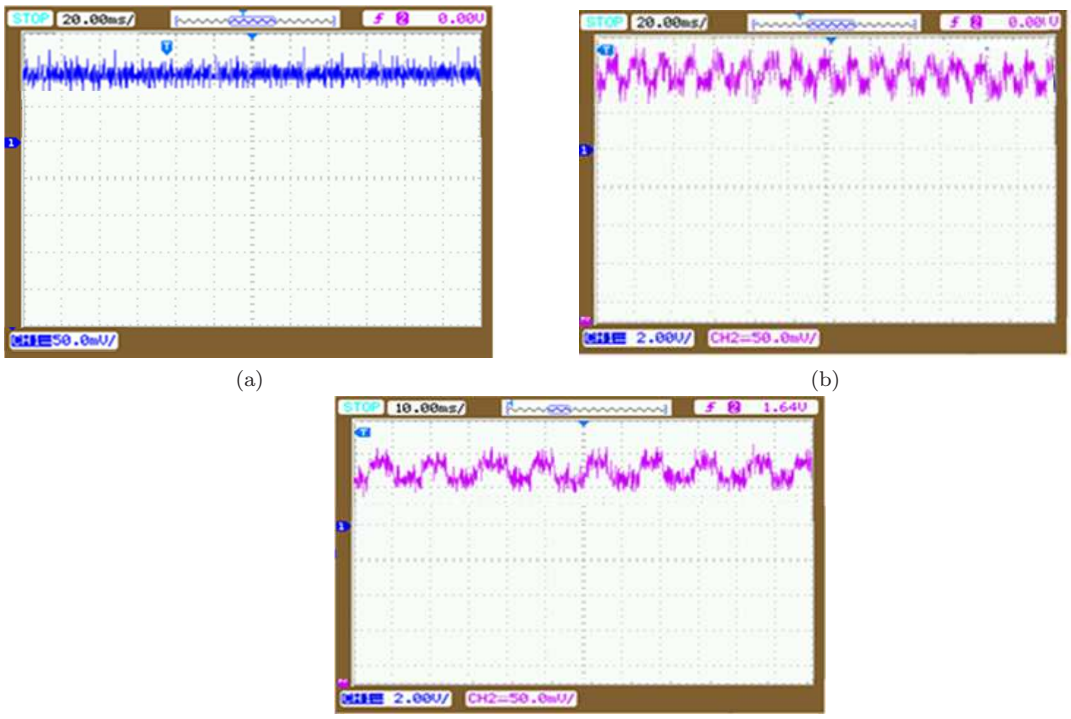

Figure 3.19: Real-time simulated MPP tracking results of the studied SSI-M6-205 PV system with (a) APO-MPPT, (b)P&O-MPPT and INC-MPPT at STC

Fig.3.20 shows comparisons of different simulated and real-time simulated MPP Tracking results such as output voltage of DC/DC boost converter at STC, input voltage for continuous step variation of solar irradiance from 500 W/m^2 to 1000 W/m^2 and output voltage for

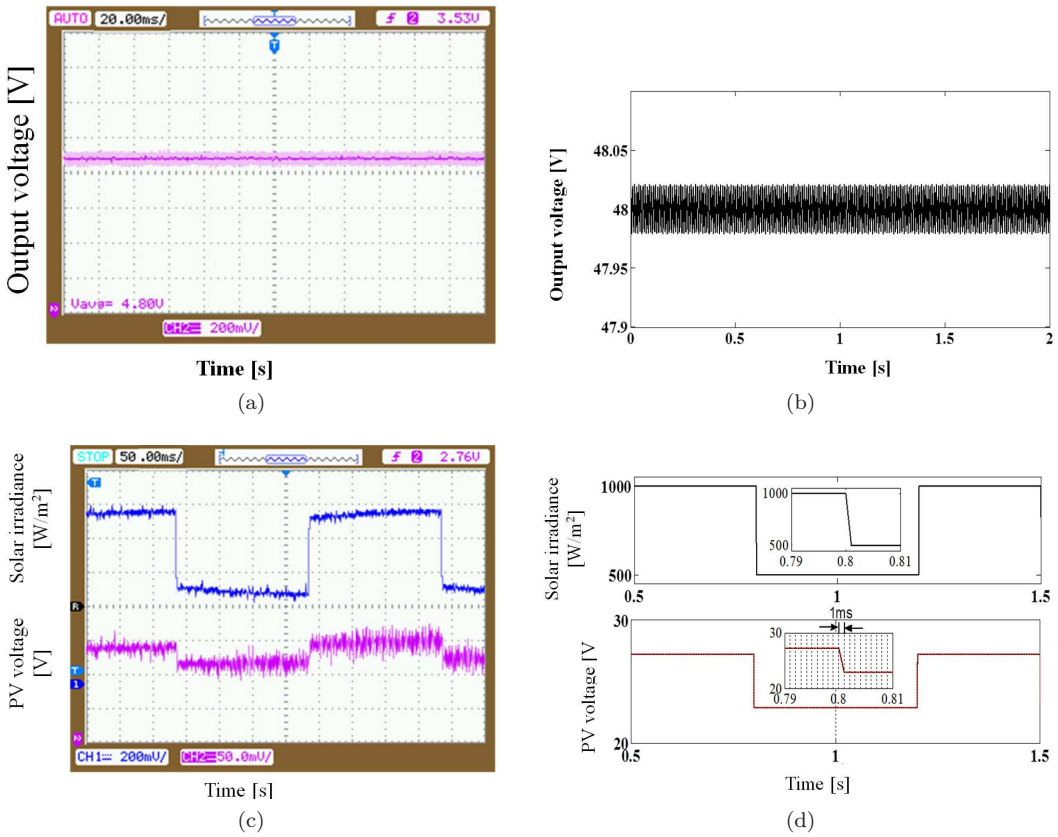

Figure 3.20: Different MPPT results of the PV system with the proposed ATAMPPT such as (a) real-time simulated output voltage and (b) simulated result of output voltage of DC/DC boost converter at STC, (c) real-time simulated PV voltage and (d) simulated PV voltage with continuous step variation of solar irradiance variation from 500W/m^2 to 1000W/m^2

step variation of solar irradiance from 500 W/m^2 to 1000 W/m^2 respectively. From these figures, it is confirmed that for every change in solar irradiance, the PV voltage v_{pv} is adjusted in around 2ms. The high frequency chattering during this variable weather condition has been maintained with in a limit i.e. 60mV. It can also be seen that for a step variation of solar irradiance from 500W/m^2 to 1000W/m^2 at 0.8s, the output voltage of DC/DC boost converter is again bounced back to 48V consuming only 2ms. Therefore, it is clear from the above results that the new ATAMPPT is performs efficiently performing for both MPPT and output voltage regulations.

Table 3.5: Components of Prototype PV System for MPPT Implementation

Component	Value
I_{sc} (A)	2.8
V_{oc} (V)	21.6
I_{mpp} (A)	2.2
V_{mpp} (V)	18.2
No. of Series Cells in each PV module	36
No. of series PV module in the PV array	5
No. of parallel PV module in the PV array	1
Inductance, L (mH)	5
Capacitance, C_1 (μF)	330
Capacitance, C_2 (μF)	580
Sampling time, T_s (μs)	1
Time interval of MPPT (s)	5
Current limit (A)	10
Voltage limit (V)	450
Load (Ω)	100

3.4.3 Experimental Results

The PV system is a stand-alone type. It consists of PV array, DC/DC boost converter, inverter, SPARTAN 3A FPGA board, signal conditioners (voltage and current sensors), personal computer and a board with analog filtering circuits. Fig.3.21 (a) shows the PV array where five PV modules are connected in series. Fig. 3.21 (b) shows the photograph of the prototype experimental set-up of the PV system and Fig. 3.21 (c) demonstrates the block diagram of the above system. The components of this PV system are shown in Table 3.5. The photograph of the FPGA board used in this work is shown in Fig.3.22 demonstrating names of all its components.

In this PV system experimental set-up, the Spartan-3A DSP Trainer Kit (Fig.3.22) has been used for FPGA control implementations [26]. In this work, instead of using costly and delicate pyranometer, solar irradiance has been estimated by using a simple and cheap indirect method. In this method, solar irradiance (G) is calculated from data of environmental temperature (T_{env}) and PV panel temperature (T_{pv}) as follows.

$$G = \frac{(T_{pv} - T_{env}) \times 800W/m^2}{(T_{NOCT} - 20)} \tag{3.34}$$

where (T_{NOCT}) is the nominal operating PV cell temperature (NOCT) = 45^0C. NOCT is the PV cell temperature measured under open-circuit when the ambient temperature, solar irradiance and wind speed are 20^0C, 800W/m^2 and 1m/s respectively.

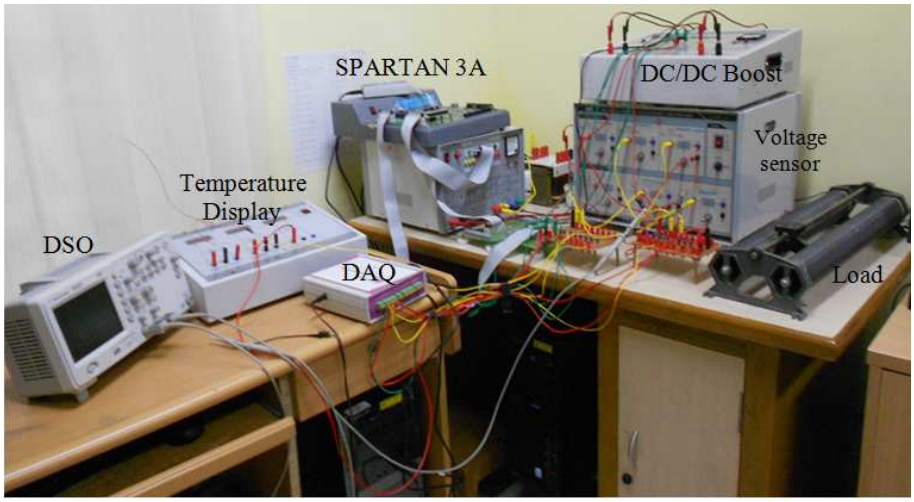

(a)

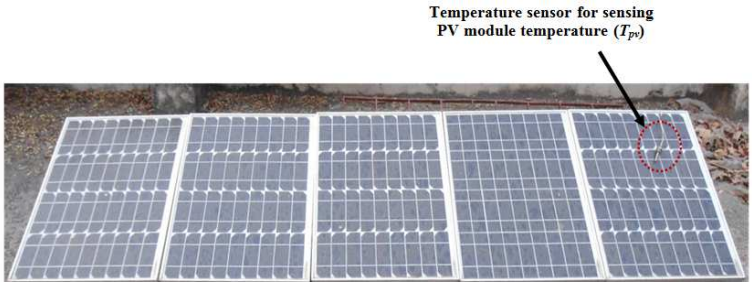

(b)

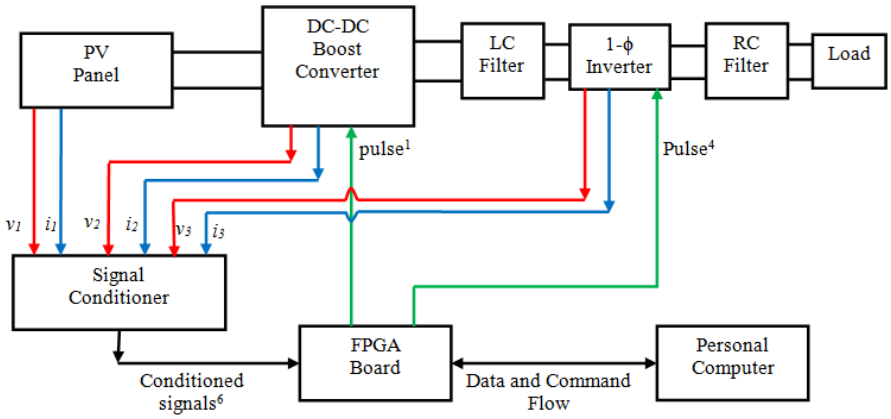

(c)

Figure 3.21: (a) PV Modules, (b) Photograph of PV system prototype and (c) Complete block diagram of the above PV system prototype

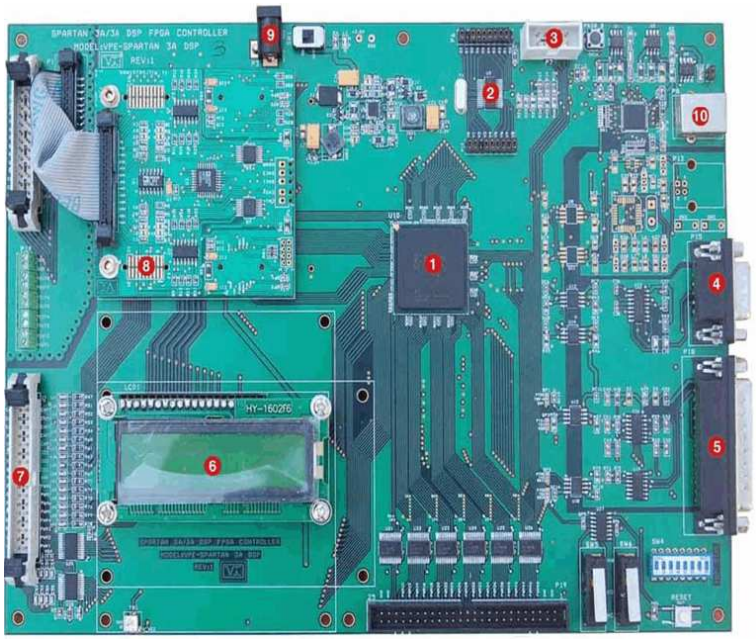

Figure 3.22: Spartan-3A DSP Trainer Kit with following components such as (1) SPARTAN-3A DSP Processor, (2) PLL Clock Setting, (3) JTAG Connector, (4) RS232 Serial Port, (5) Parallel Port, (6) LCD Display, (7) PWM Connector, (8) SDA Bus Connector, (9) Power Supply and (10) USB

3.4.4 System Architecture

For FPGA implementation, the system architecture of the control structure of the given PV system prototype is shown in Fig.3.23.

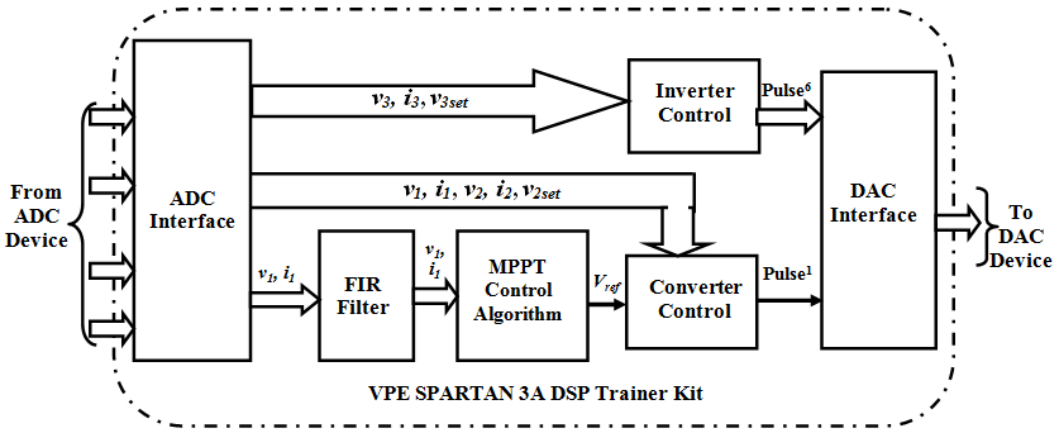

Figure 3.23: System Architecture of PV system controller

3.4.5 FPGA Simulation Results

The project status for implementation of the proposed controller in FPGA is shown in Fig.3.24. FPGA simulation results of the given PV system prototype are shown in Fig.3.25. From Fig.3.25 (a), it can be seen that time period (T) and OFF period (T_{OFF}) of the

CONV_INV Project Status (04/29/2013 - 16:31:08)			
Project File:	PULSE_PATTERN.xise	**Parser Errors:**	No Errors
Module Name:	CONV_INV	**Implementation State:**	Programming File Generated
Target Device:	xa3sd1800a-4fgg676	**•Errors:**	No Errors
Product Version:	ISE 12.1	**•Warnings:**	1256 Warnings (31 new)
Design Goal:	Balanced	**•Routing Results:**	All Signals Completely Routed
Design Strategy:	Xilinx Default (unlocked)	**•Timing Constraints:**	All Constraints Met
Environment:	System Settings	**•Final Timing Score:**	0 (Timing Report)

Figure 3.24: Simulation results from VPE SPARTAN 3A FPGA

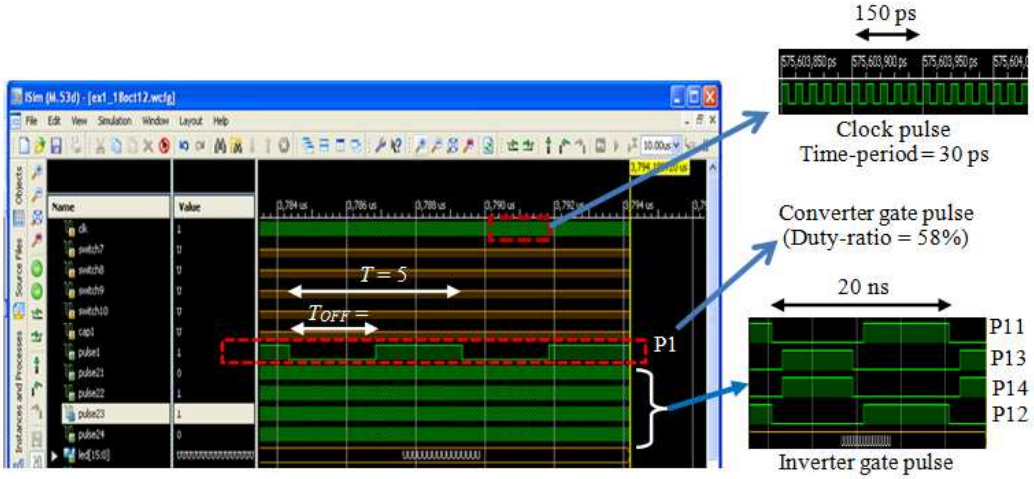

(a)

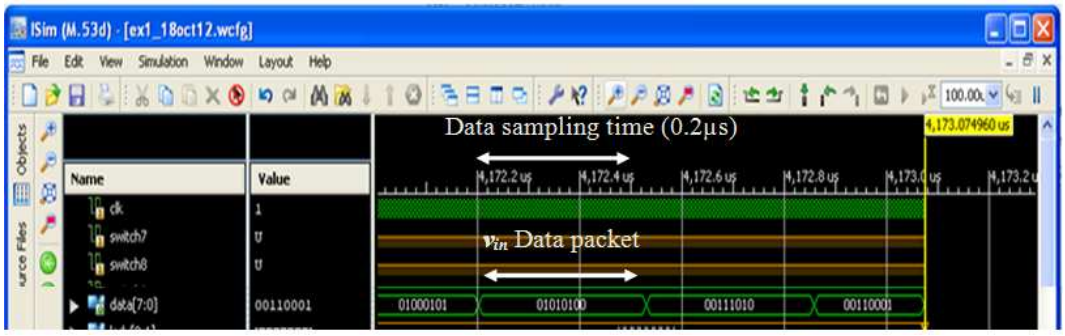

(b)

Figure 3.25: Simulation results from VPE SPARTAN 3A FPGA

converter gate pulse are 5s and 2.1s respectively. Hence, the duty-ratio of this pulse is 58% . Fig.3.25 (b) shows the data sampling time (0.2s) and flow of the PV panel voltage v_{pv} data packets.

3.4.6 System Architecture Synthesis

After modeling all blocks of the system architecture of PV system shown in Fig.3.23, the blocks are required to be synthesized. Functional performance of each of these blocks can be represented by their respective number of lines of VHDL codes, number of logic elements used and percentage utilization of the FPGA device to construct these blocks. System architecture synthesis performances of all the above blocks for the proposed ADAMPPT are shown in Table 3.6. The SPARTAN 3A FPGA used in this work contains 16,640 logic elements. Out of which only 4262 logic elements has been used for implementation of ADAMPPT. Hence, the device utilization is only 25%. In this table, the component BUFGMUX is usually used in Spartan-3, Spartan-3E and Spartan-3A devices. It represents a multiplexed global clock buffer that can be selected between two input clocks say I_0 and I_1. When the selected input (S) is Low, the signal on I_0 is selected for output (O) whilst when the selected input (S) is High, the signal on I_1 is selected for output (O) (Source: XACT Libraries Guide, Xilinx Corporation, 2001).

Table 3.6: Device Utilization Summary

Name of Block	Available	Used	Utilization (%)
Number of Slice Flip flops	33,280	2678	8
Number of 4 input Look-up Tables (LUTs)	33280	4309	12
Number of occupied Slices for logic	16640	4262	25
Total Number of 4 input LUTs	33280	5666	17
Number of bonded Input/ Output Blocks (IOBs)	519	36	6
Number of BUFGMUXs	24	2	8
NNumber of DSP48As	84	13	15
Total	117107	16966	14.5

Fig.3.26 shows comparison between the experimentally obtained and the simulated MPP tracking performances of the prototype PV system with proposed ATAMPPT. In this case, T_{pv} and T_{env} are recorded as 46^0C and 32^0C respectively. Hence, the solar irradiance can be calculated as 448W/m^2 using eq (3.34). From Fig.3.26 (a) and (b), the PV voltage is 48.9V with negligible MPPT error (V_{ref} - v_{pv}). Similarly, Fig.3.26 (c) and (d) show the simulated and experimental gate pulse of the converter for same environmental condition. It can be seen that the duty-ratio of the gate-pulse is 58% for both simulation and experiment. It can be observed that the gate-pulse validates the FPGA result as shown in Fig.3.25 (a).

MPP tracking results PV system with P&O MPPT and ATAMPPT are shown in Fig.3.27 and Fig.3.28. Fig.3.27 (a) shows simulated MPP tracking results such as PV voltage and

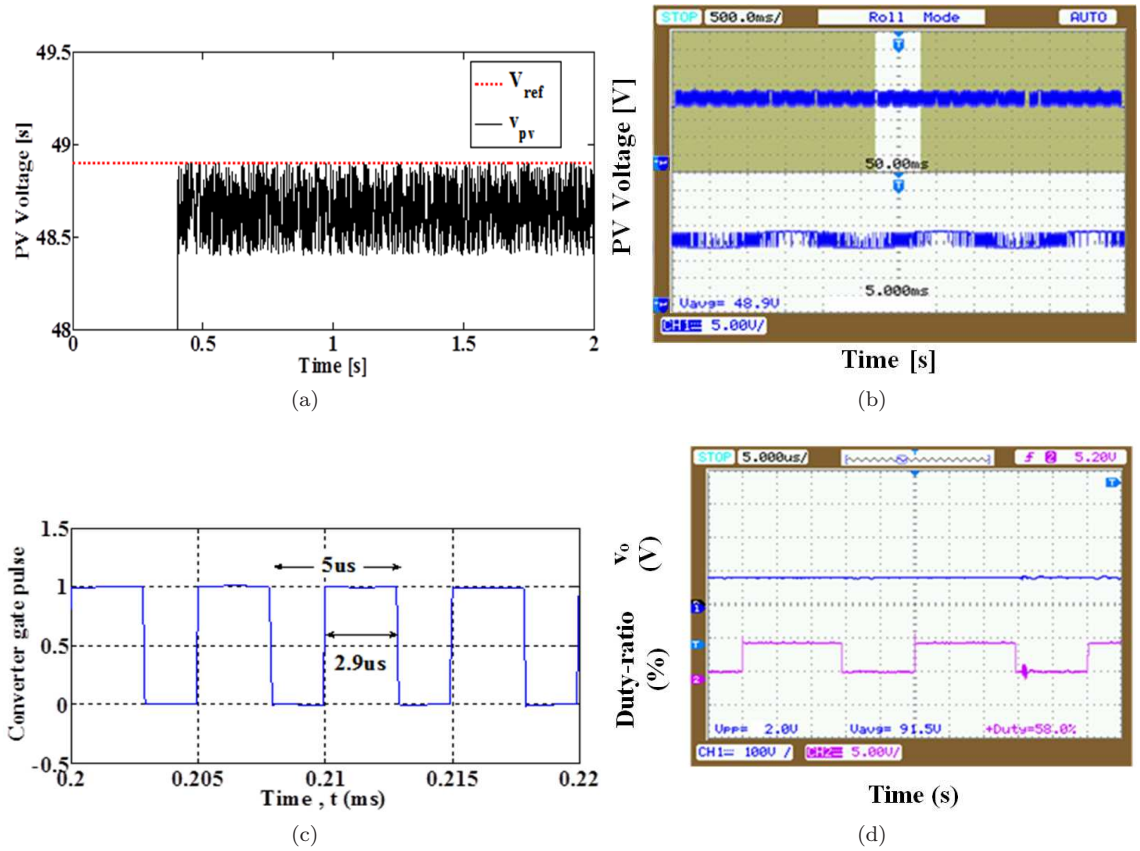

Figure 3.26: (a) Simulated PV voltage, (b) experimental PV voltage, (c) simulated converter gate pulse and (d) experimental converter gate pulse for solar irradiance of 448W/m^2

PV current of PV system with P&O-MPPT. It can be seen in this figure that PV current is changing from 0A to 2.2A taking around 0.7ms and then oscillates around 2.2A. During that period PV voltage changes from 109V to 91V and oscillates around that 91V. Fig.3.27(b) shows experimental result displaying the tracking voltage of PV system with P&O MPPT. In this figure, A denotes the point when MPPT is made ON and MPP tracking was started. Time between A and B was the MPP tracking period. After B, voltage of PV system settled at MPP voltage. It is found that tracking periods is 0.8s and voltage fluctuation at steady-state is 8V.

Similarly, Fig.3.28(a) shows simulated MPP tracking results such as PV voltage and PV current of PV system with ATAMPPT. It can be seen in this figure that PV current is changing from 0A to 2.2A taking around 0.18ms and then oscillates around 2.2A. During that period PV voltage changes from 109V to 91V and oscillates around that 91V. Fig.3.28 (b) shows experimental result of tracking voltage of PV system with ATAMPPT. It is found that tracking periods in case of ATAMPPT is 1.5s and voltage fluctuation at steady-state is 5V.

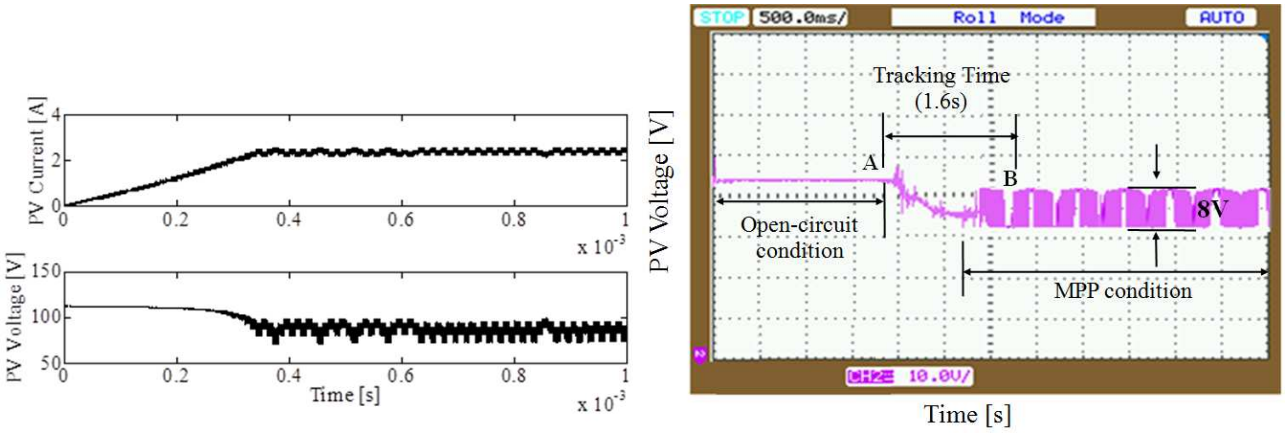

(a) (b)

Figure 3.27: MPP tracking results of prototype PV system showing (a) Simulated PV voltage and (b) Experimentally obtained PV voltage varied from open-circuit voltage to MPP voltage with P&O-MPPT (scales: x-axis 0.5s/div and y-axis 10V/div)

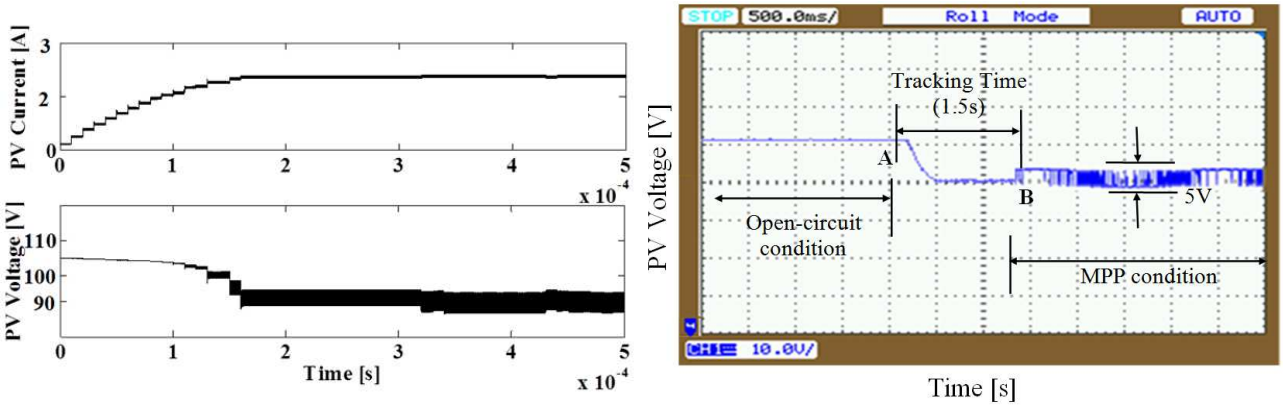

(a) (b)

Figure 3.28: (MPP tracking results of prototype PV system showing (a) Simulated PV voltage and (b) Experimentally obtained PV voltage varied from open-circuit voltage to MPP voltage with ATAMPPT (scales: x-axis 0.5s/div and y-axis 10V/div)

3.5 Chapter Summary

A new adaptive MPPT based on an auto-tuning technique called ATAMPPT is proposed in this paper for PV systems and its effectiveness are verified. The proposed MPPT tracking method can estimate the MPPs of a PV system on-line using a RLS based system identifier and a NRM technique. The ATAMPPT is compared with three existing MPPTs such as P&O, INC and APO. Simulation in MATLAB/SIMULINK, real-time simulation in OPAL-RT and experimental results using the prototype set-up are presented to validate the efficacy of this proposed approach. This auto-tuning takes place on-line and uses the on-line estimated MPPs of the PV panel. The simulation and experimental results clearly demonstrate that the new on-line auto-tuned PID-controller provides effective tracking of MPP so that maximum power can be extracted from the PV panel as well as regulates the load voltage fixed at different weather conditions.

Chapter 4

Adaptive Predictive Error Filter based MPPT for Photovoltaic Power Harvesting Application

4.1 Introduction

This chapter presents a new MPPT designed with adaptive predictive error filter based control concept. In a PV system, MPPT is employed to estimate maximum power point (MPP) voltage. A number of MPPT algorithms such as P&O, INC, P&O with adaptive perturb size etc. are proposed and implemented for PV applications [82], [49] and [48]. But one measure concern in using these MPPT algorithms is that the estimated MPP usually fluctuates around the actual reference MPP voltage depending on the perturbation size [94]. Therefore, the PV voltage v_{pv} fluctuates and needs to be adjusted such that it should be equal to MPP voltage using a DC/DC boost converter.

MPPT with an adaptive PID-controller can handle the wider range of uncertainties in the PV system and provides dynamic responses quickly by on-line tuning of the controller parameters during variations in environmental conditions [95]. The Adaptive Auto-Tuned MPPT (ATAMPPT) described in Chapter 3 uses a system identification approach to estimate the plant (PV + DC/DC boost converter) parameters and then update the controller parameters using the estimated plant parameters. Design and operation of such MPPT requires accurate estimation of plant parameters in a short period hence may be inappropriate in handling quick weather variations. Further, this ATAMPPT do not consider external disturbances. Therefore, the objective of this Chapter is to design a controller that should handle these internal uncertainties or external disturbances and hence the voltage fluctuation in v_{pv} can be reduced. Therefore, it is essential for designing a controller to harvest maximum available power in a PV system. A filter reshapes the input signal according to

some specific rules to generate an output signal.

An adaptive filter is a digital filter that changes its characteristics (frequency response) automatically by optimizing its internal parameters. In a linear adaptive filter, the adaptation algorithm follows the principle of superposition [96]. Adaptive linear finite impulse response (FIR) filters are very popular because they are easy to analyze and implement [97].

In case of prediction error filter (PEF) used in controlling a switching converter, future control variable of the converter can be derived from the past and present values of converter state variables (load voltage, inductor current, etc.) and control signal (u). In an adaptive prediction error filter (APEF), the filter parameters are set in such as a way that an objective function involving the desired signal is minimized [98], [21]. An APEF controller is usually constructed using one of the following adaptation approaches such as Weiner filter theory or Recursive least square (RLS) theory. Weiner filter theory is based on stochastic frame work as the optimum set of co-efficients of the linear filter is obtained by minimization of its mean-square-error (MSE). APEFC with Least-mean-square (LMS) algorithm is based on this Weiner filter theory. LMS algorithm is always the first choice in APEFC as it is easy for implementing its weight adaptation [99].

Although LMS algorithm has a simple structure but its main disadvantage is its slow convergence in case of large range of eigen value of the regressor covariance matrix [100]. A number of modified LMS algorithms are available in literature that can improve the performance of the original LMS algorithm by alleviating this slow convergence problem. The slow convergence problem has been solved by varying the LMS step-size with a step-size adaptation rule [11]. Different modified LMS algorithms have been proposed and implemented in signal processing applications such as Normalized LMS (NLMS) [101], Variable Step-size LMS (VSLMS), Correlation based Variable Step-size LMS (CVSLMS), Robust Correlation based Variable Step-size LMS (RCVSLMS), Gradient Adaptive-Step-size LMS (GA-SLMS) and Gradient Adaptive-Limited Step-size LMS (GA-LSLMS).

In [102], a comparison of VSLMS, CVSLMS, RCVSLMS and GA-LSLMS has been made and it is observed that GA-LSLMS is better than LMS algorithms in terms of low steady-state error and good tracking performance in presence of noise terms. Although these modified LMS algorithms are found to be better than LMS algorithms in terms of faster convergence rate and low steady-state error but becomes expensive owing to the cost of additional computational complexities [103]. The RLS algorithm is deterministic in nature. Using this algorithm, the filter coefficients are determined recursively by minimizing a weighted linear least squares cost function relating to the input signals. RLS algorithm is better than that of all LMS based algorithms with respect to quick convergence, self orthogonalyzing and less tracking error characteristics [104].

The conventional RLS-APEF controller is similar to a PD-controller. Hence, the response

time of this controller is found to be slow. By simply adding an integral-term to this RLS-APEF controller, the tracking speed can be increased and hence tracking time is reduced [98]. However, the above RLS-APEF controller algorithm uses a constant forgetting factor. It experiences slow convergence for variable tracking time-varying parameters [105]. Therefore, in this chapter a new RLS-APEFC controller has been proposed with variable forgetting factor for MPPT of a PV system. The predictive PID-controller of this MPPT suppresses voltage fluctuation better than that of a PID-controller. The PEF part of this MPPT handles the uncertainties in the PV system dynamics and reduces the effect of external disturbances such as sudden change in input solar irradiance [19].

The proposed APEF-MPPT adapts its own control parameters on-line with every change in the weather condition. Unlike most of the existing MPPTs [106], [48], [49], this MPPT is designed to perform both MPP tracking and filtering of voltage fluctuation. Hence, this MPPT can be applied directly to a PV system without any additional controller or filter. This new MPPT has following merits (i) fast response, (ii) robust and stable operation, (iii) can handle wide range of MPP, (iv) less computational complexity and (v) efficient with negligible tracking error.

4.2 Review on Adaptive Filter based Controller

4.2.1 Adaptive Filter

An adaptive system automatically adjusts or adapts to a variable environmental condition. It can be trained for some filtering or decision making performances. It performs using adaptive algorithms for adjustment of parameters of a system which needs to be adjusted. The adaptation is called open-loop adaptation if measurements of the input signal and environmental condition parameters are made. Applying the information of input signal and environmental condition for a finite period, an algorithm is formulated that is used to set the adjustment manually. A closed-loop adaptation is formulated considering output of the system.

A filter is a device or a system that processes or reshapes the input signal according to some specific rules to generate an output signal. A linear filter has a linear relationship between its input and output. This means that input and output of the filter follow the principle of superposition. A nonlinear filter has a nonlinear relationship between its input and output.

An adaptive filter is a digital filter that changes its characteristics (frequency response) automatically by optimizing its internal parameters. In a linear adaptive filter, the adaptation algorithm follows the principle of superposition whilst adaptive algorithm used a nonlinear adaptive principle in a nonlinear adaptive filter. For selection of parameters of the filter, an optimization performance function is used. According to optimization performance function

used, linear adaptive filters are of two types such as Finite impulse response (FIR) filter and Infinite impulse response (IIR) filter. FIR filter has a non-recursive structure whereas IIR filter has a recursive filter. Adaptive linear FIR filters are very popular because of ease in their analysis and implementation.

In filters, the following adaptation approaches are usually used such as Weiner filter theory, Recursive least square (RLS) theory and adaptive algorithm. The optimum set of co-efficient of the linear filter is obtained by minimization of its mean-square-error (MSE). Here, the performance index is the sum of the weighed error square for the given data. In an adaptive algorithm, the filter parameters are set in such as a way that an objective function involving the desired signal is minimized for example Newtons algorithm. Newtons algorithm suffers from singularity problem if the initial conditions are not properly chosen. LMS and RLS algorithms do not have such problems [98].

4.2.2 LMS based Predictive Error Filter (LMS-PEF)

LMS algorithm has been introduced by [107]. Since then this algorithm is well received in different problems due to its simplicity. The LMS algorithm is described in Table 4.1 and Fig.4.1.

4.2.3 Modified LMS with Adaptive Step-size Algorithms

Some modified LMS algorithms are available in literature that can improve the performance of the original LMS algorithm by solving this slow convergence problem. Using these algo-

Table 4.1: LMS algorithm

Input:
input signal samples $\{x(1), \quad x(2), \quad x(3), \quad ...\}$ reference signal r samples of control signal $\{u(1), \quad u(2), \quad u(3), \quad ...\}$ LMS step-size μ
Initialize:
weight $\omega(0) = 0$, Output error $e(0) = 1$
Computation:
for $k = 0, 1, 2, 3, ..., k_{\max}$ If $\lvert e(k)\rvert \leq \rho$: ρ is a very small positive number say (0.001) break Read a new data pair $[x(k), u(k)]$
Output error:
$e(k) = r - x(k)$
Reference error:
$\hat{e}(k) = e(k) + w(k)\, e(k-1)$
Weight adaptation:
$\Delta\omega(k) = \mu u(k)\, e(k)$; μ is fixed $\omega(k+1) = \omega(k) + \Delta\omega(k)$ end

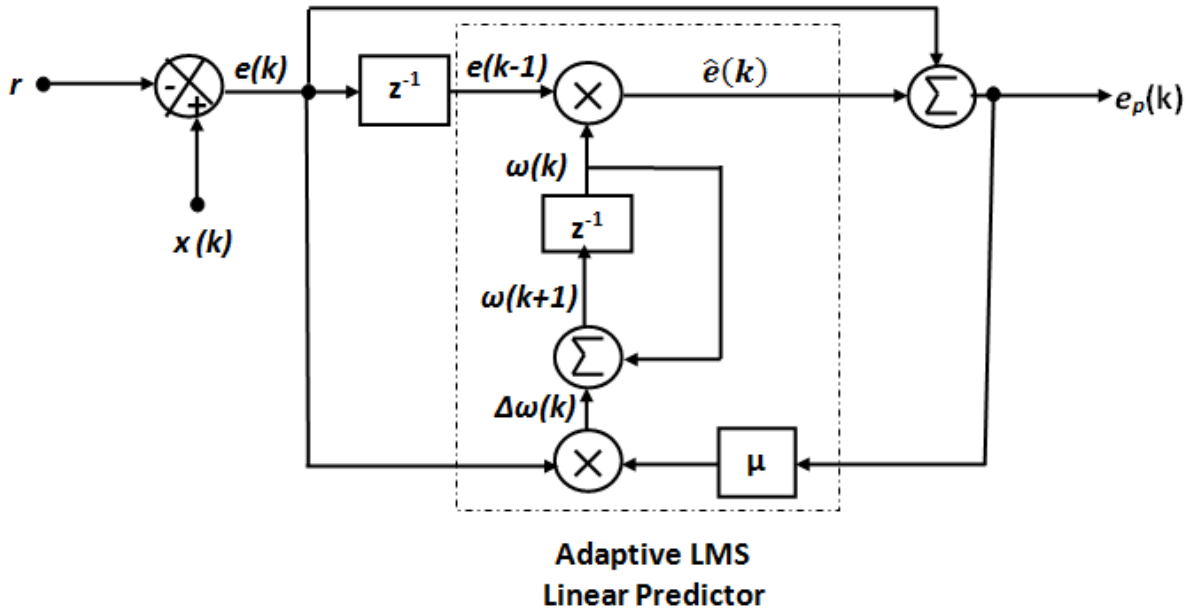

Figure 4.1: LMS-PEF Algorithm

rithms, the slow convergence problem is solved by varying the LMS step-size with a step-size adaptation rule (Fig.4.2).

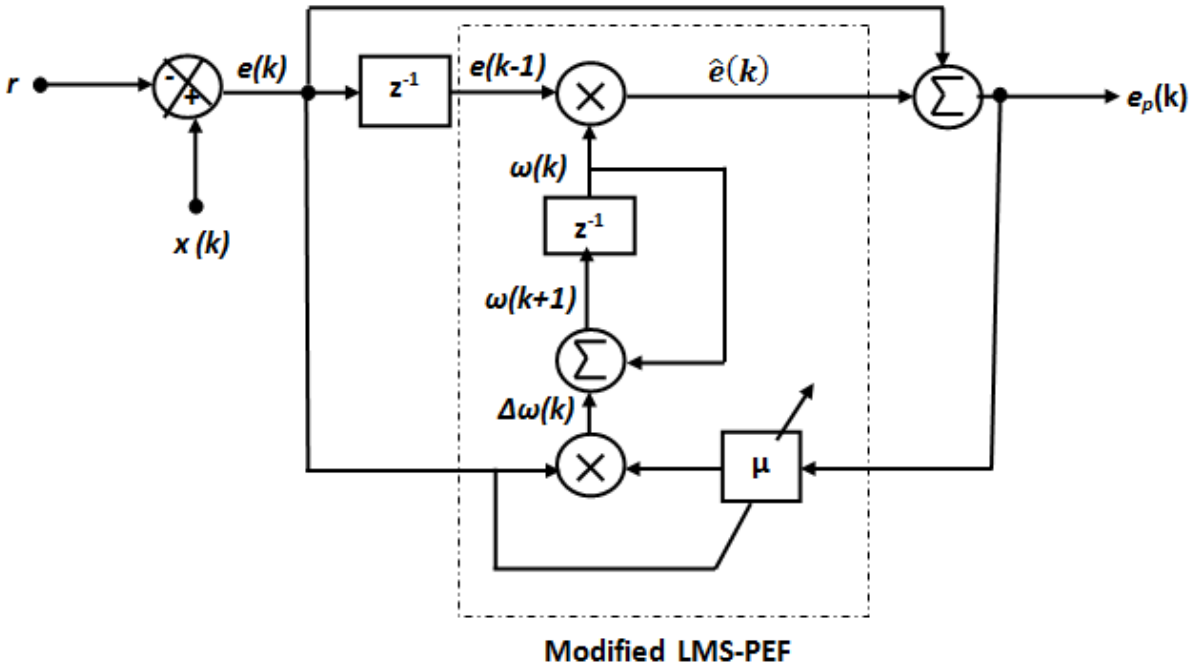

Figure 4.2: Modified LMS-PEF Algorithm

Table 4.2: Different Modified LMS-PEFs with Different Step-Size Adaptation Rule

1	Normalized LMS (NLMS) [13]
Algorithm:	$\mu = \frac{\alpha}{x^T x+\sigma}$ where $X = \begin{bmatrix} x(k) & x(k-1) & \dots & x(k-m) \end{bmatrix}^T$ α is a convergence factor such that $0 < \alpha < 2$ and σ is a small number to avoid very large step-size
Remarks:	-Independent of signal scaling and Converges faster than LMS - Complexity is slightly higher than LMS and α and σ are fixed
2	Variable Step-size LMS (VSLMS) [14]
Algorithm:	$\mu(k+1) = \begin{cases} \mu_{\max}; & if \mu'(k+1) > \mu_{\max} \\ \mu_{\min}; & if \mu'(k+1) < \mu_{\min} \\ \mu'(k+1) & otherwise \end{cases}$ where $0 < \mu_{\min} < \mu_{\max}$; $\mu_{\max} \leq \frac{2}{3Trace(R)}$ such as R is auto-correlation matrix of input PV voltages; $\mu'(k+1) = \alpha\mu(k) + \delta\|e(k)\|^2$; $e(k)$ is k^{th} sample of output error as defined in Fig.5.2 and Design parameters α and δ are defined as $0 < \alpha < 1, \quad \delta < 1$
Remarks:	-Sensitive to noise
3	Correlation based Variable Step-size LMS (CVSLMS) [15]
Algorithm:	$\mu(k+1) = \alpha\mu(k) + \delta\|e'(k)\|^2$ where $e'(k)$ is error auto-correlation estimate such as $e'(k) = \beta e(k-1) + (1-\beta)e(k-1)$; $0 < \alpha < 1; \quad 0 < \beta < 1; \quad \delta < 1$
Remarks:	(a) Rejects the effects of un-correlated noise during step-size up dation (b) At first $\|e'(k)\|^2$ is large, so $\mu(k)$ is large. (c) Near optimum, $\|e'(k)\|^2$ become smaller, so $\mu(k)$ is reduced. (d) Results in smaller step-size after convergence. Requires large steps to reach steady-state.
4	Robust Correlation based Variable Step-size LMS (RCVSLMS) [16]
Algorithm	$\mu(k+1) = \alpha\mu(k) + \delta\|e'(k)\|^2$ where $e'(k)$ is error auto-correlation estimate such as $e'(k) = \beta e(k-1) + (1-\beta)e(k)\{e(k-1) + e(k)\}$ $0 < \alpha < 1; \quad 0 < \beta < 1; \quad \delta < 1$; $\mu_{\min} < \mu < \mu_{\max}$; $\mu_{\max} = 0.01$ and $\mu_{\max} = 0.001$
Remarks:	-Low steady-state error and residual MSE than NLMS -Improved system performance and slower convergence rate than NLMS
5	Gradient Adaptive Step-size LMS (GASLMS) [17]
Algorithm:	$\mu(k) = \mu(k-1) + \frac{\rho}{2}e(k)e(k-1)X^T(k-1)X(k)$ where ρ is a small positive constant = 0.001 $e'(k) = \beta e(k-1) + (1-\beta)e(k)\{e(k-1) + e(k)\}$ $0 < \beta < 1$; $\mu_{\min} < \mu < \mu_{\max}$; $\mu_{\max} \leq \frac{2Trace(R)}{3}$
Remarks:	Less complex and Fast convergence rate than NLMS as divisible terms not present in algorithm Low steady-state error and residual MSE than RCVSLMS Probability of instability in μ if noise terms is present
6	Gradient Adaptive Limited Step-size LMS (GALSLMS) [18]
Algorithm:	$\mu(k) = \mu(k-1) + \Delta\mu(k)$; where $\Delta\mu(k) = \begin{cases} \alpha\mu(k-1); & for \Delta\beta(k) > \alpha\mu(k-1) \\ -\beta\mu(k-1); & for \Delta\beta(k) < \beta\mu(k-1) \\ \Delta\beta(k); & otherwise \end{cases}$ $\Delta\beta(k) = \rho e(k)e(k-1)X^T(k-1)X(k)$ $\alpha = \eta\mu(k-1); \quad \beta = \theta\mu(k-1)$; η and θ are positive constants
Remarks	α and β are large when $\mu(k-1)$ is large and small $\mu(k-1)$ is small Has limit on value of $\Delta\mu(k)$ Better performance than GASLMS even in presence of noise term

These modified LMS algorithms with their step-size adaptation rule and performance characteristics are given in Table 4.2 for which it is observed that GALSLMS is better among these modified LMS algorithms in terms of faster convergence rate, Low steady-state error and residual MSE and performance with noise terms. But, it is also observed that although these modified LMS algorithms are better than LMS algorithm with respect to slow convergence problem and accuracy but at the price of additional complexity [105]. RLS algorithm has good convergence speed and weight updation efficacy.

4.2.4 RLS-PEF Algorithm

The RLS algorithm is a deterministic algorithm which recursively finds the filter coefficients by minimizing a weighted linear least squares cost function relating to the input signals. This differs from the LMS algorithm in the sense that the later aims to reduce the mean square error (MSE). Table 4.3 and Fig.4.3 describe the RLS-PEF algorithm.

Table 4.3: RLS algorithm

Input:
input signal samples $\left\{x(1), \quad x(2), \quad x(3), \quad ...\right\}$ reference signal r samples of control signal $\left\{u(1), \quad u(2), \quad u(3), \quad ...\right\}$ LMS step-size μ
Initialize:
weight $\omega(0) = 0$, Output error $e(0) = 1$
Computation:
for $k = 0, 1, 2, 3, ..., k_{\max}$ If $\lvert e(k)\rvert \leq \rho$ where ρ is a very small positive number say (0.001) break Read a new data pair $[x(k), u(k)]$ Output error: $e(k) = r - x(k)$ Reference error: $\hat{e}(k) = e(k) + w(k)\, e(k-1)$ Prediction error: $e_p(k) = e(k) + \hat{e}(k)$ Kalman gain: $g(k) = \frac{P(k-1)x(k)}{\lambda + x(k)^T P(k-1) x(k)}$ Co-variance matrix: $P(k) = \frac{P(k-1) - g(k)x(k)^T P(k-1)}{\lambda}$ Weight adaptation: $\omega(k) = \omega(k-1) + e_p(k)\, g(k)$ end

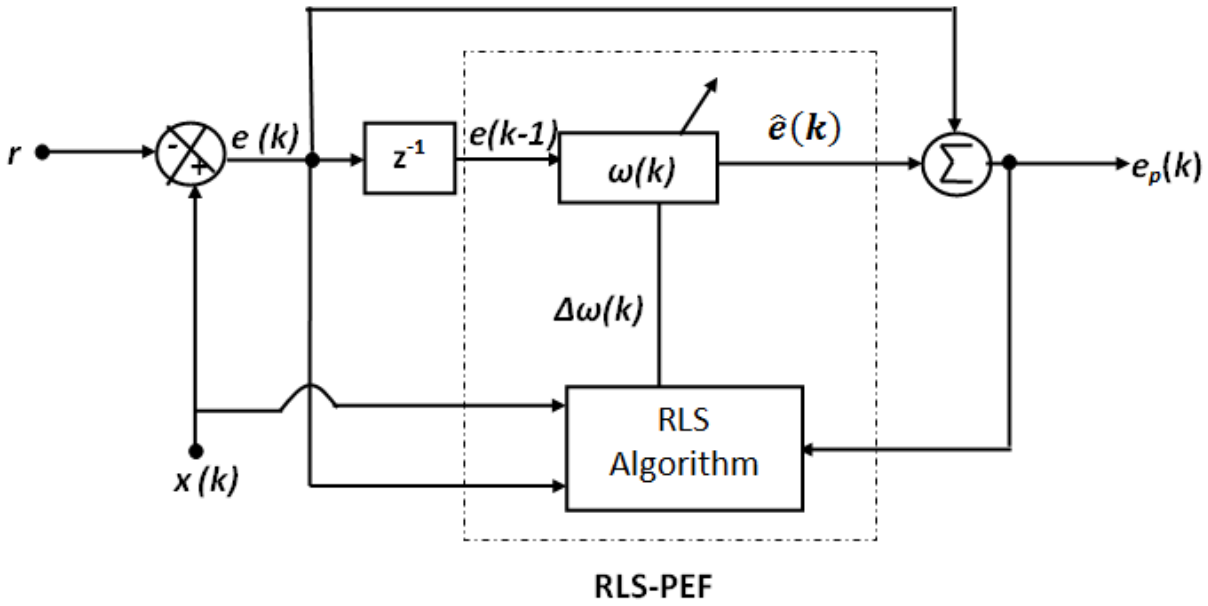

Figure 4.3: RLS-PEF Algorithm

4.3 Proposed RLS-APEFC for MPP Tracking of PV System

The studied PV system is a stand-alone energy conversion as shown in Fig.4.4(a). It consists of PV arrays with a DC/DC boost converter. This converter with the proposed RLS-APEFC MPPT serves as a MPPT converter. The boost converter is connected to a single-phase inverter, which is controlled by a PI current controller.

4.3.1 Modeling and Control of MPPT Converter

The MPPT converter is a DC/DC boost converter. The gate pulse for this MPPT converter is generated by a discrete PWM (DPWM) generator. The DPWM generator generates gate pulse by comparing control signal (u) with a triangular signal.

Here, the control signal is the duty-ratio δ of gate-pulse. The duty-ratio at k^{th} sample δ(k) is generated by the RLS-APEF MPPT controller circuit (Fig.4.4 (b)). The proposed RLS-APEF controller is similar to a discrete PID controller. The integral-term is fixed and empirically chosen referring [98], [108], [109]. Fig.4.4 (c) shows the inverter control system. In this prototype PV system, voltage fluctuation from input PV panel is handled by the proposed adaptive MPPT which performs both control and filter actions. A resistive load is connected to the PV system. In this scenario, a simple controller can be used for controlling the inverter. Therefore, a PI-controller has been used in inverter control circuit as shown in Fig.4.4 (c).

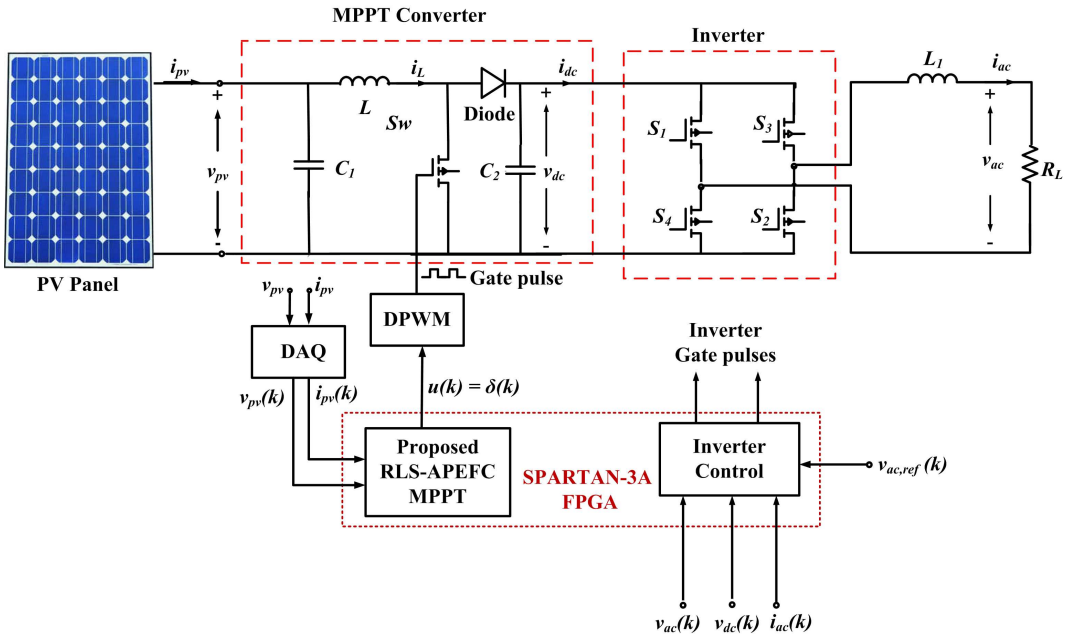

(a)

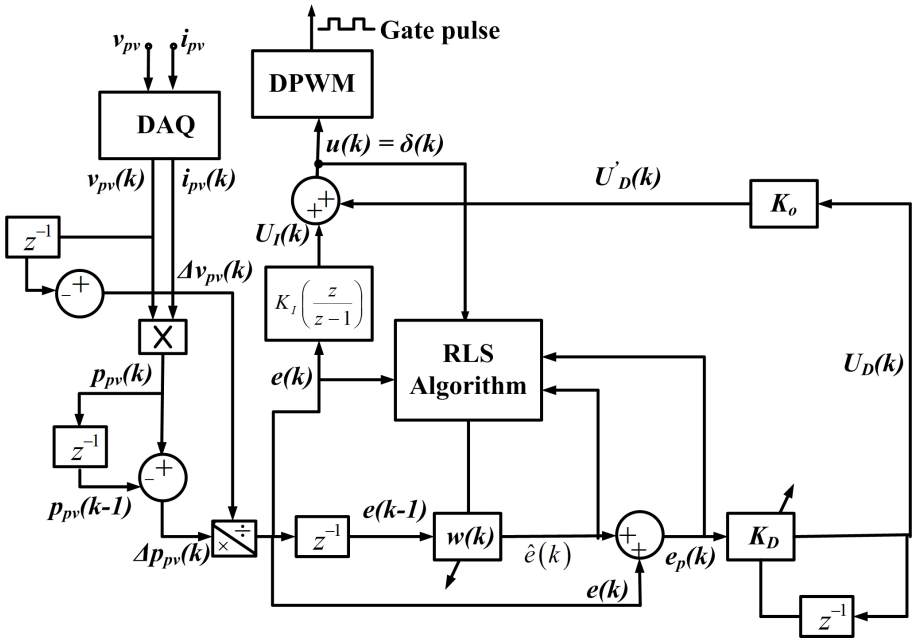

(b)

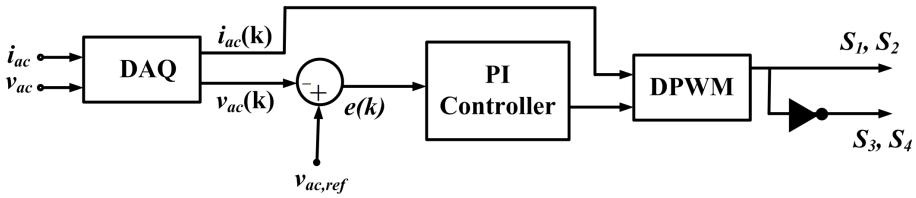

(c)

Figure 4.4: (a) Studied PV system, (b) Proposed RLS-APEF controller for MPP Tracking and (c) Inverter Control of the PV system

4.3.2 Predictive MPPT error Calculation

For MPPT operation, the controller has to generate a control signal u with a duty-ratio δ such that the PV power is maximum available power for given environmental condition. The RLS-APEF controller operates according to the PV power error signal e(k) which is calculated by comparing current k^{th} sampled PV power p_{pv} (k) with that of one step back PV power sample p_{pv} (k-1) as follows.

$$e\left(k\right)=\frac{\Delta p_{pv}\left(k\right)}{\Delta v_{pv}\left(k\right)}=\frac{p_{pv}\left(k\right)-p_{pv}\left(k-1\right)}{v_{pv}\left(k\right)-v_{pv}\left(k-1\right)} \tag{4.1}$$

This RLS-APEF controller consists of a one-tap RLS linear predictor and a summer. The MPPT error with filter weight is defined as $\hat{e}\left(k\right)$. Here, $\hat{e}\left(k\right)$ is generated as follows.

$$\hat{e}\left(k\right)=\omega\left(k\right)e\left(k-1\right) \tag{4.2}$$

where, ω(k) is the tap-weight. The values of ω(k) is updated cycle-by-cycle under the influence of prediction error e_p(k) and one step back error e(k-1) as shown in Fig.4.4 (b). This e_p(k) is calculated using the summer as follows.

$$e_p\left(k\right)=e\left(k\right)+\hat{e}\left(k\right) \tag{4.3}$$

4.3.3 Tuning of PID-parameters

Applying the RLS adapted error $\hat{e}\left(k\right)$ from eq (4.2) and actual error e(k) from eq (4.1) to a summer; it yields prediction error e_p(k) using eq (4.4). This e_p(k) is applied to tune PD-parameters such as K_P(k) and K_D(k) of the PID controller using pole-placement law as follows.

The prediction error e_p(k) in z-domain can be written as

$$E_p\left(z\right)=P_{pv}\left(z\right)\left(w_0+w_1z^{-1}+...+w_Nz^{-N}\right) \tag{4.4}$$

Eq (4.4) can be rewritten as

$$\frac{E_p\left(z\right)}{P_{pv}\left(z\right)}=w_0+w_1z^{-1}+...+w_Nz^{-N} \tag{4.5}$$

The order of this RLS-APEF is application dependent. According to pole-placement law, the order of the RLS-APEF is one order lower than that of the DC/DC boost converter used for MPPT operation []. Since, the order of the DC/DC boost converter is equal to 2; the order of the RLS-PEF would be 1. Let, the RLS-APEF is represented as

$$\frac{U_D\left(z\right)}{P_{pv}\left(z\right)}=\varepsilon_0+\varepsilon_1z^{-1} \tag{4.6}$$

where, ε_0 and ε_1 are the coefficients of the digital RLS-APEF. For boost converter, eq (4.5) should be written as follows.

$$\frac{E_p\left(z\right)}{P_{pv}\left(z\right)}=1+w_1z^{-1} \tag{4.7}$$

where $w_0 = 1$. Let, $U_D(z)$ is K_A times of $E_p(z)$ hence $U_D(z)$ can be written as

$$U_D(z) = K_A E_p(z) \tag{4.8}$$

where K_A is parameter of PD-controller and defined as follows

$$K_A = K_P + K_D z^{-1} \tag{4.9}$$

Using values of $U_D(z)$ and $E_p(z)$ from eq (4.6) and eq (4.7) respectively, K_A can be calculated as

$$K_A = \frac{\varepsilon_0 + \varepsilon_1 z^{-1}}{1 + w_1 z^{-1}} = \varepsilon_{11} + \varepsilon_{12} z^{-1} \tag{4.10}$$

Comparing eq (4.9) and eq (4.10), one would get

$$K_P = \varepsilon_{11}, \quad K_D = \varepsilon_{12} \tag{4.11}$$

With every weather change, generated PV power also varies. To extract maximum PV power in the new condition, the values of w_1, ε_0 and ε_1 change. With variation in these values w_1, ε_0, ε_1 and K_A is updated using eq (4.10). Hence, the adaptive gain factor is implemented with a single RLS tap. Again, to accelerate the tracking speed, a fixed gain K_0 has been introduced to the control loop as shown in Fig.4.4 (b) whose value is dependent on switching frequency f_s and inductance L of boost converter as follows.

$$K_0 = L f_s \tag{4.12}$$

To check its superiority with respect to convergence rate, steady-state error and performance with noise terms, tracking behavior of the studied PV system with the proposed MPPT is compared with that of RLS-APEFC MPPT [98].

4.3.4 Tap-Weight Update with Proposed MPPT

The proposed MPPT algorithm is described in Table 4.4. A RLS-APEFC MPPT is proposed by [18] for MPPT operation of PV system. The tracking operation in this MPPT is accomplished in two steps. In first step, voltage at MPP V_{ref} is calculated by a MPPT algorithm. Then in second step, PV voltage v_{pv} is adjusted to that V_{ref}. Here, the additional V_{ref} calculation step has added extra computational burden and hence is complex, lengthy and slow.

In the proposed RLS-APEFC MPPT, the additional V_{ref} calculation step is with the weight adaptation algorithm. Now the duty-ratio is self-adjusted so that PV panel output power is approaches the MPP power. Due to that computational burden has been minimized, convergence speed is increased and convergence time is also reduced.

Table 4.4: Proposed RLS-APEF adaptation algorithms for updating weight of the filter

Input:
PV voltage signal samples $\left\{v_{pv}(1), \quad v_{pv}(2), \quad v_{pv}(3), \quad ...\right\}$ PV current signal samples $\left\{i_{pv}(1), \quad i_{pv}(2), \quad i_{pv}(3), \quad ...\right\}$ Duty-ratio samples of control signal $\left\{\delta(1), \quad \delta(2), \quad \delta(3), \quad ...\right\}$ Input forgetting factor $\lambda = 0.9$ PV power signal: $P_{pv} = \left\{p_{pv}(1), \quad p_{pv}(2), \quad ...\right\} = \left\{v_{pv}(1) \times i_{pv}(1), \quad v_{pv}(2) \times i_{pv}(2), \quad ...\right\}$
Initialize:
weight $\omega(0) = 0$ And co-variance matrix $P(0) = \beta^{-1} I$; where β is a constant to initialize $P(0)$
Computation:
for $k = 0, 1, 2, 3, ..., k_{\max}$ If $e(k) \leq 0.001$ exit from "for" loop Read a new data pair $[P_{pv}(k), D(k)]$ where $P_{pv}(k) = \left[p_{pv}(k) \quad p_{pv}(k-1) \quad ... \quad p_{pv}(k-m)\right]$ and $D(k) = \left[\delta(k) \quad \delta(k-1) \quad ... \quad D(k-m)\right]$ Output error: $e(k) = \frac{\Delta p_{pv}(k)}{\Delta v_{pv}(k)} = \frac{p_{pv}(k) - p_{pv}(k-1)}{v_{pv}(k) - v_{pv}(k-1)}$ and $\hat{e}(k) = \omega(k) e(k-1)$ Prediction error: $e_p(k) = e(k) + \hat{e}(k)$ Kalman gain: $g(k) = \frac{P(k-1) D(k)}{\lambda(k) + \gamma(k)}$ Co-variance matrix: $P(k) = \frac{P(k-1) - g(k) D(k)^T P(k-1)}{\varepsilon^{-1} \gamma(k)}$ where $\gamma(k) = D^T(k) P(k-1) D(k)$, $\varepsilon = \varphi(k) - \frac{1 - \varphi(k)}{\gamma(k-1)}$ and $\varphi(k) = \left[1 + \ln(1 + \gamma(k-1)) + \left\{\frac{(\upsilon(k-1)+1)\eta(k-1)}{1+\gamma(k-1)+\eta(k-1)} - 1\right\}\left\{\frac{\gamma(k-1)}{1+\gamma(k-1)}\right\}\right]^{-1}$ In which $\upsilon(k)$ and η are defined as $\upsilon(k) = \varphi(k)(\upsilon(k-1) + 1)$ $\eta = \frac{\left[D(k) - \theta^T(k-1)\phi(k)\right]^2}{\gamma(k)}$ Forgetting Factor adaptation: $\lambda(k) = \varphi(k)\left[\lambda(k-1) + \frac{\left[D(k) - \hat{D}(k)\right]^2}{1+\gamma(k)}\right]$ Weight adaptation: $\omega(k) = \omega(k-1) + e_p(k) g(k)$ end

4.4 Results and Discussions

In this chapter, the performance of the proposed MPPT controller is verified on a SSI-M6-205 PV system [22] and prototype PV system that consists of five a PM648 PV panels connected in series. The parameters of the studied PV systems and the connected boost converter are given in Table 3.1 and Table 3.5.

4.4.1 Simulated Results

Using MATLAB/SIMULINK, the proposed APEFC based MPPT is simulated on the studied PV system. The simulated P-V and I-V characteristics of the prototype PV system at different solar radiations are shown in Fig.4.5 (a) and (b) respectively. The simulated P-V and I-V characteristics of this PV system at different solar radiations are shown in Fig.4.5 (c) and (d) respectively.

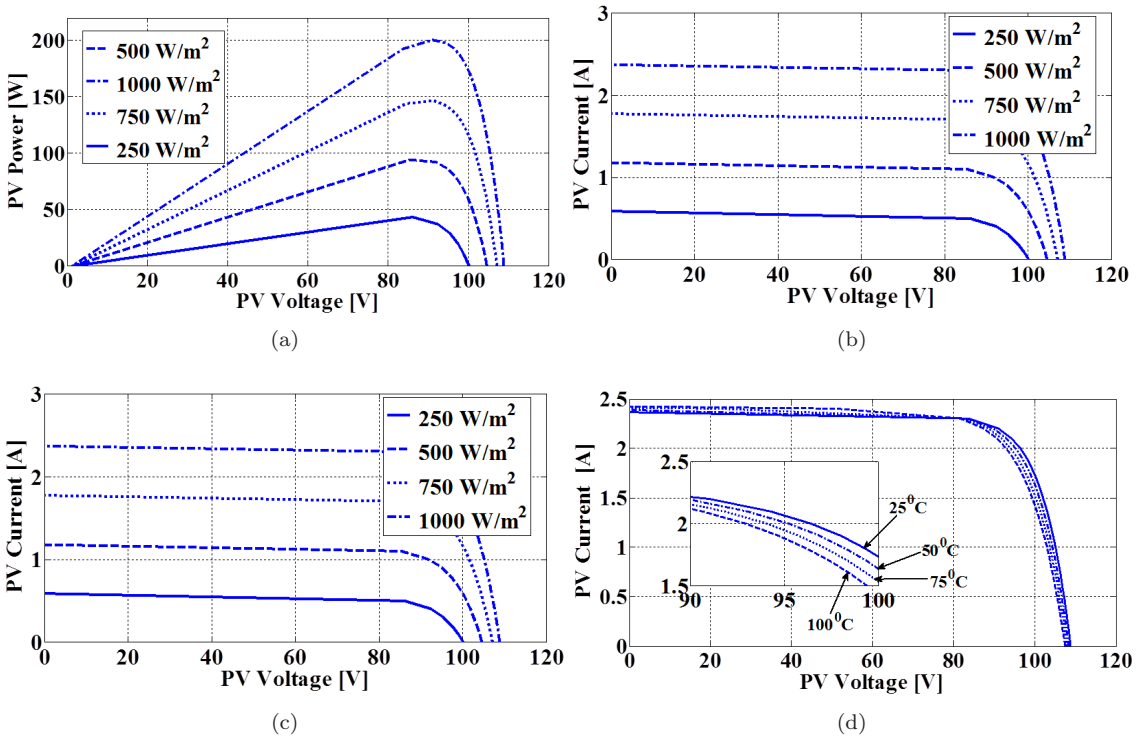

Figure 4.5: (a) P-V Characteristics at different solar irradiance, (b) I-V Characteristics at different solar irradiance, (c) P-V Characteristics at different temperature and (d) I-V Characteristics at different temperature of Prototype PV System

The simulated I-V and P-V characteristics of the prototype PV system for two cases of environmental conditions as defined by condition-I (solar irradiance 540W/m^2 and temperature 36^{0}C) and condition-II (solar irradiance 870W/m^2 and temperature 43^{0}C) are shown in Fig.4.6. (a) and (b) respectively.

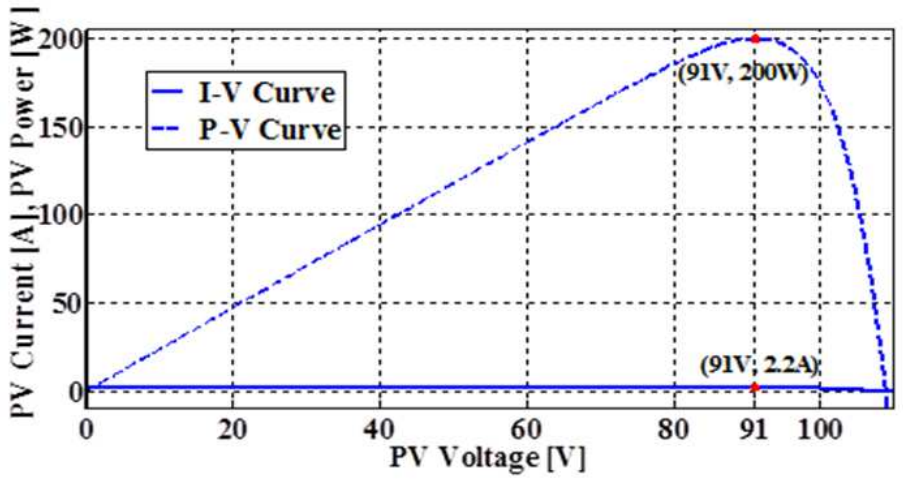

(a)

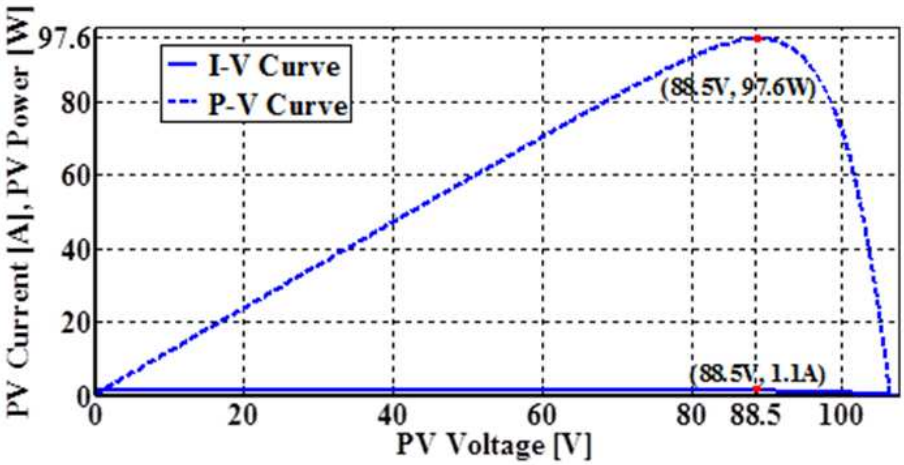

(b)

Figure 4.6: (a) Comparison of I-V and P-V Characteristics of Prototype PV System at (a) 870W/m^2 and (b) 540W/m^2

In condition-I, the MPP voltage current and power of PV system are 91V, 2.2A and 200W respectively. In condition-II, the MPP voltage current and power of PV system are 88.5V, 1.1A and 97.6W respectively.

The tuned values of filter weight and PD-parameters K_P and K_D in case of the proposed MPPT are demonstrated in Fig.4.7 (a) and (b) respectively. K_I is calculated as 0.92 as shown in Fig.4.7 (c).

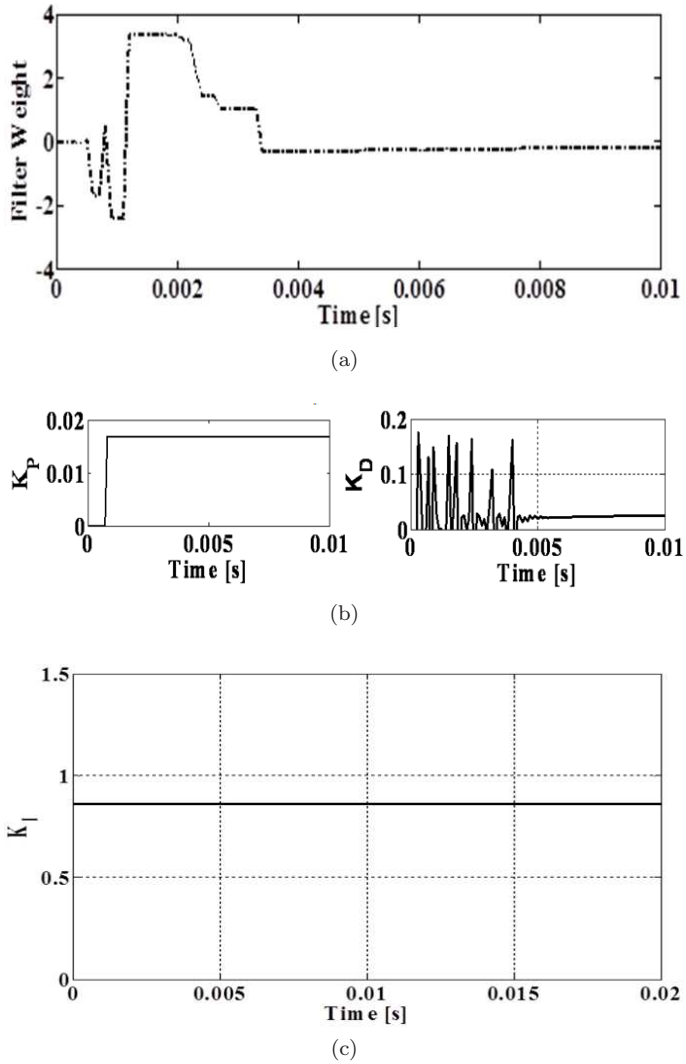

Figure 4.7: (a) Filter weight tuning, (b) calculated K_P and K_D and (c) K_I of Prototype PV System with proposed MPPT

The Bode plot of the prototype PV system with proposed MPPT at environmental conditions-I are shown in Fig.4.8. The gain margin (GM) and phase margin (PM) of these frequency responses at condition-I are 1.3192dB and 140.6564^0 respectively. Hence, it can be observed that both GM and PM are positive. Thus, it is confirmed that PV system with the proposed MPPT is stable.

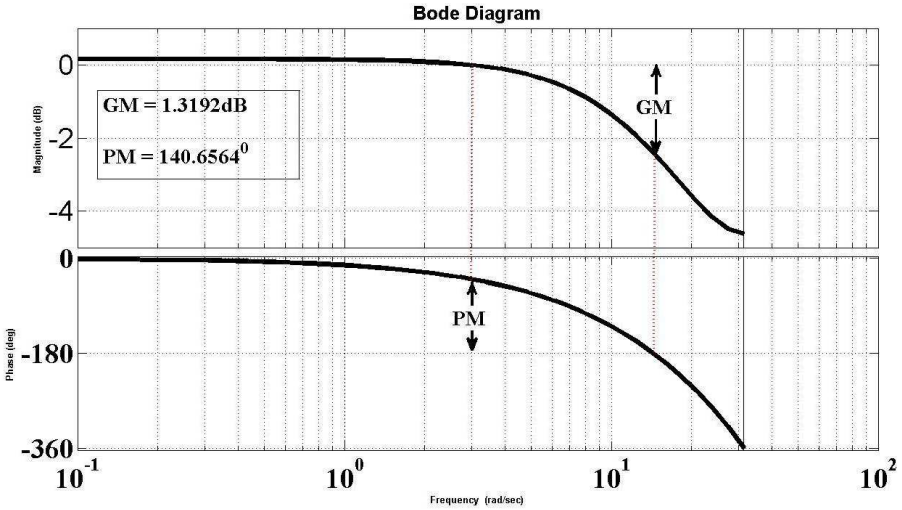

Figure 4.8: Stability studies of the studied PV System with Bode plot

The RLS-APEFC MPPT has been designed using RLS-APEFC algorithm [98] and keeping the forgetting factor fixed at 0.9. This RLS-APEFC MPPT is tested comparing its tracking performance with that of MPPTs such as ATAMPPT, LMS-APEFC, NLMS-APEFC and GALSLMS-APEFC MPPTs. Fig.4.9 (a) and (b) show the comparisons between MPP tracking response of SSI-M6-205 PV system with the above mentioned MPPTs at STC. It can be seen in these figures that rates of PV voltage adjustment for GALSLMS-APEFC and NLMS-APEFC MPPTs are faster than that of ATAMPPT. But tracking times of all these MPPTs are almost the same. This is because rate of step-size adjustment in GALSLMS-APEFC and NLMS-APEFC MPPTs are dependent on MPPT error e(k). The rate is higher if e(k) is large and reduces when e(k) approaches zero. Hence, weight adaptation of APEF is delayed and MPP tracking time is lengthened than it should be whereas in case of ATAMPPT, although rate of tracking is slower but eventually it performs similar to GALSLMS-APEFC and NLMS-APEFC MPPTs. Since, algorithm of ATAMPPT is simple and has computational burden, hence ATAMPPT is better than that of GALSLMS-APEFC and NLMS-APEFC MPPTs.

Fig.4.10 shows the comparison of simulated MPP tracking results of the prototype PV system with RLS-APEFC MPPT, ATAMPPT, LMS-APEFC, NLMS-APEFC and GALSLMS-APEFC at environmental condition-II. In this figure, it can be clearly observed that tracking speed is fastest and time is least in case of RLS-APEFC MPPT than that of GALSLMS-APEFC MPPT, NLMS-APEFC MPPT, LMS-APEFC MPPT and ATAMPPT. It can also be seen that the transient tracking response in case of RLS-APEFC MPPT is smooth and with negligible overshoot.

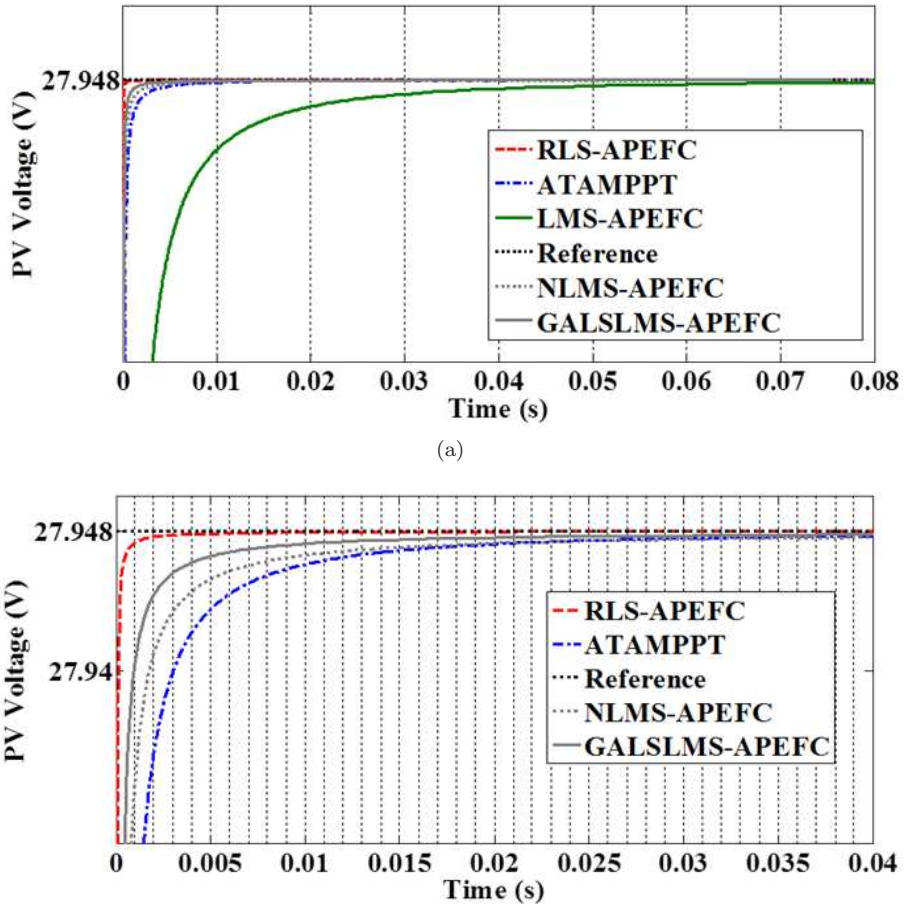

Figure 4.9: (a) Comparison of MPP voltage tracking of SSI-M6-205 PV System with RLS-APEFC, ATAMPPT, NLMS-APEFC, GALSLMS-APEFC, LMS-APEFC and ATAMPPT controllers at STC and (b) Closer view of MPP voltage tracking of PV System

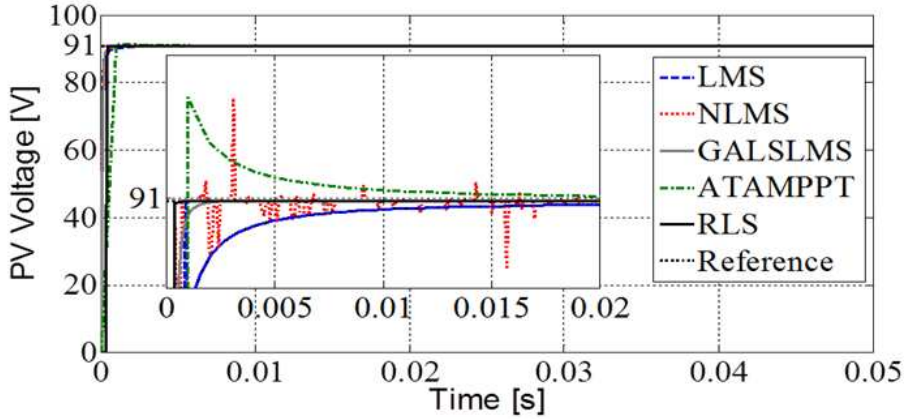

Figure 4.10: RLS-PEF Algorithm

The simulated MPP tracking result of the prototype PV system at environmental condition-II is shown in Fig.4.11 (a). From this figure, it can be clearly observed that although tracking operation in case of the proposed MPPT is delayed due to time taken in weight and forgetting factor adaptation, but tracking time in case of proposed MPPT is less than the RLS-APEFC MPPT. Because after delay, the adjustment speed of the tracking voltage increases many times than that of RLS-APEFC MPPT and hence tracking time reduces. Further, tracking error of proposed MPPT and RLS-APEFC MPPT is compared in Fig.4.11 (b).

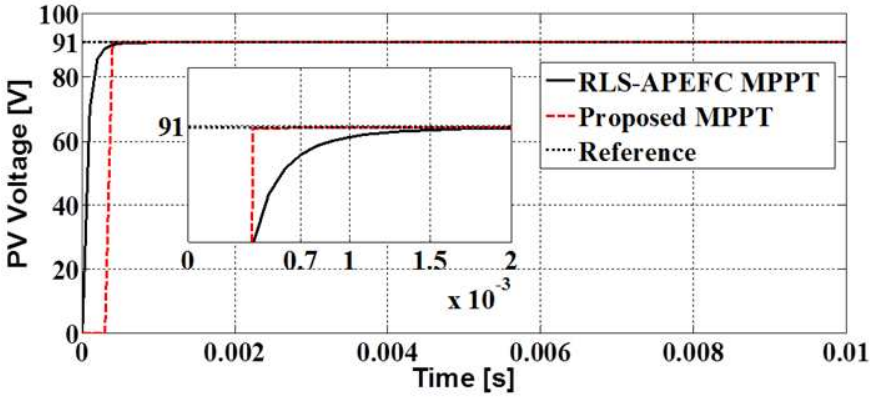

(a)

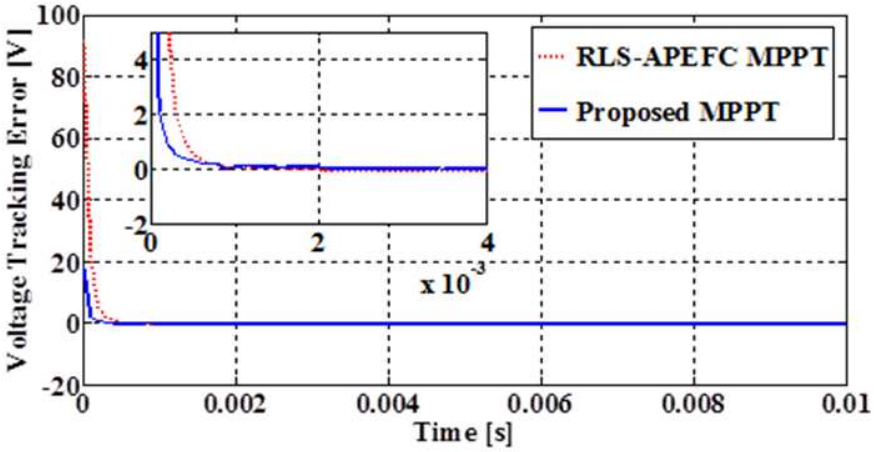

(b)

Figure 4.11: Comparison of (a) MPP voltage tracking and (b) tracking error of Prototype PV System with RLS-APEFC-MPPT and proposed MPPT

The MPP tracking time and tracking errors in case of all the MPPTs are compared in Table 4.5. From Table 4.2, it can be observed that tracking time in case of RLS-APEFC is only 5ms which is much less than that of LMS-APEFC (80ms), ATAMPPT (40ms), NLMS-APEFC (38ms) and GALSLMS-APEFC (35ms) based MPPTs. The absolute percentage errors of voltage $e_{v,mpp}$ for proposed RLS-APEFC MPPT is found to be null which is not possible in case of other MPPTs.

Table 4.5: Comparison of Tracking Behaviour of SSI-M6-205 PV System with Different APEFC-MPPTs at STC

MPPT Controller	$e_{v,mpp}$ (mV)	Tracking time (ms)
LMS-APEFC (μ=0.1)	4	80
ATAMPPT	1.6	40
NLMS-APEFC	0.5	38
GALSLMS-APEFC	0.5	25
RLS-APEFC	0.01	5

Table 4.6: Comparison of Tracking Behaviour of Prototype PV system with Different APEFC-MPPTs at Condition I

MPPT Controller	$e_{v,mpp}$ (mV)	Tracking time (ms)
Proposed APEFC-MPPT	0.03	1
RLS-APEFC MPPT	0.1	3

The MPP tracking time and tracking errors in case of the prototype PV system with the proposed MPPT and the RLS-APEFC-MPPT are compared in Table 4.6. From this table, it can be observed that tracking time in case of proposed MPPT is only 1ms whereas in case of RLS-APEFC is 3ms. The absolute percentage errors of voltage $e_{v,mpp}$ for proposed APEFC MPPT is found to be 0.03V whilst in case of RLS-APEFC MPPT, it is 0.1V.

4.4.2 Experimental Results

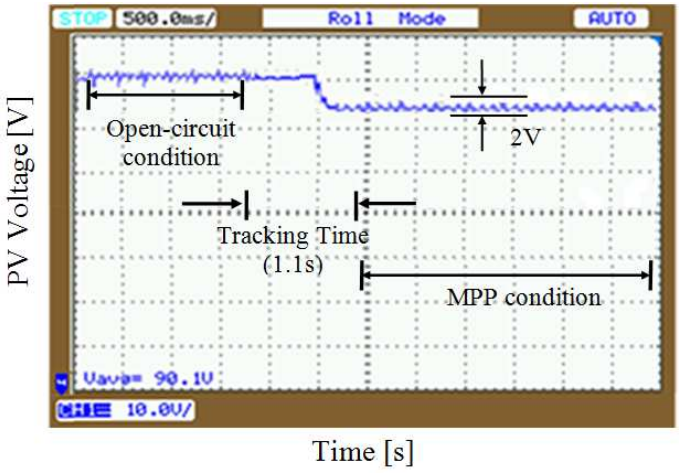

Figure 4.12: Experimental results showing MPP tracking responses of Prototype PV system using proposed MPPT for step change in solar irradiance from condition-I to condition-II (scale in x-axis: 0.5s/div and y-axis: 10V/div)

Fig.4.12 shows experimental result displaying the tracking voltage of PV system with P&O MPPT. In this figure, at first the PV system is in OFF mode. Hence, PV voltage is same as its open-circuit voltage. At A, the MPPT is switched ON. In this figure, time span between A to B is the tracking time. After B, the PV voltage oscillates around the MPP voltage. It is found that tracking periods is 1.1s and voltage fluctuation at steady-state is 2V.

Fig.4.13 shows the other experimental results of prototype PV system with proposed APEFC MPPT. The duty-ratio of MPPT converter is shown in Fig.4.16 (a). The DC-link voltage (v_{dc}) which is input to inverter is shown in Fig.4.16 (b). Fig.4.16 (c) and Fig.4.16 (d) show the load voltage (v_{ac}) and gate-pulses of inverter respectively. In Fig.4.16 (d), two sets of pulses for inverter switches are shown. The first set of pulses is for switches S_1 and S_2 whilst the second set of pulse is for switches S_3 and S_4. For an inverter, S_1 and S_2 are switched ON and OFF simultaneously and switches S_3 and S_4. Similarly, S_3 and S_4 are switched ON and OFF simultaneously. But, when S_1 and S_2 are switched ON, S_3 and S_4 are switched OFF and vice-versa. The switching period, ON time and OFF time of switches S_1 and S_2 are T_{ac} μs, t_{11} μs and t_{12} μs respectively. The switching period, ON time and OFF time of switches S_3 and S_4 are T_{ac} μs, t_{12} μs and t_{11} μs respectively. Hence, $T_{ac} = t_{11} + t_{12}$.

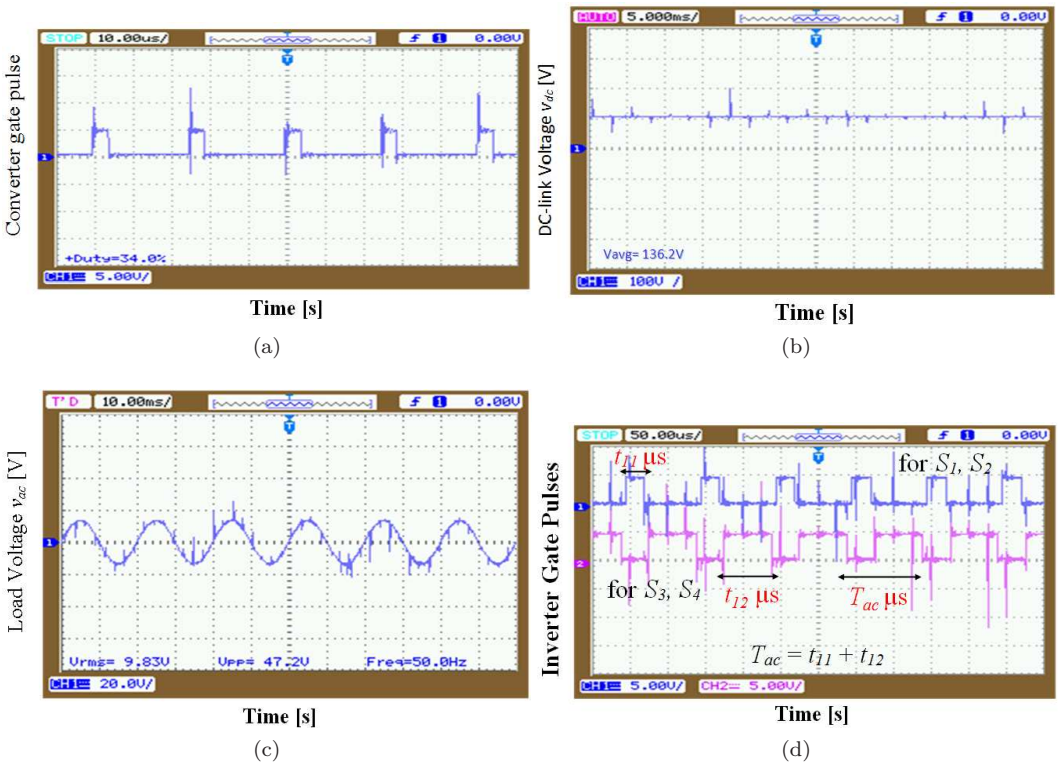

Figure 4.13: Experimental results showing different responses of Prototype PV system with proposed RLS-APEFC MPPT during MPP tracking operation such as (a) gate pulse of MPPT converter, (b) DC-link voltage (v_{dc}), (c) Load voltage (v_{ac}) and (d) gate pulses of inverter switches S_1, S_2, S_3 and S_4 at Condition-II

4.5 Chapter Summary

A new RLS-APEFC based MPPT controller is proposed in this Chapter. This proposed MPPT controller is a modified version of adaptive PID-controller where the derivative gain parameter is tuned on-line by means of an adaptive predictive filter. The proposed MPPT algorithm has been implemented on a prototype PV system. On testing in the prototype PV system, it is found that the MPP tracking performance of this new MPPT controller is efficient in terms of fast response and less steady-state error than that of LMS-APEFC, NLMS-APEFC, GALSLMS-APEFC based MPPTs and ATAMPPT. The effectiveness and accuracy of the proposed APEFC technique have been verified through numerous simulation and experimental results. This proposed RLS-APEFC MPPT is found to be computationally less complex and effective in tracking MPP of a PV system.

Chapter 5

DOUBLE INTEGRAL SLIDING MODE MPPT AND ADAPTIVE DOUBLE INTEGRAL SLIDING MODE MPPT FOR PV POWER HARVESTING APPLICATION

5.1 Introduction

This chapter proposed two new MPPT algorithms that are developed using the concept of double integral sliding mode controller (DISMC) for a stand-alone photovoltaic (PV) system. Chapter 1 has presented an APEFC-MPPT that is found to perform maximum power tracking operation with both fast response and less steady-state error than that of LMS-APEFC, NLMS-APEFC, GALSLMS-APEFC based MPPTs and ATAMPPT. But, in this MPPT technique, there are three sets of tuning algorithms are applied; one for weight w of the filter, second one for its step-size μ and third one for PD-parameters K_c and T_D. These three adaptation rules make the APEFC MPPT very complex as a whole. Although the studied PV system with this MPPT is found to be stable but stability is not guaranteed as in case of a sliding mode controller (SMC)[69].

Like a SMC, performance of DISMC is greatly influenced by the choice of the sliding surface. A DISMC uses a double integral of tracking error term in its sliding surface and can eliminate steady-state error apart from providing control in face of system uncertainties [110], [111]. But there is still difficulty of increased chattering and slow transient response in existing DISMCs [112]. In this chapter, the objective is to exploit the merits of DISMC for designing a MPPT for PV system whilst the disadvantages like chattering and slow transient responses are alleviated by choosing a new sliding surface.

It is found that MPPT based on sliding mode controller (SMC-MPPT) possesses inherent robustness of tracking control and stability against internal system parameters and load uncertainties [113]. Further, it gives high degree of flexibility in design choices and also eases in hardware implementation using DSP, Micro-controller and FPGA, etc. Due to the aforesaid benefits, SMC-MPPT is being chosen widely for controlling nonlinear systems including DC/DC converters for MPP tracking in PV systems. But, SMC-MPPT approach applied to DC/DC converter has some limitations such as variable operating frequency which results in difficulty of filter circuit design. The equivalent control of the SMC is implemented using PWM technique keeping the operating frequency constant but it suffers from non-zero steady-state error. To tackle both the above mentioned problems, a PWM based integral sliding mode controller (ISMC) [114] has been designed using an integral of error term in the sliding surface. To further improve the MPP tracking performance by adding another integral term to the sliding surface of the controller and it becomes a double integral sliding mode controller (DISMC) [110]. A number of DISMC have been reported in literature with different sliding surfaces [110], [115], [18], [116], [117], [118]. But the uncertainties and disturbance have not been considered while designing control laws hence may not adapt to the continuous and fast variation in load and external weather conditions.

5.2 Problem Formulation

Fig.5.1 describes a topology of a stand-alone PV system. It consists of a PV panel, a DC/DC boost converter, a load and a control circuit that generates PWM signal to the boost converter for MPPT operation. The output of PV current i_{pv} can be expressed as [13].

$$i_{pv} = I_{pv} - I_0 \left[\exp\left(\frac{v_{pv} + i_{pv} R_s}{N_s V_t} \right) - 1 \right] - \frac{v_{pv} + i_{pv} R_s}{R_{sh}} \tag{5.1}$$

$$I_{pv} = (I_{sc} + K_i(T - 298)) \frac{G}{1000} \tag{5.2}$$

$$V_t = \frac{a k_b}{q} T \tag{5.3}$$

$$I_0 = I_{0,ref} \left(\frac{T}{298} \right)^3 \exp\left(\frac{q E_g}{k_b n_s V_t} \left(\frac{1}{298} - \frac{1}{T} \right) \right) \tag{5.4}$$

where I_{pv}, I_0, V_t, n_s, R_s, R_{sh}, I_{sc}, K_i, G, T and k_b are photo-generated current, dark-saturation current, thermal voltage, number of series cells in a PV panel, series resistance, shunt resistance, short-circuit current, short-circuit coefficient of temperature, solar radiation, temperature and Boltzmann's constant respectively. v_{pv} and i_{pv} are output voltage and current respectively of the PV panel. $I_{0,ref}$, q, and E_g are reference dark-saturation current, charge of an electron and energy of an photon constant respectively.

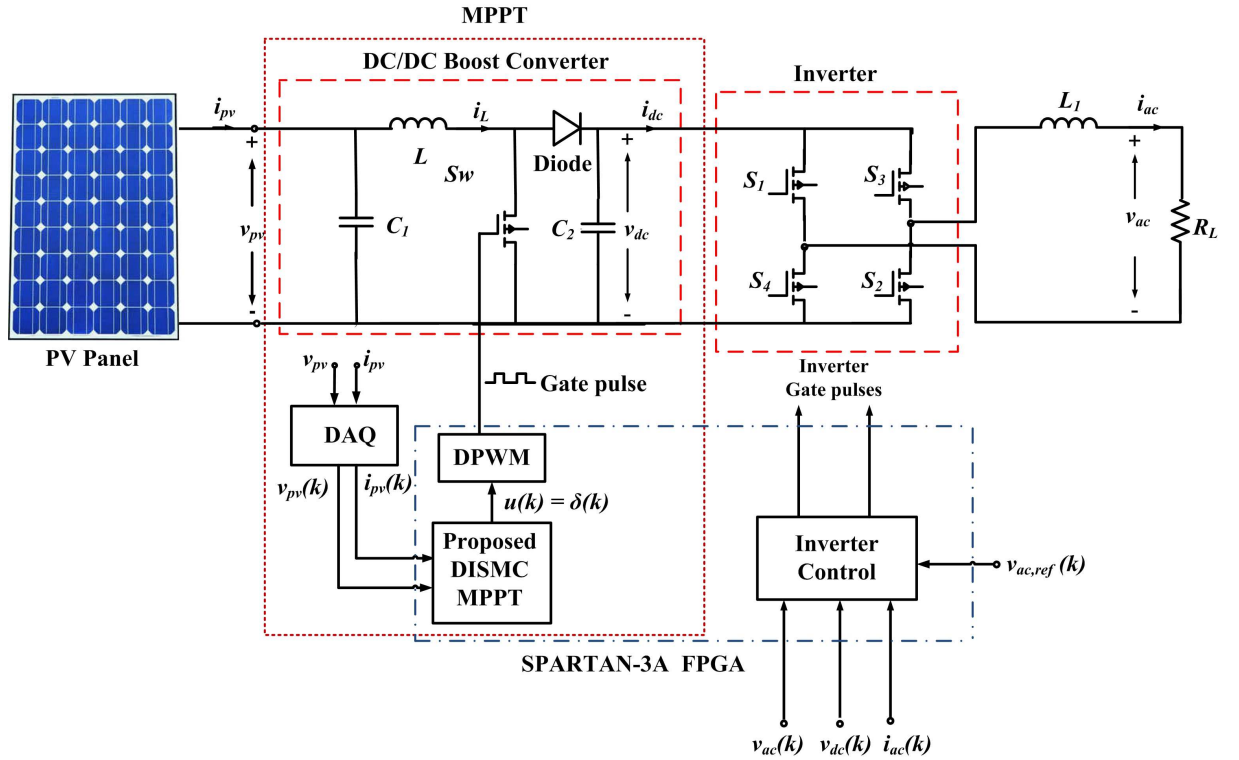

Figure 5.1: Block diagram of a simple PV system topology with DISMC based MPPT

Fig.5.2 (a) and (b) shows the converter for different switching operations. Here, u is the control signal of the boost converter which is a series of pulses with duty-ratio δ. Referring Fig.5.2 (a), when the switch (Sw) is OFF, then

$$\begin{aligned} i_L &= C_1\dot{v}_{pv} + \frac{v_{pv}}{C_1 r_{pv}} \\ \Rightarrow \dot{v}_{pv} &= \frac{1}{C_1} i_L - \frac{1}{C_1 r_{pv}} v_{pv} \end{aligned} \tag{5.5}$$

where r_{pv} is the dynamic resistance of PV panel and defined as $r_{pv} = -\frac{\partial v_{pv}}{\partial i_{pv}}$.

$$\begin{aligned} v_{pv} &= L\dot{i}_L + v_{dc} \\ \Rightarrow \dot{i}_L &= \frac{1}{L} v_{pv} - \frac{1}{L} v_{dc} \end{aligned} \tag{5.6}$$

When the switch (Sw) is ON (Fig.5.2 (b)), then

$$\begin{aligned} i_L &= C_1\dot{v}_{pv} + \frac{v_{pv}}{C_1 r_{pv}} \\ \Rightarrow \dot{v}_{pv} &= \frac{1}{C_1} i_L - \frac{1}{C_1 r_{pv}} v_{pv} \end{aligned} \tag{5.7}$$

and

$$\begin{aligned} v_{pv} &= L\dot{i}_L \\ \Rightarrow \dot{i}_L &= \frac{1}{L} v_{pv} \end{aligned} \tag{5.8}$$

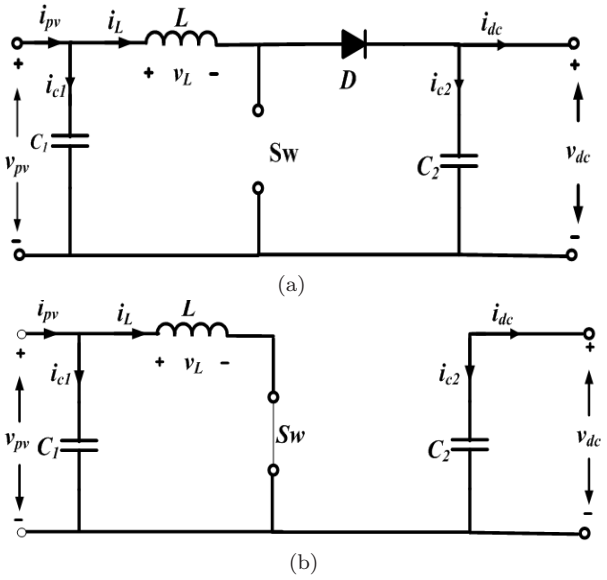

Figure 5.2: (a) Equivalent circuit of boost converter circuit when Sw is open ($u = 0$) and (b) when Sw is closed ($u = 1$)

If δ is the duty-ratio of the control signal u for controlling the switch Sw, then eq (5.4)-(5.7) can be rewritten as

$$\begin{aligned} \dot{i}_L &= \frac{1}{L} v_{pv} - \bar{\delta} \frac{1}{L} v_{dc} \\ \dot{v}_{pv} &= \frac{1}{C_1} i_L - \frac{1}{C_1 r_{pv}} v_{pv} \end{aligned} \tag{5.9}$$

where $\dot{\delta} = 1 - \delta$ .Considering v_{pv} and i_L as state variables, the dynamics of the boost converter can be written in state space form as

$$\dot{X} = f(X,t) + g(X,t)\,\bar{u} \tag{5.10}$$

where

$$\begin{aligned} X &= \begin{bmatrix} i_L & v_{pv} \end{bmatrix}^T \\ f(X) &= \begin{bmatrix} \frac{v_{pv}}{L} & -\frac{v_{dc}}{L} \\ -\frac{i_L}{C_1} & -\frac{1}{C_1 r_{pv}} v_{pv} \end{bmatrix} \\ g(X) &= \begin{bmatrix} \frac{v_{dc}}{L} & 0 \end{bmatrix}^T \\ u &= \delta \end{aligned} \tag{5.11}$$

The MPPT control problem of the PV system can be formulated as follows. For MPP tracking operation, it is intended to use a MPPT algorithm for generating reference operating voltage (V_{ref}), a DC/DC boost converter and a control circuit that supplies the switching control signal to the boost converter so that it forces the operating point of the PV system close to V_{ref}. In the single-input-single-output (SISO) state space model of PV system f is

a non-linear uncertain function whose value is estimated as $\hat{f}$.
The error of this estimation error is bounded by a known function $F(x, \dot{x})$ V/s such that

$$\left|\hat{f} - f\right| \leq F \tag{5.12}$$

Here, Control gain g_1 is estimated as $\hat{g}_1$ i.e.

$$0 < \hat{g}_{1,\min} < \hat{g}_1 < \hat{g}_{1,\max} \tag{5.13}$$

It is intended to design a robust controller that can generate u such that appropriate MPP tracking operation can be achieved in the face of internal parameter uncertainties of the PV system and converter and external disturbances due to load variation.

5.3 Proposed DISMC-MPPT

5.3.1 Design of Proposed DISMC-MPPT

The proposed continuous time DISMC-MPPT is designed as follows. It consists of a MPPT algorithm, a boost converter and the double integral sliding mode controller. The dynamics of DC/DC boost converter have been described by eq (5.9). Considering the switching control signal u from the DISMC subsystem, the inductor current (i_L) of boost converter and PV voltage (v_{pv}) are adjusted such that maximum power can be extracted from the PV system and load voltage v_{dc} can be maintained at a fixed value V_{dc}. A new MPPT algorithm that is used in this work for calculation of the reference voltage V_{ref} is shown in Table 5.1 [119].
The design steps for the new DISMC are described as follows.

Step-1: Taking the values of dc-link voltage (v_{dc}) and PV panel voltage (v_{pv}), estimate

Table 5.1: Proposed MPPT-Algorithm for calculation of V_{ref}

Step-1:	Input v_{pv} (k) and i_{pv} (k) V_{ref} (k) = v_{pv} (k)
Step-2:	Calculate $p_{pv}(k) = v_{pv}(k) \times i_{pv}(k)$
Step-3:	Calculate $dp_{pv}(k) = p_{pv}(k) - p_{pv}(k-1)$ and $dv_{pv}(k) = v_{pv}(k) - v_{pv}(k-1)$
Step-4:	Calculate $F(k) = \frac{dp_{pv}(k)}{dv_{pv}(k)}$
Step-5:	Calculate gradient of $p_{pv}(k)$ as $grd(k) = \frac{F(k)-F(k-1)}{v_{pv}(k)-v_{pv}(k-1)}$
Step-6:	If $F(k) > 0 \quad \alpha = \varepsilon$ where α is the step-size and ε is a very small positive number Else if $F(k) < 0 \quad \alpha = -\varepsilon$ Else if $F(k) = 0 \quad \alpha = 0$
Step-7:	Update $V_{ref}(k+1) = V_{ref}(k) - \alpha g(k)$

the percentage duty-ratio (δ) for the boost converter as

$$\delta = \frac{(v_{dc} - v_{pv})}{v_{dc}} \times 100 \tag{5.14}$$

This δ should track δ_{ref} where is given as

$$\delta_{ref} = \frac{(v_{dc} - V_{ref})}{v_{dc}} \times 100 \tag{5.15}$$

Step-2: Select a switching surface $S_1(X,t) = 0$ (where, X is the state vector of the system to be controlled) that provides the desired asymptotic behavior in steady state. The sliding surface can be defined as [14, 15]

$$S_1 = \left[\frac{d}{dt} + \beta\right]^{n-1} e_1 \tag{5.16}$$

where n is the order of the sliding surface and e_{11} is the tracking error. If

$$n = 1 \Rightarrow S_1 = e_1 \tag{5.17}$$

In this work, tracking error e is defined as

$$e_1 = e_{11} + e_{12} + e_{13} \tag{5.18}$$

where

$$\begin{aligned} e_{11} &= [(V_{ref} - v_{pv}) + (v_{dc,ref} - v_{dc})] \\ e_{12} &= \int [(V_{ref} - v_{pv}) + (v_{dc,ref} - v_{dc})]\, dt \\ e_{13} &= \int \left\{ \int [(V_{ref} - v_{pv}) + (v_{dc,ref} - v_{dc})]\, dt \right\} dt \end{aligned} \tag{5.19}$$

Here, $v_{dc,ref}$ is the desired dc-link voltage of the PV system. In this tracking error (e_1) consists of the input voltage error (for MPPT purpose) and output voltage error (for regulation of output voltage). The significance of considering output voltage error is highly recommended for supplying battery or other DC loads.

Step-3: Obtain the equivalent control (u_{eqv}) by applying invariance condition,

$$S_1(x,t) = 0;\ \ \dot{S}_1(x,t) = 0 \ \ \Rightarrow u \cong u_{eqv} \tag{5.20}$$

The existence of the equivalent control u_n ensures the feasibility of a sliding motion over the switching surface

$$S_1(x,t) = 0 \tag{5.21}$$

Equivalent switching signal (u_{eqv}) can be calculated by solving following equations.

$$\dot{S}_1(x,t) = 0 \tag{5.22}$$

Solving eq (5.22), one can obtain

$$u_{eqv} = -\hat{g}^{-1}\left[\hat{f} + e_{11} + e_{12}\right] = \hat{g}^{-1}\hat{u} \tag{5.23}$$

where

$$\hat{u} = -\left[\hat{f} + e_{11} + e_{12}\right] \tag{5.24}$$

Step-4: Consider a nonlinear control signal or input (u_n) to ensure that Lyapunov's stability criterion is feasible which is given as

$$S\dot{S} < 0 \tag{5.25}$$

The nonlinear switching control (u_n) required for taking care of the external disturbances. In this work, u_n is chosen as

$$u_n = -\hat{g}^{-1}K|S_1|^{\alpha} sat\left(\frac{S_1}{\phi}\right); 0 < \alpha < 1 \tag{5.26}$$

$$sat\left(\frac{S_1}{\phi}\right) = \begin{cases} 1; & \left|\frac{S_1}{\phi}\right| \leq 1 \\ sgn\left(\frac{S_1}{\phi}\right); & \left|\frac{S_1}{\phi}\right| > 1 \end{cases} \tag{5.27}$$

The exponential term $|S|^{\alpha}$ empowers the u_n such that the reaching speed increases when the state is far away from the sliding surface, but the reaching speed reduces near the sliding surface. Chattering magnitude can be reduced by interpolating u_n in a thin boundary layer of thickness . Further, K in eq (5.26) has to be large enough so that the reaching condition $S_1\dot{S}_1 < 0$ is satisfied. K can be calculated from the reachability condition as

$$\frac{1}{2}\frac{d}{dt}S_1^2 \leq -\eta\,|S_1| \tag{5.28}$$

Integrating eq (5.28) between t=0 and t=t_{reach}, the reaching time (t_{reach}) can be calculated as

$$t_{reach} \leq \frac{S_1\,(t=0)}{\eta} \tag{5.29}$$

Eq (5.29) suggests that starting from any initial condition, the state trajectory reaches the sliding surface in a finite time smaller than $\frac{S_1(t=0)}{\eta}$. Further, from eq (5.28), K can be calculated as

$$K \geq \hat{g}g^{-1}\left(\hat{f} - F\right) + \hat{f} + \hat{g}g^{-1}\,(e_{11} + e_{12}) \tag{5.30}$$

Step-5: Calculate the switching control signal as

$$u = u_{eqv} + u_n = g^{-1}\left[\hat{u} - K|S_1|^{\alpha} sat\left(\frac{S_1}{\phi}\right)\right] \tag{5.31}$$

The structure of the proposed continuous time double integral sliding mode controller (DISMC) based MPPT is shown in Fig.5.3. The dashed lines in this figure denote the signal-flow in the circuit.

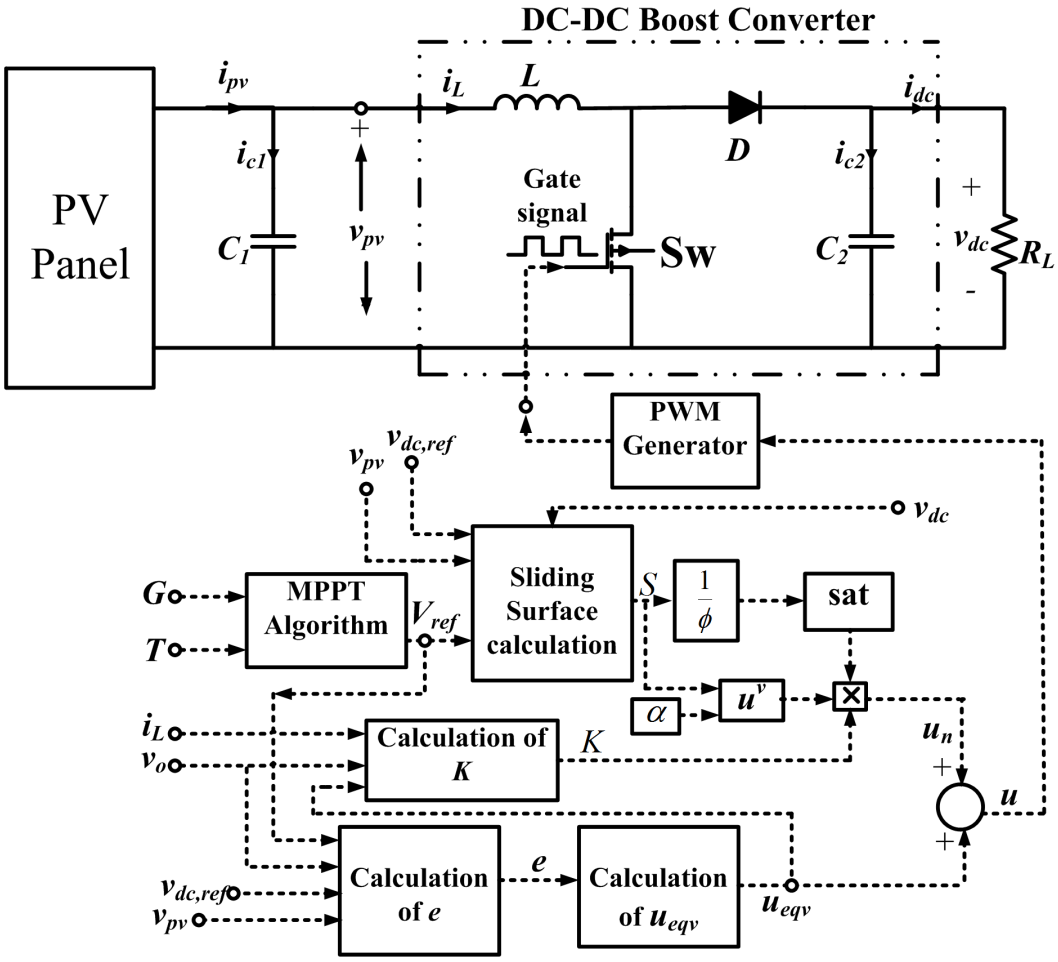

Figure 5.3: Structure of the proposed DISMC-MPPT

This switching operation causes high frequency chattering in the output. The chattering magnitude (h) in PV voltage output signal (v_{pv}) can be calculated as follows.

$$h = h_1 - h_2 \tag{5.32}$$

where, h_1 and h_2 are the upper and lower bound of the chattering in v_{pv}. Similarly, the steady-state error (SSE) of v_{pv} during tracking operation can be calculated as

$$SSE = V_{ref} - \left[h_2 + \frac{(h_1 - h_2)}{2}\right] \tag{5.33}$$

where, V_{ref} is the reference PV voltage at which the operating point of the PV system lies at MPP, h_1 and h_2 are the upper and lower limits of the chattering in v_{pv}. The objective of the proposed DISMC is to minimize the steady-state error with low chattering magnitude.

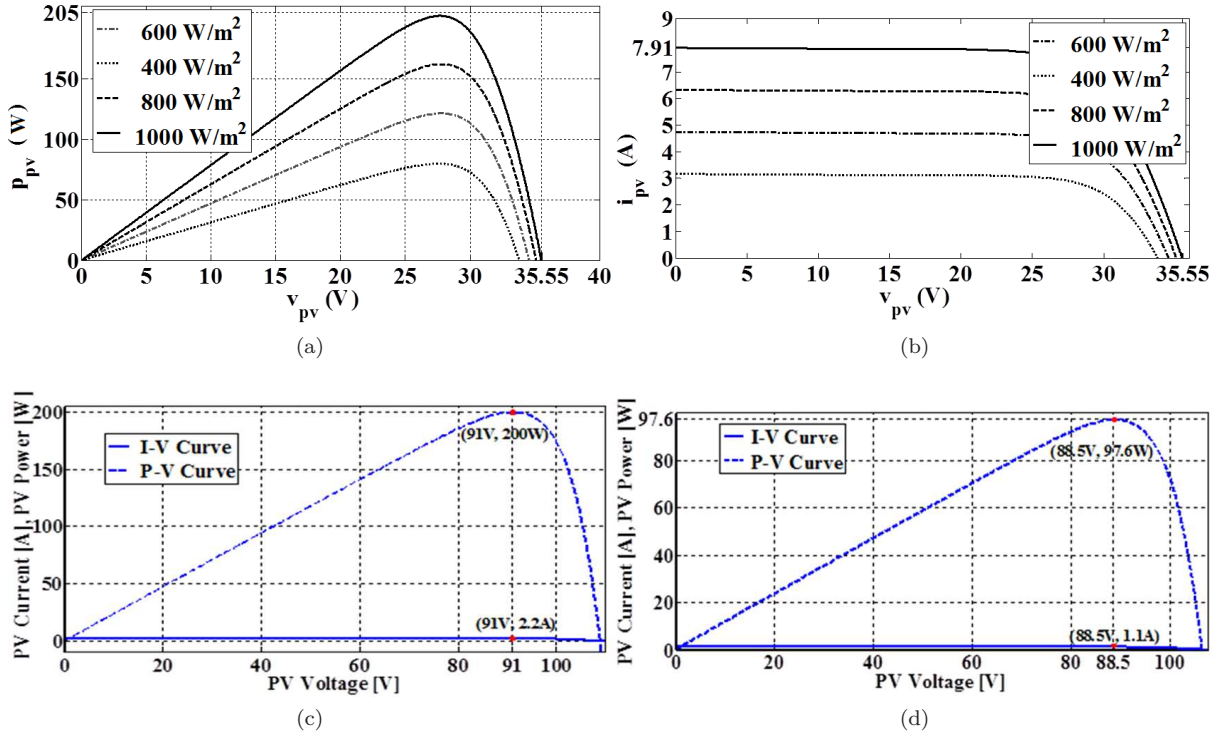

Figure 5.4: (a) P-V Characteristics, (b) I-V Characteristics of SSI-M6-205 solar panel at different solar radiations and Comparison of I-V and P-V Characteristics of Prototype PV System at (c) 870W/m^2 and (d) 540W/m^2

5.4 Results and Discussions of Proposed DISMC-MPPT

5.4.1 Simulation Results

The MPPT tracking performance of the proposed DISMC-MPPT was verified on SSI-M6-205 PV panel [22] and the prototype PV system introduced in Chapter 4. Referring to [22], I-V and P-V characteristics of the studied PV panel are shown in Fig.5.4. These simulated tracking performances are evaluated and tested using MATLAB/SIMULINK.

In this work, the studied PV panel voltage at MPP is taken as Vref for the DISMC-MPPT controller and is calculated online for every change in solar irradiance or temperature using eq (5.15) and eq (5.16). The values of Values of V_{oc} and V_{ref} for the SSI-M6-205 PV system are calculated using eq (5.15) and eq (5.16) for different solar irradiance or temperature can be seen in Table 5.2. In this DISMC-MPPT, nonlinear control signal u_n is calculated using eq (5.30). For this calculation, 0.97 and 0.01 are found to be more effective empirically chosen values for of m and ϕ respectively. The parameters f, for the tested PV system have been calculated from eq (5.11) considering the STC condition where $i_L = i_{pv} = I_{mpp} = 7.31$A, $v_{pv} = 28.04V$ and $v_{dc} = 48V$.

Similarly, $\hat{g}_{1,\max}$ and $\hat{g}_{1,\min}$ are calculated considering the upper bound ($v_{pv,max}$) and lower bound ($v_{pv,min}$) of the PV voltage v_{pv} at STC as 28.1V and 27.9V. For efficient tracking of the

V_{ref} of the studied PV panel, the parameters of the values of different components are used in this work as shown in Table 5.3. In this table, the values of the components of the given DC/DC boost converter i.e.; inductor (L) and capacitors (C_1 and C_2) are constant. The MPP tracking characteristics using DISMC-MPPT have been studied for two distinct cases such as constant condition (solar radiation $G = 1000$ W/m^2 and temperature $T = 25^0$C) and variable weather condition (step change in G from 500 W/m^2 to 1000 W/m^2 at 1 s, T = 25^0C). As expected, the inclusion of two extra integral terms in DISMC provides the benefits of superior MPP tracking performance compared to that of sliding mode controller MPPT (SMC-MPPT) integral sliding mode controller MPPT (ISMC-MPPT) defined as follows.

$$\begin{aligned} S_{SMC} &= e_{11} = [(V_{ref} - v_{pv}) + (v_{dc,ref} - v_{dc})] \\ S_{ISMC} &= e_{11} + e_{12} = e_{11} + \int e_{11} dt \end{aligned} \tag{5.34}$$

Fig.5.5 shows the steady-state waveform of sliding surface function S_1. It also shows the components of S_1 i.e., voltage error (e_{11}), integral of voltage error (e_{12}) and double integral of voltage error (e_{13}) separately. In this figure, the error components e_{11}, e_{12} and e_{13} are found to be of very small range close to zero; hence ensure the existence of sliding operation. Further, the value of S_1 which is sum of e_1, e_2 and e_3 is lesser than 1mV which means S_1 is satisfying the design condition $S_1 < \phi$ where $\phi = 0.01$. To compare the steady-state error (SSE) and chattering yielded by the three controllers (i.e. SMC, ISMC and DISMC), any arbitrary time instant i.e. between t=0.12s to t=0.2s has been considered. Taking reading of upper chattering bound (h_1) and lower chattering bound (h_2), the values of the chattering magnitude (h) and SSE were calculated using eq (5.36) and eq (5.37) respectively as shown in Table 5.3. It can be seen in this Table 5.3 that both the chattering magnitude and SSE in case of DISMC-MPPT are less than that of the other two controllers. The ISMC-MPPT needs slightly higher settling time i.e. 0.014s. SMC-MPPT still not settled until 1.05s. Different MPP tracking performances obtained using SMC, ISMC and DISMC are compared in Fig.5.6 considering the given conditions of case-2. From the figure, it is found that maximum overshoot in case of DISMC-MPPT is less than that of ISMC-MPPT.

Table 5.2: Estimated V_{ref} of the Studied PV System using the proposed MPPT Algorithm given in Table 5.1

Solar Irradiance $\boldsymbol{G}$ (W/m^2)	Open-circuit Voltage V_{oc} (V)	Calculated MPP Voltage V_{ref} (V)
250	32.98	25.99
500	34.26	27
750	35.02	27.59
1000	35.55	28.04

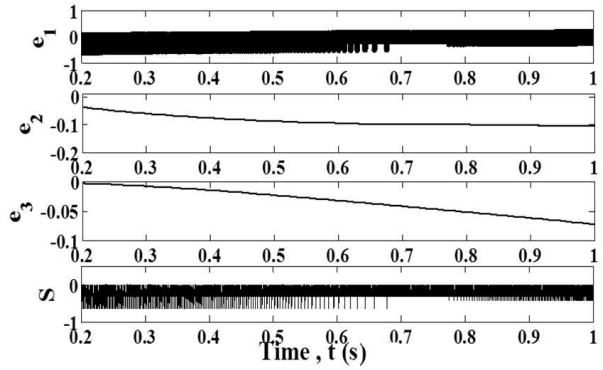

(a)

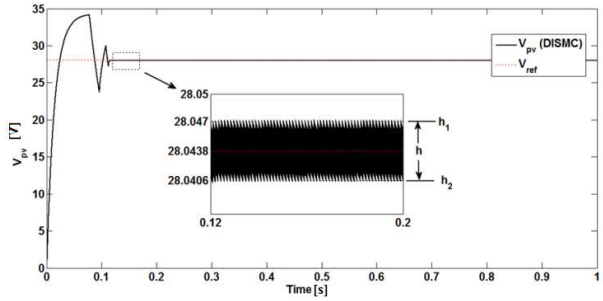

(b)

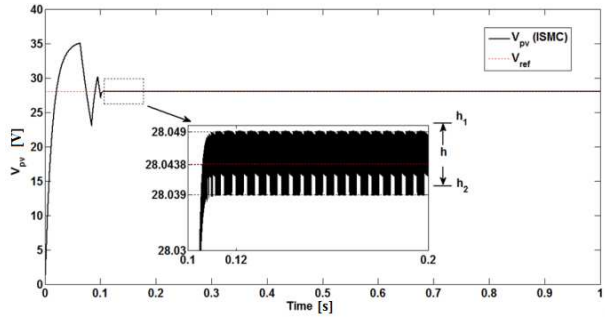

(c)

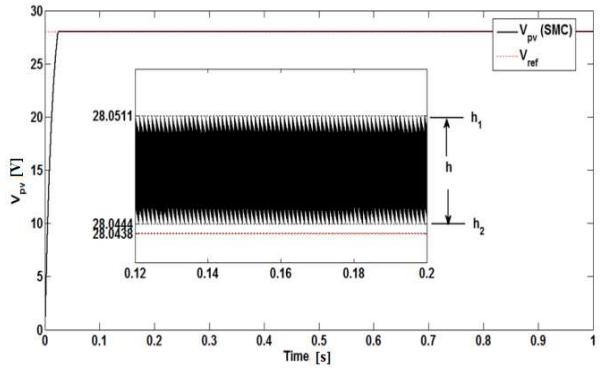

(d)

Figure 5.5: (a) MPP Tracking error e_{11}, e_{12} and e_{13} and sliding function S_1 of proposed DISMC-MPPT at 1000 W/m^2 and 25^{0}C and (b) Comparison v_{pv} of PV system with DISMC-MPPT, ISMC-MPPT and SMC-MPPT at 1000 W/m^2,25^{0}C

Table 5.3: The value of different components of the proposed DISMC-MPPT

Components	**SSI-M6-205 PV System**	**Prototype PV System**
R_L [Ω]	10	100
L [mH]	8	5
C_1 [μF]	850	380
C_1 [μF]	525	330
Switching frequency (f_s) [KHz]	10	10
β	0.8	0.8
m	10	10
v_{pv} [V]	0-36	0-113 V
v_{pv} [V]	48 V	260 V
r_{pv} [Ω]	2-14	0-10

Table 5.4: Comparison of chattering and steady state error (SSE) of the studied PV Panel at 1000 W/m^2, 25^0C using SMC-MPPT, ISMC-MPPT and Proposed DISMC-MPPT controller

Parameters	SMC-MPPT SMC-MPPT	ISMC-MPPT ISMC-MPPT	Proposed DISMC-MPPT
V_{ref} (V)	28.0438	28.0438	28.0438
h_1 (V)	28.0511	28.049	28.047
h_2 (V)	28.0444	28.039	28.0406
h (V)	0.77	0.01	0.0064
SSE (mV)	-3.9	-0.2	0
SSE (% of V_{ref})	13	0.8	0
Maximum Overshoot (%)	0.4562	6.9562	5.4562
Settling Time (s)	> 1	0.12	0.11

Considering the MPP tracking response for an arbitrary time span between t=0.995s and t=1.05s (Fig.5.6), it can be observed that DISMC-MPPT is settling around 1.01s, hence needs 0.01s of settling time.

5.4.2 Real-time Simulation Results

Real-time simulated voltage tracking results of SSI-M6-205 PV system with DISMC-MPPT, ISMC-MPPT and SMC-MPPT are shown in Fig.5.7 (a), (b) and (c) respectively. From these figures, it is found that the chattering height in case of DISMC-MPPT is only 0.15mV which is less than that of ISMC-MPPT (0.2mV) and SMC-MPPT (0.3mV). It can also be seen that chattering in PV current is just 0.1mA in case of DISMC-MPPT. Real-time simulated voltage tracking results of SSI-M6-205 PV system with DISMC-MPPT, ISMC-MPPT and SMC-MPPT for step-change solar irradiance are shown in Fig.5.8 (a), (b) and (c) respectively. Here, Fig.5.8 (a) shows the continuous change in solar irradiance as 1000-700-500 W/m^2. For these variable solar irradiances, the voltage tracking results of PV-system

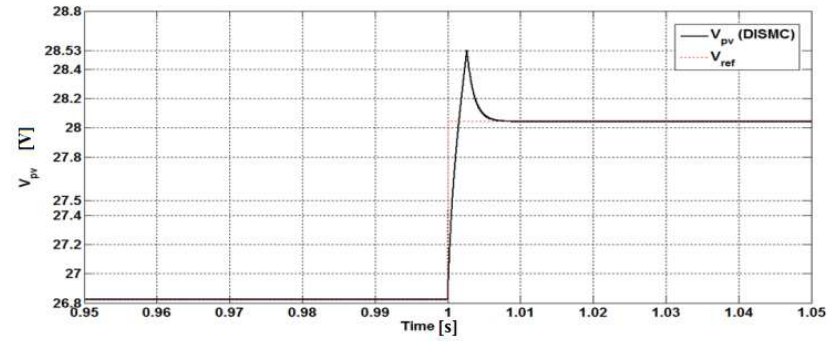

(a)

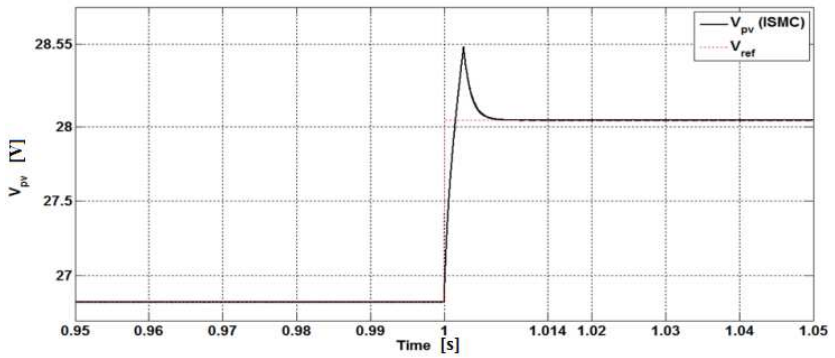

(b)

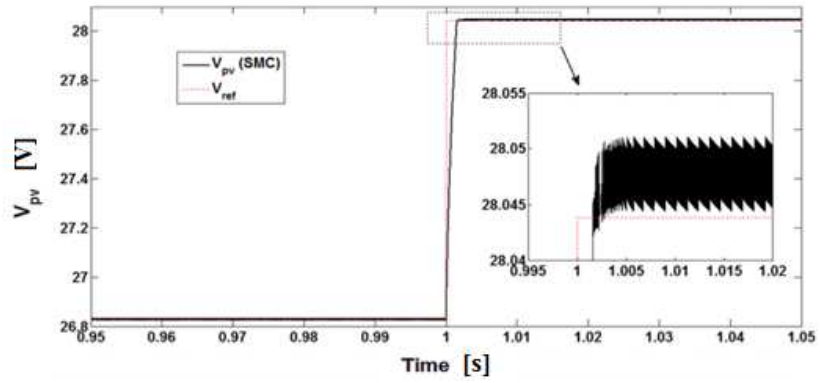

(c)

Figure 5.6: Comparison of v_{pv} tracked by (a) DISMC-MPPT, (b) ISMC-MPPT and (c) SMC-MPPT for step solar irradiance change from 500 W/m^2 to 1000 W/m^2 at t=1s

with ISMC-MPPT and SMC-MPPT are shown in Fig.5.8 (b). In this figure, it can be seen that PV voltage in case of ISMC-MPPT is smoother than that of SMC-MPPT. Fig.5.8 (c) shows the PV voltage in case of DISMC-MPPT for continuous change in solar irradiance between 1000 W/m^2 and 500 W/m^2. Here, the PV voltage is also smooth with less chattering and is also changing fast with change in solar irradiance. From these real-time responses, it is clear that DISMC-MPPT can perform efficiently in variable solar irradiance also.

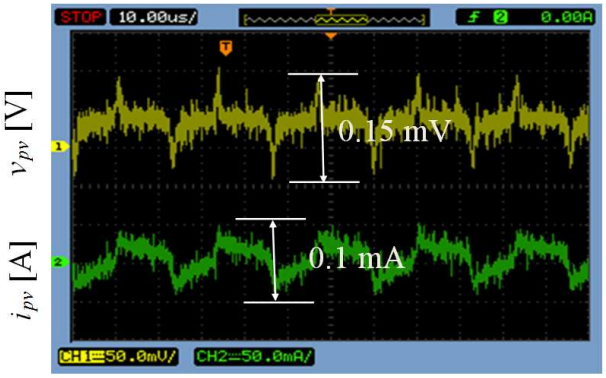

(a)

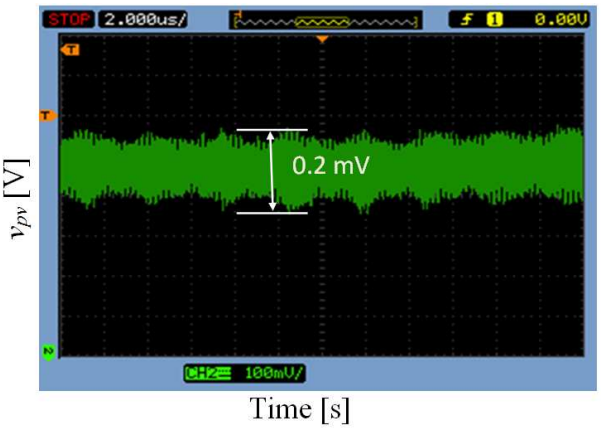

(b)

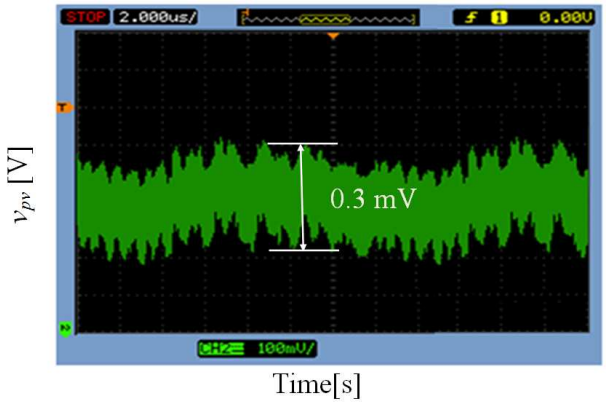

(c)

Figure 5.7: Comparison of real-time simulated voltage tracking results in case of (a) DISMC-MPPT, (b) ISMC-MPPT and (c) SMC-MPPT at STC

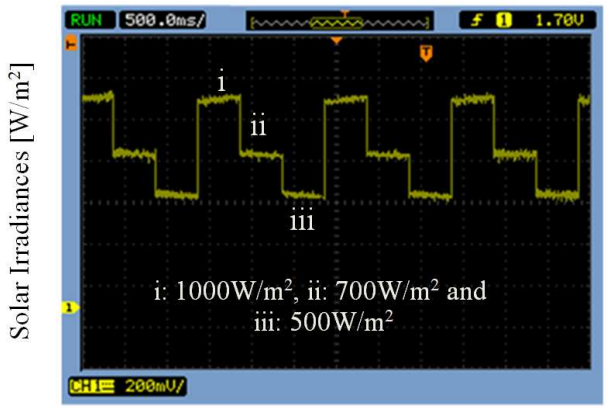

(a)

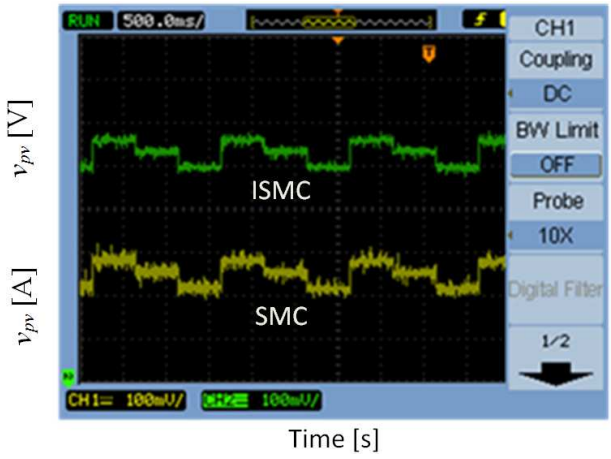

(b)

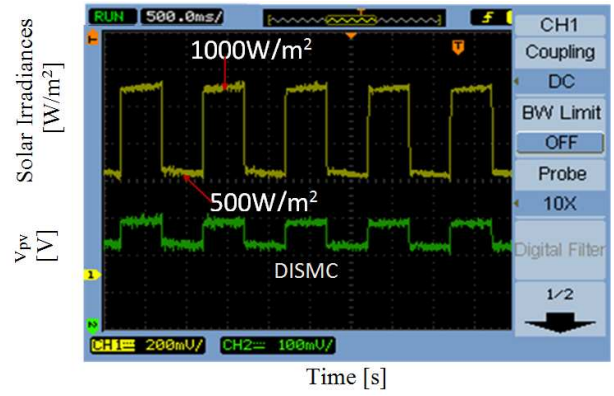

(c)

Figure 5.8: Different real-time simulated tracking results (a) continuous step-change in solar irradiance as 1000-700-500 W/m^2, (b) tracking voltage v_{pv} in case of ISMC-MPPT and SMC-MPPT, (c) tracking voltage v_{pv} in case of DISMC-MPPT continuous step-change in solar irradiance between 1000 and 500 W/m^2

5.4.3 Experimental Results

Fig.5.9 (a) shows the experimentally obtained MPP tracking performances of the prototype PV system with proposed DISMC-MPPT at constant weather condition (solar irradiance of 448 W/m^2 and PV panel temperature of 420C). In this case, it can be seen that chattering in PV voltage is approximately 1volt only. Fig.4.11 (b) further shows the experimentally obtained tracking PV system voltage for change in solar irradiance from 448 W/m^2 to 580 W/m^2. It can be seen that MPP tracking period is only 0.8secs. Maximum overshoot in PV system voltage during change in solar irradiance is around 10V. But, the PV voltage is settling quickly with only two overshoots. Fig.5.9 (c) shows experimental result displaying the tracking voltage of PV system with the proposed DISMC-MPPT. In this figure, at first the PV system is in OFF mode. Hence, PV voltage is same as its open-circuit voltage. At A, the MPPT is switched ON. In this figure, time span between A to B is the tracking time. After B, the PV voltage oscillates around the MPP voltage. It is found that tracking periods is 0.76s and voltage fluctuation at steady-state is 2.5V.

5.4.4 Remarks from the Proposed DISMC-MPPT

Advantages The proposed DISMC-MPPT is found to perform MPP tracking more efficiently than that of SMC-MPPT and ISMC-MPPT in the following fields.

1. High frequency chattering is less than that of SMC-MPPT and ISMC-MPPT
2. Steady state tracking error SSE is found to be almost null in case of DISMC-MPPT whilst there are SSEs present in case of SMC-MPPT and ISMC-MPPT
3. MPP tracking time is less than that of SMC-MPPT and ISMC-MPPT

Disadvantages

1. Complex computation
2. Difficult to calculate correct value of K as only its lowest probable value is only known
3. Tracking performances such as steady-state error and tracking time depend on values and which are empirically chosen fixed values
4. Maximum overshoot is high such as 5.4562V
5. MPP tracking time is still high such as 0.11s

Hence, there is a scope of improvement of the proposed DISMC-MPPT by designing a new DISMC-MPPT that would retains the merits of the proposed DISMC-MPPT and can elevate some of its demerits. Therefore, a new adaptive DISMC-MPPT has been designed which is presented in next section.

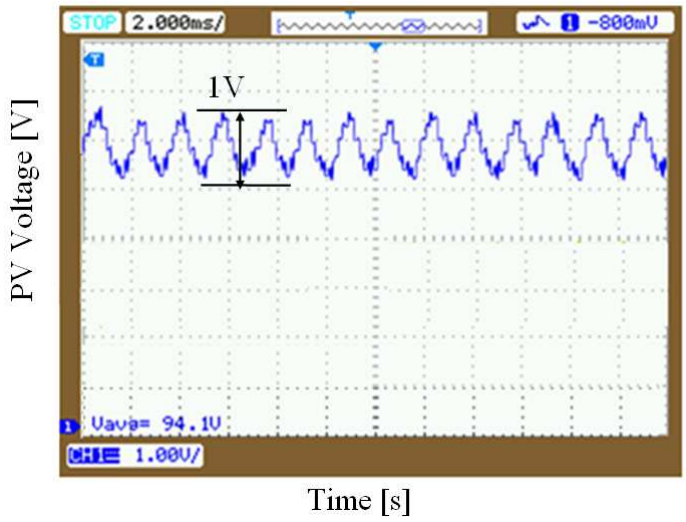

(a)

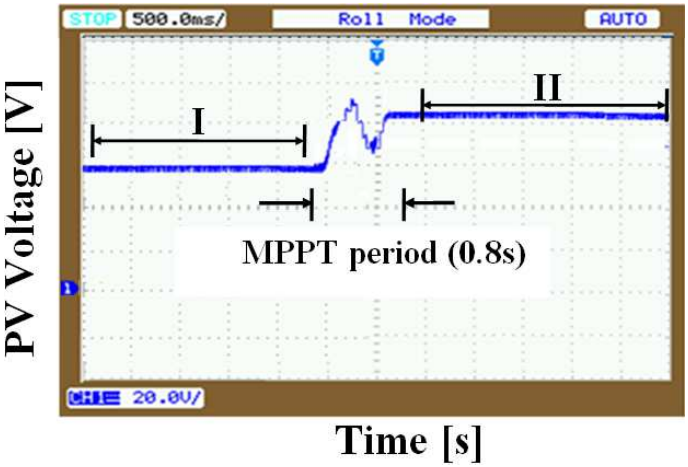

(b)

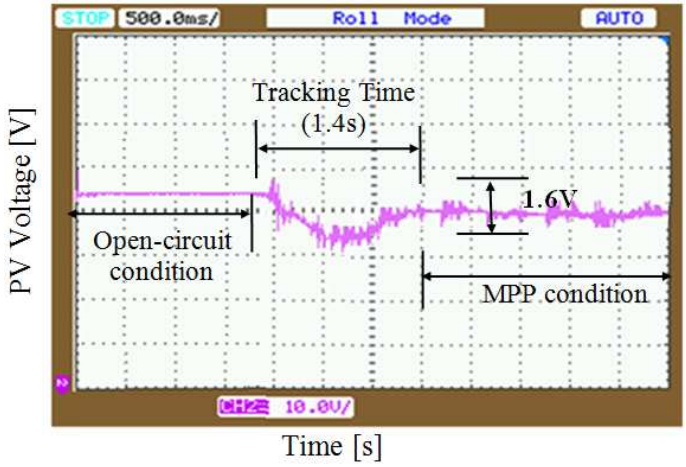

(c)

Figure 5.9: Experimental Tracking Results of the studied PV System using DISMC-MPPT at different conditions such as (a) at constant environmental condition, (b) at step change in solar irradiance from 448 W/m^2 to 580 W/m^2 and (c) at change in PV voltage from open circuit to MPP condition.

5.5 Proposed Adaptive DISMC-MPPT

The design of the proposed adaptive DISMC-MPPT systems considers the uncertainties in weather conditions and variations in load. In this MPPT, sliding surface is being adapted according to change in weather. It has been implemented using a pulse-width-modulator (PWM) controlled DC/DC converter to keep the switching frequency constant. Thus designing the control and filter circuits becomes simpler. Usually in a DC/DC converter, the duty-ratio δ of the switching signal u is such that $0 \leq \delta \leq 1$. The proposed DISMC-MPPT has the PWM-based switching signal u; hence it has only two logic-states 0 and 1. The general switching law for a DC/DC boost converter is as follows.

$$\begin{aligned} u = 1; \quad when \quad S_2 < 0 \\ 0; \quad when \quad S_2 > 0 \end{aligned} \tag{5.35}$$

where S_2 is the proposed sliding surface that is defined as

$$S_2 = a_1 e_{21} + a_2 e_{22} + a_3 e_{23} + a_4 e_{24} \tag{5.36}$$

The terms a_1-a_4 represent the sliding surface coefficients. The terms e_{21}-e_{24} are various error signals and are defined as follows.

$$\begin{aligned} e_{21} &= i_{ref} - i_L \\ e_{22} &= V_{ref} - \beta v_{pv} \\ e_{23} &= \int (V_{ref} - \beta v_{pv})\, dt \\ e_{24} &= \int \left[\int (V_{ref} - \beta v_{pv})\, dt \right] dt \end{aligned} \tag{5.37}$$

$$i_{ref} = m\,(V_{ref} - \beta v_{pv}) \tag{5.38}$$

where m is voltage error's gain constant. On differentiating the state variables of eq (5.37) leads to

$$\begin{aligned} \dot{e}_{21} &= \frac{d}{dt}\left[i_{ref} - i_L\right] = \frac{m\beta}{C_1} i_{c1} - \frac{v_{pv}}{L} + \frac{v_{dc}}{L} - \frac{v_{dc}}{L} u \\ \dot{e}_{22} &= \frac{d}{dt}\left[V_{ref} - \beta v_{pv}\right] = \frac{\beta}{C_1} i_{c1} \\ \dot{e}_{23} &= V_{ref} - \beta v_{pv} \\ \dot{e}_{24} &= \int \left[V_{ref} - \beta v_{pv}\right] dt \end{aligned} \tag{5.39}$$

Taking derivative of S_2 gives

$$\dot{S}_2 = a_1 \dot{e}_{21} + a_2 \dot{e}_{22} + a_3 \dot{e}_{23} + a_4 \dot{e}_{24} \tag{5.40}$$

The equivalent control signal (u_{eq}) can be obtained by solving eq (5.40)

$$\dot{S}_2 = 0 \tag{5.41}$$

Applying eq (5.39) and eq (5.40) in eq (5.41) and then solving this eq (5.41), u_{eq} is obtained as follows.

$$v_{dc}u_{eq} = \frac{\beta L}{C_1}\left(\alpha + \frac{a_2}{a_1}\right) i_{c1} - v_{pv} + v_{dc} + \frac{a_3 L}{a_1}\left(V_{ref} - \beta v_{pv}\right) + \frac{a_4 L}{a_1}\int \left[V_{ref} - \beta v_{pv}\right] dt \tag{5.42}$$

Hence, equivalent control signal is

$$u_{eq} = \frac{\beta L}{v_{dc}C_1}\left(m + \frac{a_2}{a_1}\right) i_{c1} - \frac{v_{pv}}{v_{dc}} + 1 + \frac{a_3 L}{v_{dc}a_1}\left(V_{ref} - \beta v_{pv}\right) + \frac{a_4 L}{v_{dc}a_1}\int \left[V_{ref} - \beta v_{pv}\right] dt \tag{5.43}$$

Let, v_{con} is the switching control voltage, then

$$v_{con} = K_1 i_{c1} - v_{pv} + v_{dc} + K_2 e_{22} + K_3 e_{23} \tag{5.44}$$

where

$$\begin{aligned} v_{con} &= v_o u_{eq} \\ K_1 &= \frac{\beta L}{C_1}\left(\alpha + \frac{a_2}{a_1}\right) \\ K_2 &= \frac{a_3 L}{a_1} \\ K_3 &= \frac{a_4 L}{a_1} \end{aligned} \tag{5.45}$$

The DISMC-MPPT sliding surface parameters K_1, K_2 and K_3 are chosen such that existence and stability conditions would be satisfied. The circuit diagram of this DISMC-MPPT is shown in Fig.5.10. The functional responsibility of the proposed DISMC-MPPT is that for a given DC/DC boost converter with fixed values of capacitances C_1, C_2 and inductance L, it is required to find K_1, K_2 and K_3 such that the PV system satisfied reaching and stability conditions.

5.5.1 Reaching Condition

Reaching condition is to be satisfied in order to ensure that the state trajectory of the system will be directed always towards the sliding surface from any initial conditions. In order to achieve this, the product of sliding function and its first derivative term must be negative according to Lyapunov's stability concept. Hence,

$$\lim_{S_2 \to 0} S_2 \dot{S}_2 < 0 \tag{5.46}$$

Referring eq (6.24) and (6.50), in a boost converter, if and when

$$\begin{aligned} u &= 1 \\ \dot{S}_2 &> 0 \\ K_1 i_{c1} + K_2 e_{22} + K_3 e_{23} &< v_{pv} \end{aligned} \tag{5.47}$$

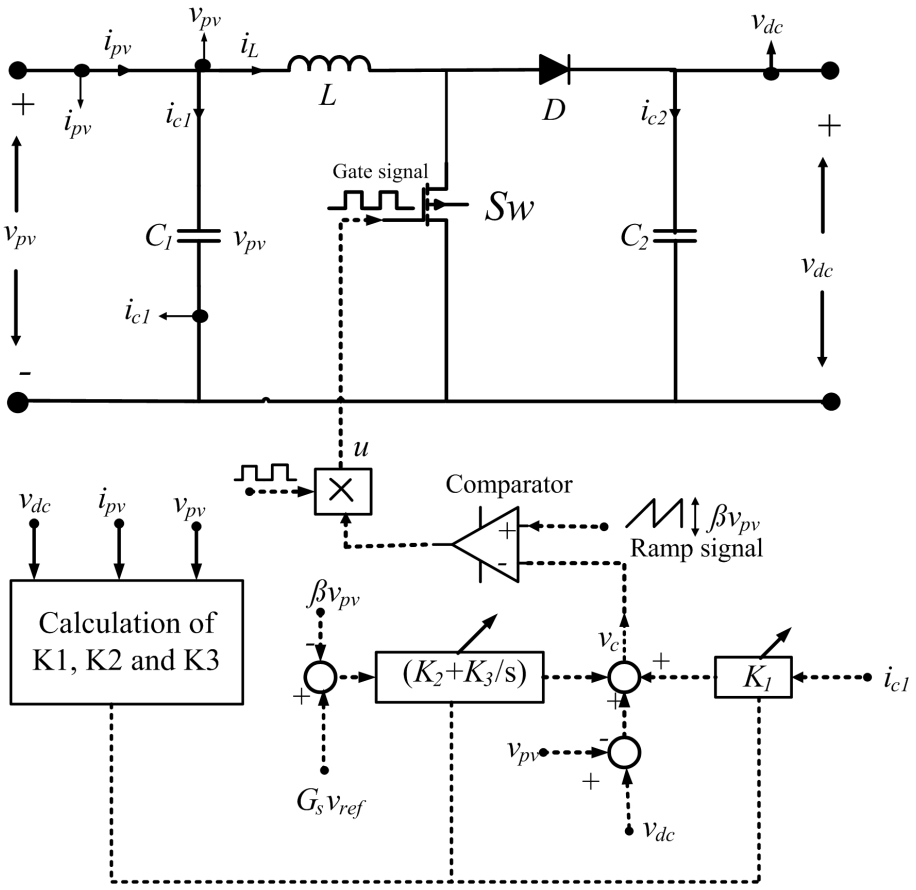

Figure 5.10: Controller circuit diagram of the proposed adaptive DISMC-MPPT

$$\begin{aligned} u &= 0 \\ \dot{S}_2 &< 0 \\ K_1 i_{c1} + K_2 e_{22} + K_3 e_{23} &> (v_{pv} - v_{dc}) \end{aligned} \tag{5.48}$$

At steady state eq (5.47) and eq (5.48) can be rewritten as follows

$$K_1 i_{c1(\min)} + K_2 e_{22(\max)} + K_3 e_{23(\max)} < v_{pv(ss)} \tag{5.49}$$

$$K_1 i_{c1(\max)} + K_2 e_{22(\min)} + K_3 e_{23(\min)} > \left(v_{pv(ss)} - v_{dc(\min)}\right) \tag{5.50}$$

where v_{pv}(ss) is the PV panel voltage at steady-state, $v_{dc(min)}$ is the minimum output voltage $e_{22(min)}$ and $e_{22(max)}$ are minimum and maximum value of error e_{22} $e_{23(min)}$ and $e_{23(max)}$ are minimum and maximum value of error e_{23}, $i_{c1(min)}$, $i_{c1(max)}$ are minimum and maximum capacitor current i_{c1} respectively.

5.5.2 Stability Condition

This condition ensures that the state trajectory remains in the sliding surface. The proposed adaptive DISMC-MPPT consists of both the current and voltage state variable terms in its

structure. Hence, the sliding motion equation ($S_2 = 0$) cannot be solved analytically. It can be solved by using the PV system and controller dynamics given by eq (5.8) and equivalent control signal given by eq (6.47) as follows.

At first, u_{eq} from eq (5.43) is applied in eq (5.8) to get

$$\begin{aligned} \dot{i}_L &= \frac{K_1}{L} i_L - \frac{K_1}{L r_{pv}} v_{pv} + \frac{K_2}{L} \left(V_{ref} - \beta v_{pv}\right) + \frac{K_3}{L} \int \left(V_{ref} - \beta v_{pv}\right) dt \\ \dot{v}_{pv} &= \frac{1}{C_1} i_L - \frac{1}{C_1 r_{pv}} v_{pv} \end{aligned} \tag{5.51}$$

Eq (5.51) can be rewritten as

$$\begin{aligned} \dot{\tilde{i}}_L &= \beta_{11} \tilde{i}_L + \beta_{12} \tilde{v}_{pv} + \beta_{13} \int \tilde{v}_{pv} dt \\ \dot{\tilde{v}}_{pv} &= \beta_{21} \tilde{i}_L + \beta_{22} \tilde{v}_{pv} + \beta_{23} \int \tilde{v}_{pv} dt \\ \frac{d}{dt}\left(\int \tilde{v}_{pv} dt\right) &= \beta_{31} \tilde{i}_L + \beta_{32} \tilde{v}_{pv} + \beta_{33} \int \tilde{v}_{pv} dt \end{aligned} \tag{5.52}$$

where

$$\begin{aligned} \tilde{i}_L = i_L, \quad & \tilde{v}_{pv} = V_{ref} - \beta v_{pv}, \\ \beta_{11} = \frac{K_1}{L}, \quad & \beta_{12} = -\left(\tfrac{K_1}{r_{pv} L} + \tfrac{K_2}{L}\right), \\ \beta_{13} = \frac{K_1}{L}, \quad & \beta_{21} = \tfrac{1}{C_1}, \\ \beta_{22} = -\frac{1}{C_1 r_{pv}}, \quad & \beta_{23} = 0, \\ \beta_{31} = \beta_{33} = 0, \quad & \beta_{32} = 1 \end{aligned} \tag{5.53}$$

Characteristics equation of the linearized PV system is

$$\begin{vmatrix} s - \beta_{11} & -\beta_{12} & -\beta_{13} \\ -\beta_{21} & s - \beta_{22} & -\beta_{23} \\ -\beta_{31} & -\beta_{32} & s - \beta_{33} \end{vmatrix} = 0 \tag{5.54}$$

$$\Rightarrow s^3 + \beta_1 s^2 + \beta_2 s + \beta_3 = 0 \tag{5.55}$$

where

$$\begin{aligned} \beta_1 &= -\left(\beta_{11} + \beta_{22}\right) \\ \beta_2 &= -\beta_{23} + \beta_{11}\beta_{22} - \beta_{12} z_{21} \\ \beta_3 &= \beta_{11}\beta_{23} - \beta_{13}\beta_{21} \end{aligned} \tag{5.56}$$

Characteristic equation (6.60) can be used to apply Routh-Hurwitz criterion for determining stability condition as follows

$$\begin{array}{lll} s^3 & 1 & \beta_2 \\ s^2 & \beta_1 & \beta_3 \\ s^1 & \frac{\beta_3-\beta_1\beta_2}{\beta_1} & 0 \\ s^0 & \beta_3 & 0 \end{array} \tag{5.57}$$

Referring (6.62), at critically stable conditions,

$$\frac{\beta_3 - \beta_1\beta_2}{\beta_1} = 0 \tag{5.58}$$

The above discussed reaching and stability conditions should be satisfied to ensure the close-loop stability of the system. For that, K_1, K_2 and K_3 should be chosen such that eq (5.45), eq (5.49) and eq (5.50) are valid.

5.5.3 Adaptive Tuning of DISMC Parameters K_1, K_2 and K_3

A second-order stable system with un-damped natural frequency ω_n and damping-ratio ζ is usually in the form of

$$\frac{d^2x}{dt^2} + 2\zeta\omega_n\frac{dx}{dt} + \omega_n^2 = 0 \tag{5.59}$$

Laplace Transform of (5.59) is

$$\left(s^2 + 2\zeta\omega_n s + \omega_n^2\right) X(s) = 0 \tag{5.60}$$

$$\Rightarrow s^2 + 2\zeta\omega_n s + \omega_n^2 = 0 \tag{5.61}$$

The PV system is also a second-order system with $\omega_n = \frac{v_{pv}}{v_{dc}}\sqrt{\frac{1}{LC_1}}$. In this PV system, in critically stable condition V_{pv} will be equal to V_{ref} at steady-state if

$$i_{ref} - i_L = 0 \Rightarrow e_{21} = 0 \tag{5.62}$$

At steady-state, the following condition is also satisfied.

$$S_2 = 0 \Rightarrow a_1e_{21} + a_2e_{22} + a_3e_{23} + a_4e_{24} = 0 \tag{5.63}$$

Applying eq (5.62) in eq (5.63)

$$a_2e_{22} + a_3e_{23} + a_4e_{24} = 0 \tag{5.64}$$

or

$$a_2e_{22} + a_3\int e_{22}dt + a_4\iint e_{22}dtdt = 0 \tag{5.65}$$

Laplace Transform of eq (5.65) is

$$a_2E_{22}(s) + \frac{a_3}{s}E_{22}(s) + \frac{a_4}{s^2}E_{22}(s) = 0 \tag{5.66}$$

or

$$s^2 + \frac{a_3}{a_2}s + \frac{a_4}{a_2} = 0 \tag{5.67}$$

Comparing eq (5.67) with eq (5.60), the following relationships can be derived

$$\begin{aligned} 2\zeta\omega_n &= \frac{a_3}{a_2} \\ \omega_n^2 &= \frac{a_4}{a_2} \end{aligned} \tag{5.68}$$

or

$$\begin{aligned} \frac{a_3}{a_2} &= 2\zeta\frac{1}{\sqrt{LC_1}}, \\ \frac{a_4}{a_2} &= LC_1 \end{aligned} \tag{5.69}$$

Comparing eq (5.45) and eq (5.69)

$$\begin{aligned} \frac{K_2}{K_3} &= \frac{a_3}{a_4} = \frac{2\zeta}{\omega_n} \\ a_1 &= \frac{a_3 L}{K_2} \\ K_1 &= \frac{\beta L}{C_1}\left(m + \frac{a_2}{a_3 L}K_2\right) \end{aligned} \tag{5.70}$$

If t_s is the settling-time of the PV system with DISMC and can be described by

$$\begin{aligned} t_s &= \frac{4}{\zeta\omega_n} \\ \Rightarrow \zeta\omega_n &= \frac{4}{t_s} \end{aligned} \tag{5.71}$$

Then, eq (5.71) can be rewritten as

$$\begin{aligned} \frac{K_2}{K_3} = \frac{8}{t_s\omega_n^2} &= \frac{8 \times LC_1}{t_s}\left(\frac{v_{dc}}{v_{pv}}\right)^2 \\ \Rightarrow K_3 &= \left(\frac{t_s}{8 \times LC_1}\right)\left(\frac{v_{pv}}{v_{dc}}\right)^2 K_2 \end{aligned} \tag{5.72}$$

Using eq (5.70) and eq (5.71) in eq (5.72), one can get

$$K_1 = \frac{\beta L}{C_1}\left(m + \frac{t_s}{8L}K_2\right) \tag{5.73}$$

Again referring eq (5.73), the following relationship is valid for critically stable condition.

$$\begin{aligned} K_2 &= \frac{K_3 L}{K_1 - \frac{L}{C_1 r_{pv}}} \\ K_3 &= \frac{K_2}{L}\left(K_1 - \frac{L}{C_1 r_{pv}}\right) \end{aligned} \tag{5.74}$$

Solving eq (5.70) to eq (5.74), the following formulas are derived for finding the values of K_1, K_2 and K_3

$$\begin{aligned} K_1 &= \frac{t_s}{8C_1}\left(\frac{v_{pv}}{v_{dc}}\right)^2 + \frac{L}{C_1 r_{pv}} \\ K_2 &= \frac{8}{\beta t_s}\left(\frac{t_s}{8}\left(\frac{v_{pv}}{v_{dc}}\right)^2 + \frac{L}{C_1 r_{pv}} - m\beta L\right) \\ K_3 &= \frac{K_2}{L}\left(K_1 - \frac{L}{C_1 r_{pv}}\right) \end{aligned} \tag{5.75}$$

In eq (5.75), L and C_1 are fixed. The value of m, β and t_s can be chosen by the designer. But, the value of r_{pv} is dependent on weather condition hence r_{pv} changes with every variation in weather conditions. Since K_1, K_2 and K_3 are function of r_{pv}, their values also adopted with r_{pv} using eq (5.75). Due to PWM control action in the DISMC-MPPT, there is a high frequency switching operation.

5.6 Results and Discussions for Proposed Adaptive DISMC-MPPT

5.6.1 Simulation Results

Like the the DISMC-MPPT, the MPPT tracking performance of the proposed adaptive DISMC-MPPT was verified on SSI-M6-205 PV panel and the prototype PV system. Simulated MPP tracking results are derived from these PV systems using their model constructed in MATLAB/SIMULINK and then applying the proposed adaptive DISMC-MPPT (Fig.5.10) in those PV models.

For these PV models, the sliding mode controller parameters K_1, K_2 and K_3 of the proposed adaptive DISMC-MPPT are calculated using eq (5.75). Fig.5.11 shows the update of these parameters K_1, K_2 and K_3 along with V_{ref} for change in solar irradiance from 100W/m^2 to 1000W/m^2 with 100W/m^2 step-size. It can be seen that V_{ref} as well as parameters K_1, K_2 and K_3 are getting updated with each values of solar irradiance.

In Fig.5.12, it can be seen that for every change in G; V_{ref} varies and v_{pv} is quickly adjusted by the proposed MPPT to follow V_{ref} such that every-time the power drawn from the PV panel (p_{pv}) is the maximum possible one. For this maximization of PV panel power process, the PV panel current (i_{pv}) and dynamic resistance (r_{pv}) are also adjusted accordingly. Further, to test the efficacy of the proposed DISMC-MPPT, its performances are compared with that of two existing DISMC-MPPTs with different sliding surfaces such as DISMC-MPPT with sliding surface SS1 [117] and DISMC-MPPT with sliding surface SS2 [111] .

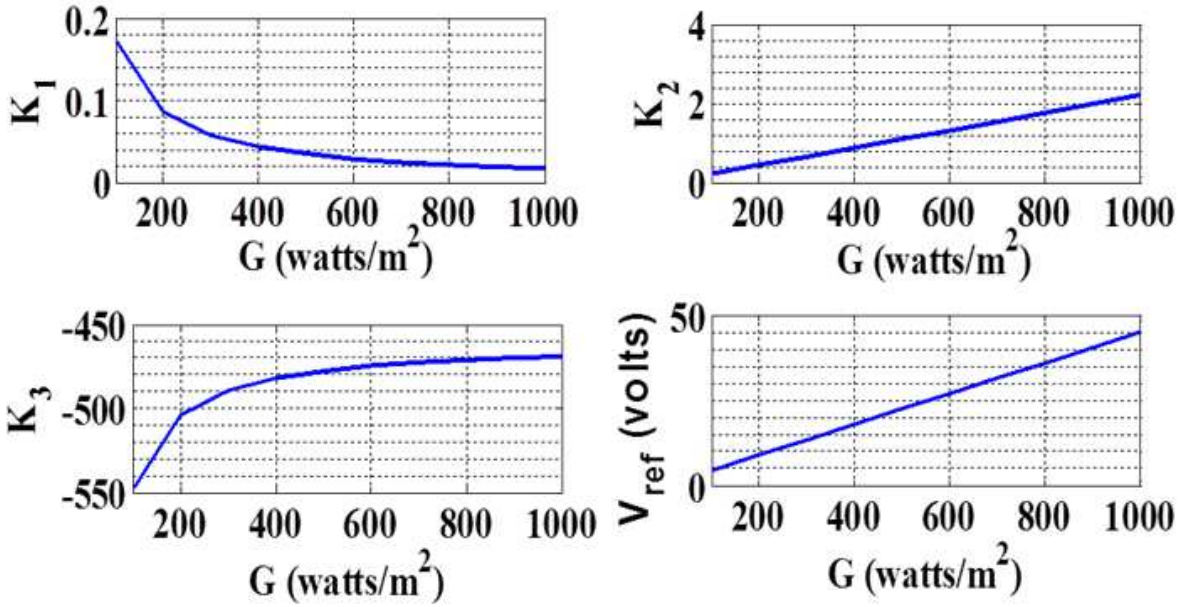

Figure 5.11: Values of K_1, K_2 and K_3 and V_{ref} of the tested PV system with DISMC-MPPT for variations in G from 100W/m^2 to 1000W/m^2

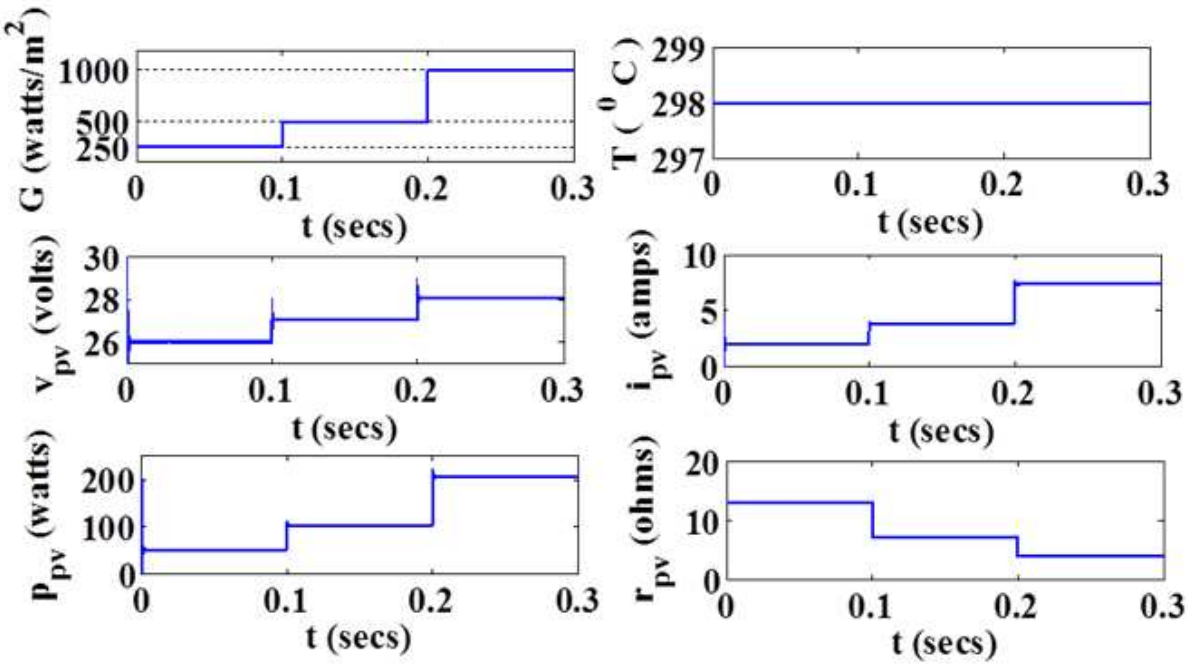

Figure 5.12: PV system output results at (v_{pv}), output current (i_{pv}), output power (p_{pv}) and output resistance (r_{pv}) at constant temperature (T) and variable solar irradiance (G)

Fig.5.13 compares the chattering and steady-state error (SSE) of the three MPPTs. In this figure, h_1 and h_2 are the highest and lowest chattering points respectively of the v_{pv} signals during steady-state of the chattering operation. The chattering magnitude (h) and SSE can be calculated eq (6.36) and (6.37) respectively. It can be seen that the proposed adaptive DISMC-MPPT has less SSE (2mV) and less h (2.8mV) than that of DISMC-MPPTs with sliding surface SS1 [117] and sliding surface SS2 [111] respectively.

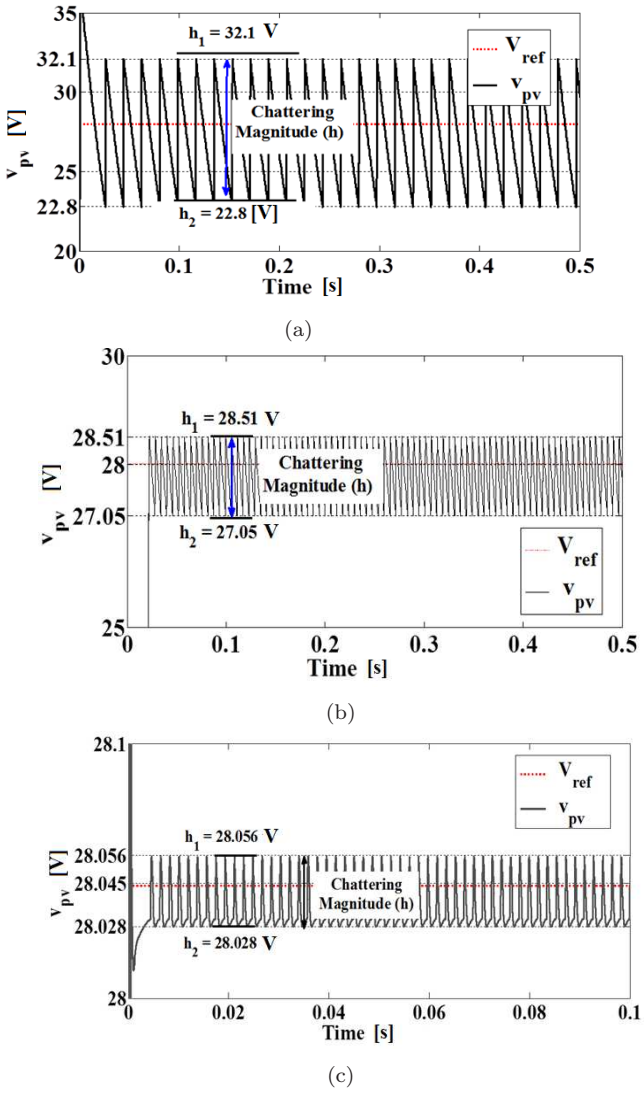

Figure 5.13: Comparison of PV panel output voltage signal at 1000 W/m^2 and 25^{0}C for (a) DISMC-MPPT with Jiao's sliding surface SS1, (b) DISMC-MPPT with sliding surface SS2 (c) Proposed DISMC-MPPT controller with adaptive K_1, K_2 and K_3

Further, when only structures of the above three DISMC-MPPTs are compared, then it is found that the proposed DISMC-MPPT has only three control variables i.e. v_{pv}, v_{dc} and i_{C1} similar as DISMC-MPPT with SS1 [117]. Hence, it needs only one current sensor for measurement of i_{C1}. But, DISMC-MPPT with SS2 [111] needs four control variables i.e. v_{pv},

v_{dc}, i_L and i_{C1} and two current sensors for measurements of i_L and i_{C1}. The current sensor is both expensive and adds complexity to the controller circuit. Hence, the proposed adaptive DISMC-MPPT is less expensive and complex compared to DISMC-MPPT with SS2 [111]. For a DISMC-MPPT, reaching-time to sliding surface, settling-time and maximum overshoot are three other important factors besides chattering phenomenon and SSE. Fig.5.14 shows the comparison of the three studied MPPT controllers for reaching-time and settling-time at 1000W/m^2 and 25^{0}C.

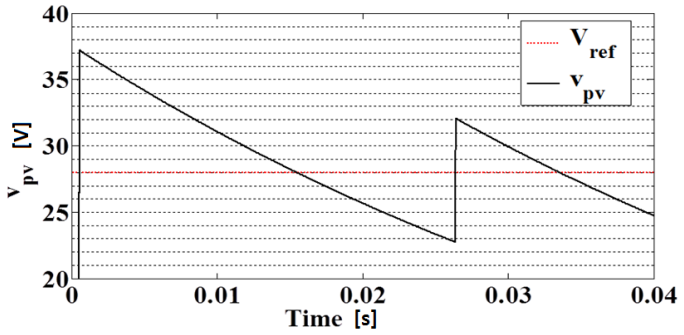

(a)

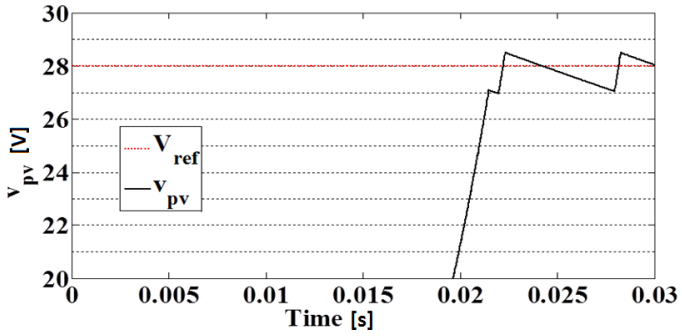

(b)

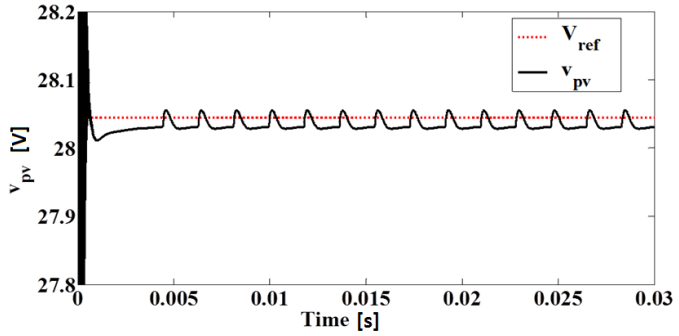

(c)

Figure 5.14: Comparison of reaching-time of (a) DISMC-MPPT [117], (b) DISMC-MPPT [111] and (c) Proposed adaptive DISMC-MPPT for the studied SSI-M6-205 PV panel output voltage signal at STC

From the figure, it is found that although reaching-time of the DISMC-MPPT with SS1 [117]is $\leq$ 5ms but its settling-time (25ms) is more than settling time (5ms) of proposed

Table 5.5: Comparison of chattering and steady state error of the studied PV Panel at 1000 W/m^2 and 25^0C using DISMC-MPPT with sliding surface SS1 [117], Adaptive DISMC-MPPT with SS2 [111] sliding surface SS2 and Proposed DISMC-MPPT controller

DISMC Types	h_1 (V)	h_2 (V)	Chattering h (V)	SSE (V)	Reaching time (ms)	Settling time (ms)
Proposed Adaptive DISMC	28.056	28.028	0.028	0.002	< 5	5
DISMC [111]	28.51	27.05	1.46	0.26	< 22	22
DISMC [117]	32.1	22.8	9.3	0.59	< 5	> 25

adaptive DISMC-MPPT. Also, the proposed adaptive DISMC-MPPT has less reaching-time and settling-time compared to that of DISMC-MPPT with SS2 [111]. The reason of faster response of the proposed DISMC-MPPT is because during the start-up, the sliding function of this DISMC with single current sensor is crossing the origin and the system representing point is very close to origin. Hence, the reaching time is less. Comparison of reaching and settling times of v_{pv} for PV system with proposed DISMC and DISMCs with that of DISMC [117] and DISMC [111]s at constant weather condition of 1000 W/m^2 and 25^0C are shown in Table 5.5.

Fig.5.15 shows the behavior of the v_{pv} signal during step-change in solar irradiance from 500 W/m^2 to 1000 W/m^2. Referring to Fig.5.15, it is found that the proposed adaptive DISMC-MPPT efficiently settled v_{pv} with in a span of 2ms which is less compared to that of DISMC-MPPT [117] (20ms) and DISMC-MPPT [111](2.5ms).

The overall behavior of the proposed adaptive DISMC-MPPT along with DISMC-MPPT [117] and DISMC-MPPT [111] have been summarized in Table 5.6. From Table 5.6, it is clear that the proposed adaptive DISMC-MPPT has less number of control variables and requires only one current sensor. Hence, its controller circuit is less expensive and has less complex control behavior. Further, the proposed DISMC-MPPT performs efficiently with less maximum over-shoot and chattering. Using this MPPT controller, the required reaching-time and settling-time are also very less. It also adjusts v_{pv} efficiently during variation in input solar radiation.

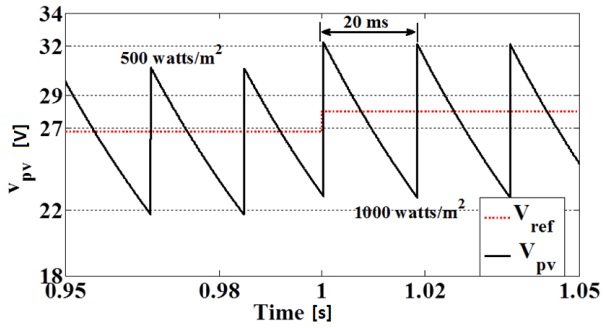

(a)

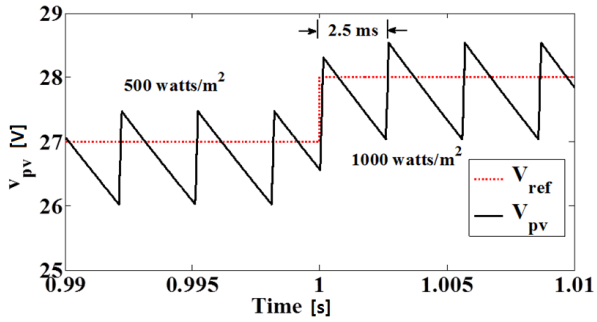

(b)

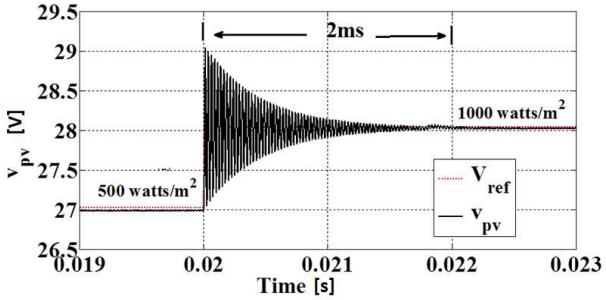

(c)

Figure 5.15: Comparison of MPP tracking results of (a) DISMC-MPPT with sliding surface SS1 [117], (b) DISMC-MPPT controller with sliding surface SS2 [111]and (c) Proposed DISMC-MPPT during step-change in solar irradiation from 500 W/m^2 to 1000 W/m^2

5.6.2 Real-time Simulation Results

The real-time simulation studies of the proposed adaptive DISMC-MPPT are done using the layout of the real-time HIL simulation set-up shown in Fig.3.16 of Chapter 4. It should be noted that the sampling time of the real-time simulation by OPAL-RT is considered to be 0.1ms. To verify the efficacy of this adaptive DISMC-MPPT, real-time voltage tracking results in case of this DISMC-MPPT is compared with that of the proposed DISMC-MPPT. Further, real-time voltage tracking results in case of this DISMC-MPPT is compared with that of the DISMC-MPPT [111] and DISMC-MPPT [117].

Fig.5.16 (a) shows the real-time tracking voltage of the studied SSI-M6-205 PV system with the proposed adaptive DISMC-MPPT for continuous step-change in solar irradiance

Table 5.6: Comparative studies of Simulated Results of MPPT controller properties and Tracking responses in case of Proposed Adaptive DISMC-MPPT with that of DISMC-MPPT [117], DISMC-MPPT [111] and Proposed DISMC-MPPT

Controller Properties	DISMC-MPPT	DISMC-MPPT	Proposed Adaptive DISMC-MPPT	Proposed DISMC-MPPT
Number of current sensors	Three	Two	Two	Two
Sliding surface parameters	Fixed	Fixed	Fixed	Adaptive
Complexity	More	Less	Less	Less
Control Variables	v_{pv}, v_{dc}, i_{pv}, i_L and i_{C1}	v_{pv}, v_{dc}, i_{pv}, i_{C1}	v_{pv}, v_{dc}, i_{pv}, i_{c1}	v_{pv}, v_{dc}, i_{c1}
Expensive	more	less	less	less
Reaching time	22 ms	$<$ 5ms	$<$ 5 ms	110 ms
Settling-time	22 ms	$>$ 25ms	5 ms	5 ms
Chattering	1.43V	9.3V	28mV	12.5mV
SSE (%)	2.2	3.9	0.08	0.7
Settling-time during step-change in input	2.5ms	20ms	2ms	2ms
Maximum overshoot (%)	1.78	14.27	3.57	19.5

between 500W/m^2 and 1000W/m^2. It can be seen in this figure that time taken by solar irradiance to change from 500W/m^2 to 1000W/m^2 is 0.5ms. For that change in solar irradiance, PV voltage is taking 18ms to change. Hence, MPP tracking time in this case is 17.5ms. Again, the real-time tracking results in case of this proposed adaptive DISMC-MPPT is compared with that of proposed DISMC-MPPT in Fig.5.16 (b) for continuous step-change in solar irradiance between 500W/m^2 and 1000W/m^2. From this figure, it can be observed that the PV voltage signal for adaptive DISMC-MPPT has 12.5mV of voltage chattering height and 18ms of settling time. The voltage chattering height and settling time in case of proposed DISMC-MPPT with fixed sliding surface are 25.8mV and 26ms respectively. Therefore, the MPP tracking time in this case is 25.5ms. Analyzing the real-time tracking results shown in Fig.5.16 (a) and (b), it is clear that tracking performance in case adaptive DISMC-MPPT is better than that of DISMC-MPPT.

5.6.3 Experimental Results

Fig.5.17 shows different experimental results from prototype PV system with the proposed adaptive DISMC-MPPT. The PV voltage at 958W/m^2 and 45^0C of weather condition is shown in Fig.5.17 (a). The value of PV voltage output for this weather condition is measured as 94.1V. Similarly, PV voltage at 916W/m^2 and 41^0C of weather condition is shown in Fig.5.17 (a). PV voltage output in this case is measured as 93.4volts. Fig.5.17 (c) shows

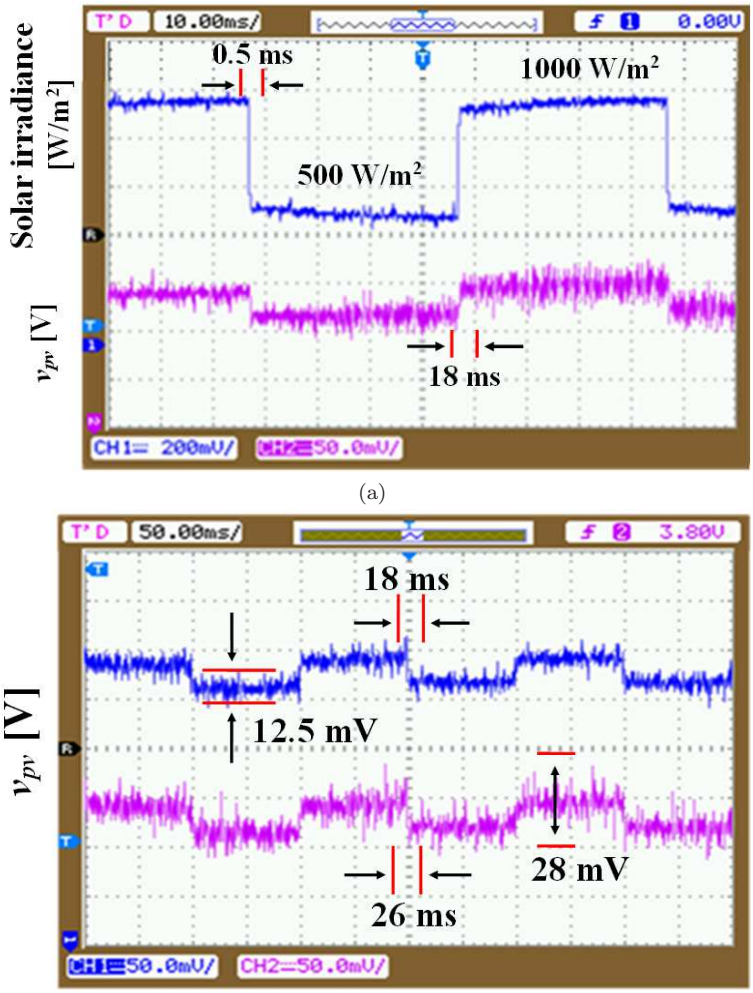

Figure 5.16: Real-time tracking responses of PV system with Proposed DISM Current Controller using OPAL-RT for (a) v_{pv} with proposed adaptively chosen of K_1, K_2 and K_3 and (b) v_{pv} with empirically chosen fixed value of K_1, K_2 and K_3

experimental result displaying the tracking voltage of PV system with the proposed adaptive DISMC-MPPT when MPPT is switched ON. In this figure, at first the PV system is in OFF mode. Hence, PV voltage is same as its open-circuit voltage. At **A**, the MPPT is switched ON. In this figure, time span between **A** to **B** is the tracking time. After **B**, the PV voltage oscillates around the MPP voltage. It is found that tracking periods is 0.9s and voltage fluctuation at steady-state is 1V.

Fig.5.18 (a)-(d) show different experimental results from the prototype PV system with proposed adaptive DISMC-MPPT during MPP tracking operation at 248W/m^2 and 32^{0}C. PV voltage at this condition is obtained as 62.4V as shown in Fig.5.18 (a). This Fig.5.18 (a) also shows that duty-ratio of gate pulse of converter is 52.4%. It is shown in Fig.5.18 (b) that the dc-link voltage is 128V. Fig.5.18 (c) shows the AC load voltage signal at output of the single phase inverter in which frequency is 50Hz and peak-peak voltage is 66V. Hence,

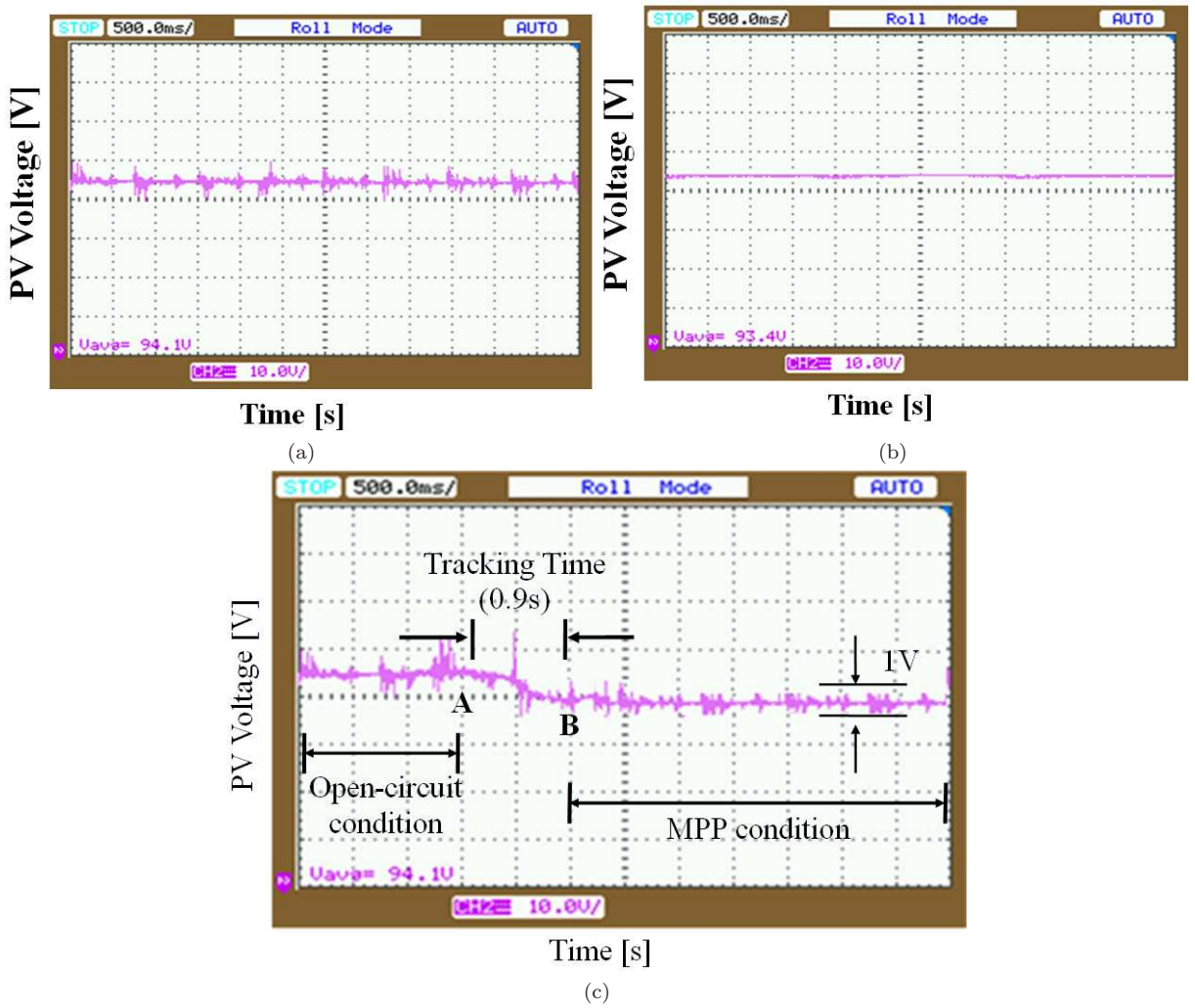

Figure 5.17: Experimental PV voltage of prototype PV system at (a) 958W/m^2 and 45^0C, (b) 916W/m^2 and 41^0C, (c) change in weather conditions from 916W/m^2 and 41^0C to 958W/m^2 and 45^0C

the RMS load voltage is 46.7V. At last Fig.5.18 (d) shows the gate pulses of the inverter.

5.7 Chapter Summary

A DISMC-MPPT and an adaptive DISMC-MPPT are proposed in this chapter. These two DISMC-MPPTs have been developed with new sliding surfaces. In the first proposed DISMC-MPPT, controller coefficients are taken fixed whilst in the proposed adaptive DISMC-MPPT, controller coefficients are updated with changing weather conditions. The PWM mechanism adds advantages such as simple control structure and fixed frequency operation to these two DISMC-MPPTs. With simulation and real-time simulation results, the MPP tracking capability of the proposed DISMC-MPPT is verified to be better than that of ISMC-MPPT and SMC-MPPT. The selection of the sliding mode control coefficients in case of the proposed adaptive DISMC-MPPT taking account the reaching and

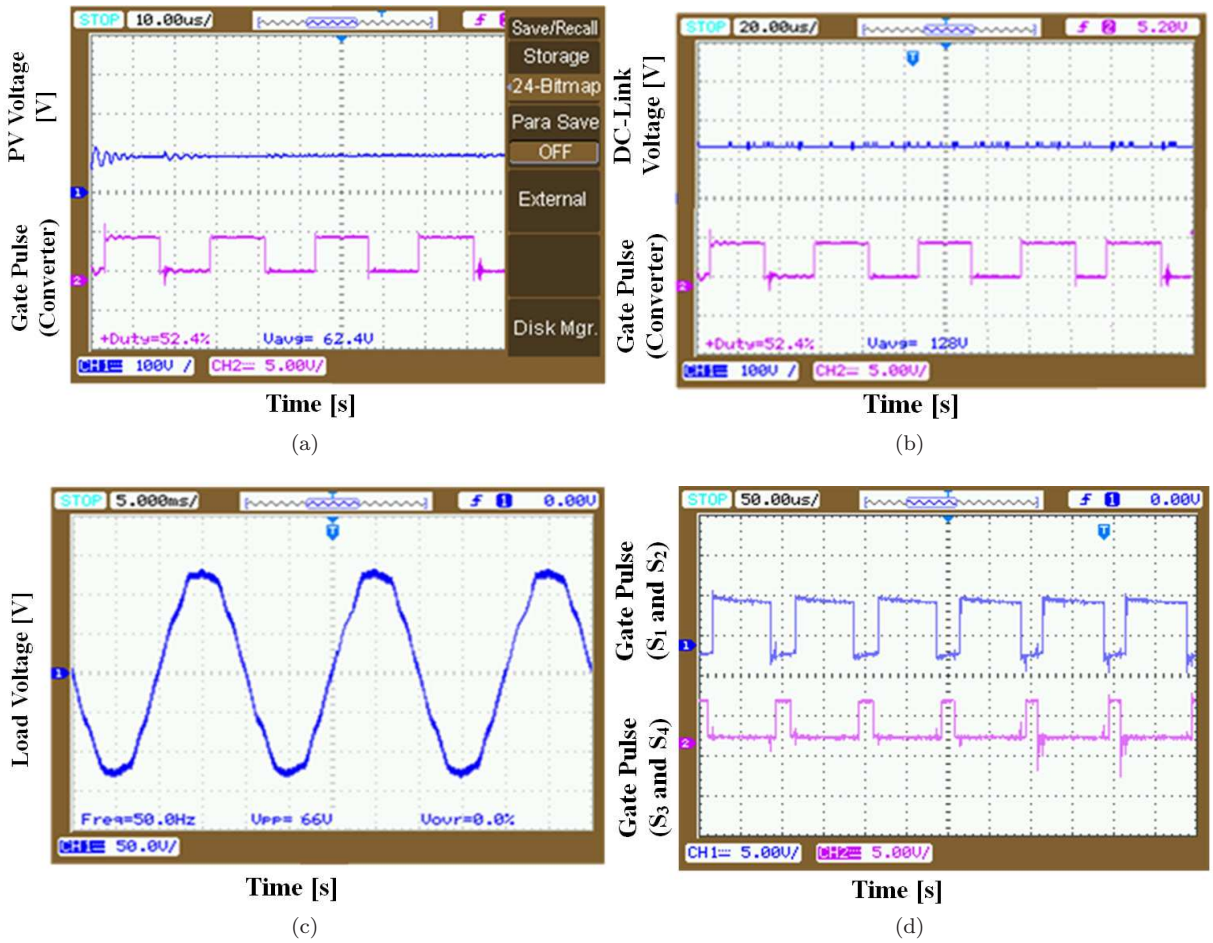

Figure 5.18: Experimental results of prototype PV system showing (a) PV voltage and DC/DC boost converter gate pulse during MPP tracking task, (b)DC/link voltage and DC/DC boost converter gate pulse during MPP tracking task, (c) AC load voltage at output of Inverter and (d) Inverter gate pulses for solar irradiance of 448W/m^2

stability conditions facilitates with fast response and guaranteed stability. The efficacy of the proposed adaptive DISMC-MPPT is verified comparing with proposed DISMC-MPPT, DISMC-MPPT [111] and DISMC-MPPT [117]. From these comparisons, it is found that with less number of components and control variables than DISMC-MPPT [111], the proposed adaptive DISMC-MPPT needs less reaching time than that of DISMC-MPPT [111]. Similarly, the proposed adaptive DISMC-MPPT has less chattering compared to the DISMC-MPPT [117] and proposed DISMC-MPPT. Hence, the proposed adaptive DISMC-MPPT is found to be an efficient MPP tracking of PV system perfectly balancing the control structure complexity, chattering in output signal and response time. The verification of efficacy of this proposed adaptive DISMC-MPPT is supported with experimental, simulation and real-time simulation results.

Chapter 6

Self-tuned Adaptive Maximum Power Point Tracker for a Photovoltaic System for a Photovoltaic System

6.1 Introduction

This chapter proposes a new self-tuning MPPT that is designed with an incremental proportional integral derivative (IPID) controller for a stand-alone photovoltaic (PV) system. It has been discussed in Chapter 3, 4 and 5 that PID-controller is the most popular controllers in MPPT applications because of its simple structure [120]. Uncertainties in the input PV voltage occur due to varied weather conditions and load connected to PV system. There may be rapid or sudden variations in load or input voltage. Under such situations, a fixed gain PID-controller may not adapt to the changing weather conditions. These variations in weather conditions result in fast changes in the DC/DC converter control signals in the MPPT of the PV system which may cause instability. This instability issue in the situation of rapid input and output variations in the switched converter can be avoided using an IPID controller [121]. Because, this IPID-controller limits the speed of the control signal and hence the control signal varies slowly providing efficient regulation of converter avoiding instability issue [122]. Hence, the same concept can be extended to a MPPT for a PV system.

For successful MPP tracking, parameters of IPID-controller such as K_C, T_I and T_D must be appropriately chosen. Usually, tuning of these controller parameters are based on observations on duty-ratio and PV voltage relationship of the MPPT converter of the PV system for a fixed period. The load characteristics or external disturbances are not considered in the PV system [122].

The MPPT converter may suffer from aging problem, uncertainties in load and input voltage fluctuations affecting its dynamic behavior. IPID-controller with fixed values of K_C, T_I

and T_D are unsuitable for above situations. Therefore, adaptive controllers such as DISMC-MPPTs (Chapter 5) are preferred for robust tracking operations. The DISMC-MPPT with adaptive sliding surface described in the same Chapter 6 is showing better tracking results than that of P&O-MPPT, INC-MPPT, APO-MPPT, ATAMPPT and APEFC-MPPT with less voltage and current fluctuations, less tracking error and less tracking time.

But, the performance of adaptive DISMC-MPPT is dependent on the selection of its sliding surface. An appropriate tuning rule is necessary to tune parameters of this sliding surface. Again, although the DISMC-MPPT is robust in nature while tracking operation, but it is designed around non-linear models of PV panel and DC/DC boost converter of the PV system. In nonlinear models of PV system, on-line parameter extraction is not possible because of intrinsic nature of the PV system dynamics. The parameters used in these nonlinear models are usually calculated off-line using some parameter extraction algorithms and then made adaptive using some approximation rules chosen. It is also found that external disturbances are not considered while identifying the PV system dynamics. Therefore, there is requirement of new MPPTs that is designed with a black-box model of PV system that is identified on-line considering error in measurement (disturbances) [123].

It is observed from literature that instead of designing adaptive controllers using a non-linear MPPT converter model, it would be easier and effective to design those controllers on a linearized MPPT converter model. Further, instead of linearizing the nonlinear MPPT converter model circuit using small signal analysis, on-line system identification techniques can be used to identify parameters of a pre-defined linearized structure such as ARX of the MPPT converter. In on-line system identification techniques, no detail a prori knowledge of converter is required. Also, error in measurement can also be considered [87]. In order to improve MPP tracking adaptations such as response time and tracking accuracy of the PV system, self-adjusting fuzzy MPPT controllers have been used in [124]. But stability proof of these fuzzy MPPTs is very difficult because of lack of accurate mathematical descriptions [125]. Self-tuning controller is one of such type of adaptive controllers that uses linearized plant model [87].

Self-tuning algorithm follows two distinct steps namely (i) on-line parameters estimation of a pre-defined linearized structure of the DC/DC boost converter and (ii) generation of the control signal designing a suitable control law. For identification of converter model, Least-square (LS) or Recursive Least-square (RLS) methods can be employed. For rapid variations of the parameters, RLS is preferable because by assigning a forgetting factor, the MPPT converter model parameters can be identified [126]. Minimum variance (MV) and Generalized Minimum variance (GMV) are two suitable control laws used in self-tuning controller. MV cannot deal with a NMP system (a system with the zeros outside the unit circles). Situations of NMP usually resulted because of inappropriate selection of sampling

period in control algorithm. In this situation, a dead-bit response (closed loop poles lie in origin) exists in the converter. To handle that a large control signal is required that is practically infeasible as control signal of a boost converter lies between 0 and 1. GMV can deal with NMP problem by introducing three scalar weights P, Q and R in its cost function to avoid dead-bit situations. But, it is very difficult to make choice of P, Q and R in its cost function so that perfect balance in control action would be maintained [127]. Incremental GMV (IGMV) control law [89] can be used where the cost function has only a single weighing parameter that can be easily tuned.

Self-tuning control techniques have been applied successfully to a number of systems such as voltage regulation of DC/DC converters and inverters. However, there is a little application of self-tuning control technique to a PV system [128]. Therefore, in this work, a new self-tuned-MPPT with RLS based parameter estimation, IGMV based control law and IPID-controller has been designed and implemented in a PV system. The performances of this self-tuned-MPPT are verified through both simulation and experimental studies pursued using a developed PV control set-up that has FPGA platform for implementation of the control algorithms.

6.2 Problem Formulation

The equivalent circuit of a PV system is shown in Fig.6.1 (a). When solar radiation G falls on the PV system,current I_{ph} is generated at the output terminals of the PV system. The PV system voltage v_{pv} and current i_{pv} and are available. Applying Kirchoff's current law at output terminal of the circuit shown in Fig.6.1 (a), the current-voltage (I-V) characteristics can be expressed as in eq (6.1).

$$i_{pv} = I_{pv} - I_0 \left[\exp\left(\frac{v_{pv} + i_{pv}R_s}{N_s V_t}\right) - 1\right] - \frac{v_{pv} + i_{pv}R_s}{R_{sh}} \tag{6.1}$$

where I_0 is the dark-saturation current, n_s, R_s and R_{sh} are number of series cells in the PV panel, series resistance and shunt resistance respectively. V_t is the thermal voltage of the PV system given by eq (6.2).

$$V_t = \frac{a k_b T}{q} \tag{6.2}$$

where a is diode-ideality factor, k_b is Boltzmanns constant, T is junction temperature and q is the charge of an electron. The output power of the PV system is given by eq (6.3).

$$p_{pv} = v_{pv} \times i_{pv} \tag{6.3}$$

There exists a single point called Maximum Power Point (MPP) at any solar irradiance at which output power of the PV system is the maximum as shown in Fig.Fig.6.1 (b).

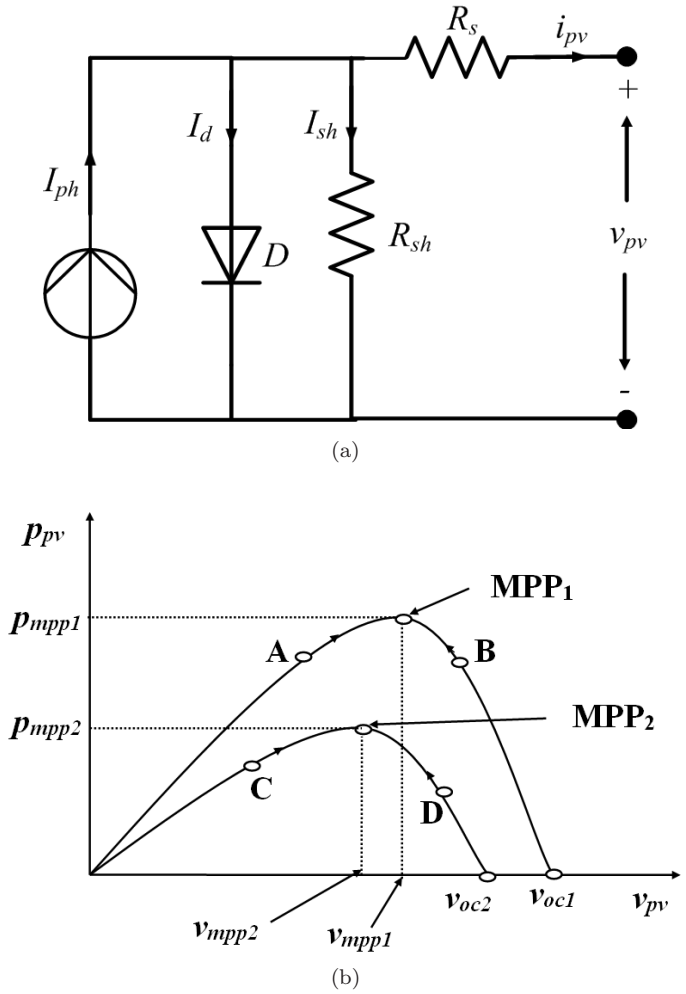

Figure 6.1: (a) Equivalent circuit model of a PV Panel and (b) P-V characteristics of a PV Panel at different weather conditions

6.3 Proposed Self-Tuning MPPT

6.3.1 Tracking error calculation

At MPP, the power from PV panel is maximum. Therefore the following relation holds good.

$$\frac{dp_{pv}}{dv_{pv}} = 0 \tag{6.4}$$

In a MPPT (Fig.6.2), In MPPTs like P&O, ATAMPPT and DISMC, tracking of MPP is done as follows. The voltage at MPP v_{mpp} is calculated using a MPPT algorithm (Fig.6.2). Then the operating point of the PV system can be adjusted to track this calculated v_{mpp} by using a DC/DC boost converter. Further, a controller is used in the PV system to perform this tracking task to help of a DC/DC boost converter. Therefore, in these MPPTs, MPP tracking of PV system is done following three distinct steps such as in step 1, the voltage at MPP v_{mpp} is calculated using a MPPT algorithm. In step 2, the tracking error is calculated using a comparator and in step 3, the control signal u can be calculated using a controller.

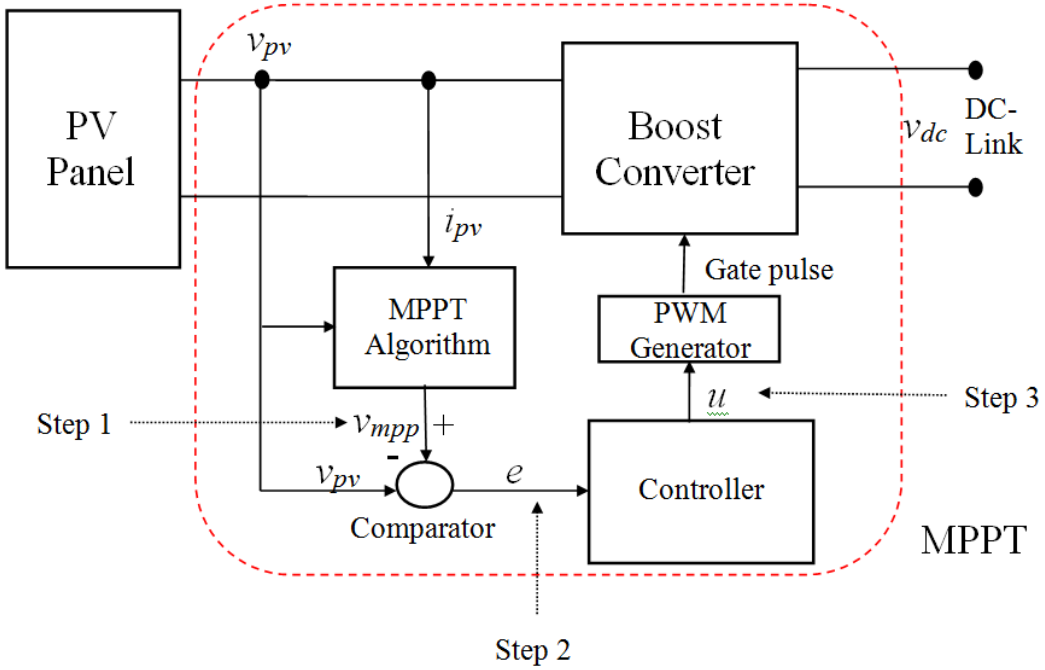

Figure 6.2: PV system with the proposed Self-Tuned-MPPT

Efficient design of MPPT algorithm and controller is the focus in a PV system in order to achieve good performances and power conversion efficiency of the entire PV system. Using eq (6.3) in eq (6.4),

$$i_{pv} + v_{pv}\frac{di_{pv}}{dv_{pv}} = 0 \tag{6.5}$$

At any operating condition other than MPP such as A, B, C or D, eq (6.5) may be generalized as

$$i_{pv} + v_{pv}\frac{di_{pv}}{dv_{pv}} = \psi; \quad \psi \neq 0 \tag{6.6}$$

Dynamic resistance of a PV panel can be defined as

$$r_{pv} = -\frac{dv_{pv}}{di_{pv}} \tag{6.7}$$

Applying eq (6.7) in eq (6.6), one gets

$$i_{pv} - \frac{v_{pv}}{r_{pv}} = \psi \Rightarrow v_r - v_{pv} = \psi' \tag{6.8}$$

where

$$\begin{cases} v_r = i_{pv} r_{pv} \\ \psi' = r_{pv} \times \psi \end{cases} \tag{6.9}$$

When the operating point approaches MPP, $\psi \to 0$ and hence $\psi' \to 0$ as $r_{pv} \neq 0$. Therefore, to operate the PV system always at MPP,ψ' must be zero. In this chapter, ψ' is considered as the tracking error e of the PV system. Hence, by setting $\psi' \to 0$, tracking error $e \to 0$ can be made and hence $v_{pv} \to v_{mpp}$. Fig.6.3 depicts the PV system with the proposed MPPT.

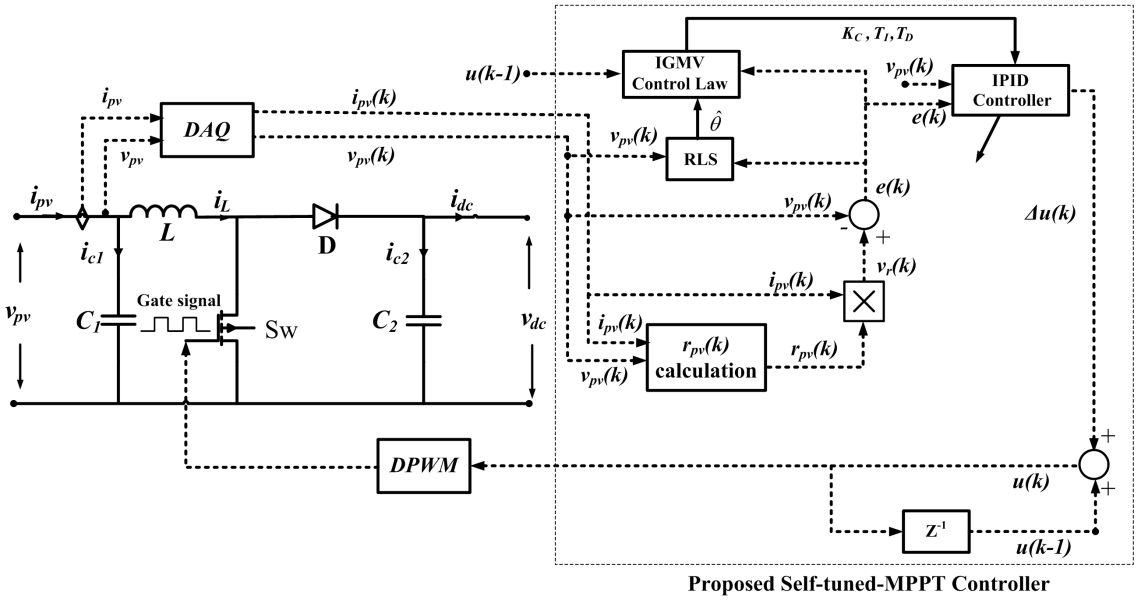

Figure 6.3: PV system with the proposed Self-Tuned-MPPT

6.3.2 MPPT Converter Model

The MPPT converter used in this chapter is a DC/DC boost converter. The control input of a boost converter is its duty-ratio of the gate signal. In this application, the output of this MPPT converter is the PV voltage as here input voltage is supposed to be controlled. The dynamic characteristic of the boost converter with unknown parameters can be expressed as a quadratic system as follows.

$$A\left(z^{-1}\right) v_{pv}\left(k\right) = z^{-d} B\left(z^{-1}\right) u\left(k-1\right) + \xi\left(k\right) \tag{6.10}$$

where u(k) is control input, $\xi\left(k\right)$ is the probability or observation noise, z^{-1} is the backward-shift operator and d is the number of backward-shift or time-delay or dead-time such that $d \geq 1$.

$$\begin{aligned} A\left(z^{-1}\right) &= 1 + a_1 z^{-1} + a_2 z^{-2} \\ B\left(z^{-1}\right) &= b_0 + b_1 z^{-1} + ... + b_m z^{-m} \\ z^{-1} v_{pv}\left(k\right) &= v_{pv}\left(k-1\right) \end{aligned} \tag{6.11}$$

6.3.3 IPID Controller

Instead of PID-controller, an incremental PID-controller (IPID-controller) has been used in this chapter. The control law of this controller prevents the rapid change of control input u by controlling change in u which is instead of u. This provides appropriate control action to the boost converter for maintaining its stability. The IPID-control law can be defined as

follows.

$$\Delta u\left(k\right)=K_{c}\frac{T_{s}}{T_{I}}e\left(k\right)-K_{c}\left(\Delta+\Delta^{2}\frac{T_{D}}{T_{s}}\right)v_{pv}\left(k\right) \tag{6.12}$$

where T_s, K_C, T_I and T_D are the sampling time, proportional gain, integral time and derivative time respectively. The required control signal $u\left(k\right)$ can be updated as

$$u\left(k\right)=u\left(k-1\right)+\Delta u\left(k\right) \tag{6.13}$$

The parameter $\Delta=1-z^{-1}$ and e(k) is the k^{th} sampled control error which can be calculated as

$$e\left(k\right)=\psi'\left(k\right)=v_{r}\left(k\right)-v_{pv}\left(k\right) \tag{6.14}$$

Here, the parameters T_s, K_C, T_I and T_D are usually the control parameters. Hence, it is essential to use appropriate values of these parameters. Hence, incremental generalized minimum variance (IGMV) based self-tuning control law is used for tuning these parameters.

6.3.4 Tuning of IPID Controller

In this chapter, the IPID controller is tuned using IGMV control law. This control law uses the concept of minimization of the following cost function as in [].

$$J_{s}=\Xi\left[\phi^{2}\left(k+k_{m}+1\right)\right. \tag{6.15}$$

where

$$\Xi\left[\bullet\right]=\text{Mathematical expectation operator} \tag{6.16}$$

and $\phi\left(k+k_{m}+1\right)$ is the generalized output and is given by

$$\phi\left(k+k_{m}+1\right)=\Gamma\left(z^{-1}\right)e\left(k+k_{m}+1\right)+w\Delta u\left(k\right) \tag{6.17}$$

where w is the weighing factor of the control input. $\Gamma\left(z^{-1}\right)$ is an user-defined polynomial such as

$$\Gamma\left(z^{-1}\right)=1+\Gamma_{1}z^{-1}+\Gamma_{2}z^{-2}+... \tag{6.18}$$

The cost function J_s defined in eq (6.15) can be minimized using the following Diophantine equation

$$\Gamma\left(z^{-1}\right)=\Delta A\left(z^{-1}\right)E\left(z^{-1}\right)+z^{-(k_{m}+1)}F\left(z^{-1}\right) \tag{6.19}$$

where

$$\begin{aligned}E\left(z^{-1}\right)&=1+\varepsilon_{1}z^{-1}+...+\varepsilon_{k_{m}}z^{-k_{m}}\\F\left(z^{-1}\right)&=f_{0}+f_{1}z^{-1}+f_{2}z^{-2}\end{aligned} \tag{6.20}$$

where the degree of polynomials $E\left(z^{-1}\right)$ and $F\left(z^{-1}\right)$ are k_m and 2 respectively as all the parameters of the polynomials E and F are unique. Now, minimizing eq (6.19), the following control law can be obtained.

$$F\left(z^{-1}\right)e\left(k\right)+\left\{E\left(z^{-1}\right)B\left(z^{-1}\right)+w\right\}\Delta u\left(k\right)=0 \tag{6.21}$$

Now, applying the value of e(k) from eq (6.15) in eq (6.14), the IPID-control law can be rewritten as follows.

$$\Delta u\left(k\right)=K_c\frac{T_s}{T_I}\left(v_r\left(k\right)-v_{pv}\left(k\right)\right)-K_c\left(\Delta+\Delta^2T_D\right)v_{pv}\left(k\right) \tag{6.22}$$

Eq (6.22) can be simplified as

$$\Delta u\left(k\right)=K_c\frac{T_s}{T_I}v_r\left(k\right)-K_c\left(\frac{T_s}{T_I}+\Delta+\Delta^2\frac{T_D}{T_s}\right)v_{pv}\left(k\right) \tag{6.23}$$

Applying Taylors series, Eq (6.23) can be expanded as

$$\Delta u\left(k\right)=K_c\frac{T_s}{T_I}v_r\left(k\right)-K_c\left\{\left(\frac{T_s}{T_I}+1+\frac{T_D}{T_s}\right)-\left(1+2\frac{T_D}{T_s}\right)z^{-1}+\frac{T_D}{T_s}z^{-2}\right\}v_{pv}\left(k\right) \tag{6.24}$$

or

$$\Delta u\left(k\right)=K_c\frac{T_s}{T_I}v_r\left(k\right)-C\left(z^{-1}\right)v_{pv}\left(k\right) \tag{6.25}$$

where

$$C\left(z^{-1}\right)=K_c\left\{\left(\frac{T_s}{T_I}+1+\frac{T_D}{T_s}\right)-\left(1+2\frac{T_D}{T_s}\right)z^{-1}+\frac{T_D}{T_s}z^{-2}\right\} \tag{6.26}$$

At steady-state, $E\left(z^{-1}\right)$ and $B\left(z^{-1}\right)$ can be replaced by $E(1)$ and $B(1)$. Hence, eq (6.21) becomes

$$F\left(z^{-1}\right)e\left(k\right)+\tau\Delta u\left(k\right)=0 \tag{6.27}$$

where $\tau:=E\left(1\right)B\left(1\right)+w$. Then,

$$\frac{F\left(z^{-1}\right)}{\tau}e\left(k\right)+\Delta u\left(k\right)=0 \tag{6.28}$$

Applying value of from eq (6.15) in eq (6.28), one gets

$$\frac{F\left(z^{-1}\right)}{\tau}\left(v_r\left(k\right)-v_{pv}\left(k\right)\right)+\Delta u\left(k\right)=0 \tag{6.29}$$

Eq (6.29) can be rearranged as

$$\Delta u\left(k\right)=\frac{F\left(z^{-1}\right)}{\tau}v_{pv}\left(k\right)-\frac{F\left(z^{-1}\right)}{\tau}v_r\left(k\right) \tag{6.30}$$

Comparing eq (6.27) and eq (6.30) yeilds

$$C\left(z^{-1}\right)=\frac{F\left(z^{-1}\right)}{\tau} \tag{6.31}$$

Applying value of $C\left(z^{-1}\right)$ from eq (6.26) and $F\left(z^{-1}\right)$ from eq (6.21) in eq (6.31), it becomes

$$K_c\left\{\left(\frac{T_s}{T_I}+1+\frac{T_D}{T_s}\right)-\left(1+2\frac{T_D}{T_s}\right)z^{-1}+\frac{T_D}{T_s}z^{-2}\right\}=-\left\{\frac{f_0}{\tau}+\frac{f_1}{\tau}z^{-1}+\frac{f_2}{\tau}z^{-2}\right\} \quad (6.32)$$

Comparing the coefficients of the order of back-ward-shift operator in eq (6.32), K_C, T_I and T_D can be calculated as follows.

$$\begin{aligned} K_C &= \frac{f_1+2f_2}{\tau}T_s \\ T_I &= \frac{-\left(f_1+2f_2\right)}{f_0+f_1+f_2}T_s \\ T_D &= \frac{-f_2}{f_1+2f_2}T_s \end{aligned} \quad (6.33)$$

6.3.5 System Identification of PV System with a MPPT

The parameter vector of the PV system is given by

$$\theta=\begin{bmatrix} a_1 & a_2 & b_1 & b_2 & ... & b_m \end{bmatrix}^T \quad (6.34)$$

The linear mathematical model of the PV system is described in eq (6.10) is in Auto-Regressive exogenous (ARX) form. It can be rewritten as

$$v_{pv}\left(k\right)=-a_1v_{pv}\left(k-1\right)-a_2v_{pv}\left(k-2\right)+b_0u\left(k-d\right)+...+b_1u\left(k-d-k_m\right)+\xi\left(k\right) \quad (6.35)$$

Eq (6.35) can again be rewritten as

$$v_{pv}\left(k\right)=\varphi^T\left(k\right)\theta+\xi\left(k\right) \quad (6.36)$$

where, φ is known as vector of observations or regression vector and defined as

$$\varphi\left(k\right)=\begin{bmatrix} -v_{pv}\left(k-1\right) & -v_{pv}\left(k-2\right) & u\left(k-d\right) & ... & u\left(k-d-k_m\right) \end{bmatrix}^T \quad (6.37)$$

Tuning of parameters of IPID-controller such as K_C, T_I and T_D based on IGMVC law are possible only if the PV system parameters θ is known. But, actually exact values of these parameters θ are not known a priori. Hence, estimation of the values of a_i and b_i can be made by using a parameter estimation algorithm. In this work, a RLS based estimation algorithm is used which is described as follows. Considering $\xi\left(k\right)$ is zero, eq (6.36) can be rewritten in regressor form as

$$v_{pv}\left(k\right)=\varphi^T\left(k\right)\theta\left(k\right) \quad (6.38)$$

RLS algorithm can be applied directly to estimate $\hat{\theta}$ as follows.

$$\hat{\theta}\left(k\right)=\hat{\theta}\left(k-1\right)+K\left(k\right)\left[v_{pv}\left(k\right)-\varphi^T\left(k\right)\hat{\theta}\left(k-1\right)\right] \quad (6.39)$$

$$K\left(k\right)=\frac{C\left(k-1\right)\varphi^T\left(k\right)}{\lambda+\varphi^T\left(k\right)C\left(k-1\right)\varphi\left(k\right)} \quad (6.40)$$

Table 6.1: Values of theta for Different Input Voltages

	Solar	irradiance	$[\mathrm{W}/m^2]$	
Theta	250	500	750	1000
a_1	590.5038	596.1201	603.9981	615.6499
a_2	590.0195	596.1991	603.3781	615.1781
b_0	590.5544	596.1845	604.1915	615.4930
b_1	16.2521	16.4144	16.6289	16.9513

Table 6.2: Values of IPID-Controller Parameters for Different Input Voltages

	Solar	irradiance $[\mathrm{W}/m^2]$
IPID-parameters	500	1000
K_C	1.6261	0.1003
T_I	9.4941	9.4968
T_D	1254.7	1254.7

$$C(k) = \frac{\left[I - K(k)\,\varphi^T(k)\right] C(k-1)}{\lambda} \tag{6.41}$$

where $\hat{\theta}$, K(k), λ and C(k) are estimated value of θ , Kalman-gain matrix, forgetting factor such that $0 < \lambda < 1$ and covariance-matrix respectively at k^{th} sample.

6.4 Results and Discussions of Proposed Self-tuned MPPT

6.4.1 Simulation Results

For designing the proposed self-tuning MPPT, the unknown parameters (a_1, a_2, b_0 and b_1) of linear MPPT converter mathematical model given in eq (6.10) are estimated using RLS algorithms. The estimated MPPT converter parameters (a_1, a_2, b_0 and b_1) and calculated IPID-controller parameters K_C, T_I and T_D using IGMV control law for different weather conditions are shown in Table 6.1 and 6.2 respectively.

Comparison of RLS estimated P-V characteristics of the PV array with that of the actual is shown in Fig.6.4(a). The corresponding estimation of PV power error is shown in Fig.6.4 (b). From these two figures, it is clear that the estimated P-V curve closely matches with the actual P-V curve.

Considering the parameters estimated by RLS, now the different control laws of self-tuning control schemes i.e. pole-placement, GMV and IGMV were verified for MPPT of the studied PV system. Fig.6.5 shows the MPP tracking performances of the proposed self-tuning MPPT with different control laws considering a PID-controller.

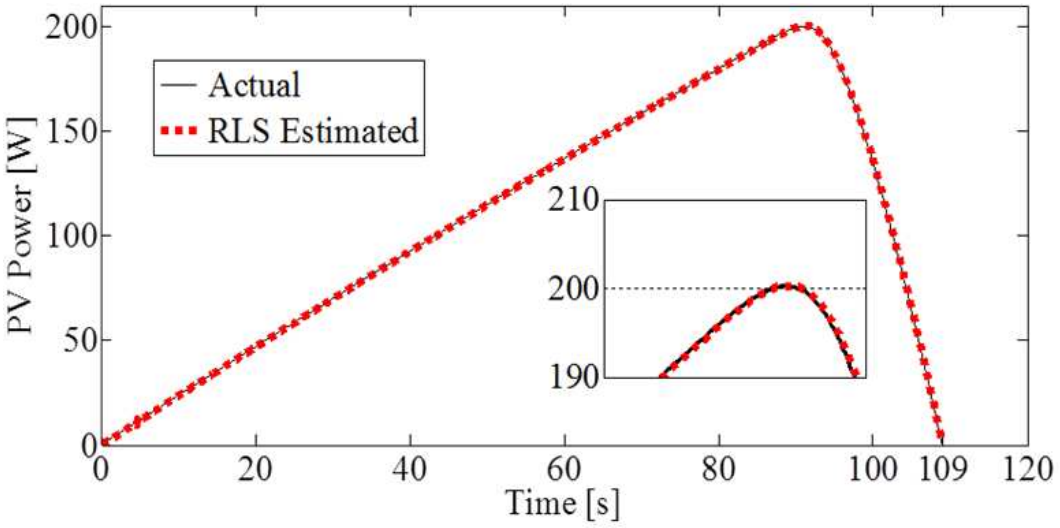

(a)

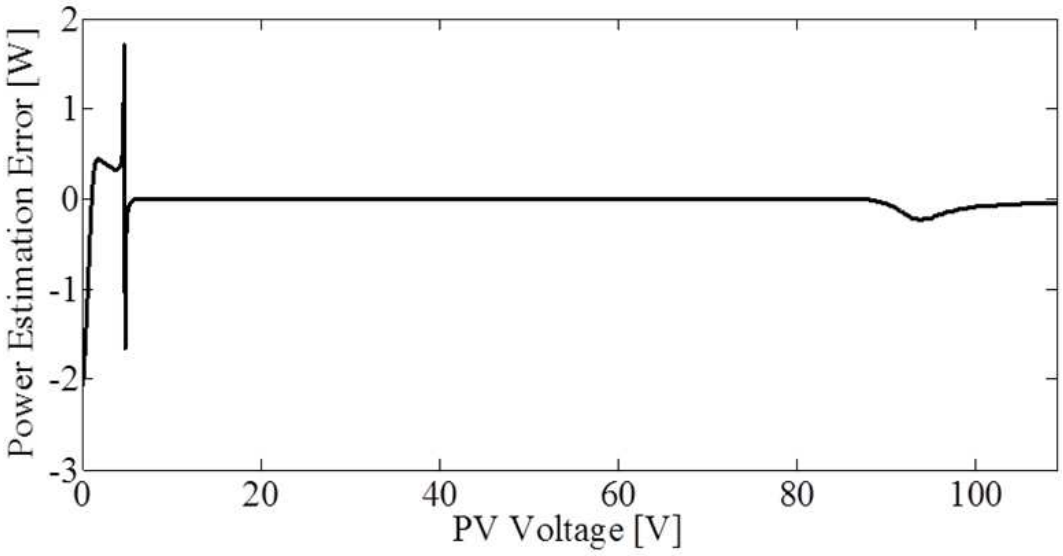

(b)

Figure 6.4: (a) Comparison of P-V characteristics of RLS identified ARX model with that of actual P-V characteristic of studied prototype PV array and (b) estimated PV power error using RLS algorithm

Fig.6.6 shows the same MPP tracking performances considering an IPID-controller. These two figures envisage that although the tracking speed in case of IGMV tuning law is low but maximum overshoot of tracking voltage and tracking time is also less than that of GMV and pole-placement tuning laws. Again, proposed self-tuning MPPT with IPID-controller and IGMV tuning law has yielded the lowest overshoot with lesser tracking time than in case of MPPTs with GMV and pole-placement.

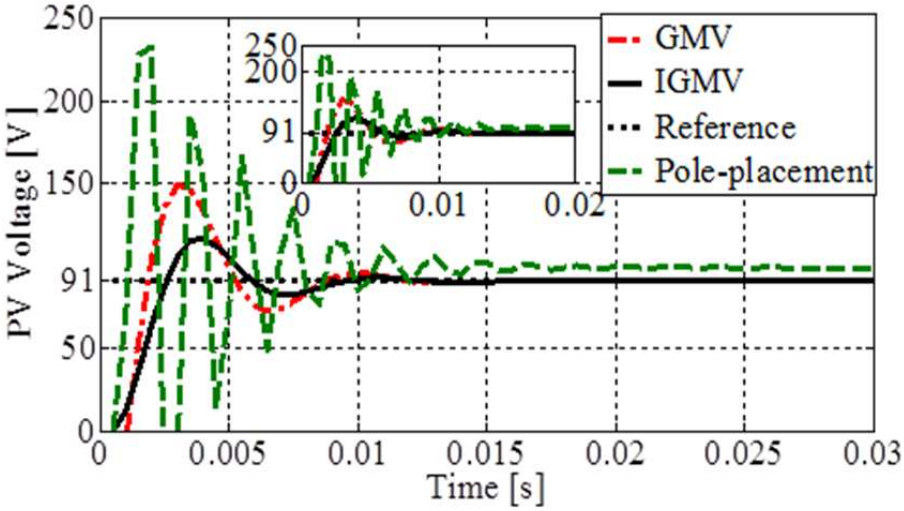

Figure 6.5: Comparison of MPP tracking response of the studied PV system with the Self-Tuned MPPT, IGMV-MPPT, Pole-placement-MPPT and GMV-MPPT using PID-controller

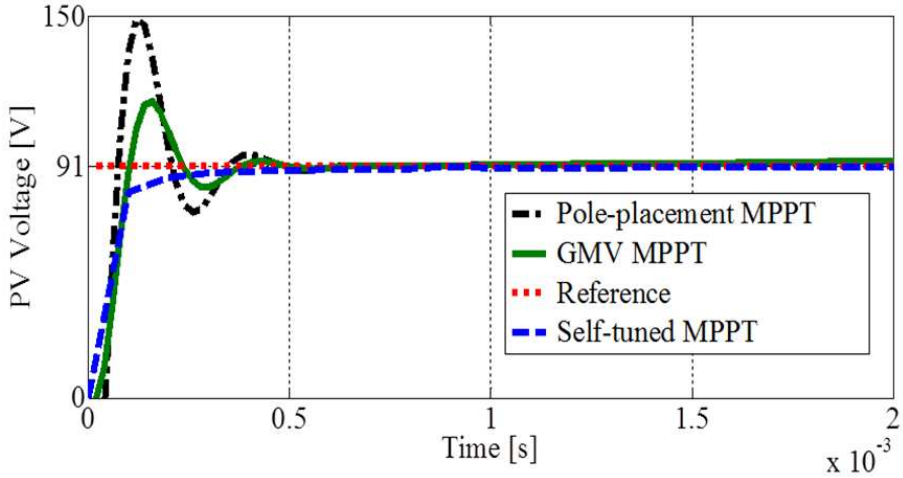

Figure 6.6: Comparison of MPP tracking response of the studied PV system with the Self-Tuned MPPT, IGMV-MPPT, Pole-placement-MPPT and GMV-MPPT using IPID-controller

Tracking response of the PV system with the proposed self-tuned MPPT has been compared with that of an auto-tuned MPPT in Fig.6.7. This shows that the tracking of the PV voltage is faster than that of the auto-tuned MPPT with less overshoot of PV voltage during the tracking period.

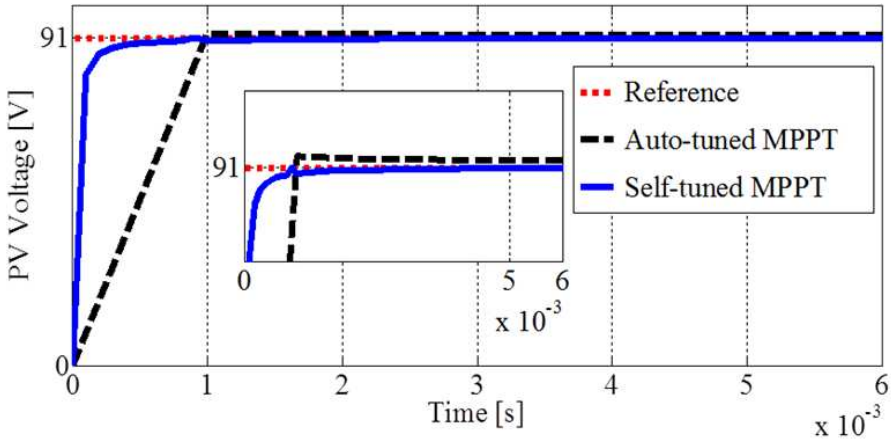

Figure 6.7: Comparison of MPP tracking response of the studied PV system with the proposed Self-Tuned MPPT and Auto-tuned MPPT

Fig.6.8 shows the PV tracking response of the PV system with the proposed self-tuned MPPT with IGMV control law for step-change in weather conditions. In this changing condition, actual MPP voltage changes from 91V to 87V. It can be seen in Fig.6.8 that the proposed self-tuned MPPT with IPID controller adjusts the PV voltage to the MPP voltage taking less than 5ms with less tracking error than that of proposed self-tuned MPPT with PID controller.

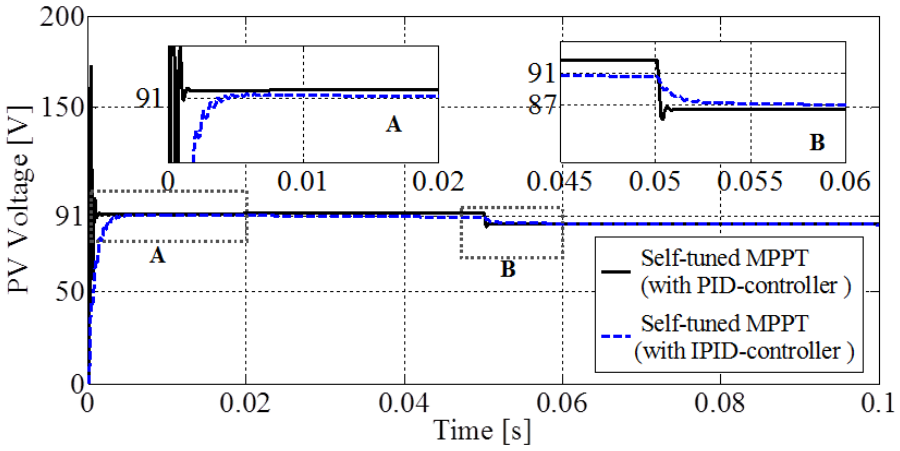

Figure 6.8: Comparison of MPP tracking response of the studied PV system with the proposed Self-Tuned MPPT with (a) PID-controller and (b) IPID-controller

6.4.2 Experimental Results

This section describes the experimental results obtained from experimentation conducted on PV system on set-up shown in Fig.6.9 for complete validation of the proposed STC based IPID-controller. Here, IPID, STC and PWM algorithms are implemented in SPARTAN 3A FPGA board. In this set-up, the input and output voltages of the given DC/DC boost

converter are sensed using voltage sensors. The sensed data is then sampled using a data acquisition (DAQ) and then those sampled signals are fed to the FPGA board. The FPGA is interlinked with a personal computer (PC).

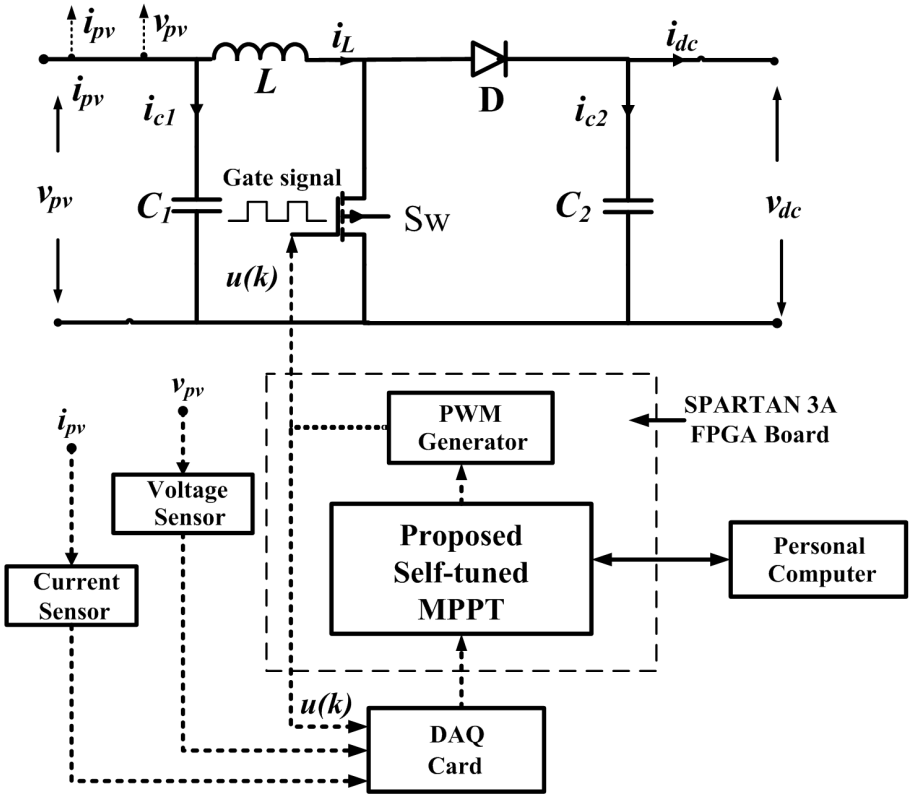

Figure 6.9: Experimental set-up used for validation of the proposed Self-tuned-MPPT

Fig.6.10 (a) shows simulated MPP tracking performances such as PV voltage and PV current of PV system when the self-tuned MPPT. It can be seen from this figure that PV current is changing from 0A to 2.2A taking around 0.7s and then oscillates around 2.2A. During that period PV voltage changes from 109V to 91V and oscillates around that 91V. Fig.6.10 (b) shows experimental result displaying the tracking voltage of PV system with the self-tuned MPPT when MPPT is switched ON. In this figure, at first the PV system is in OFF mode. Hence, PV voltage is same as its open-circuit voltage. At A, the MPPT is switched ON. In this figure, time span between A to B is the tracking time. After B, the PV voltage oscillates around the MPP voltage. It is observed from Fig.6.10 (b) that tracking periods is 0.6s and voltage fluctuation at steady-state is 0.5V. Fig.6.11 shows the PV voltage and PV current of the studied PV system with proposed self-tuned MPPT during MPP tracking. The corresponding gate pulse is shown in Fig.6.12.

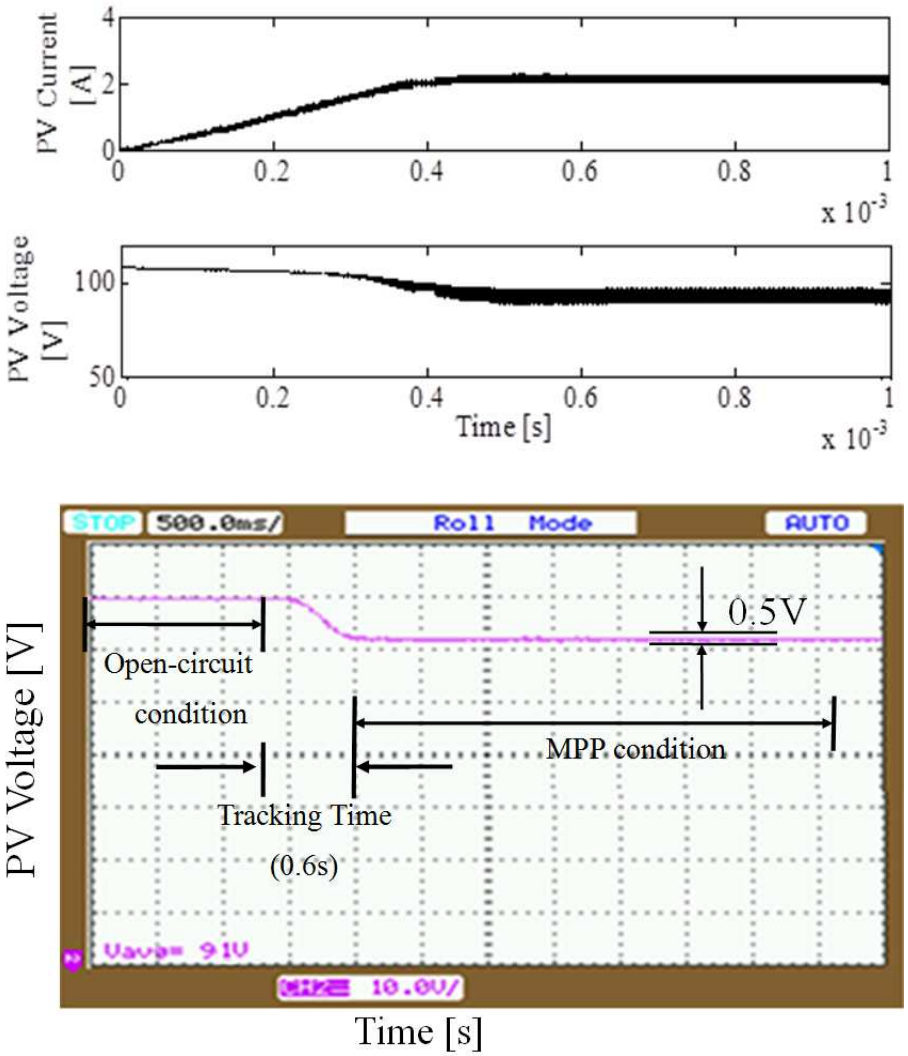

Figure 6.10: MPP tracking results of prototype PV system showing (a) simulated PV voltage and (b) experimentally obtained PV voltage varied from open-circuit voltage to MPP voltage with Proposed Self-tuned MPPT (scales: x-axis 0.5s/div and y-axis 10V/div)

6.4.3 Comparison of Performances of the Developed MPPT Algorithms

The simulated MPP tracking performances of the proposed self-tuning MPPT has been compared with that of existing MPPTs such as P&O MPPT and adaptive P&O MPPT, Auto-tuned MPPT proposed in Chapter 3, APEFC-MPPT proposed in Chapter 4, DISMC-MPPT and adaptive DISMC-MPPT proposed in Chapter 5. In Table 6.3, comparison have been done taking account of tracking times, fluctuations or chattering in PV voltage, steady-state errors (SSE), maximum overshoots and MPPT efficiencies of the studied MPPTs. From this table, it is clear that MPP tracking characteristics of proposed self-tuned MPPT is better than other studied MPPTs because tracking time, fluctuation in PV voltage, SSE, maximum overshoot are less with high MPPT efficiency. The experimental MPP tracking results of all the above MPPTs are compared in Table 6.4. In this table, tracking time and fluctuations

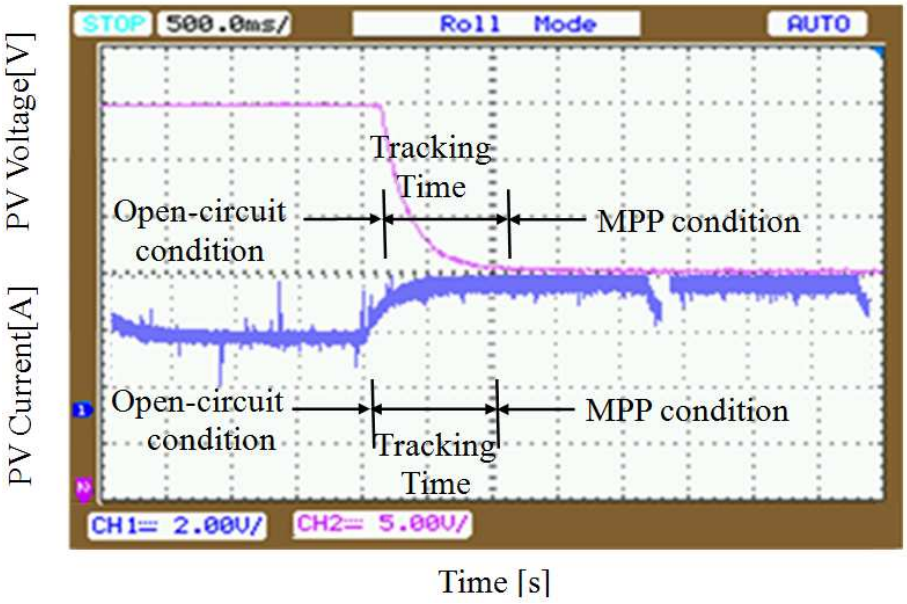

Figure 6.11: Experimental results showing (a) PV voltage and PV current of the prototype PV system with proposed self-tuned MPPT (PV voltage scales: x-axis 0.5s/div and y-axis 50V/div, PV current scales: x-axis 0.5s/div and y-axis 2A/div)

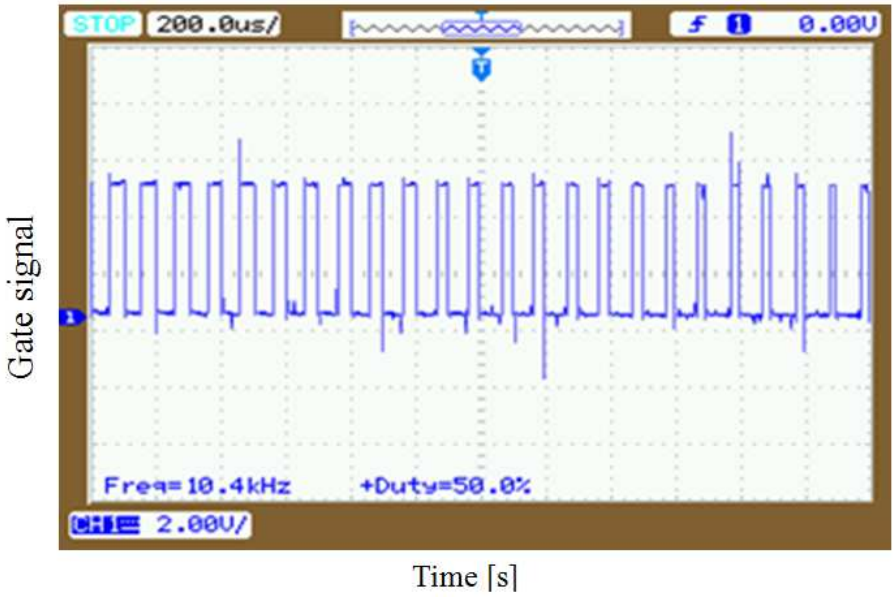

Figure 6.12: Experimental responses showing gate signal generated by the PWM signal generator

Table 6.3: Comparison of Simulated MPP tracking performance of Proposed self-tuning MPPT with different MPPTs

Type of MPPT	Tracking time (s)	Chattering (V)	SSE (%)	Maximum overshoot (%)	MPPT Efficiency (%)
P&O	0.75	6	3.5	1.78	96.5
Incremental Conductance	0.74	6.5	2.5	0.5	97.5
Adaptive P&O	0.17	1.5	0.5	0.3	99.5
ATAMPPT	0.45	0.5	2.0	10.7	98
APEFC	0.005	0.05	0.092	0.89	99.908
DISMC	0.025	4.6	0.7	19.5	99.3
Adaptive DISMC	0.26	0.8	0.08	3.57	99.02
Self-tuned	0.01	0.1	0.02	0.535	99.98

Table 6.4: Comparison of Experimental MPP tracking performance of Proposed self-tuning MPPT with different MPPTs

Type of MPPT	Tracking time (s)	Chattering (V)
P&O	1.6	8.0
ATAMPPT	1.5	5.0
APEFC	1.1	2.0
DISMC	1.4	1.5
Adaptive DISMC	0.9	1.0
Self-tuned	0.6	0.5

or chattering in PV voltage are shown. It can be seen that studied prototype PV system with self-tuned MPPT is taking only 0.6s time for adjusting PV voltage to MPP voltage with voltage fluctuations of only 0.5V. On the other hand, tracking time in case of P&O, ATAMPPT, APEFC, DISMC-MPPT and adaptive DISMC-MPPT are 1.6s, 1.5s, 1.1s, 1.4s and 0.9s respectively. Similarly, tracking voltage in case of P&O, ATAMPPT, APEFC, DISMC-MPPT and adaptive DISMC-MPPT are 8V, 5V, 2V, 1.5V and 1V respectively.

6.5 Remarks on the Proposed Self-tuning MPPT

The following advantages are observed from the proposed self-tuned MPPT

- The MPPT performance is achieved in a single step like APEFC-MPPT of Chapter 4.
- This MPPT is able to provide less high frequency chattering in PV voltage tracking.
- There is less steady state tracking error SSE in case of this MPPT.
- PV system has less MPP tracking time with this time.

- In this case, maximum overshoot during the transient period of MPP tracking is less.

6.6 Chapter Summary

This chapter proposed a self-tuning MPPT with IPID-controller, RLS identifier and IGMV control law for a PV system. The reliability of the proposed MPPT is verified by artificially adding disturbances in input PV voltage and a variable delay time element in the control loop of the PV system. The effectiveness of the proposed MPPT has been validated through both simulation and experimental studies. From the simulation and experimental results, it is found that the proposed self-tuning MPPT is better than that of other developed MPPTs such as ATAMPPT, APEFC, DISMC-MPPT and adaptive DISMC-MPPT.

Chapter 7

Conclusion and Suggestions for Future Work

This chapter presents the overall conclusion and also suggests some future scope of research work as an extension of the work pursued in this thesis.

7.1 Overall Conclusions

This thesis has presented new algorithms for parameter extraction of a PV panel and maximum power control problems of a stand-alone PV system.

An extensive review on mathematical modeling of PV panels, different parameter extraction techniques and maximum power control techniques have been pursued and presented in chapter 1. Remarks on the review on parameter extraction and MPPT algorithms are presented with broad categorization of existing parameter extraction techniques into three groups such as analytic, iterative and evolutionary computational techniques. Further, merits and demerits of the available parameter extraction techniques reported in the literature are discussed.

Subsequently, literature on available MPPT algorithms have been reviewed and analyzed with respect to their merits, demerits and applications etc. Further, necessity of designing new adaptive MPPTs to achieve higher MPPT efficiency is explored.

A new algorithm called hybrid NRM and another new evolutionary computational algorithm called BFO based parameter extraction algorithm are proposed for PV panel in Chapter 2. The proposed hybrid NRM alleviates singularity problem during convergence and exhibits faster convergence and more accurate than that of the NRM algorithm [38] and an existing comprehensive parameter extraction technique [44]. But, this hybrid NRM suffers from problem of dependency of its speed of convergence on initial conditions of the unknown PV panel parameters. Thus, it may not be suitable for fast changing weather conditions and partial shading conditions.

Therefore, another algorithm using proposed BFO has been proposed for parameter extraction. It does not suffer from singularity problem during convergence and efficiently works in both fast changing weather conditions and partial shading conditions. Thus, the BFO based parameter extraction algorithm is found to perform better in extraction of PV panel parameters than that of the hybrid NRM algorithm.

The thesis then focussed on development of new adaptive MPPT algorithms. A new auto-tuned adaptive MPPT technique called ATAMPPT has been proposed for maximum power control of PV systems in Chapter 3. The ATAMPPT algorithm accomplishes estimation of the MPPs of a PV system on-line using a RLS algorithm and a NRM algorithm. Its effectiveness is verified comparing with three existing MPPTs such as P&O, INC and APO using simulation results obtained from MATLAB/SIMULINK, real-time simulation results obtained from OPAL-RT and experimental results obtained using a 0.2kW prototype PV control set-up.

Further, a new MPPT called Adaptive predictive error filter based MPPT (APEFC MPPT) has been designed in chapter 4. using recursive least square (RLS) with a variable forgetting factor and adaptive predictive error filter based controlling concept. This MPPT alleviates the shortcomings of ATAMPPT i.e. requirement of accurate estimated PV panel parameters in a short period hence may be inappropriate in handling quick weather variations. Further, this MPPT considers external disturbances. The proposed APEFC is an adaptive PID-controller. Here, the APEF part of this APEFC MPPT is an adaptive PD-controller where the proportional and derivative gains are tuned on-line by pole-placement algorithm. The integral term only acts as catalyst in the APEFC-MPPT and hence speeds up the dynamic response of the PV system. Therefore, an empirically chosen fixed value of integral gain has been used. The weight of the adaptive predictive error filter of this APEFC-MPPT is updated using a RLS algorithm that has a variable forgetting factor. In this chapter, four other APEFCs have also been presented that are designed with four different algorithms such as RLS algorithm with fixed forgetting factor, LMS , normalized LMS (NLMS), gradient adaptive limited step LMS (GALSLMS). From simulated and experimental studies with the prototype PV system, it is observed that the proposed APEFC-MPPT with adaptive RLS algorithm possesses both faster response and lesser steady-state error than that of ATAMPPT and all other APEFCs with RLS, LMS, NLMS and GALSLMS algorithms. This MPPT is also capable of both tracking and filtering operations.

The proposed APEFC-MPPT of chapter 4 is found to be computationally complex with still high steady-state error and chattering in PV voltage. Although the PV system with this MPPT is observed to be stable, but the stability can not be guaranteed. Therefore, double integral sliding mode controller based MPPT (DISMC-MPPT) has been designed in chapter 5. Because, it is observed that a DC/DC converter with a DISMC exhibits

fast dynamic response, less steady-state error and reduced chattering. Two new MPPTs that have developed exploiting the concept of DISMC for the PV system namely DISMC-MPPT and adaptive DISMC-MPPT. These MPPTs have been designed to ensure guaranteed stability of the PV system. Sliding surface plays significant role in efficiency of DISMC-MPPT. In literature, two distinct sliding surfaces have been used namely sliding surface 1 (SS1) [111] and sliding surface 2 (SS2) [117]. DISMC with SS1 has less number of components and control variables but has higher chattering in PV voltage whereas DISMC with SS1 has less chattering and fast tracking but has more number of control variables hence expensive and complex. Therefore, a new sliding surface has been selected to design the two proposed DISMC-MPPTs. In the proposed DISMC-MPPT, sliding surface is assumed to be fixed whilst in the proposed adaptive DISMC-MPPT; sliding surface is updated to cope with the changing weather conditions. From simulation and real-time simulation, it is observed that the MPP tracking performance of the proposed DISMC-MPPT is better than that of ISMC-MPPT [110]and SMC-MPPT [69]. The selection of the sliding mode control coefficients in case of the proposed adaptive DISMC-MPPT are made considering the reaching and stability conditions thus facilitates in achievement of fast response and guaranteed stability. From experimental, simulation and real-time simulation results, it is further found that the proposed adaptive DISMC-MPPT performs better MPP tracking compared to the proposed DISMC-MPPT, DISMC-MPPT with SS1 and DISMC-MPPT with SS2 in terms of control structure complexity, chattering in output signal and response time.

Although DISMC-MPPT with adaptive sliding surface yields better tracking results than that of P&O-MPPT, INC-MPPT, APO-MPPT, ATAMPPT and APEFC-MPPT with less voltage and current fluctuations, less tracking error and less tracking time but, the performance of adaptive DISMC-MPPT is dependent on the selection of its sliding surface. Therefore, there is need of designing a new MPPT using a black-box model of PV system that is identified on-line considering error in measurement (disturbances). A self-tuning MPPT embedded with IPID-controller, RLS identifier and IGMV control law for a PV system is proposed in chapter 6. The self-tuned MPPT, tracking of MPP is done in a single step by taking $\frac{dp_{pv}}{dv_{pv}}$ as cost function. It does not require extra algorithm for MPP calculation. Instead of PID, this MPPT has incremental PID-controller. The effectiveness of the proposed MPPT is validated pursuing simulation and experimental studies. Comparison of MPP tracking results of the self-tuning MPPT with that of from existing MPPTs like ATAMPPT, APEFC-MPPT, DISMC-MPPT and adaptive DISMC-MPPT is prove that the Self-tuned adaptive MPPT works better in terms of settling time, steady-state error, voltage fluctuations in steady-state and %age of maximum overshoot with more accuracy and MPPT efficiency.

7.2 Contributions of the Thesis

The contributions of this thesis are as follows.

- An iterative parameter extraction algorithm called hybrid NRM algorithm is proposed in Chapter 2. This algorithm can accurately extract parameters of PV panels taking less time than that of the NRM [38] and comprehensive algorithm [44]. This hybrid algorithm does not suffers from singularity problem [22], [129].
- An evolutionary computational parameter extraction algorithm called Bacterial Foraging Optimization (BFO) is also proposed in Chapter 2. It is global optimization algorithm and hence can efficiently extract parameters of PV panels both in non-shading and shading conditions. It also does not suffers from singularity problem.
- An auto-tuning Adaptive MPPT called ATAMPPT is proposed in Chapter 3. It is designed with an adaptive auto-tuner. Tracking performance of this MPPT is observed to be better than of P&O, INC and an P&O with adaptive perturbation size in terms of tracking time, tracking error and voltage fluctuation [130].
- An APEFC-MPPT is proposed in Chapter 4. It is designed with an adaptive predictive error filter whose weights are being updated using RLS algorithm with variable forgetting factor. It is capable of both MPP tracking and filtering operations. MPP tracking time and steady-state error in case of this APEFC-MPPT is found to be better than that of ATAMPPT.
- One DISMC-MPPT and another adaptive DISMC-MPPTs are proposed with new sliding surfaces in Chapter 5. The adaptive DISMC-MPPT is designed with an adaptive sliding surface [116], [111] and [112]. These DISMC-MPPTs have guarantted stability and superior tracking performances than that of the APEFC-MPPT.
- A Self-tuned adaptive incremental PID (IPID) based MPPT is presented which uses an ARX mathematical model of PV system in Chapter 6. For parameter estimation of this ARX model, an RLS algorithm is employed. For tuning IPID parameters, an IGMV control law has been used.

7.3 Suggestions for Future Work

In this thesis, a number of parameter extraction for PV system modeling have been developed. Further, the thesis proposed new MPPT algorithms for stand-alone PV systems. However, an immediate extension of the thesis work is to apply these algorithms for a Grid connected PV system. An utility Grid may have a large number of conventional and nonconventional sources. Connecting the PV system to the utility network may introduce different

dynamics to the existing PV system. If the PV system is not properly controlled, then Grid may become unstable. But, the dynamics of PV system is dependent greatly on fluctuation of solar irradiance and temperature. Thus, when this PV system connected to Grid together with other conventional power sources, there is a strong research need of study of dynamic stability of the PV system [131], [132], [133], [134] and [135].

Thesis Disseminations

Journal Papers

1. B. Subudhi and R. Pradhan, "A Comparative Study on PV Panel Parameter Extraction Methods", International Journal on Renewable Energy Technology (Inderscience), vol. 3, no. 3, pp. 295-315, 2012.

2. B. Subudhi and R. Pradhan, "A Comparative Study of Maximum Power Point Tracking Techniques for Photovoltaic System", IEEE Transactions on Sustainable Energy, vol. 4, no. 1, pp. 89-98, 2013.

3. R. Pradhan and B. Subudhi, "An Adaptive Double-Integral-Sliding-Mode-Maximum-Power-Point-Tracker for a Photovoltaic System", Control Engineering Practice (Revised copy submitted).

4. R. Pradhan and B. Subudhi, "Double Integral Sliding Mode MPPT Control of a Photovoltaic System", IEEE Transactions on Control Systems Technology (Under Review).

5. R. Pradhan and B. Subudhi, "An Adaptive Predictive Error Filter based Maximum Power Point Tracker for a Photovoltaic System", IET Power Electronics (Revised copy submitted).

6. R. Pradhan and B. Subudhi, "Design and Real-time Implementation of a New Auto-tuned Adaptive MPPT Control for a Photovoltaic System", International Journal on Power and Energy System, Elsevier (Under Review).

7. R. Pradhan and B. Subudhi, "A Self-Tuned Adaptive Maximum Power Point Tracker for a Photovoltaic System", IEEE Transactions on Sustainable Energy (Revised copy submitted).

Conference Papers

1. R. Pradhan, B. Subudhi and P.K. Ray, "A Real-time linearized Maximum Power Point Tracker for Photovoltaic System", IEEE PEDS-2013, 22-25 April 2013, Kitakyushu, Japan.

2. R. Pradhan and B. Subudhi, "An Adaptive Prediction Error Filter for Photovoltaic Power Harvesting Applications", IEEE INDICON-2012, Kochi, Kerala, 7-9 December, 2012.

3. R. Pradhan and B. Subudhi, "A Steepest-Descent based Maximum Power Point Tracking Technique for a Photovoltaic Power System", IEEE ICPCES-2012, MNNIT, Allahabad, UP, 17-19 December 2012.

4. R. Pradhan and B. Subudhi, "A New Digital Double Integral Sliding Mode Maximum Power Point Tracker for Photovoltaic Power Generation Application", ICSET-2012, Kathmandu, Nepal, 24-27 September 2012.

5. B. Subudhi and R. Pradhan, "Characteristics Evaluation and Parameter Extraction of a Solar Array Based on Experimental Analysis", IEEE PEDS-2011, Singapore, 5-8 December 2011.

6. B. Subudhi and R. Pradhan, "A Comparative Study on Solar Parameter Extraction Methods", NSC-2010, Surathkal, Karnataka, 10-12 December, 2010.

Raseswari Pradhan

She born to Smt. Gitanjali Pradhan and Mr. Sitaram Pradhan in 2^{nd} June, 1979 in Tora, Bargarh, Orissa. After Getting her Bachelor in Engineering Engineering, she has five years of work experience.

E-mail: rase1512@gmail.com

Qualifications

- Ph.D. (Continuing)
  National Institute of Technology Rourkela
- M.E. (Power System)
  Jadavpur University, Kolkata, West Bengal
- B.E. (Electrical Engineering)
  I.G.I.T. Sarang, Utkal University, Odisha
- +2 (Science)
  Council of Higher Secondary Education, Odisha
- 10^{th}
  Board of Secondary Education, Odisha

Publications

- 04 Journal Articles
- 09 Conference Papers

Present Address

Assistant Professor-II,
School of Electrical Engineering, KIIT University
Bhubaneswar, Odisha, India

Permanent Address

Jita Tikra, Tora
Bargarh-768040, Odisha, India

Bibliography

[1] K. Peng, Kuiqing, Y. Xu, Y. Wu, Y. Yan, S. Lee, and J. Zhu, "Aligned single-crystalline si nanowire arrays for photovoltaic applications," *Small*, vol. 1, no. 11, pp. 1062–1067, 2005.

[2] R. Karki and B. Roy, "Reliability/cost implications of pv and wind energy utilization in small isolated power systems," *IEEE Transactions on Energy Conversion*, vol. 16, no. 4, pp. 368–373, 2001.

[3] B. Parida, S. Iniyan, and R. Goic, "A review of solar photovoltaic technologies," *Renewable and Sustainable Energy Reviews*, vol. 15, no. 3, pp. 1625–1636, 2011.

[4] Y. Hamakawa, "Recent advances in solar photovoltaic technology and its new role for environmental issue," *Renewable energy*, vol. 5, no. 1, pp. 34–43, 1994.

[5] H. Ravaee, F. Saeid, and S. Faramarz, "Artificial neural network based model of photovoltaic thermal (pv/t) collector," *Journal of Mathematics and Computer Science*, vol. 4, no. 3, pp. 411–417, 2012.

[6] G. K. Singh, "Solar power generation by pv (photovoltaic) technology: A review," *Energy*, vol. 53, no. 1, pp. 1–13, 2013.

[7] K. H. Solangi, M. R. Islam, R. Saidur, N. A. Rahim, and H. Fayaz, "A review on global solar energy policy," *Renewable and Sustainable Energy Reviews*, vol. 15, no. 4, pp. 2149–2163, 2011.

[8] Y. Kuwano, "The future of photovoltaic power generation," in *Proc. Symposium by Semiconductor Equipment and Materials International (SEMI)*, 2011.

[9] A. Mohamed, M. Elshaer, and O. Mohammed, "Control enhancement of power conditioning units for high quality pv systems," *Electric Power Systems Research*, vol. 90, no. 1, pp. 30–41, 2011.

[10] M. Datta, S. Tomonobu, Y. Atsushi, F. Toshihisa, and K. C.-H. Kim, "A coordinated control method for leveling pv output power fluctuations of pvdiesel hybrid systems connected to isolated power utility," *IEEE Transactions on Energy Conversion*, vol. 24, no. 1, pp. 153–162, 2009.

[11] P. Tech, "Gujarat's 214mw solar park named as asia's largest single pv plant," in *http://www.pv-tech.org/news*, 23 April, 2012.

[12] P. P. Dash, "Design methodology and stability analysis for a photovoltaic (pv) plant interfaced with a distribution network," in *PhD Dissertation, The University of Western Ontario*, 2008.

[13] P. Denholm and R. M. M. Margolis, "Evaluating the limits of solar photovoltaics (pv) in traditional electric power systems," *Energy policy*, vol. 35, no. 5, pp. 2852–2861, 2007.

[14] E. Roman, A. R. Alonso, E. S. I. Pedro, and G. Damian, "Intelligent pv module for grid-connected pv systems," *IEEE Transactions on Industrial Electronics*, vol. 53, no. 4, pp. 1066–1073, 2006.

[15] A. C. Kyritsis, E. C. Tatakis, and N. P. Papanikolaou, "Optimum design of the current-source flyback inverter for decentralized grid-connected photovoltaic systems," *IEEE Transactions on Energy Conversion*, vol. 23, no. 1, pp. 281–293, 2008.

[16] W. El-Khattam and M. Salama, "Distributed generation technologies, definitions and benefits," *Electric Power Systems Research*, vol. 71, no. 2, pp. 119–128, 2004.

[17] Sunways, "Examining architectures of photo-anode and photovoltaic tandem cells for solar water splitting," in *http://www.sunways.eu*, 2012.

[18] H.-L. Tsai, C.-S. Tu, and Y.-J. Su, "Development of generalized photovoltaic model using matlab/simulink," in *World Congress on Engineering and Computer Science*, 2008, pp. 846–851.

[19] A. Celik and N. Acikgoz, "Experimental verification of the operating current of mono-crystalline photovoltaic modules using four- and five- parameter models," *Applied Energy*, vol. 84, no. 1, pp. 1–15, 2007.

[20] B. Subudhi and R. Pradhan, "Characteristics evaluation and parameter extraction of a solar array based on experimental analysis," in *Proc.* 9^{th} *IEEE Power Electronics and Drives Systems (PEDS), Surathkal, Karnataka*, 5-8 December, 2011, pp. 340–344.

[21] T. Easwarakhanthan, J. Bottin, I. Bouhouch, and C. Boutrit, "Nonlinear minimization algorithm for determining the solar cell parameters with microcomputers," *IEEE Transactions on Aerospace and Electronic Systems*, vol. 4, no. 1, pp. 1–12, 1986.

[22] B. Subudhi and R. Pradhan, "A comparative study on parameter estimation methods," *International Journal on Renewable Energy Technology (Inderscience)*, vol. 3, no. 3, pp. 295–315, 2012.

[23] M. Ameli, S. Moslehpour, and M. Shamlo, "Economical load distribution in power networks that include hybrid solar power plants," *Electric Power Systems Research*, vol. 78, no. 1, pp. 1147–1152, 2008.

[24] N. Femia, P. Giovanni, S. Giovanni, and V. Massimo, "Optimization of perturb and observe maximum power point tracking method," *IEEE Transactions on Power Electronics*, vol. 20, no. 4, pp. 963–973, 2005.

[25] J. M. Carrasco, L. G. Franquelo, J. T. Bialasiewicz, R. G. E. Galvn, M. Prats, J. Leon, and N. Moreno-Alfonso, "Power-electronic systems for the grid integration of renewable energy sources: A survey," *IEEE Transactions on Industrial Electronics*, vol. 53, no. 4, 2006.

[26] F. Blaabjerg, Z. Chen, and S. Kjaer, "Power electronics as efficient interface in dispersed power generation systems," *IEEE Transactions on Power Electronics*, vol. 19, no. 5, 2004.

[27] T. T. N. Khatib, A. Mohamed, N. Amin, and K. Sopian, "An efficient maximum power point tracking controller for photovoltaic systems using new boost converter design and improved control algorithm," *WSEAS Transactions on Power System*, vol. 5, no. 2, pp. 53–63, 2010.

[28] V. Salas, E. Olias, A. Lazaro, and A. Barrado, "Evaluation of a new maximum power point tracker applied to the photovoltaic stand-alone systems," *Solar Energy Materials and Solar Cells*, vol. 87, no. 1-4, pp. 807–815, 2005.

[29] L. P. G. Accetta and L. Ferrarini, "Energy production estimation of a photovoltaic system with temperature-dependent coefficients," in *3rd IEEE International Conference on Sustainable Energy Technologies, (IEEE ICSET 2012)*, 2012, pp. 189–195.

[30] S. Chowdhury and H. Saha, "Maximum power point tracking of partially shaded solar photovoltaic arrays," *Solar Energy Materials and Solar Cells*, vol. 94, no. 1, pp. 1441–1447, 2010.

[31] M. Valentini, A. Raducu, D. Sera, and R. Teodorescu, "Pv inverter test setup for european efficiency, static and dynamic mppt efficiency evaluation," in 11^{th} *International Conference on Optimization of Electrical and Electronic Equipment*, 2008, pp. 433–438.

[32] H. N. Zainudin and S. Mekhilef, "Comparison study of maximum power point tracker techniques for pv systems," in *Proc.* 14^{th} *International Middle East Power Systems Conference, Egypt*, 19-21 December, 2010.

[33] M. de Blas, J. Torres, E. Prieto, and A. Gracia, "Selecting a suitable model for characterizing photovoltaic devices," *Renewable Energy*, vol. 25, no. 3, pp. 371–380, 2002.

[34] R. Chenni, M. Makhlouf, T. Kerbache, and A. Bouzid, "A detailed method for photovoltaic cells," *Energy*, vol. 32, no. 9, pp. 1724–1730, 2007.

[35] K. Kennerud, "Analysis of performance degradation in cds solar cell," *IEEE Transactions on Aerospace and Electronic Systems*, vol. 5, no. 6, pp. 912–917, 1969.

[36] N. Enebish, D. Agchbayar, S. Dorjkhand, and I. Y. D. Baatar, "Numerical analysis of solar cell current-voltage characteristics," *Solar Energy Materials and Solar Cells*, vol. 29, no. 3, pp. 201–208, 1993.

[37] J. Gow and C. Manning, "Development of a photovoltaic array model for use in power- electronics simulation studies," *IEE Proceedings-Electric Power Applications*, vol. 146, no. 2, pp. 193–200, 1999.

[38] K. Bouzidi, M. Chegaar, and A. Bouhemadou, "Solar cell parameters evaluation considering the series and shunt resistances," *Solar Energy Materials and Solar Cells*, vol. 91, no. 18, pp. 1647–1651, 2007.

[39] E. Matagne, R.Chenni, and R. E. Bachtiri, "A photovoltaic cell model based on nominal data," in *Power Engineering, Energy and Electrical Drives POWERENG Conference*, 2007, pp. 562–565.

[40] C. Carrero, J. Rodriguez, D. Ramirez, and C. Platero, "Simple estimation of pv modules loss resistances for low error modeling," *Renewable Energy*, vol. 35, no. 5, pp. 1103–1108, 2010.

[41] V. Brano, A. Orioli, G. Ciulla, and A. Gangi, "An improved five-parameter model for photovoltaic modules," *Solar Energy Materials and Solar Cells*, vol. 94, no. 8, pp. 1358–1370, 2010.

[42] D. Sera, R.Teodorescu, and P. Rodriguez, "Pv panel model based on datasheet values," in *Proc. IEEE Conference on Industrial Electronics (ISIE), Taipei, Taiwan*, 5-8, November 2007, pp. 2392 – 2396.

[43] J. C. H. Phang, D. S. H. Chan, and J. R. Phillips, "Accurate analytical method for the extraction of solar cell," *Electronics Letter*, vol. 20, no. 10, pp. 406–408, 1984.

[44] M. Villalva and J. Gazoli, "Comprehensive approach to modeling and simulation of photovoltaic arrays," *IEEE Transactions on Power Electronics*, vol. 24, no. 5, pp. 1198–1208, 2009.

[45] K. Ishaque, Z. Salam, and H. Taheri, "Simple, fast and accurate two-diode model for photovoltaic modules," *Solar Energy Materials and Solar Cells*, vol. 95, no. 2, pp. 586–594, 2011.

[46] M. Eghbal, T. Saha, and K. Hasan, "Transmission expansion planning by meta-heuristic techniques: A comparison of shuffled frog leaping algorithm, pso and ga," in *IEEE General Meeting in Power and Energy Society*, 2011, pp. 1–8.

[47] J. Soon and K.-S. Low, "Photovoltaic model identification using particle swarm optimization with inverse barrier constraint," *IEEE Transactions on Power Electronics*, vol. 27, no. 9, pp. 3975–3983, 2012.

[48] V. Salas, E. Olias, A. Barrado, and A. Lazaro, "Review of the maximum power point tracking algorithms for stand-alone photovoltaic systems," *Solar Energy Materials and Solar Cells*, vol. 90, no. 11, pp. 1555–1578, 2006.

[49] T. Esram and P. Chapman, "Comparison of photovoltaic array maximum power point tracking techniques," *IEEE Transactions on Energy Conversion*, vol. 22, no. 2, pp. 439–449, 2007.

[50] M. A. S. Masoum, H. Dehbonei, and E. F. Fuchs, "Theoretical and experimental analyses of photovoltaic systems with voltage and current based maximum power point tracking," *IEEE Transactions on Energy Conversion*, vol. 17, no. 4, pp. 514–522, 2002.

[51] N. F. D. Granozio, G. Petrone, G. Spagnuolo, , and M. Vitelli, "Optimized one-cycle control in photovoltaic grid connected applications for photovoltaic power generation," *IEEE Transactions on Aerospace Electronics System*, vol. 42, no. 3, pp. 954–972, 2006.

[52] S. Jain and V. Agarwal, "A dsp-based single-stage maximum power point tracking pv inverter," *IEEE Power Electronics Letter*, vol. 2, no. 1, pp. 16–19, 2004.

[53] O. L-Lapena, M. T. Penella, and M. Gasulla, "A new mppt method for low-power solar energy harvesting," *IEEE Transactions on Industrial Electroncs*, vol. 57, no. 9, pp. 3129–3138, 2010.

[54] C. Hua and C. Shen, "Study of maximum power tracking techniques and control of dc/dc converters for photovoltaic power system," in *Proc.* 29^{th} *Annual Power Electronics Specialist Conference, Japan*, 17-22 May, 1998, pp. 86–93.

[55] Y. H. Lim and D. C. Hamill, "Simple maximum power point tracker for photovoltaic arrays," *Electronics Letter*, vol. 36, no. 11, pp. 997–999, 2000.

[56] F. Liu, Y. Kang, Y. Zhang, and S. Duan, "Comparison of p&o and hill climbing mppt methods for grid-connected pv generator," in *Proc.* 3^{rd} *IEEE Conference on Industrial Electronics Applications, Singapore*, 3-5 June, 2008, pp. 1–6.

[57] A. Safari and S. Mekhilef, "Simulation and hardware implementation of incremental conductance mppt with direct control method using cuk converter," *IEEE Transactions on Industrial Electronics*, vol. 58, no. 4, pp. 1154–1161, 2011.

[58] A. Garrigos, J. M. Blanes, J. A. Carrascoa, and J. B. Ejea, "Real time estimation of photovoltaic modules characteristics and its application to maximum power point operation," *IEEE Transacions on Aerospace Electronics System*, vol. 32, no. 6, pp. 1059–1076, 2007.

[59] K. K. Tse, M. T.Ho, H. S.-H. Chung, and S.Y.Hui, "A novel maximum power point tracker for pv panels using switching frequency modulation," *IEEE Transactions on Power Electronics*, vol. 17, no. 6, pp. 980–989, 2002.

[60] T. Esram, J. W. Kimball, P. T. Krein, P. L. Chapman, and P. Midya, "Dynamic maximum power point tracking of photovoltaic arrays using ripple correlation control," *IEEE Transactions on Power Electronics*, vol. 21, no. 5, pp. 1282–1291, 2006.

[61] L. Li-qun and W. Zhi-xin, "A rapid mppt algorithm based on the research of solar cell's diode factor and reverse saturation current," *WSEAS Transactions on Systems*, vol. 7, no. 5, pp. 568–579, 2008.

[62] T. Noguchi and H. Matsumoto, "Maximum power point tracking method of photovoltaic using only single current sensor," in *Proc.* 10^{th} *European Conference on Power Electronics Applications, Toulouse*, 2-4 September, 2003, pp. 1–8.

[63] C. Liu, B.Wu, and R. Cheung, "Advanced algorithm for mppt control of photovoltaic systems," in *Canadian Solar Building Conference*, 2004, pp. 1–8.

[64] D. P. Holm and M. E. Ropp, "Comparative study of maximum power point tracking algorithms," *Progress in photovoltaics: Research and Applications*, vol. 11, no. 1, pp. 47–62, 2003.

[65] D. Shmilovitz, "On the control of photovoltaic maximum power point tracker via output parameters," *IEE Proceedings-Electric Power Applications*, vol. 152, no. 2, pp. 239–248, 2005.

[66] N. Pongratananukul, "Analysis and simulation tools for solar array power systems," in *Ph.D. dissertation, Department of Electrical and Computer Engineering, University Central Florida, Orlando, FL*, 2005.

[67] Y. B. T.L. Kottas and A. Karlis, "New maximum power point tracker for pv arrays using fuzzy controller in close cooperation with fuzzy cognitive networks," *IEEE Transactions on Energy Conversion*, vol. 21, no. 3, pp. 793–803, 2006.

[68] T. Hiyama and K. Kitabayashi, "Neural network based estimation of maximum power generation from pv module using environment information," *IEEE Transactions on Energy Conversion*, vol. 12, no. 3, pp. 241–247, 1997.

[69] C.-C. Chu and C.-L. Chen, "Robust maximum power point tracking method for photovoltaic cells: A sliding mode control approach," *Solar Energy*, vol. 83, no. 8, pp. 1370–1378, 2009.

[70] W. Xiao, W. Dunford, P. Palmer, and A. Capel, "Application of centered differentiation and steepest descent to maximum power point tracking," *IEEE Transactions on Industrial Electronics*, vol. 54, no. 5, pp. 2539–2549, 2007.

[71] C. Rodriguez and G. A. J. Amaratunga, "Analytic solution to the photovoltaic maximum power point problem," *IEEE Transactions on Circuits Systems-1*, vol. 54, no. 9, pp. 2054–2060, 2007.

[72] R. Ramprava and B. L.Mathur, "Intelligent controller based maximum power point tracking for solar pv system," *International Journal on Computer Appllications*, vol. 12, no. 10, pp. 37–41, 2011.

[73] B. Amrouche, M. Belhamel, and A. Guessoum, "Artifical intelligence based p&o mppt method for photovoltaic systems," in *Review of Renewable Energy ICRESD*, 2007, pp. 11–16.

[74] C. Larbes, S. M. A. Cheikh, T. Obeidi, and A. Zerguerras, "Genetic algorithm optimized fuzzy logic control for the maximum power point tracking in photovoltaic system," *Renewable Energy*, vol. 34, no. 10, pp. 2093–2100, 2009.

[75] M. S. Aldobhani and R. John, "Mppt of pv system using anfis prediction and fuzzy logic tracking," in *Proc. International Multi-Conference of Engineering and Computer Science, Hong Kong*, 19-21 March, 2008, pp. 11–16.

[76] P. Tsao, S. Sarhan, and I. Jorio, "Distributed mppt for pv arrays," in *Proc.* 34^{th} *IEEE PV Specialized Conference, PA USA*, 7-12 June, 2009, pp. 2378–2384.

[77] G. Petrone, G. Spagnuolo, R. Teodorescu, M. Veerachary, and M. Vitelli, "Reliability issues in photovoltaic power processing systems," *IEEE Transactions on Industrial Electronics*, vol. 55, no. 7, pp. 2569–2580, 2008.

[78] A. R. Paja, G. Spagnuolo, G. Petrone, M. Vitelli, and J. D. Bastidas, "A multivariablemppt algorithm for granular control of pv systems," in *Proc. IEEE International Symposium on Industrial Electronics, Bari, Italy*, 4-7 July, 2010, pp. 3433–3437.

[79] J. Slotine and W. Li, *Applied Non-linear Control*. New Jersey, USA: Prentice Hall, 1991.

[80] B. Subudhi and R. Pradhan, "Characteristics evaluation and parameter extraction of a solar array based on experimental analysis," in *IEEE* 9^{th} *International Conference on Power Electronics and Drive Systems (PEDS), Singapore*, 5-8 December, 2011, pp. 340–344.

[81] A. Iqbal, A. Rub, and S. M. Ahmed, "Adaptive neuro-fuzzy inference system based maximum power point tracking of a solar pv module," in *Proc. IEEE International Energy Conference and Exhibition, 2010*, 2010, pp. 51–56.

[82] B. Subudhi and R. Pradhan, "A comparative study of maximum power point tracking techniques for photovoltaic system," *IEEE Transactions on Sustainable Energy*, vol. 4, no. 1, pp. 89–98, 2013.

[83] P. Kakosimos, A. Kladas, and S. Manias, "Fast photovoltaic system voltage or current oriented mppt employing a predictive digital current-controlled converter," *IEEE Transactions on Industrial Electronics*, vol. 60, no. 12, pp. 5673–5685, 2013.

[84] D. Petreus, T. Patatau, S. Daraban, C. Morel, and B. Morley, "A novel maximum power point tracker based on analog and digital control loops," *Solar Energy*, vol. 85, no. 3, pp. 588–600, 2011.

[85] P. Kakosimos and A. Kladas, "Implementation of photovoltaic array mppt through fixed step predictive control technique," *Renewable Energy*, vol. 36, no. 9, pp. 2508–2514, 2011.

[86] L. Piegari and R. Rizzo, "Adaptive perturb and observe algorithm for photovoltaic maximum power point tracking," *IET Renewable Power Generation*, vol. 4, no. 4, pp. 317–328, 2010.

[87] W. Xiao, M. Lind, W. Dunford, and A. Capel, "Real-time identification of optimal operating points in photovoltaic power systems," *IEEE Transactions on Industrial Electroics*, vol. 53, no. 4, pp. 1017–1026, 2006.

[88] Y. Kondo, V. Phimmasone, Y. Ono, and M. Miyatake, "Mppt based on standalone water pumping system," in *Proc. IEEE International Conference on Electrical Machanical Systems (Incheon), Hong Kong*, 24-28 January, 2010, pp. 593–596.

[89] T. Yamamoto and S. Shah, "Design and experimental evaluation of a multivariable self-tuning pid controller," *IEE Proceedings-Control Theory Appllications*, vol. 151, no. 5, pp. 645–652, 2004.

[90] Z. Zhao and A. Prodica, "Limit-cycle oscillations based auto-tuning system for digitally controlled dc-dc power supplies," *IEEE Transactions on Power Electronics*, vol. 22, no. 6, pp. 2211–2222, 2007.

[91] W. Stefanutti, P. Mattavelli, S. Sagginni, and M. Ghioni, "Auto-tuning of digitally controlled dc-dc converters based on relay feedback," *IEEE Transactions on Power Electronics*, vol. 22, no. 1, pp. 199–207, 2007.

[92] K. Rifai, "Nonlinearly parameterized adaptive pid control for parallel and series realization," in *American Control Conference 2009 (ACC2009)*, 2009, pp. 170–174.

[93] L. Gauchia and J. Sanz, "A per-unit hardware-in-the-loop simulation of a fuel cell/battery hybrid energy system," *IEEE Transactions on Industrial Electronics*, vol. 57, no. 4, pp. 1186–1194, 2010.

[94] M. Masoum, H. Dehbonei, and E. Fuchs, "Theoretical and experimental analysis of photovoltaic systems with voltage and current based maximum power point tracking," *IEEE Transactions on Energy Conversion*, vol. 19, no. 5, pp. 514–522, 2004.

[95] C. Chan, "A nonlinear control for dc-dc converters," *IEEE Transactions on Power Electronics*, vol. 22, no. 1, pp. 216–222, 2007.

[96] I. Atlas and A. Sharaf, "A photovoltaic array simulation model for matlab/simulink gui environment," in 5^{th} *International Conference on Clean Electrical Power (ICCEP), Capri, Italy*, 21-23 May, 2007, pp. 341–345.

[97] M. Alcono-Garcia and J. Ruiz, "Real-time identification of optimal operating points in photovoltaic power systems," *IEEE Transactions on Industrial Electronics*, vol. 53, no. 4, pp. 1017–1026, 2006.

[98] R. Pradhan and B. Subudhi, "An adaptive prediction error filter for photovoltaic power harvesting applications," in *Proc. IEEE Annual India Conference (INDICON), Kochi, Kerala*, 7-9 December, 2012, pp. 115–120.

[99] B. Widrow, J. M. McCool, M. G. Larimore, and C. R. Johnson, "Stationary and nonstationary learning characteristics of the lms adaptive filter," *Proceedings of the IEEE*, vol. 64, no. 8, pp. 1151–1162, 1976.

[100] R. A. Gonzalo, "A general weighted median filter structure admitting negative weights," *IEEE Transactions on Signal Processing*, vol. 46, no. 12, pp. 3195–3205, 1998.

[101] H.-C. Shin, A. H. Sayed, and W.-J. Song, "Variable step-size nlms and affine projection algorithms," *IEEE signal processing letters*, vol. 11, no. 2, pp. 132–135, 2004.

[102] M.H.Shaheed, "Performance analysis of fout-types of conjugate gradient algorithms in the nonlinear dynamic modelling of a trms using feedforward neural networks," in *Proc. IEEE International Conference on Systems, Man and Cybernetics, Hague, Netherlands*, 10-13 October 2004, pp. 5985–5990.

[103] T. D. Slock, "On the convergence behavior of the lms and the normalized lms algorithms," *IEEE Transactions on Signal Processing*, vol. 41, no. 1, pp. 2811–2825, 1993.

[104] B. Subudhi, P.K.Ray, and A.M.Panda, "Recursive estimation of power system frequency by advanced signal processing techniques," *International Journal, AMSE, France*, vol. 82, no. 1, pp. 16–26, 2009.

[105] S. Jung and P. Park, "Variable forgetting factor recursive total least squares algorithm for fir adaptive filtering," in *Proc. International Conference on Electronics Engineering and Informatics, Phuket, Thailand*, 1-2 September, 2012, pp. 170–174.

[106] R. Pradhan, B. Subudhi, and P. Ray, "A real-time linearized maximum power point tracker for photovoltaic system," in *IEEE 10*10^{th} *International Conference on Power Electronics and Drive Systems (PEDS), Kitakyushu, Japan*, 22-25 April, 2013, pp. 962 – 967.

[107] S. S. Haykin and B. Widrow, *Least-mean-square adaptive filters.* New York, USA: Wiley-Interscience, 2003.

[108] L. Guo, J. Hung, and R. Nelms, "Evaluations of dsp-based pid and fuzzy controllers for dc-dc converters," *IEEE Transactions on Industrial Electronics*, vol. 56, no. 6, pp. 2237–2248, 2009.

[109] M. Algreer, M. Armstrong, and D. Griaouris, "Adaptive pd+i control of a switch-mode dc-dc power converter using a recursive fir predictor," *IEEE Transactions on Industry Applications*, vol. 47, no. 5, pp. 2135–2144, 2011.

[110] C. W. Tan, T. C. Green, and C. A. H. Aramburo, "An improved maximum power point tracking algorithm with current-mode control for photovoltaic applications," in *Proc. IEEE International Conference on Power Electronics and Drives Systems (PEDS), Malaysia*, @8 November - 1 December, 2005, pp. 489–494.

[111] S. Tan, Y. Lai, and C. Tse, "Indirect sliding mode control of power converters via double integral sliding surface," *IEEE Transactions on Power Electronics*, vol. 23, no. 2, pp. 600–611, 2008.

[112] R. Pradhan and B. Subudhi, "A new digital double integral sliding mode maximum power point tracker for photovoltaic power generation application," in 3^{rd} *IEEE International Conference on Sustainable Energy Technologies, (IEEE ICSET), Kathmandu, Nepal*, 24-27 September, 2012, pp. 183–188.

[113] H.Serhoud and D.Benattous, "Sliding mode control of maximum power point tracker for photovoltaic array," in *Proc. International Symposium on Environmental Friendly Energies in Electrical Applications, Newcastle upon Tyne, United Kingdom*, 25-27 June, 2010, pp. 1–5.

[114] Y. Niu, Y. D. W. Ho, and J. Lam, "Robust integral sliding mode control for uncertain stochastic systems with time-varying delay," *Automatica*, vol. 41, no. 5, pp. 873–880, 2005.

[115] S. Tan, Y. Lai, C. Tse, L. Salamero, and C. Wu, "A fast-response sliding mode controller for boost-type converters with a wide range of operating conditions," *IEEE Transactions on Industrial Electronics*, vol. 54, no. 6, pp. 3276–3286, 2007.

[116] Y. Jiao and F. Luo, "An improved sliding mode controller for boost converter in solar energy system," in *Proc.* 4^{th} *IEEE Congress on Industrial Electronics and Applications (ICIEA 2009), Singopre*, 25-27 May, 2009, pp. 805–810.

[117] Y. Jiao, F. Luo, and M. Zhu, "Generalized modeling and sliding mode control for n-cell cascade super-lift dc-dc converters," *IET Power Electronics*, vol. 4, no. 5, pp. 532–540, 2010.

[118] Y. Jiao and F. Luo, "An improved sliding mode controller for boost converter in solar energy system," in *4th IEEE Congress on Industrial Electronics and Applications (ICIEA 2009), China*, 2009.

[119] R. Pradhan and B. Subudhi, "A steepest-descent based maximum power point tracking technique for a photovoltaic power system," in *IEEE* 2^{nd} *International Conference on Power, Control and Embedded Systems (ICPCES), Allahabad*, 17-19 December, 2012, pp. 1–6.

[120] K. H. Ang, C. Gregory, and L. Yun, "Pid control system analysis, design and technology," *IEEE Transactions on Control Systems Technology*, vol. 13, no. 4, 2005.

[121] L. Shen, Z. Liu, Z. Zhang, and X. Shi, "Frame-level bit allocation based on incremental pid algorithm and frame complexity estimation," *Journal of Visual Communication and Image Representation*, vol. 20, no. 1, 2009.

[122] C. Alippi and G. Cristian, "An adaptive system for optimal solar energy harvesting in wireless sensor network nodes," *IEEE Transactions on Circuits and Systems I*, vol. 55, no. 6, 2008.

[123] F. Alonge, F. Ippolito, F. Raimondi, and S. Tamminaro, "Nonlinear modeling of dc/dc converters using the hammersteins approach," *IEEE Transactions on Power Electronics*, vol. 22, no. 4, 2007.

[124] Z. Cheng, H. Yang, and Y. Sun, "Fpga-based pv systems fuzzy mppt control algorithm," in *IEEE* 7^{th} *International Conference on Fuzzy Systems and Knowledge Discovery*, 2010, pp. 1244–1248.

[125] D. Sera, R. Teodorescu, J. Hantschel, and M. Knoll, "Optimized maximum power point tracker for fast-changing environmental conditions," *IEEE Transactions on Industrial Electronics*, vol. 55, no. 7, 2008.

[126] G. Evans, *Self-tuning and Adaptive Control Coursework*.

[127] Welsted, *Self-tuning Controllers:A Reivew of Developments*. Secaucus, NJ, USA: Springer-Verlag New York, Inc., 2008.

[128] K. Burnham, I. Zajic, and J. Linden, *Knowledge-Based Intelligent System Advancements: System and Cybernatic Approaches*. Secaucus, NJ, USA: Springer-Verlag New York, Inc., 2010.

[129] B.Subudhi and R.Pradhan, "A comparative study on solar parameter extraction methods," in 34^{th} *National System Conference, Surathkal, Karnataka*, 10-12 December, 2010, pp. 1–6.

[130] R. Pradhan and B. Subudhi, "An adaptive prediction error filter for photovoltaic power harvesting applications," in *IEEE Annual Indian Conference INDICON, Kerala*, 7-9 December, 2012, pp. 115–120.

[131] S. Kim, M. B. Kim, and M. J. Youn, "New maximum power point tracker using sliding-mode observer for estimation of solar array current in the grid-connected photovoltaic system," *IEEE Transactions on Industrial Electronics*, vol. 53, no. 4, pp. 1027–1035, 2006.

[132] S. Ganguly, N. C. Sahoo, and D. Das, "Multi-objective particle swarm optimization based on fuzzy-pareto-dominance for possibilistic planning of electrical distribution systems incorporating distributed generation," *International Journal on Fuzzy Sets and Systems*, vol. 213, no. 1, pp. 47–73, 2013.

[133] R. Mahanty, "Large value ac capacitor for harmonic filtering and reactive power compensation," *IET, Generation Transmission Distribution*, vol. 2, no. 6, pp. 876–891, 2008.

[134] J. Moscinski and Z. Ogonowski, *Advanced Control with MATLAB and SIMULINK*. New Delhi: Ellis Horwood, 1996.

[135] A. Chakraborty and S. Halder, *Power System Analysis, Operation and Control*. New Delhi: Third Edition, PHI Publication, 2010.